Photoredox-Catalyzed Decarboxylative Radical Conjugate Addition-Elimination-Oxa-Michael Reaction: A Sustainable Approach to Potent HIV-1 Protease Inhibitors

Dissertation

Zur Erlangung des Doktorgrades der Naturwissenschaften

Dr. rer. nat.

der Fakultät für Chemie und Pharmazie

der Universität Regensburg

vorgelegt von

Tomislav Krolo

aus Bad Abbach

Regensburg, Juli 2022

Meiner Familie

Table of contents

Abbreviations

Ac	acetyl	4-CzIPN	1,2,3,5-tetrakis(carbazole-9-yl)-4,6-dicyanobenzene
AIBN	2,2`-azobis(isobutyronitrile)	d	day(s)
AIDS	Acquired Immunodeficiency Syndrome	DABCO	1,4-diazabicyclo[2.2.2]octane
APCI	atmospheric pressure chemical ionization	dap	2,9-bis(*para*-anisyl)-1,10-phenanthroline
aq.	aqueous	dba	dibenzylideneacetone
Ar	aryl	DBU	1,8-diazabicyclo-[5.4.0]undec-7-ene
ART	antiretroviral therapy	DCA	9,10-dicyanoanthracene
Bn	benzyl	DCC	dicyclohexylcarbodiimide
Boc	*tert*-butyloxycarbonyl	DCM	dichloromethane
bpy	2,2`-bipyridine	DcRCA	decarboxylative radical conjugate addition
*t*Bu	*tert*-butyl	DcRCAE	decarboxylative radical conjugate addition-elimination
° C	degree celsius	*de*	diastereomeric excess
c	concentration	DIPEA	*N,N*-diisopropylethylamine
Cbz	benzyloxycarbonyl	DMA	*N,N*-dimethylacetamide
CCDC	Cambrigde Crystallographic Data Center	DMAP	4-dimethylaminopyridine
CFL	compact fluorescence lamp	DMF	*N,N*-dimethylformamide
Cp	cyclopentanyl	DMSO	dimethylsulfoxide
CpO	cyclopentanonyl	*dr*	diastereomeric ratio

dtbbpy	4,4'-di-*tert*-butyl-2,2'-bipyridine	LED	light-emitting diode
EA	ethyl acetate	M	molar; mega
EI	electron ionization	Me	methyl
equiv	equivalents	MeCN	acetonitrile
ESI	electrospray ionization	MeOH	methanol
Et	ethyl	mg	milligram
et al.	et alia	min	minutes(s)
EtOAc	ethyl acetate	mp	melting point
EWG	electron-withdrawing group	mRNA	messenger ribonucleic acid
FDA	Food and Drug Administration	m/z	mass-to-charge ratio
Fmoc	fluorenylmethoxycarbonyl	nM	nanomolar
g	gram	nm	nanometer
gem	geminal	NMR	nuclear magnetic resonance
h	hour(s)	PC	photocatalyst
HIV	human immunodeficiency virus	PG	protecting group
HPLC	high-performance liquid chromatography	Ph	phenyl
HRMS	high resolution mass spectrometry	PI	protease inhibitor
Hz	hertz	pM	picomolar
IC_{50}	half maximal inhibitory concentration	ppm	parts per million
IR	infrared	ppy	2-phenylpyridine
J	coupling constant	*i*Pr	*iso*-propyl
K	Kelvin	quant	quantitative
LED	light-emitting diode	R	arbitrary residue

R$_f$	retention factor	TBAF	tetrabutylammonium fluoride
rac	racemic	Tf	triflyl
RNA	ribonucleic acid	TFA	trifluoroacetic acid
rt	room temperature	THF	tetrahydrofuran
s	second(s)	Thr	threonine
sat.	saturated	TLC	thin layer chromatography
SCE	standard calomel electrode	TMS	trimethylsilyl
Ser	serine	UV	ultraviolet
SET	single electron transfer	vs.	versus
SOMO	single occupied molecular orbital	W	Watt
TBA	tetrabutylammonium		
TBADT	tetrabutylammonium decatungstate		

Indication of relative and absolute stereochemistry is given as follows:

= relative stereochemistry

= absolute stereochemistry
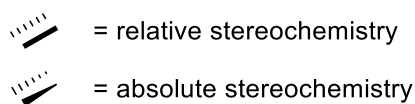
A Introduction

1 Photoredox-catalyzed decarboxylative radical conjugate addition to alkenes: a sustainable protocol for C-C bond formations

1.1 Carboxylic acids as a green alternative for efficient radical generation

In the last two decades mankind witnessed the most significant transformation since the industrial revolution in the 19th century and the beginning of a new era in society, politics and industry – the digitalization. The technological progresses and advancements, especially since the millennium, led to a whole new economy and industry, entirely changing and facilitating our way of living on all levels, including mobility, the access to information and entertainment. Furthermore, these ongoing innovations accelerated the development of new methods in science and research due to completely new and prior unimaginable possibilities in data handling and information processing, which consequently resulted in an overall better understanding of complex processes in our environment. This new knowledge gathered over the last decades together with the public`s opportunity of facile and instant access to information led to the emergence of new values and principles in society and politics, with the topic of sustainability being one of the most prominent ones.

This idea of sustainability and the corresponding redefinition of existing standards in our society is fueled by the recent acceleration of global warming and climate change, resulting in an increased number of extreme weather events and natural catastrophes wordwide.[1] The growing public awareness of this dramatic evolution generates the pressing need for new and more sustainable processes on all scales, including the shift of our mobility away from fossil fuels towards greener alternatives. The transition of these ideas and principles into general chemistry and especially into the chemical industry, the industrial sector with the biggest energy consumption in Germany in 2020 and still mainly relying on fossil fuels as feedstocks, is of paramount importance.[2,3]

The basis of this idea of sustainability in the chemical sector was set by Anastas and Warner with the development of the concept of "Sustainable Chemistry" or "Green Chemistry" in 1998.[4,5] A focal point of this revolutionary philosophy is, besides the efficient utilization of catalytic methods under atom economic aspects, the usage of renewable feedstocks such as biomass.[6] The interest of the chemical industry in large scale industrial conversion of biomass into bulk and fine chemicals increased significantly over the last two decades, which is not only

a consequence of the attempt of compensating the expected degression of petroleum production, but also to reduce increasing dependency on specific fossil fuel exporting countries. In fact, stringent legislation regarding greenhouse gas emissions and the need to adapt to an overall shift in society and politics towards more sustainable principles to improve public confidence and remove distrust in the chemical industry contributed considerably to this elevated interest in renewable resources as green feedstocks.[7]

A key functionality for the generation of platform and fine chemicals including natural products and pharmaceuticals from renewable resources derived raw compounds is the carboxyl group present in carboxylic acids, which can be targeted in this context as chemo- and regioselective leaving group, thus serving as a versatile connection point for the construction of carbon-carbon frameworks.[8,9,10] Carboxylic acids are one of the most abundant class of compounds, making them widely available in industry and academia. Their presence in various naturally occurring compound classes like amino acids, fatty acids and sugar acids showcase their remarkable structural diversity including numerous centers of chirality. This structural value combined with the characteristics of carboxylic acids serving as non-toxic, bench stable, inexpensive and widely available reagents make these the ideal substrates for the sustainable synthesis of valuable products and pharmaceuticals.[11]

Their synthetic value can be attributed to the aforementioned carboxylate group, which can be considered as a chemo- and regioselective leaving group upon decarboxylation. During the process of decarboxylation, a traceless extrusion and elimination of CO_2 from the reaction mixture occurs, thus providing entropic driving force without any influence on the underlying reaction system.[12,13] Pioneered by the works of Kolbe[14], Hunsdiecker[15] and Barton[16] for the understanding of radical generation via decarboxylation, numerous novel methods for efficient decarboxylation approaches have been developed in the last decades.[12,17]

One of the most promising approaches among recent advances for efficient radical decarboxylation procedures is the utilization of visible-light mediated coupling processes. The development of visible-light photoredox catalysis has led to a paradigm shift in organic synthesis, enabling heretofore inaccessible reaction pathways and unprecedented reactivity patterns[18,19,20]. Furthermore, mild reaction conditions under low-energy irradiation allow for high functional group tolerance and thus chemoselectivity, circumventing drawbacks of earlier decarboxylation methods including harsh conditions and the use of toxic and unstable reagents for radical generation.[11] The use of a library of different and versatile transition-metal based and organic photocatalysts with tunable reactivity, owing to their specific photophysical and

electrochemical properties, enables the synthetic chemist a myriad of chemical transformations, thus opening the door for the utilization of varying radical precursors and different types of carboxylic acids for the facile generation of a series of different radical intermediates.[21]

The mode of activation in a photoredox-catalyzed decarboxylation involves typically three steps: after an initial deprotonation of carboxylic acid **1**, carboxylate anion **2** is formed, which is subsequently oxidized via single electron transfer (SET) by the excited photocatalyst in a second step to oxygen-centered radical intermediate **3** (Scheme 1). Extrusion of CO_2, generating carbon-centered radical species **4**, completes the decarboxylation process and therefore enables various C-C bond forming reactions with suitable alkene acceptors.[11,22]
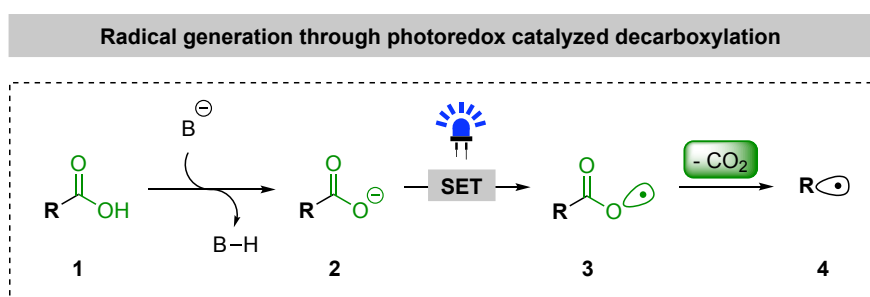
Scheme 1. Extrusion of CO_2 via photoredox-catalyzed decarboxylation.[11]

The addition efficiency of generated radical **4** to an electron-deficient alkene and the resulting chemoselective advantage of a radical-addition process compared to a typical addition of a nucleophile to an alkene is considerably high. Nucleophilic carbon-centered radicals can add to an electron-deficient alkene with a rate on the order of 10^6 M^{-1} s^{-1}.[23] This rate is distinctly faster than that of undesired side reactions, including typical atom-transfer reactions from sensitive functional groups present in the reaction medium such as alcohols and amines, which proceed with a rate on the order of 10^2 M^{-1} s^{-1}.[21,24] This chemoselective "headstart" enables the radical conjugate addition to proceed in the presence of unprotected functional groups, further streamlining synthetic processes.[11]

The versatility of a visible-light photoredox catalyzed decarboxylation allows the application of different types of carboxylic acids as radical precursors, including α-amino (**5**), α-oxo (**7**), α-alkyl (**9**), aryl acetic acids (**11**) and α-oxy-carboxylic acids (**13**) (Scheme 2). This structural variety of the underlying acid precursors allows for the efficient generation of a wide range of radicals after decarboxylation, with examples being α-amino radicals (**6**), acyl radicals (**8**), alkyl radicals with different substitution patterns (**10**), benzyl radicals (**12**) and α-oxy radicals (**14**), hence enabling an extremely broad set of alkene acceptor functionalization depending on the employed precursor.
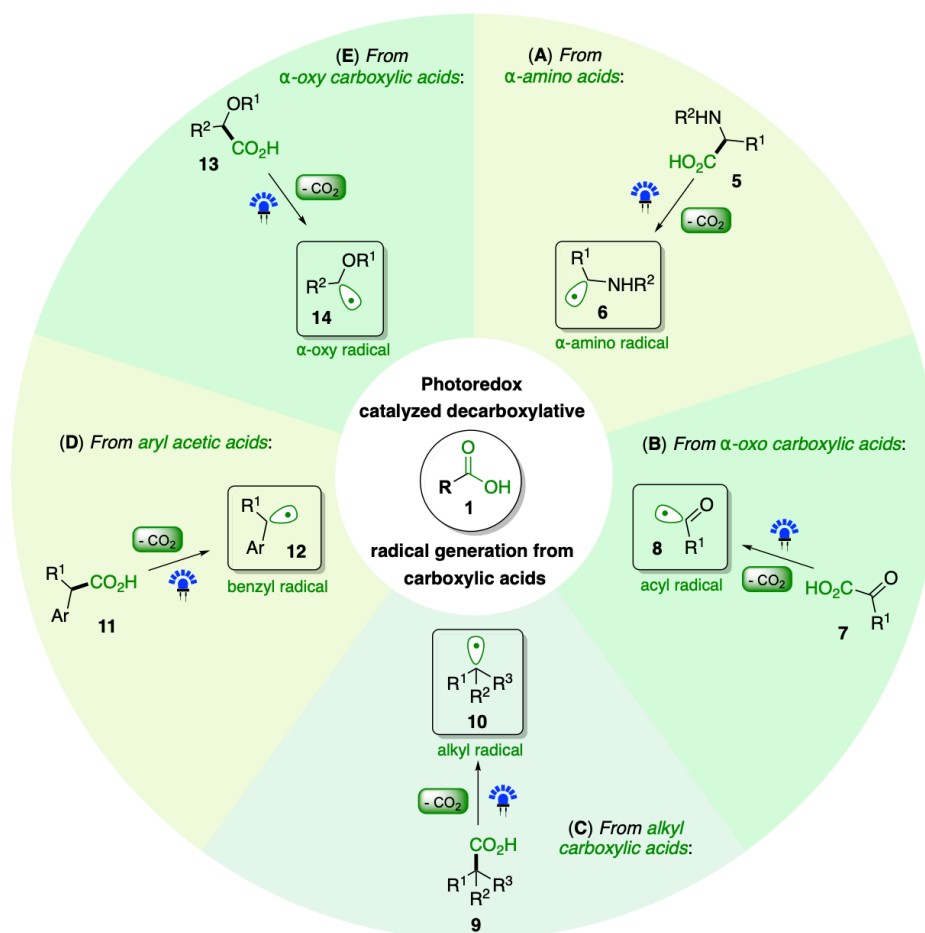
Scheme 2. Visible-light induced radical generation from different types of carboxylic acids.

In the following chapter, a brief summary of recent examples of photoredox catalyzed decarboxylative radical conjugate addition reactions is presented, highlighting the versatility of this powerful method. Due to operational, ecological and economical drawbacks of the utilization of pre-functionalized redox active esters like *N*-(acyloxy)phthalimide (NHPI) esters as radical precursors, only the conversion of free and inactivated carboxylic acids is covered.[11] In order to give the reader an extensive overview of the synthetic variety of the different described substrates, this summary is divided into five chapters, originating from the types of radical precursors and their corresponding radical intermediates exhibited in Scheme 2, thus immediately showcasing the synthetic value of typical carboxylic acid classes as bench stable chemicals.

It should be noted that not all of the described methodologies are limited to the class of carboxylic acid substrates they are assigned to, in fact, a considerable amount of the highlighted works show a broad scope of different employed acids as precursors, which will be mentioned in the respective examples. Nonetheless, the covered reports show in most cases a clear focus on a specific class of employed substrates, representing the majority of the scope, with the acid substrate of the respective assigned category being the most prominent one.

1.2 Abundant α-amino acids as precursors for the formation of nucleophilic α-amino radicals

Amino acids are highly desirable substrates for chemical syntheses owing to their properties of being abundant, readily available, non-toxic and predominantly inexpensive, bench stable reagents. After successful photochemical decarboxylation, a $C(sp^3)$-centered α-amino radical is formed, exhibiting a strongly nucleophilic character which is distinctly higher compared to the nucleophilicity of typical alkyl radicals without an adjacent heteroatom. This distinct nucleophilic character of α-amino radicals, representing one of the most nucleophilic radicals known, originates from an efficient π-interaction of the nitrogen-atom with the adjacent alkyl radical.[25,26] Resonance donation from the lone pair on the nitrogen results in a raised single occupied molecular orbital (SOMO), representing primarily the unhybridized *p*-orbital, thus considerably enhancing the nucleophilic character of the neighboring radical and enabling highly efficient conjugate addition to a variety of electron-deficient alkenes.[26]

A pioneering protocol for the efficient generation of nucleophilic radicals from amino acids was reported by MacMillan and co-workers in 2014, enabling radical conjugate addition to a variety of different Michael acceptors.[27] With iridium-based photocatalyst **18** and K_2HPO_4 as the preferred deprotonation system, efficient decarboxylation of amino acids **15** was observed under irradiation with a 26 W fluorescent light bulb, yielding adducts **17** after radical conjugate addition to electron-deficient alkenes **16** (Scheme 3). The mild reaction conditions allowed for the derivatization of a library of Michael acceptors including α,β-unsaturated aldehydes, ketones, esters, imides and sulfones. Furthermore, the synthetic utility of this powerful methodology was demonstrated by a three-step synthesis of medicinal agent (±)-pregabalin with the photoredox-catalyzed decarboxylative 1,4-addition as key step.[27,28] Besides amino acids as employed precursors, also other carboxylic acids including α-oxy- and hydrocarbon-substituted acids were successfully utilized as substrates.
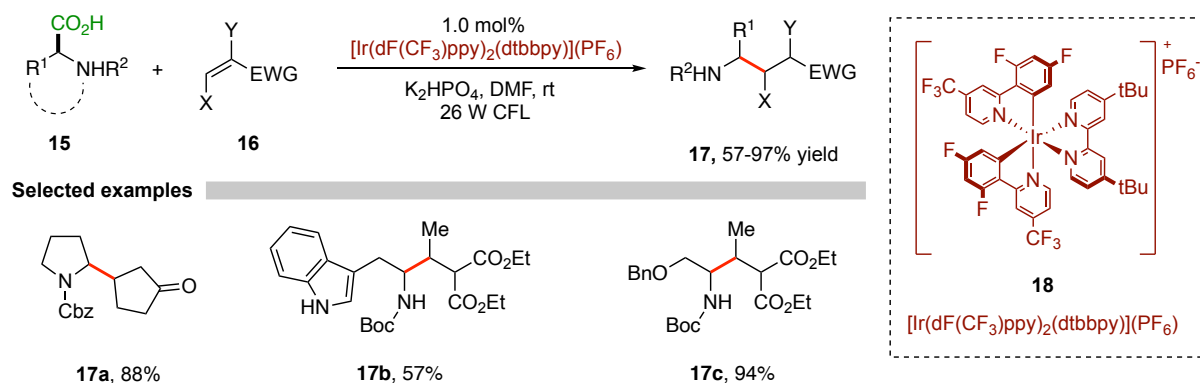
Scheme 3. Decarboxylative radical conjugate addition by the group of MacMillan.[27]

The MacMillan group expanded their previously developed methodology successfully to a decarboxylative peptide macrocyclization protocol by utilizing peptides bearing *N*-terminal Michael acceptors, thus enabling an intramolecular cyclization after decarboxylation of the C-terminal acid functionality (Scheme 4).[29] In contrast to the aforementioned procedure, a high catalyst loading of photocatalyst **18** was employed, adapting to the required low concentration levels of substrates in the reaction medium in order to circumvent undesirable oligomerization pathways. A wide range of diverse and linear peptides **19**, ranging from 3 to 15 amino acids, was successfully converted to the corresponding cyclic peptides **20**, representing a privileged class of pharmacophores with increased biological activity and target selectivity due to conformational rigidity.[30] The preparative utility of this method was once again highlighted by the synthesis of macrocyclic peptide and somatostatin analogue COR-005, being currently evaluated in clinical trials.[29] In 2021, Ruf and co-workers extended this work to the C-terminal modification of small peptide substrates by broadening the scope of Michael acceptors to acyclic unsaturated ketones and less electrophilic Michael systems such as cinnamic esters and vinyl-substituted (hetero)aromatic systems.[31]
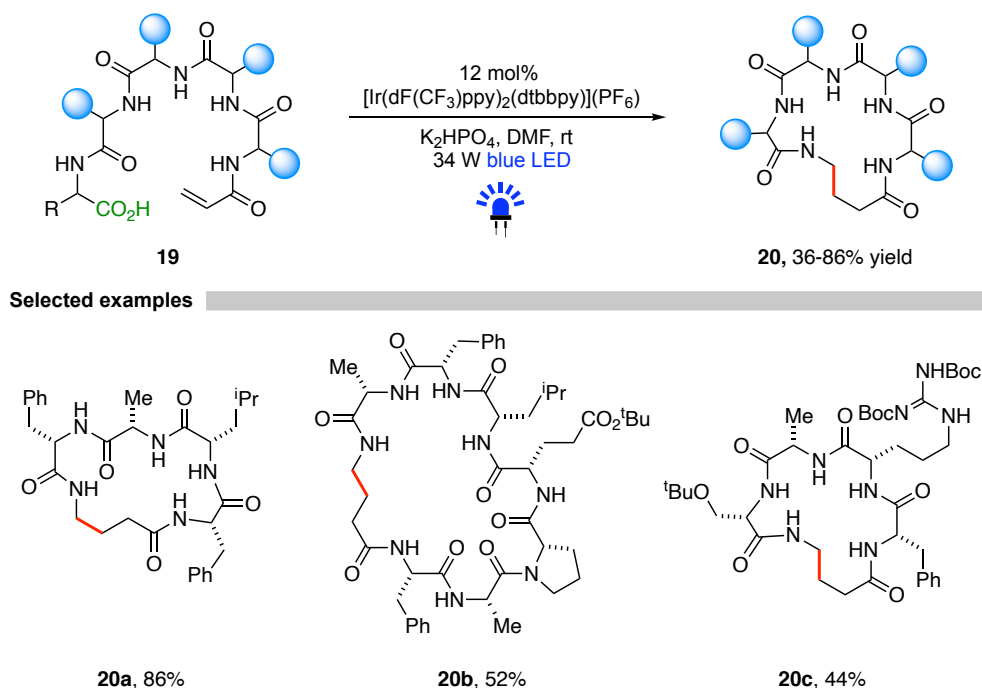
Scheme 4. Decarboxylative peptide macrocyclization.[29]

In 2014, MacMillan et al. successfully demonstrated the photoredox-catalyzed α-vinylation of amino acids **15** with vinyl sulfones **21** as coupling reagents, providing synthetically valuable allylic amines **22** in an efficient manner (Scheme 5).[32] Catalyzed by [Ir(dF(CF$_3$)ppy)$_2$(dtbbpy)](PF$_6$) (**18**), a broad scope of various allylic amines was synthesized

at slightly elevated temperatures of 50 °C, providing the respective products in good to excellent yields. High functional group tolerance with respect to both starting materials along with an excellent control of olefin geometry underlines the efficiency of this powerful method (Scheme 5, A). The proposed mechanism of this transformation involves initial steps of deprotonation and oxidation of amino acid **15** by the excited photocatalyst, generating nucleophilic radical **23** after CO_2-extrusion (Scheme 5, B). Subsequent radical addition to vinyl sulfone **21** provides β-sulfonyl radical **24** as an intermediate, which after elimination of a sulfinyl radical generates allylic amine **22** as the desired product. Reduction of liberated sulfinyl radical to the sulfinate anion regenerates the photocatalyst, thereby closing the catalytic cycle.[32]
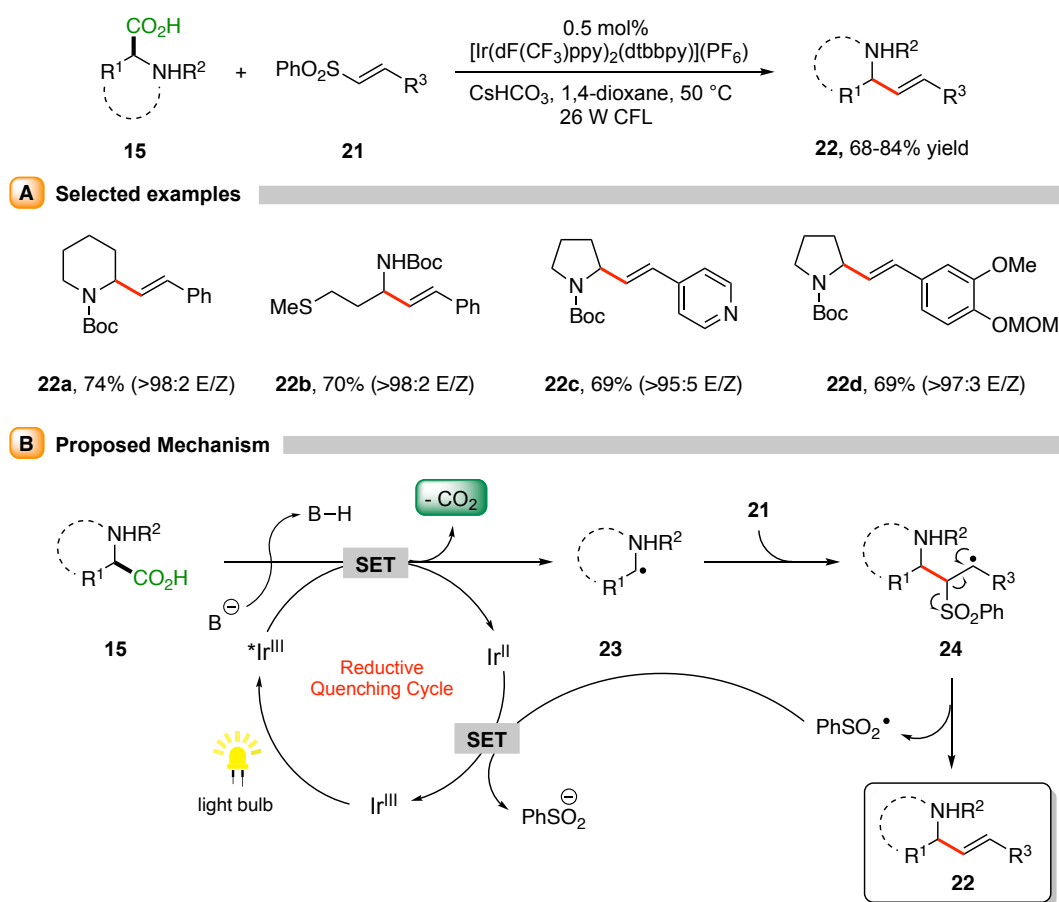
Scheme 5. Visible light-mediated α-vinylation of amino acids.[32]

Photocatalytic direct decarboxylative allylation was achieved in 2017 by Zhu and co-workers. This optimized protocol with [Ir(ppy)$_2$(bpy)](PF$_6$) as the photocatalyst allows the functionalization of various *N*-arylglycine derivatives **25** utilizing allyl sulfone **26** as the radical acceptor (Scheme 6). The corresponding homoallylic amines **27** were obtained in moderate to excellent yields of 23–95%, indicating a significant dependence of the efficiency of the underlying catalytic process on the electronic properties of the employed *N*-arylglycine substrate as precursor.[33]
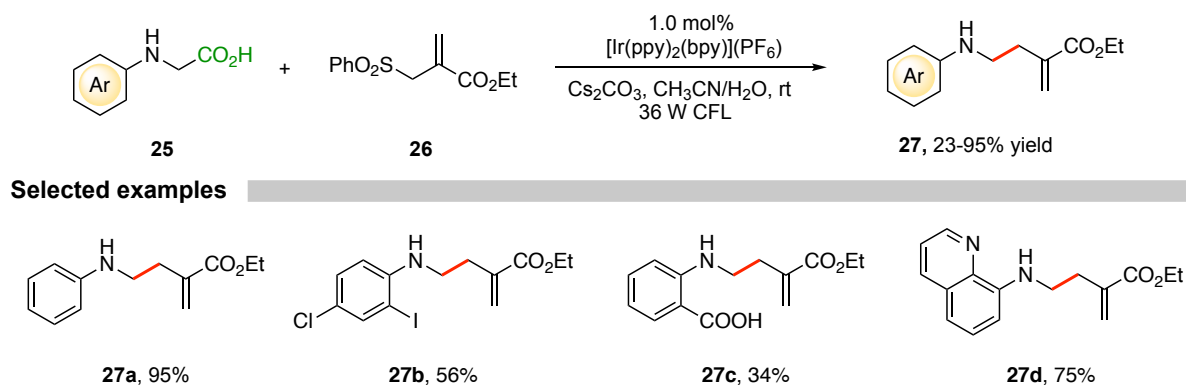
Scheme 6. Direct decarboxylative allylation of N-arylglycine derivatives.[33]

An interesting variation of MacMillan's aforementioned α-vinylation of amino acids[32] was introduced 2018 by Opatz and his research group, reporting the successful synthesis of vinyl sulfones and α,β-unsaturated nitriles from amino acids by utilizing either bis-vinylsulfone **28** or sulfonilated nitrile **29** as the coupling reagent (Scheme 7).[34] The organic photocatalyst 9,10-dicyanoanthracene (DCA) efficiently promoted the vinylsulfonylation and acrylonitrile incorporation into substrates **15**, yielding the corresponding sulfones **30** and acrylic nitriles **31** in moderate to good yields. The synthetic utility of this methodology was showcased by a three-step synthesis of potent cysteine protease inhibitor K11777, underlining the importance of vinyl sulfones as potential electrophilic warheads in covalent inhibitors.[34,35]
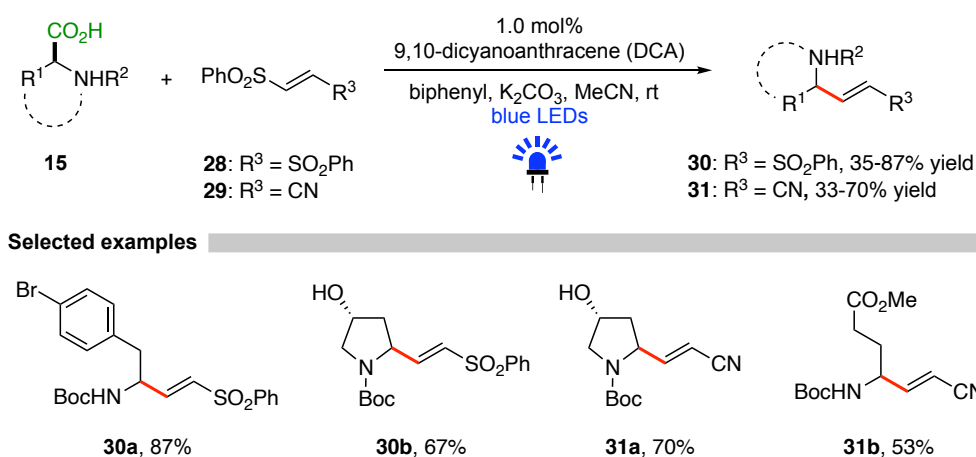
Scheme 7. Photoredox-catalyzed formation of vinyl sulfones and acrylic nitriles from amino acids.[34]

In the same year, the groups of Aggarwal and Noble reported a novel visible light induced decarboxylative radical addition-polar cyclization cascade approach for the synthesis of functionalized cyclopropanes from various carboxylic acid derivatives including α-amino acids.[36] While efficient transformations were also observed for iridium-based photocatalysts, the more economical, cyanobenzene-based organic photocatalyst 4CzIPN (**36**) was found to be even more powerful for inducing the desired transformation (Scheme 8).

Under irradiation with a blue LED, a library of amino acids **15** was converted to cyclopropyl boronic esters **34** and cyclopropyl esters **35** in yields up to 99% by conjugate addition to the respective chlorinated alkenes **32** and **33**. The proposed mechanism reveals a specific feature of this protocol (Scheme 8, B). After in-situ deprotonation of amino acid **15**, the oxidation by the excited organic photocatalyst **PC*** with subsequent decarboxylation occurs, resulting in α-amino radical **23** and the reduced photocatalyst species **PC*−**. Radical addition to either homoallyl chloride **32** or **33** generates intermediate **37**, which in a next step undergoes reductive termination to anionic species **38**, regenerating the ground state of the photocatalyst **PC**. At this stage, typically and often reported simple protonation of anion **38** to undesired product **39** occurs, which is circumvented in this example by the presence of an adjacent chlorine moiety. Nucleophilic attack of stabilized anion **38** furnishes the respective cyclopropane esters **34** and **35** after a polar 3-*exo-tet* cyclization, highlighting the special character of this transformation.[36] Furthermore, this methodology demonstrated its synthetic value by a series of late stage functionalizations of complex carboxylic acids including fibrate Gemfibrozil and vitamin E derivative Trolox.[36]
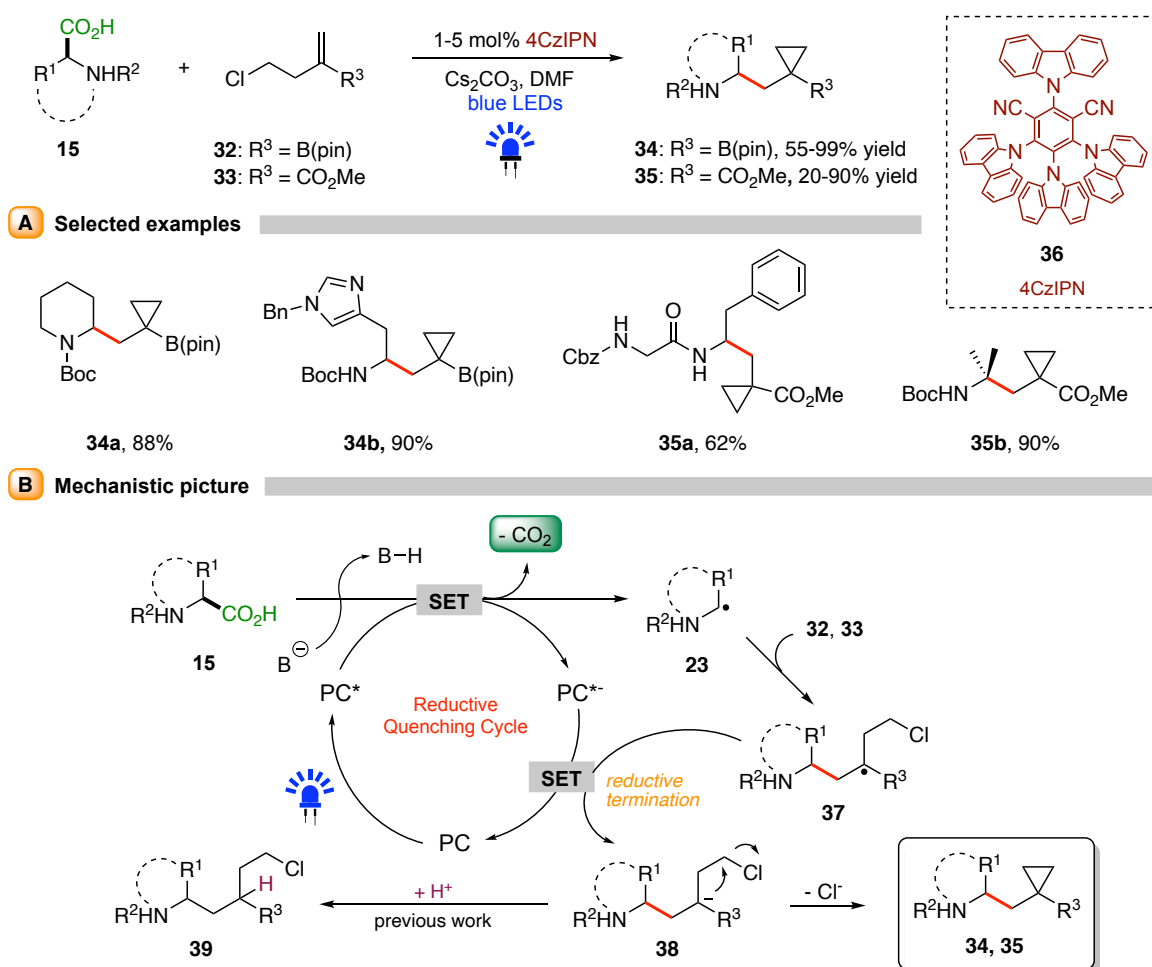
Scheme 8. Decarboxylative radical addition-polar cyclization cascade to functionalized cyclopropanes.[36]

A remarkable and exotic protocol for the efficient utilization of α-amino radicals was developed by Cintrat and co-workers in 2020 with the photochemical strain-release-driven cyclobutylation of various amino acids.[37] The uniqueness in this report is based on the employed radical acceptors, being highly strained and sulfonated bicyclo[1.1.0]butanes (BCB, **40**) instead of alkenes, exhibiting remarkable ring strain energy of 64 kcal mol^{-1} (Scheme 9).[38] The reason for the incorporation of this special example into this summary which meant to cover exclusively radical conjugate to alkenes is the strong π-character of the central C-C σ-bond present in the BCB framework, thus opening the possibility to serve as a surrogate for the corresponding olefin. Generation of highly nucleophilic α-amino radicals from amino acids **15** under iridium-based photocatalysis furnished 1,3-disubstituted cyclobutanes **41** in yields ranging from 26 to 95%, even enabling late-stage functionalization of antihypertensive drugs Ramipril (**41c**) and Valsartan (**41d**) in moderate yields. Deuterium-labelling experiments supported the presence of a transient sulfonyl anion during the mechanistic pathway, hence showing faster reduction and protonation processes compared to often occurring telomerization of BCBs.[37]
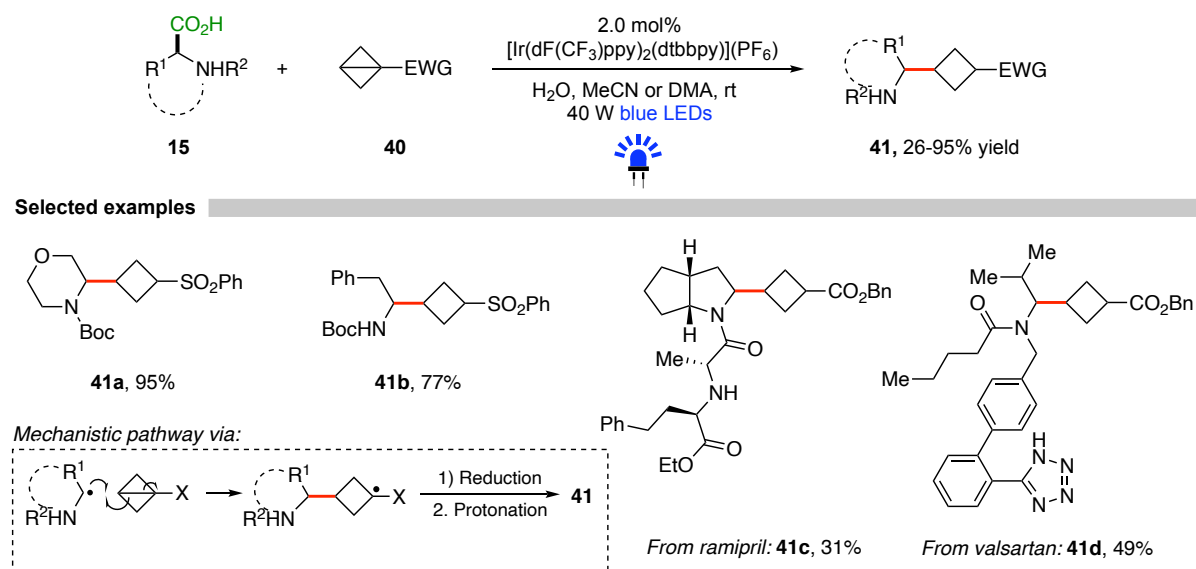
Scheme 9. Strain-release-driven cyclobutylation of amino radicals.[37]

1.3 Acyl radicals from α-oxocarboxylic acids as versatile coupling initiators

Carbon-centered sp^2 hybrid radicals possess distinctly varied fundamental electronic properties compared to their C(sp^3)-centered analogs, originating from their respective hybrid orbitals being located closer to the nucleus due to their higher s-character, making C(sp^2)-centered radicals generally more electrophilic than similarly substituted alkyl radicals.[26] Acyl radicals represent a special class of sp^2-hybridized radicals in which the present π-bond involves oxygen as a heteroatom containing two non-bonding electron pairs, therefore enabling efficient π-interaction with the adjacent radical.[39] This stabilizing effect is enhanced by conformational rigidity of the lone pair, being a consequence of the restricted rotation around the π-bond, thus maximizing interaction with the SOMO and leading to radicals of considerably nucleophilic character.[26]

One of the first photoredox-catalyzed protocols for the generation of acyl radicals from α-oxocarboxylic acids was developed by Fu and co-workers in 2015.[40] This methodology allows the efficient synthesis of *γ*-carbonyl compounds **44** starting from arylated α-keto acids **42** by decarboxylative 1,4-addition to various Michael acceptors **43** (Scheme 10, A).
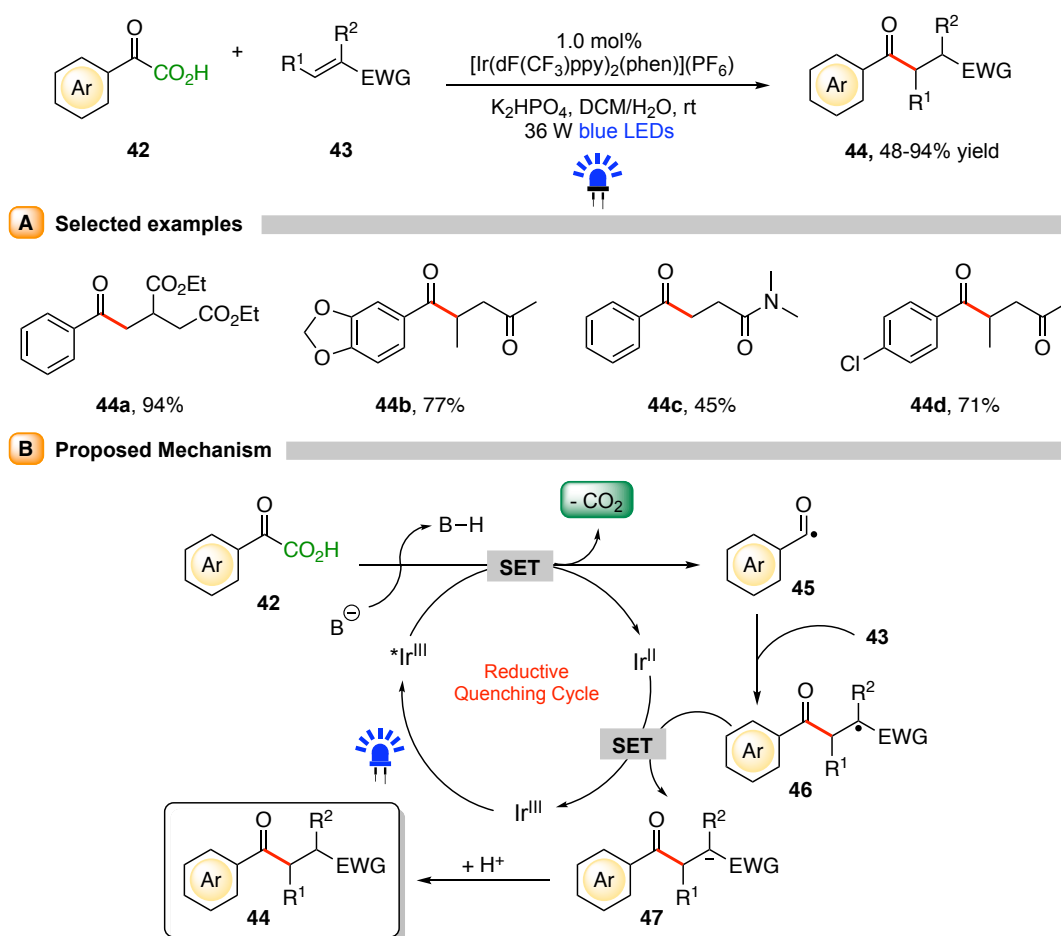
Scheme 10. Decarboxylative 1,4-addition of α-oxocarboxylic acids.[40]

Mild reaction conditions involving blue light irradiation under iridium-photocatalysis facilitated the conversion of several phenylacetic acids with varying electronic properties, enabling efficient 1,4-additions to a library of Michael acceptors including α,β-unsaturated esters, cyclic and acyclic ketones, aldehydes, amides and nitriles. The proposed mechanism of this transformation involves deprotonation of α-keto acid **42** followed by oxidation via SET and extrusion of CO_2, furnishing acyl radical **45** which adds in a second step to Michael acceptor **43** (Scheme 10, B). Radical intermediate **46** is reduced to anion **47**, thereby closing the photocatalytic cycle and yielding the desired product **44** after a final protonation step.[40] The groups of Shi and Lei expanded this work later by utilizing activated alkenes including styrenes and 1,1-diphenylethene derivatives as radical acceptors, yielding a diverse set of aryl ketones.[41]

In 2017, the group of Zhu reported an interesting visible-light mediated cross-coupling protocol of α-oxocarboxylic acids with styrenes for the synthesis α,β-unsaturated ketones via a domino-fluorination-protodefluorination cascade (Scheme 11).[42] The critical part of this strategy involves the formation of a new C–F bond promoted by a fluorine atom transfer from fluorinating agent Selectfluor to the corresponding benzyl radical generated after the acyl radical addition to styrene **48** during the photocatalytic process. The formation of a conjugated π-system acts as a driving force for the subsequent sequential elimination of hydrogen fluoride, furnishing the arylated α,β-unsaturated ketones **49** in overall good yields.
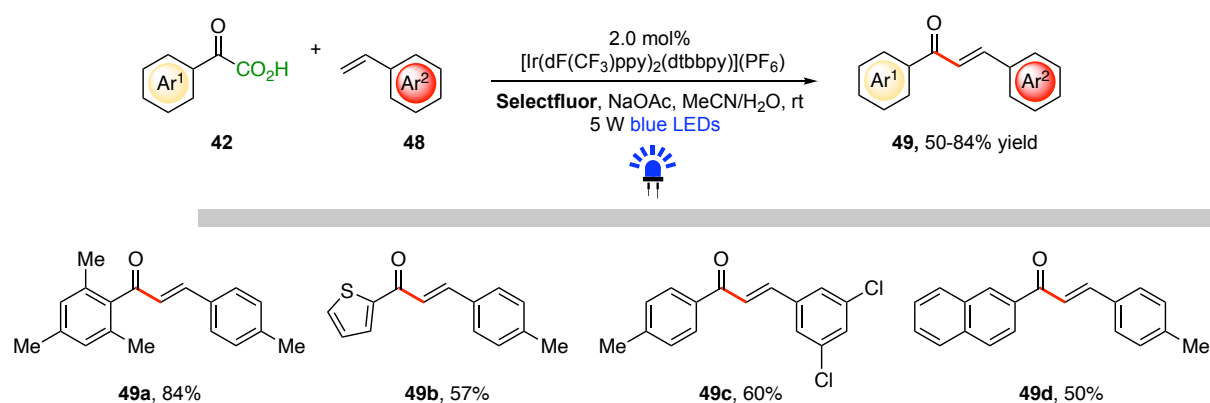
Scheme 11. Synthesis of α,β-unsaturated ketones via a domino-fluorination-protodefluorination cascade.[42]

Another methodology involving fluorine species not only during the mechanistic pathway but also in the specific radical conjugate addition products was introduced by Zhou and co-workers, providing an efficient route towards γ,γ-difluoroallylic ketones **52** (Scheme 12).[43] By utilizing α-trifluoromethyl alkenes **51** as radical acceptors, numerous successful decarboxylative/defluorinative transformations were carried out, tolerating a broad range of functional groups including the presence of thiophens under iridium-photocatalyzed conditions,

furnishing the corresponding *gem*-difluoroalkenes **52** in yields ranging from 48–91%. This protocol was not limited to α-keto acids as radical precursors, numerous amino acids were also successfully employed as radical generating substrates, affording various 1,1-difluorohomoallylic amines as products.
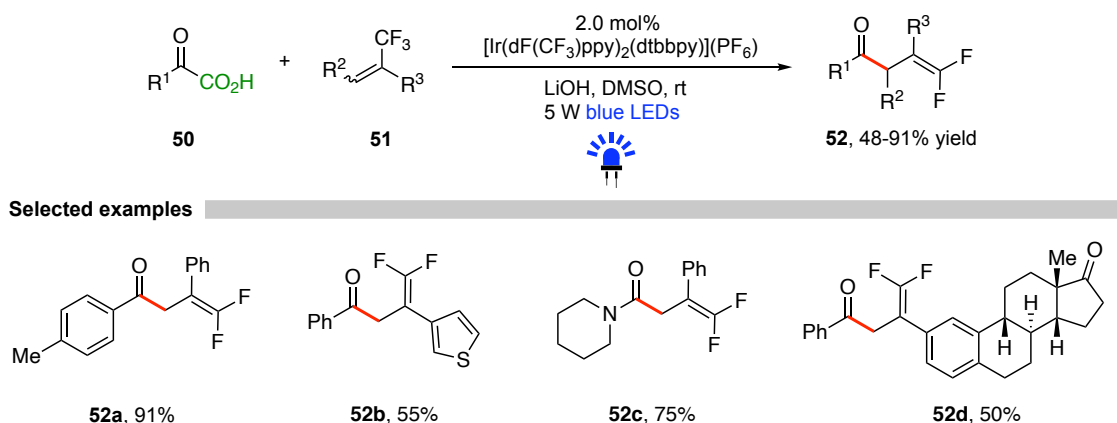
Scheme 12. Decarboxylative/defluorinative cascade to γ,γ-difluoroallylic ketones.[43]

While typically α-keto acids are utilized as acyl radical precursors, Feng and co-workers developed in 2018 the first successful decarboxylation of a special class of carboxylic acid derivatives, namely oxamic acids.[44] The resulting carbamoyl radicals turned out to be efficient coupling intermediates with various mono-and disubstituted alkenes **54**, furnishing after a sequence of intermolecular radical addition, intramolecular cyclization and aromatization diverse 3,4-dihydroquinolin-2(1*H*)-ones **55** in moderate to good yields (Scheme 13, A). The proposed mechanism of this valuable transformation commences with the formation of carbamoyl radical **56** from oxamic acid **53** after CO_2-elimination in the absence of a typically required base (Scheme 13, B). Intermolecular radical addition to alkene **54** leads to the formation of intermediate **57**, which in a next step undergoes intramolecular homolytic aromatic substitution to cyclohexadienyl radical **58**. The photocatalytic cycle is terminated by single electron reduction of oxygen present in the reaction mixture. The generated oxygen radical anion subsequently abstracts a hydrogen atom from aryl radical **58**, yielding desired quinolinone **55** and, in a last protonation step, H_2O_2 as byproduct (Scheme 13, B).[44]

In the same year, the group of Xu reported a specialized decarboxylative protocol, enabling two different reaction pathways starting from the same class of α-oxocarboxylic acids as radical precursors.[45] Depending on the substitution pattern of the employed substrate, either a simple decarboxylation occurs for primary and secondary alkylsubstituted α-keto acids **59**, generating a typical acyl radical under the present photochemical conditions and affording after radical addition to Michael acceptors **61** the corresponding γ-ketoesters **62** (Scheme 14, pathway **A**).
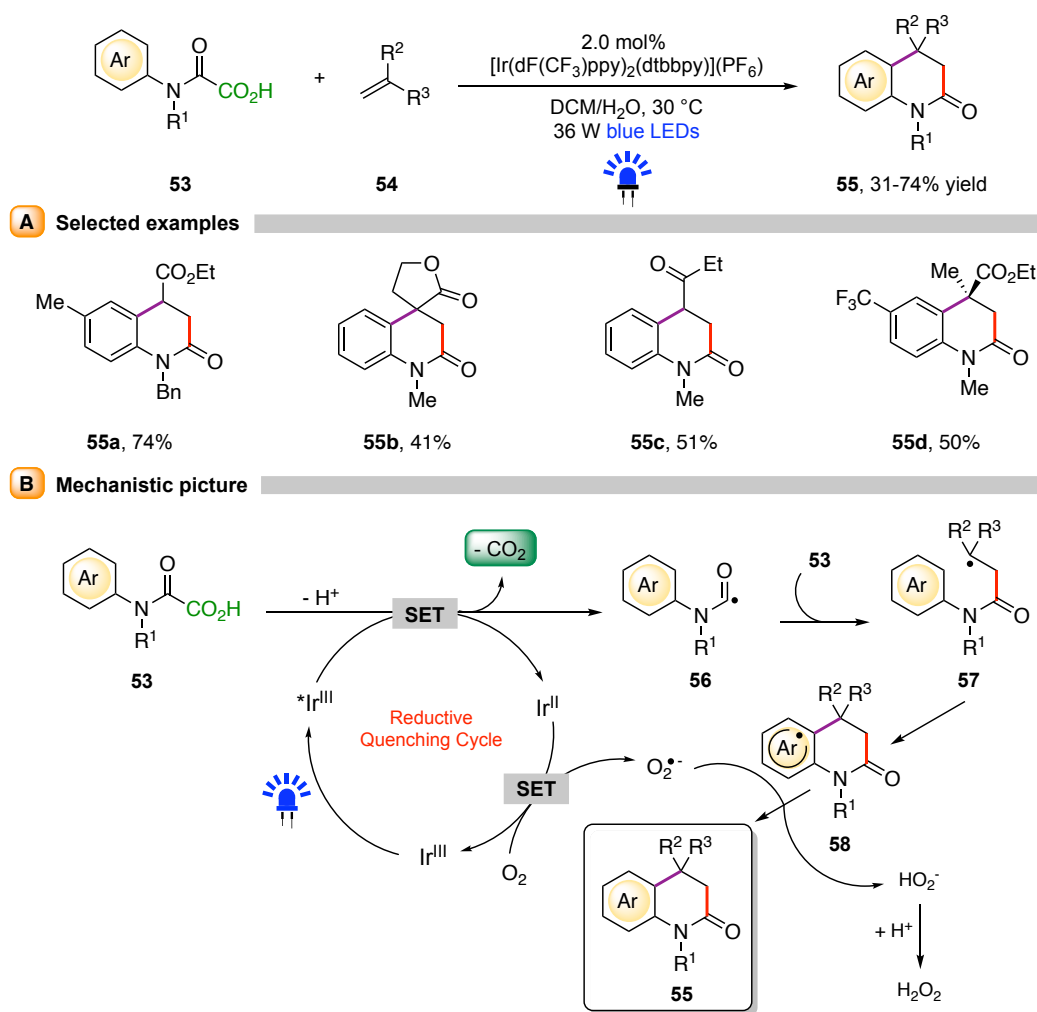
Scheme 13. Synthesis of quinolinones starting from oxamic acids via photoredox-catalyzed decarboxylation.[44]

By changing the substitution pattern of the keto-acid to tertiary alkyl substitution (substrate **60**), in addition to the expected decarboxylative acyl radical generation, a decarbonylation process occurs, generating the corresponding highly stabilized tertiary carbon radicals after CO-extrusion, thus yielding a series of quarternary carbons **63** as products after conjugated addition to electron-deficient alkenes **61** (Scheme 14, pathway **B**). It should be noted that primary alkyl ketoacids undergo exclusively the decarboxylation reaction and tertiary alkyl substrates are also exclusively prone to rapid decarboxylation-decarbonylation processes. However, secondary alkyl keto acids furnish the respective products of both possible reaction pathways, with the decarboxylation pathway **A** being the prominent one and yielding γ-ketoesters **62** as major products. Altering the reaction conditions with secondary substituted keto acids as substrates to heating under reflux changes the rates of product formation and shifts the outcome of the reaction towards the decarboxylation-decarbonylation pathway **B**, affording mainly tetra-substituted adducts **63**.[45]
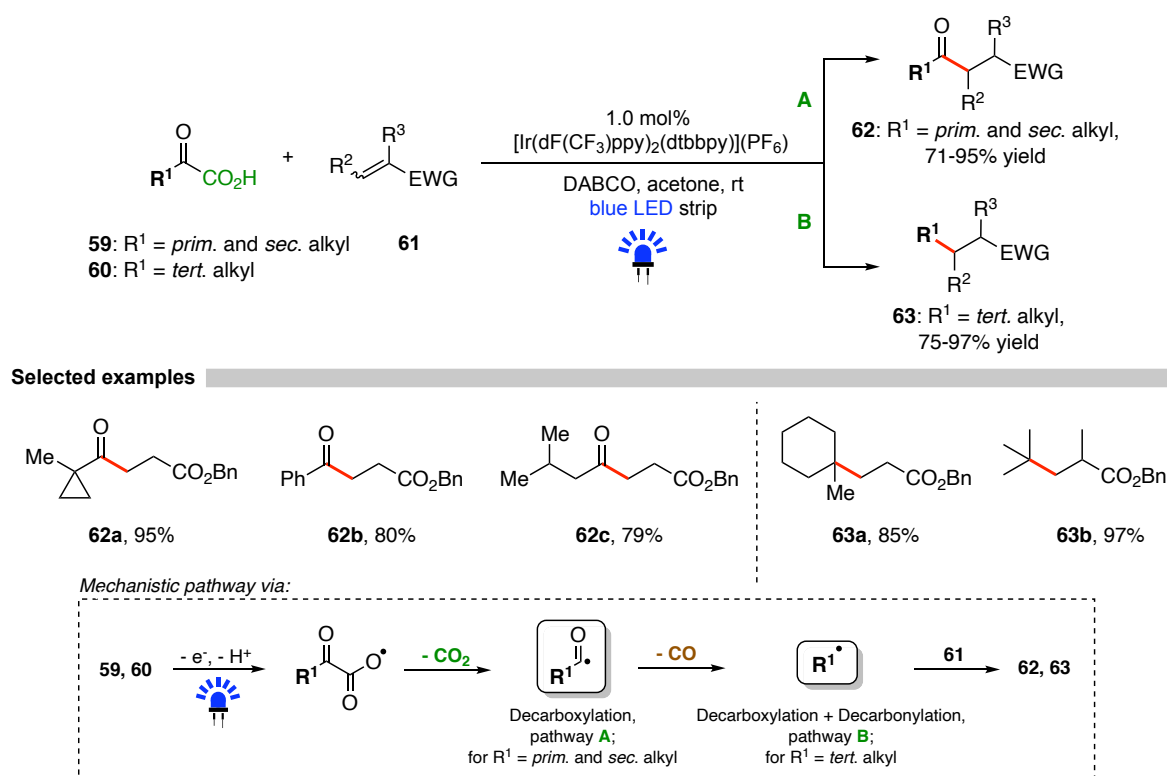
Scheme 14. Decarboxylation vs. decarboxylation-decarbonylation pathway.[45]

1.4 Decarboxylative photoredox-processes involving C(sp³)-centered alkyl radicals

The class of alkyl radicals is probably the one with the broadest spectrum in terms of radical reactivity and performance in radical conjugate addition reactions. The stability and electronic properties of hydrocarbon-substituted radicals is strongly dependent on the respective substitution pattern: stabilization of alkyl radicals occurs through hyperconjugative donation of adjacent alkyl groups, the higher the degree of substitution, the greater the hyperconjugation and thus the nucleophilicity of the respective radicals.[26] Consequently, tertiary alkyl radicals are strongly nucleophilic, whereas secondary and especially primary radicals are typically not overly effective in radical couplings involving electron-deficient alkenes, especially compared to α-heteroatom-substituted C(sp³)-centered radicals.

In 2018, Aggarwal and co-workers utilized various hydrocarbon-substituted carboxylic acids as alkyl radical precursors for the decarboxylative radical addition to boronic esters.[46] Under blue light irradiation and iridium-based photocatalysis, carboxylic acids **64** were successfully converted to their corresponding alkylated boronic esters **66** via a radical conjugate addition to vinyl boronic acid pinacol ester **65** (Scheme 15).

Both cyclic and acyclic carboxylic acids turned out to be efficient substrates for the desired transformation and exemplary late-stage functionalizations, whereas no example of a successful radical coupling of a primary carboxylic acid is reported, being a consequence of the instability of primary alkyl radicals. Besides hydrocarbon-substituted carboxylic acids, a broad range of α-amino acids was covered in this work, affording an extensive series of γ-amino boronic esters.
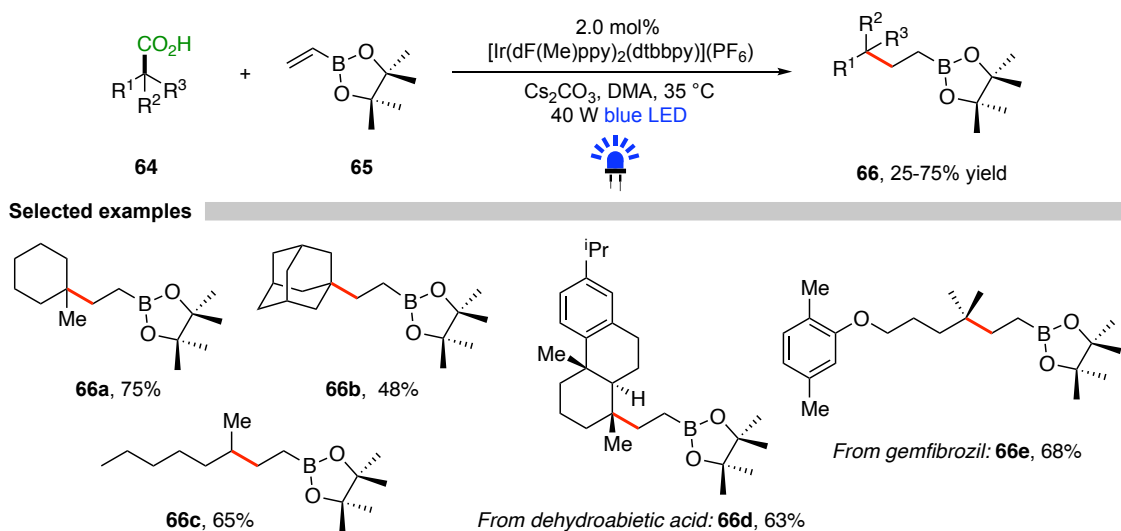
Scheme 15. Decarboxylative radical addition to vinyl boronic esters.[46]

In the next year later, König et al. reported a prolific protocol for the decarboxylative hydrazination of inactivated alkyl carboxylic acids enabled by cerium photocatalysis via a Ligand to Metal Charge Transfer (LMCT) as catalytic key step.[47] Irradiation with a 455 nm blue light LED induced the photocatalytic conversion of a broad series of carboxylic acids **64**, affording a variety of hydrazine derivatives **68** after radical addition to di-*tert*-butylazodicarboxylate (DBAD, **67**) (Scheme 16, A). Alkyl carboxylic acids with all degrees of substitution furnished the corresponding hydrazines **68** in good to excellent yields, highlighting the synthetic value of this methodology, especially considering the coupling efficiency of otherwise rather inefficient primary alkyl radicals in underlying radical additions. The proposed mechanism commences with an activation of Ce^{III} species **A** either via SET by *N*-centered radical **71** or, as an alternative pathway, by the photoactivated species DBAD* (E* = 1.66 V vs. SCE in MeCN), generating Ce^{IV} species **B**.[48] Coordination of carboxylic acid **64** after deprotonation leads to the formation of Cerium complex **C**, which in a next step undergoes the photoinduced Ce-O(CO) homolytic cleavage, referred to as photoinduced LMCT, regenerating Ce^{III} species **A** and affording carboxy radical **69**.[49] Alkyl radical **70** is formed after extrusion of CO$_2$, which is subsequently trapped by DBAD **67** to furnish *N*-centered radical **71**. A concluding SET-protonation cascade results in the formation of product **68** (Scheme 16, B).[47]
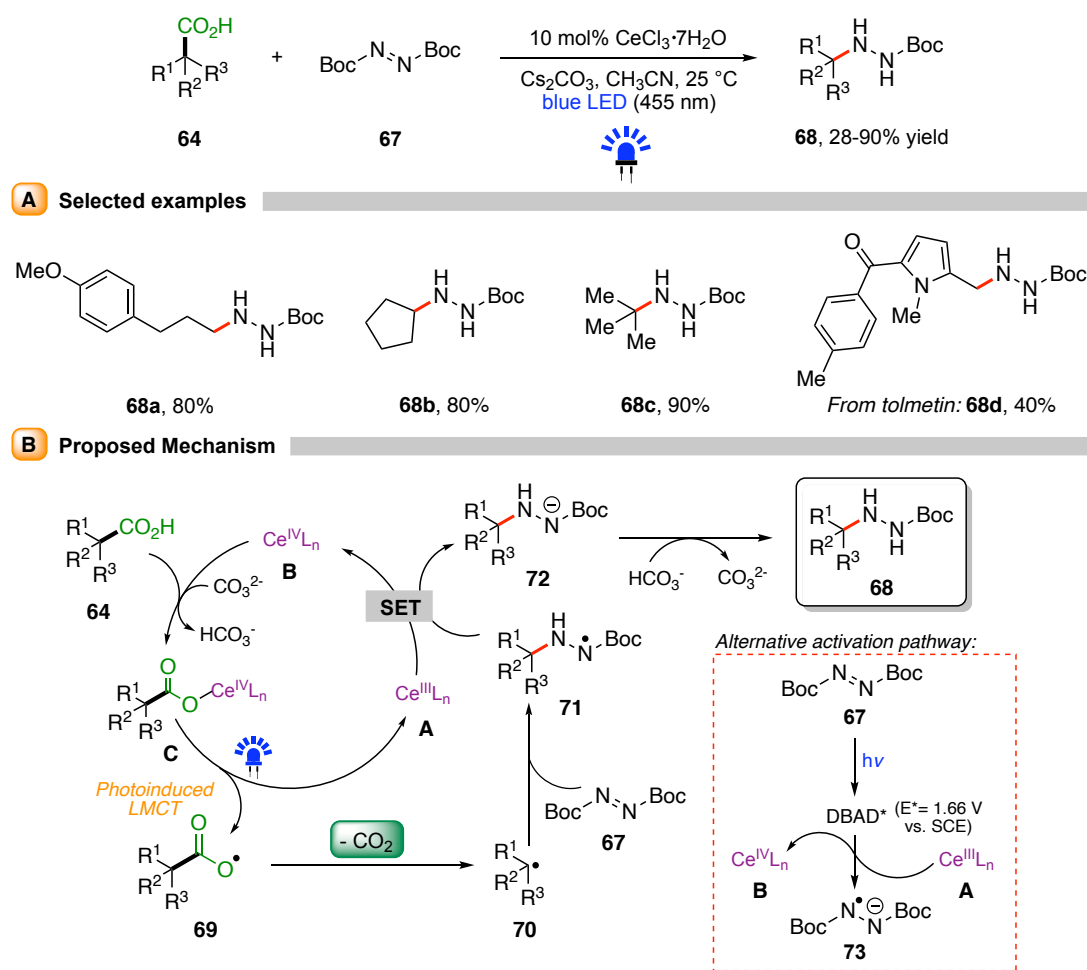
Scheme 16. Cerium-photocatalyzed, decarboxylative hydrazination of alkyl carboxylic acids.[47]

A novel photoredox-catalyzed decarboxylative methodology for the synthesis of unnatural amino acids was introduced by Schubert and co-workers in 2020.[50] Alkyl radical insertion onto dehydroalanine derivative **74** in the presence of organic photocatalyst 4CzIPN afforded a diverse set of coupling products **75**, enabling the introduction of numerous alkyl side chains for the generation of new α-alkylsubstituted amino acid derivatives (Scheme 17).
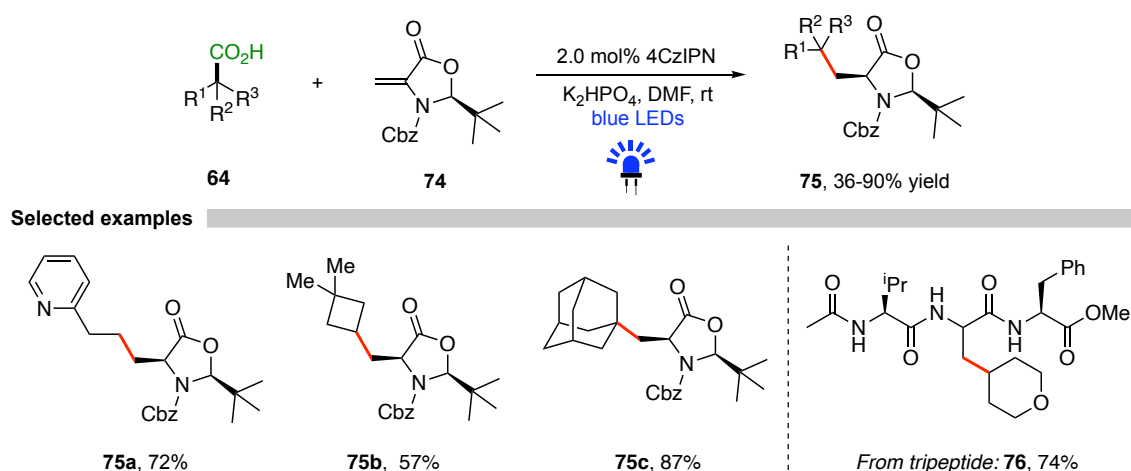
Scheme 17. Photocatalyzed derivatization of dehydroalanine.[50]

Both cyclic and acyclic primary, secondary and tertiary carboxylic acids **64** were efficient substrates for the underlying transformation, furnishing the corresponding products **75** with excellent diastereoselectivity. Additional derivatization of tripeptides afforded alkylated peptides **76**, enabling a delayed introduction of side chains and representing a valuable protocol for a late-stage enhancement of solubility and lipophilicity properties of peptides.[50,51]

Very recently, the group of Sureshkumar reported a visible-light mediated decarboxylative protocol for the efficient alkylation of vinylcyclopropanes.[52] Radical generation from carboxylic acids **64** under iridium-photocatalysis afforded after successful radical addition to a series of vinylcyclopropanes **77** the corresponding homoallylic and disubstituted adducts **78** (Scheme 18). The coupling reaction proceeded smoothly with secondary and tertiary alkyl carboxylic acids as radical precursors, delivering the desired adducts in yields ranging from 48–93% with high *E/Z* selectivity. This protocol was not limited to hydrocarbon-substituted carboxylic acids as radical precursors, numerous amino acids were also successfully employed as substrates, affording a variety of homoallylic amino acid derivatives as the corresponding products.
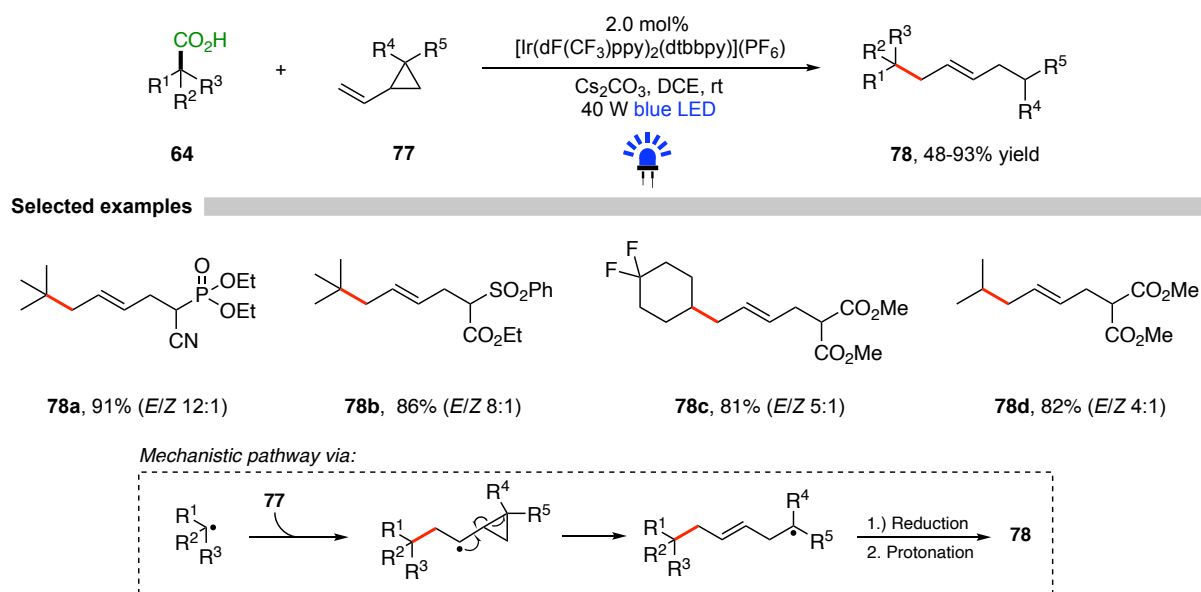
Scheme 18. Visible-light mediated decarboxylative alkylation of vinylcyclopropanes.[52]

1.5 Photoredox-catalyzed benzylation from aryl acetic acids

Benzyl radicals, obtained in the context of this overview through decarboxylation of aryl acetic acids, are a special representative of the class of carbon-centered alkyl radicals. The adjacent aryl group in α-position to the radical bearing carbon atom enables an efficient delocalization of the respective radical, resulting in resonance stabilization originating from π-interaction with the aryl group.[53] Additional hyperconjugative effects of potential other present alkyl substituents on the benzylic carbon atom make the benzyl radical a considerably stable radical reagent, exhibiting a typically higher nucleophilic character compared to typical $C(sp^3)$-centered alkyl radicals with the same degree of substitution.

In 2013, the first example of iridium-based photocatalysis was developed by the group of Nishibayashi, reporting a radical conjugate addition of benzyl radicals to electron-deficient alkenes after oxidative decarboxylation of arylacetic acids.[54] This pioneering work set the precedent of modern photoredox catalysis by utilizing $[Ir(ppy)_2(bpy)](BF_4)$ as the photocatalyst under white LED illumination, furnishing radical coupling products **81** after successful decarboxylation of aryl acetic acids **79** (Scheme 19). Efficient addition to highly electron-deficient Michael acceptors **80** was only observed for *para*-amino substituted arylacetic acids as substrates, affording aniline-substituted adducts **81** in moderate to excellent yields.
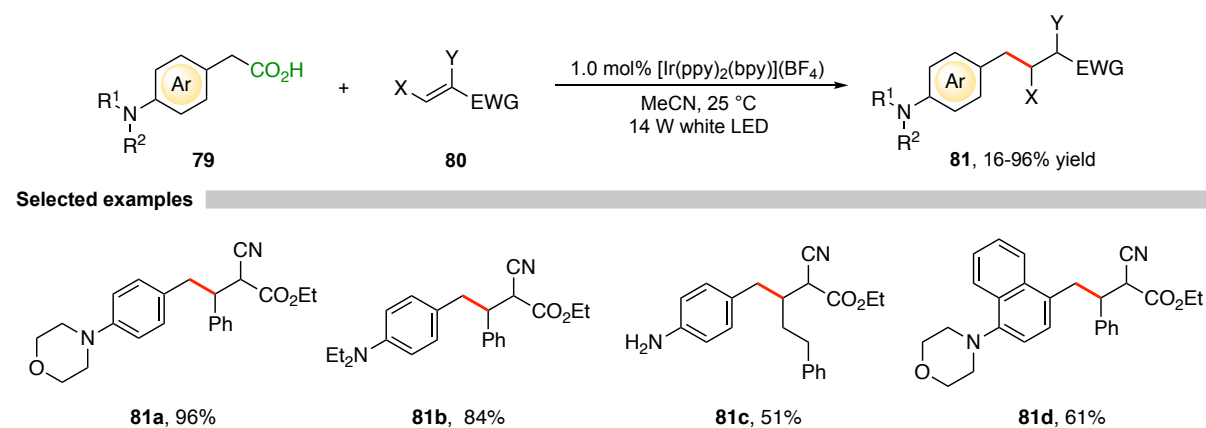
Scheme 19. Pioneering visible-light mediated decarboxylation of arylacetic acids.[54]

Three years later, Ravelli and co-workers developed a valuable extension of Nishibayashi's work, significantly broadening the scope of tolerated arylacetic acids as benzyl radical precursors.[55] Successful benzylation of highly electrophilic olefins **83** was achieved for a wide range of arylacetic acids **82**, including various activated and inactivated arylated acids and heteroaromatic analogues (Scheme 20). Tetrabutylammonium decatungstate as the photocatalyst under irradiation at 310 nm efficiently induced decarboxylation and benzyl radical formation, affording the corresponding radical addition products **84** in 37–99% yield.
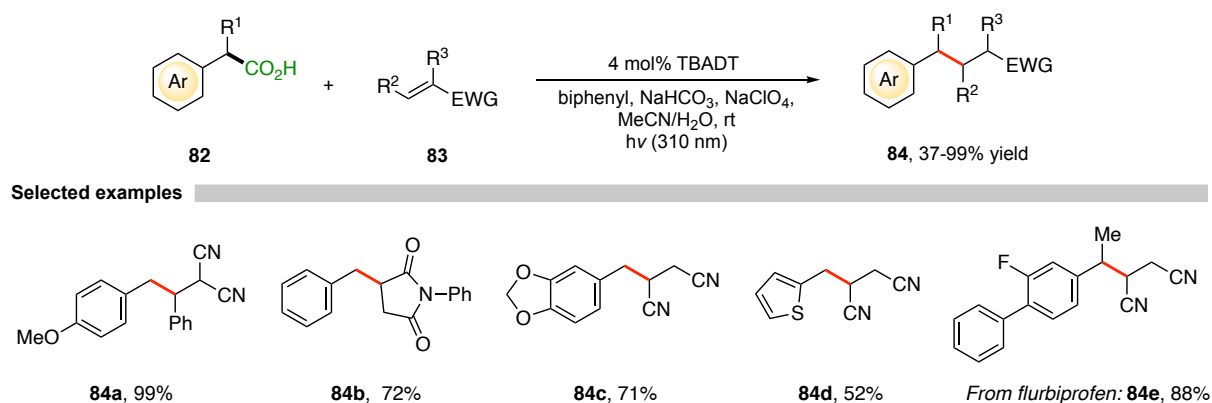
Scheme 20. Photocatalyzed benzylation of electrophilic olefins.[55]

An interesting variation of the employed radical acceptor in photoredox catalyzed decarboxylative benzylations was reported by Weng and Lu in 2018.[56] Instead of highly electron-deficient alkenes, arylated imines **85** were subjected to the photocatalytic benzylation protocol under blue-light irradiation and iridium-photocatalysis, affording a broad range of β-arylethylamines **86** in moderate to good yields (Scheme 21). The product formation step in this transformation involves a radical-coupling between a reduced imine species and the after oxidation generated benzyl radical, opposed to often occurring radical-polar crossover pathways with reductive termination during typical photocatalyzed processes.
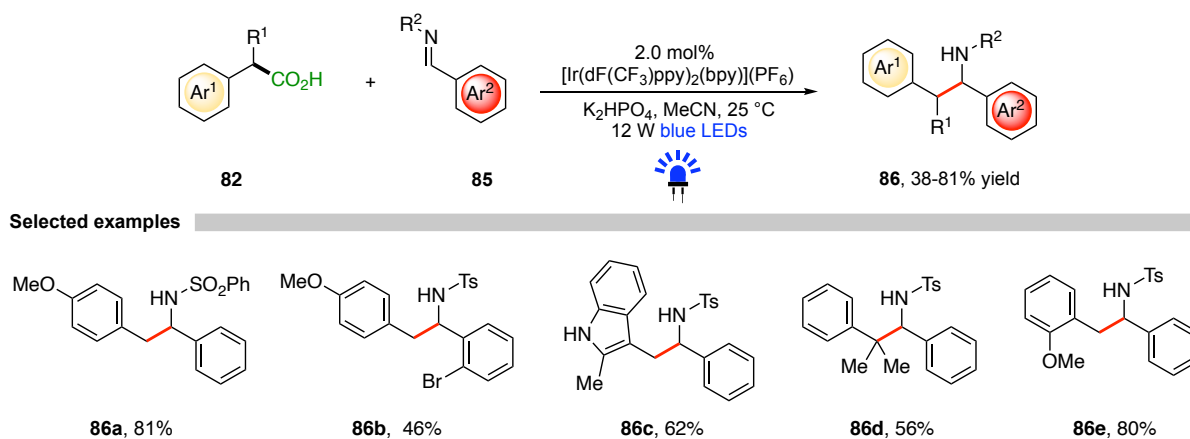
Scheme 21. Photocatalytic benzylation of arylated imines.[56]

1.6 Decarboxylative conjugate addition reactions involving α-oxy radicals

Another representative class of radicals with an adjacent heteroatom next to the radical bearing carbon is, besides the already in chapter 1.2 discussed α-amino radicals, the group of α-oxy radicals. Generated by photoredox-catalyzed decarboxylation of α-oxy carboxylic acids, α-oxy radicals are considered to be considerably nucleophilic, originating from efficient resonance donation from the free lone pair located on the oxygen atom. However, compared to its nitrogen containing counterpart, α-oxy radicals are typically less nucleophilic than α-amino radicals, being a consequence of the higher electronegativity of oxygen compared to nitrogen, thus lowering the nucleophilic character.[26]

In 2017, Xu and co-workers reported a photocatalytic decarboxylative Michael addition of glyoxalic acid acetals, serving as a formyl equivalent and thus allowing for the photochemical introduction of protected aldehydes via conjugate addition.[57] Under blue light irradiation and iridium-based catalysis, several acetals **87** were successfully converted to the corresponding addition products **89** after decarboxylative coupling to electron-deficient alkenes **88** in moderate to excellent yields (Scheme 22, A).
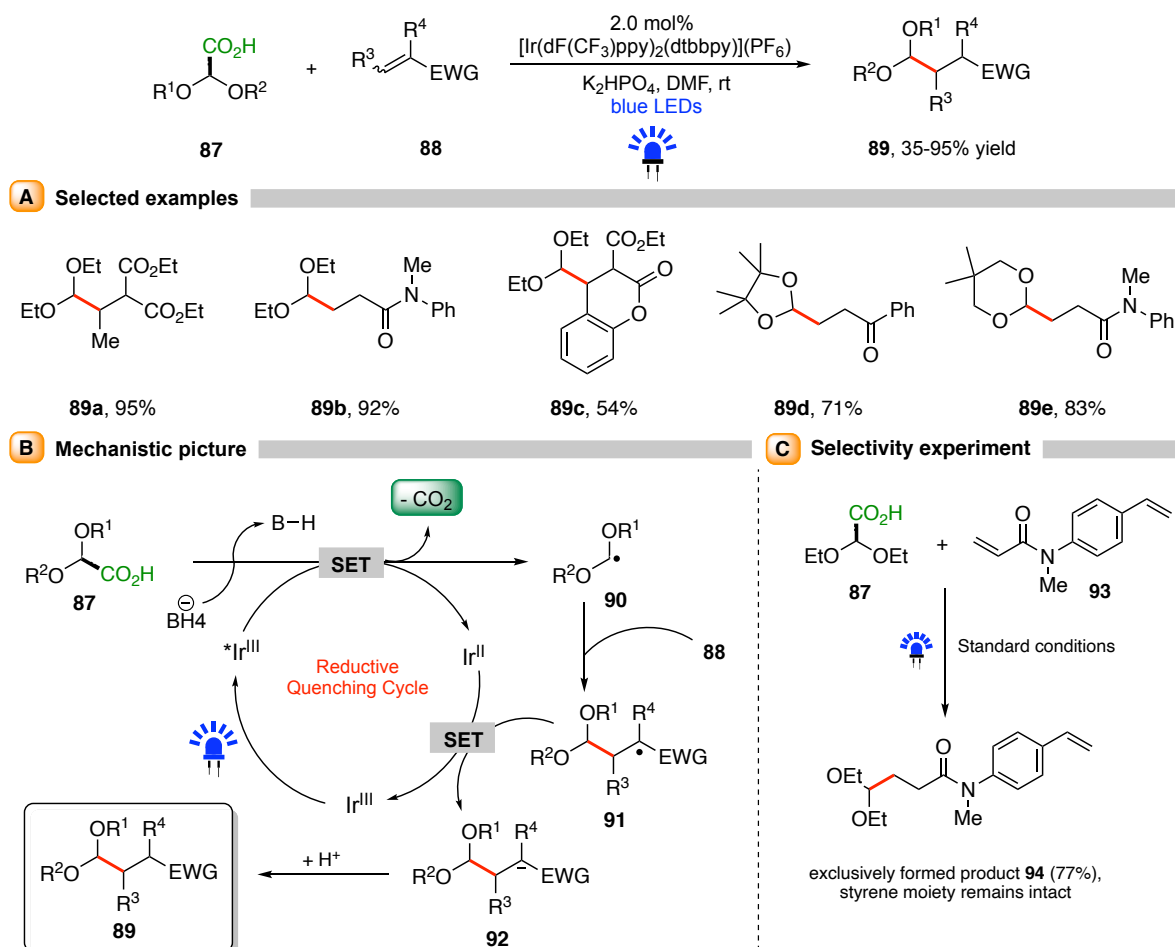
Scheme 22. Michael addition of glyoxalic acid acetals via photoredox-catalyzed decarboxylation.[57]

The proposed mechanism of this transformation involves decarboxylation of glyoxalic acid **87** to α-oxy-radical **90**, leading to the formation of radical coupling intermediate **91** after trapping with alkene **88** (Scheme 22, B). Typical reductive termination with subsequent protonation yields protected aldehyde **89**. Interestingly, intramolecular selectivity experiments of substrate **93** revealed a preferential radical attack of the electron deficient double bond present in the radical acceptor, leaving the electron-rich styrene moiety intact (Scheme 22, C).[57]

A synthetic counterpart of Xu`s method was developed in the same year by the group of Mariano and Wang, reporting an organo-photoredox-catalyzed hydroformylation of various styrenes.[58] Utilization of 4CzIPN as organic photocatalyst enabled the efficient conversion of diethoxyacetic acid (**95**) after radical coupling to activated aryl olefins **96** and subsequent acidic one-pot treatment with HCl, affording the corresponding liberated aldehydes **97** in yields ranging from 50–90% (Scheme 23). The reported reactions were performed in both batch and flow set ups, allowing efficient late-stage installation of aldehyde groups into various biologically relevant substrates containing a styrene moiety.[58]
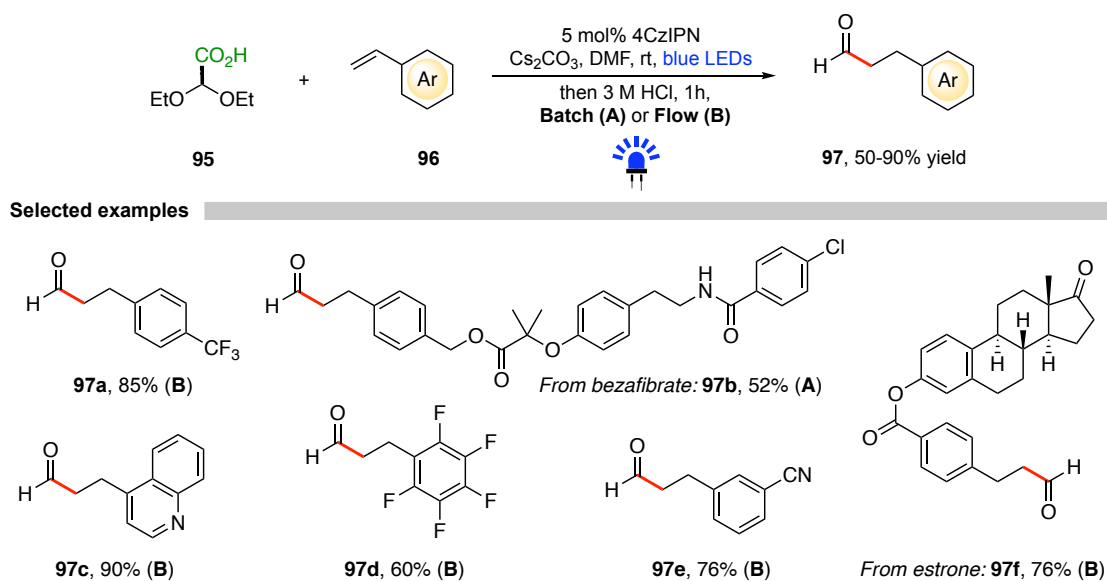
Scheme 23. Visible-light mediated hydroformylation of styrenes.[58]

An interesting variation of the employed radical acceptor was introduced by Jin and co-workers in 2018, utilizing α-aryl vinylphosphonates as activated alkenes.[59] An iridium-based photocatalyst efficiently induced the underlying transformation between α-oxy carboxylic acids **98** and arylated vinylphosphonate **99**, affording the respective ether adducts **100** in excellent yields (Scheme 24). Changing the substrate and subjecting glyoxalic acid acetals **87** to the optimized reaction conditions, the corresponding arylated acetal derivatives are formed, which are subsequently cleaved via treatment with $LiBF_4$ to γ-phosphonated aldehydes **101**.
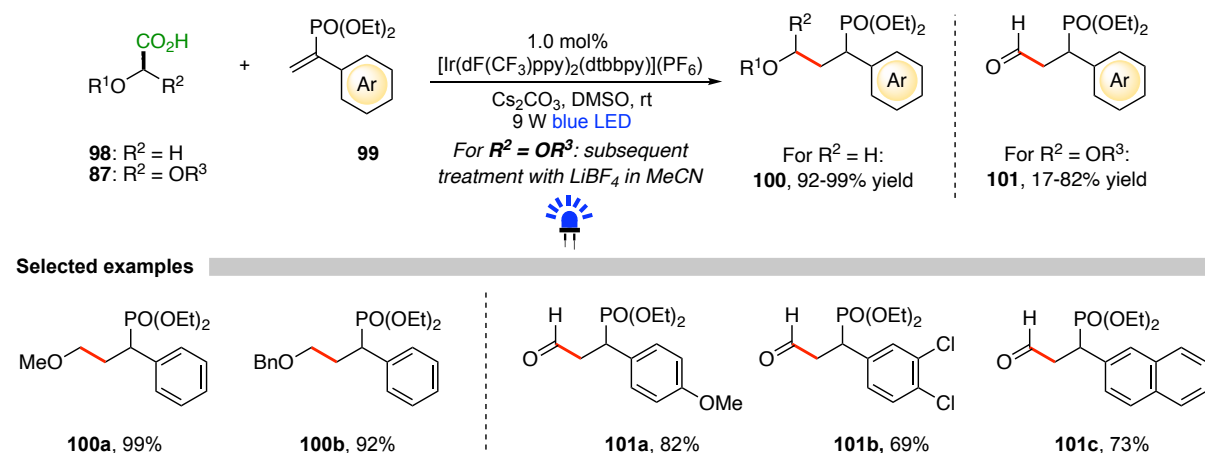
Scheme 24. Photocatalytic decarboxylative coupling involving aryl vinylphosphonates.[59]

This protocol was not limited to α-oxy carboxylic acids as radical precursors, numerous alkyl carboxylic acids were also successfully employed as substrates, affording a variety of alkylated aryl phosphonates as corresponding products.

In conclusion, the development of photoredox-catalyzed decarboxylative radical conjugate addition emerged as a powerful tool for C–C bond formations for both synthetic and medicinal chemists to construct a variety of valuable functionalities and frameworks. The flexibility of the general method allows for the generation of new structural motifs under benign conditions under high functional group tolerance, thus allowing numerous selective late-stage functionalizations, further underlying the high synthetic value of these methodologies. The utilization of carboxylic acids as radical precursors combined with the concept of visible-light mediated photocatalysis showcases the sustainable character of photocatalytic decarboxylative couplings, making it highly desirable to further research and expand this prolific strategy into new synthetic areas in both academic and industrial sectors.

2 4-Hydroxy-2-cyclopentenone as valuable, renewable resources derived substrate[a]

The desire of implementing the revolutionary principles of "Green Chemistry" in both diverse academic and industrial chemical sectors is an honorable goal and of utmost importance in order to shape the future of society towards more sustainable pathways.[5] Besides the development of sustainable catalytic strategies and the direct utilization of naturally occurring platform chemicals like carboxylic acids, the efficient conversion of renewable resources to the corresponding valuable bulk- and fine chemicals is considered as a central issue in this development.

However, especially compared to the utilization of fossil fuels as chemical feedstocks, numerous barriers arise when attempts are made to convert renewables into suitable basic chemicals due to their differing chemical nature and structure. Renewable resources derived carbohydrates, predominantly hydrophilic and high-functionalized, require, in contrast to fossil resources based hydrocarbons, basically hydrophobic and lacking of functional groups, completely opposed techniques to be efficiently converted into beneficial intermediate products.[61] Furthermore, the utilization of biomass for industrial chemical bulk conversions leads, due to the primary application of starch as starting material, inevitably to conflicts and collisions with the food production, wherefore it is special concern to harness agricultural waste arising during typical food production processes as a basis for further chemical transformations.[62]

A representative example of one of these usable, on a large-scale available waste materials is bagasse, containing cellulose, hemicellulose, lignin and xylane, a representative of the hemicellulose family which is mainly composed of xylosepolymer. Bagasse is generated as the main waste product during the conversion of sugar cane, with 125 kg of dry bagasse accumulated for every converted ton of sugar cane, making it a widely and easily available starting material for further value-generating transformations.[63,64] Treatment of hemicellulose with diluted acid induces a hydrolytic cleavage of the sugar polymers present in hemicellulose and producing monomer *D*-Xylose (**102**), which is in a second step converted to bulk chemical furfural (**103**) after subsequent acidic dehydration under high temperatures (200-250 °C, Scheme 25).[64,65]

---

[a]This chapter is partially based on a short section of the introduction part of my masterthesis: T. Krolo, *Photochemical derivatization of 4-hydroxy-2-cyclopentenone and derivatives*. Masterthesis, University of Regensburg, Regensburg, **2018**.[60]

Conversion of hemicellulose originating from waste product bagasse
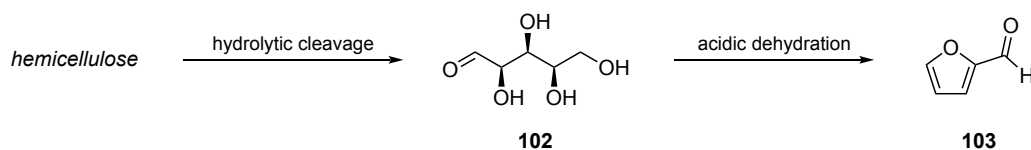
Scheme 25. Hydrolytic cleavage of hemicellulose.

Furfural (**103**) itself serves as a versatile building block for the synthesis of numerous important fine chemicals in organic synthesis, thus being often referred to as a synthetically meaningful platform chemical, making a library of derivatives directly accessible through simple conversions (Scheme 26).

Furfural as platform chemical
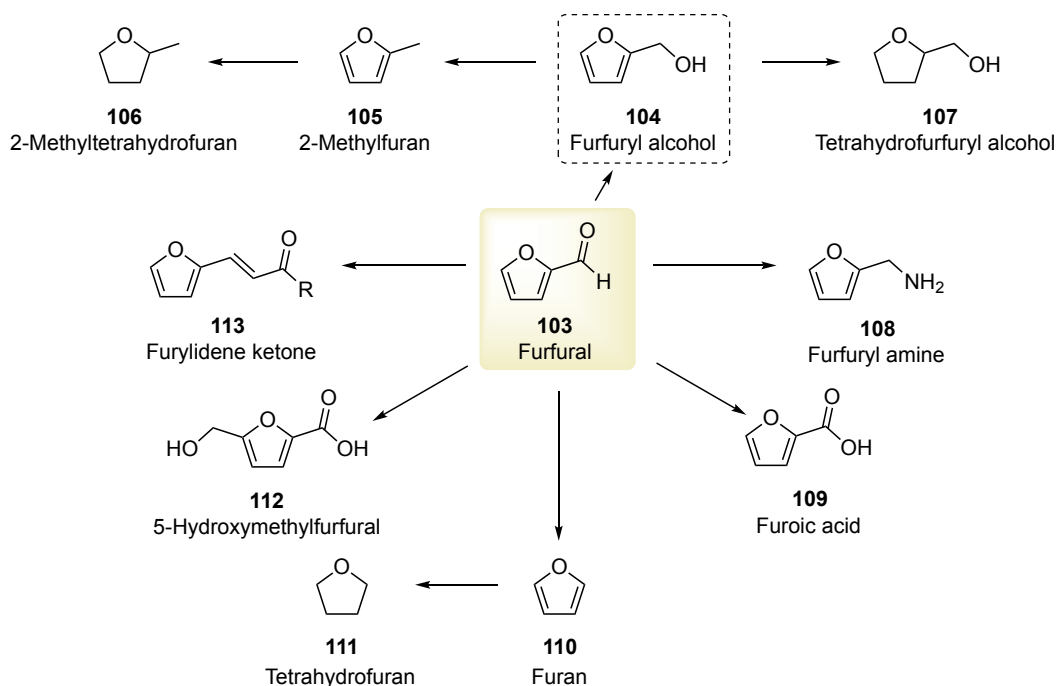
Scheme 26. Directly accessible derivatives from Furfural.[65]

Furfuryl alcohol (**104**) is directly accessible from furfural (**103**) and is industrially produced by catalytic hydrogenation of **103** in ton scale.[65] Furfuryl alcohol (**104**) has the remarkable ability to undergo exotic skeletal transformations, thus allowing the direct synthesis of 4-hydroxy-2-cyclopentenone (**116**) via the famous *Piancatelli* rearrangement, which is believed to proceed through a sequence concluding with a 4π-conrotatory electrocyclic ring closure (Scheme 27).[66]

Piancatelli **rearrangement**
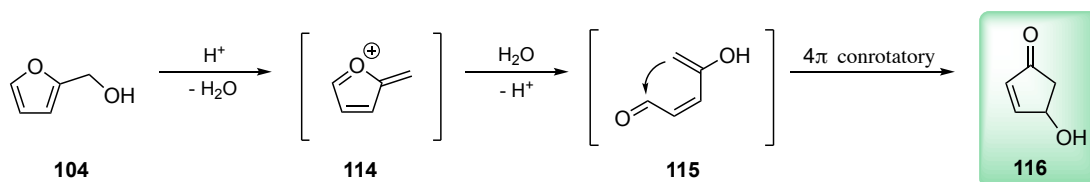
Scheme 27. Synthesis of 4-hydroxy-2-cyclopentenone via Piancatelli rearrangement.[62,66]

4-Hydroxy-2-cyclopentenone (**116**) is a versatile substrate and exhibits a high functional group density distributed over the five-membered ring, thus opening access to a variety of possible transformations, leading to specific utility as promising intermediate in the synthesis of complex structures. Furthermore, 4-hydroxy-2-cyclopentenone (**116**) was found to be a widespread core fragment in various natural products including prostanoids, indenones and alkaloids.[67]

Remarkably, Reiser and co-workers established a highly efficient protocol for the synthesis of cyclopentenone **116** via the Piancatelli rearrangement from alcohol **104** by developing a continuous flow system utilizing a microreactor set-up, thus providing access to **116** on a multi-gram scale (Figure 1).[62]
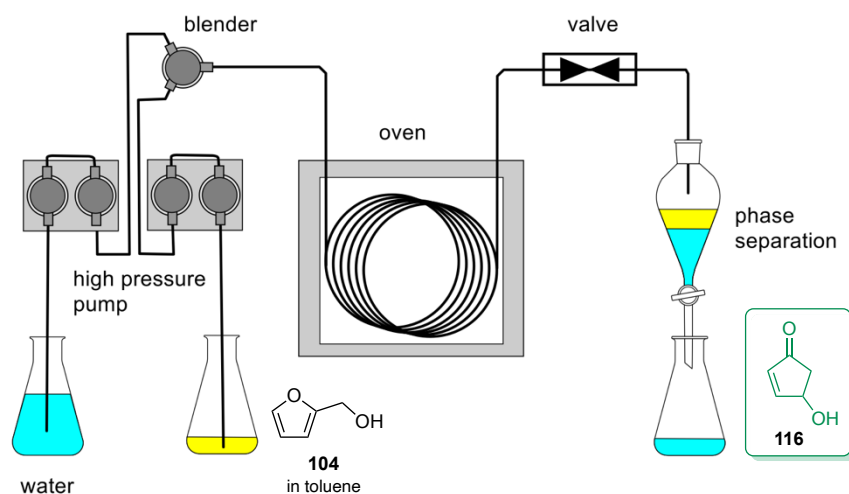
Figure 1. Continous flow set-up for a Piancatelli rearrangement.[62,68]

During this process, a solution of alcohol **104** in toluene and water (pH = 4) are injected via a high-pressure pump and subsequently mixed with a blender. A contact time of less than one minute in an oven with a temperature of 240 °C leads to the formation of two separated phases, with the aqueous phase containing the desired product **116**. Simple phase separation followed by extraction and evaporation of water gives rise to cyclopentenone **116** in 87% yield and 97% purity.[62]

Considering the synthetic availability of 4-hydroxy-2-cyclopentenone (**116**) on multi-gram scale combined with its easy accessibility from renewable, non-edible resources make it an optimal substrate for chemical reactions from the perspective of sustainability adhering to the principles of green chemistry.

3 Photochemical reactivity of 4-hydroxy-2-cyclopentenone and derivatives

The combined application of the earlier highlighted approach of photoredox-catalyzed decarboxylative radical conjugate addition together with renewable resources-derived 4-hydroxy-2-cyclopentenone (**116**) as versatile substrate create a highly desirable and sustainable environment for chemical transformations. From a photochemical point of view, the enone moiety present in **116** is of biggest interest for further visible-light induced transformations, representing a cyclic Michael acceptor functionality being frequently targeted in photocatalysis. Consequently, the first studies regarding the photochemical behavior of **116** and derivatives were performed during my masterthesis, revealing remarkable and interesting reactivity patterns (Scheme 28).[60]

Photochemical behavior of 4-hydroxy-2-cyclopentenone derivatives
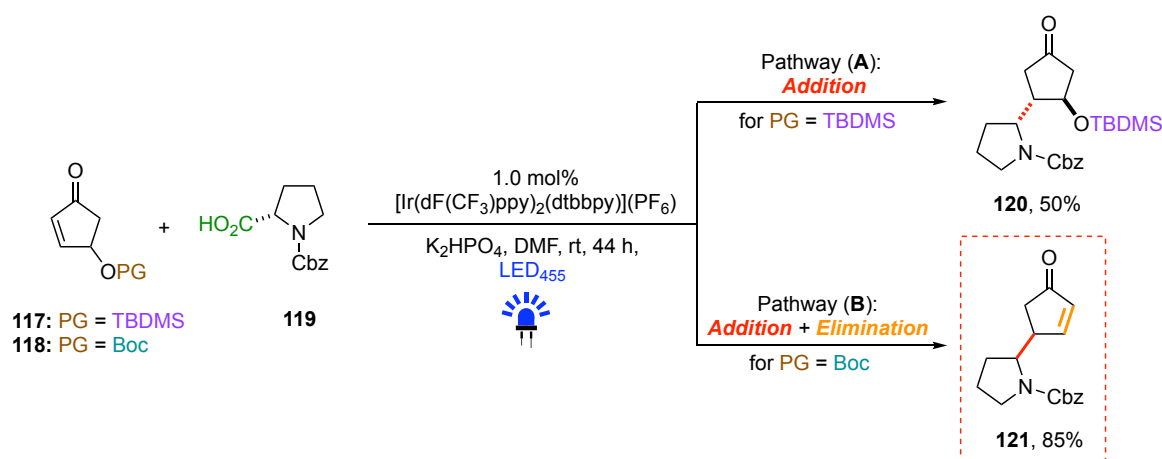
Scheme 28. Reactivity of 4-hydroxy-2-cyclopentenone derivatives under photocatalytic conditions.[60]

Inspired by the works of MacMillan and co-workers, 4-hydroxy-2-cyclopentenone (**116**) and the corresponding protected derivatives were examined as Michael acceptors under the reported photocatalytic conditions.[27] Interestingly, decarboxylative radical coupling with Cbz-Pro-OH (**119**) led to the occurrence of two different reaction pathways, depending on the employed protecting group (PG). The expected radical addition product **120** was observed when silyl-protected cyclopentenone **117** was utilized as substrate (pathway (**A**), Scheme 28), whereas the Boc-protected analogue **118** gave rise to unexpected adduct **121**, generated by radical addition of the amino acid residue followed by subsequent elimination of the Boc-protected hydroxyl functionality, thus regenerating the initial enone structure (pathway (**B**), Scheme 28). This specific reactivity pattern enables further derivatizations at the regenerated enone functionality in **121** and allows for the implementation of novel and valuable strategies targeting this variegated moiety, which will be thoroughly discussed in this present thesis.

B   Present work: Results and Discussion

1   Visible light mediated decarboxylative radical addition-elimination-oxa Michael reaction cascade as key step to valuable fused cyclic ethers[b]

1.1 Cyclopentanonyl- and cyclopentyl-fused cyclic ethers – a widespread motif in nature and drug discovery

Cyclopentanonyl-fused small-sized, 5–7-membered cyclic ethers are a privileged class of heterocyclic motifs frequently found in many natural-occurring organic compounds and drug candidates with intriguing biological properties (Scheme 29). For instance, the cyclopentanonyl-fused tetrahydrofuran (CpO-THF) framework occurs in a functionalized ergosteroid, asperflotone (**122**), which demonstrates inhibitory activity against lipopolysaccharide-activated IL-6 production in THP-1 cells (IC_{50} = 22 μM).[70] This moiety is also found in A-seco limonoid zumsin (**123**) that shows potent antifeedant activities.[71] In addition, the CpO-THF moiety serves as a synthetic intermediate in total syntheses of various natural products such as (−)platensimycin,[72] resiniferatoxin,[73] oolongtheanins,[74] and Thromboxane A_2.[75]
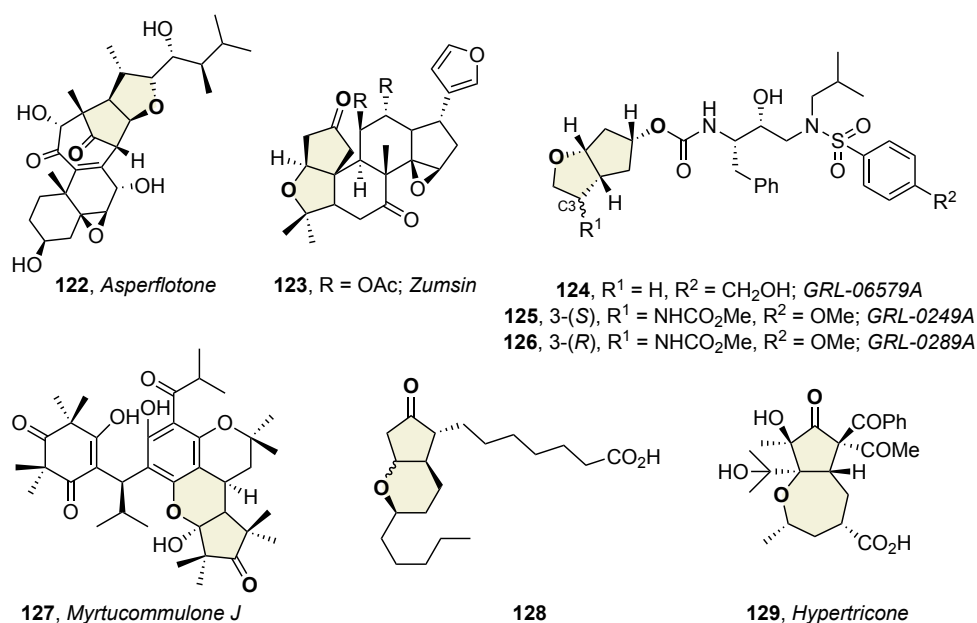
Scheme 29. Examples of cyclopentanonyl-fused cyclic ethers in natural products and drug candidates.

Its carbonyl-reduced form, i.e. the cyclopentyl-fused tetrahydrofuran (Cp-THF) moiety, is also a pharmacologically significant molecular framework which occurs in several natural prostaglandins such as PGI_2 and Beraprost.[76]

---

[b]This chapter is partially based on: T. Krolo, A. Bhattacharyya, O. Reiser, *Org. Lett.* **2021**, *23*, 6283-6287.[69]

Most notably, a series of extremely potent HIV-1 protease inhibitors **124–126** containing the Cp-THF core was designed and synthesized by Ghosh and co-workers upon realizing the complications related to the emergence of drug resistance in antiretroviral therapies and drawing inspiration from the success of Darunavir, an FDA-approved drug for HIV/AIDS patients (IC_{50} = 0.003 µM).[77] Subsequent structural analysis revealed that appropriate functionalization at the C3-position of the Cp-THF moiety could effectively enhance the potency of the drug candidates. The diastereomeric GRL-0249A (**125**, IC_{50} = 1.6 nM, K_i = 1.8 pM) and GRL-0289A (**126**, IC_{50} = 4.6 nM, K_i = 4.0 pM) bearing *N*-methyl carbamate groups at C3 were found to be among the most effective clinical candidates along with C3-unsubstituted (**124**, GRL-06579A, IC_{50} = 1.8 nM) or hydroxy-substituted (IC_{50} = 2.9 nM) derivatives.[78,79] The one- and two carbon higher homologues of CpO-THF structural frameworks also construct molecular cores of biologically active natural products such as the phloroglucinol derivative Myrtucommulone J (**127**),[80] prostaglandin by-product **128**,[81] and heartwood root and leaf-constituent hypertricone (**129**).[82]

Considering their significant biological impacts, several methods have been developed for the construction of CpO-THF molecular scaffolds over the years. The notable mention includes conjugate addition of mixed vinyl cuprate to THF-fused cyclopentenal followed by trapping with TMSCl and subsequent ozonolysis,[83] Swern oxidation of the corresponding alcoholic precursors,[84] intramolecular oxy-Michael addition to enone,[73,85] intramolecular cyclization of hydroxyimines,[86] *5-exo*-cyclization of alkyl radicals to a ketene intermediate[87] and nickel-catalyzed cyclization of alkynylenones in the presence of organozincs.[88] A few methods were also developed for its one-carbon higher homologues, including intramolecular terminal alkyne-carbene couplings or transition-metal catalyzed C-H insertion approaches.[89] However, most of the reported syntheses rely on the use of toxic reagents, suffer from relatively low yields and require often special and pre-designed substrates.

1.2 HIV-1 protease inhibitors: Medicinal relevance and synthetic approaches

The most significant and promising class of compounds containing the variegated CpO- or Cp-THF motif are HIV-1 protease inhibitors, finding great application in the treatment of *Human Immunodeficiency Virus* (HIV) infections. HIV is a member of the *Retroviridae* family and genetically related to the Lentivirus genus, whose infections typically lead to a chronic course of disease, accompanied by a long period of clinical latency and persistent viral replication.[90]

Specific isolates of HIV are clustered into two different types, namely HIV-type 1 (HIV-1), characterized by a pandemic occurrence worldwide, and HIV-type 2 (HIV-2), being restricted to regions in Western and Central Africa, with both types 1 and 2 potentially causing *Acquired Immunodeficiency Syndrome* (AIDS).[90] Since the start of the pandemic, an estimated 79 million infections were registered with HIV, leading to overall 36 million cases of death being a consequence of AIDS-related illnesses. In 2020, 1.5 million new infections with HIV occurred which were accompanied by 680 000 fatalities, with a center of these terrific statistics being numerous developing countries in Africa due to the lack of medicinal treatment originating from poor medicinal infrastructure.[91] Even if these statistics are shocking and generate a pressing need for immediate action, an HIV infection, once a fatal diagnosis, is nowadays considered a chronic but mostly manageable disease due to the emergence of antiretroviral therapy (ART).[92] This medicinal approach dramatically improved the prognosis and life expectancy of HIV patients, reducing the morbidity and mortality of AIDS by suppressing viral replication and allowing immunorestoration.[93,94]

HIV-1 Protease Inhibitors (PIs) play, besides reverse transcriptase inhibitors, a major role in these promising therapeutic methodologies. [95] A better understanding of the mode of inhibition of PIs and their respective function in suppression of viral replication can be gained by taking a deeper look into a HIV life cycle, which typically entails seven steps (Figure 2).[96]
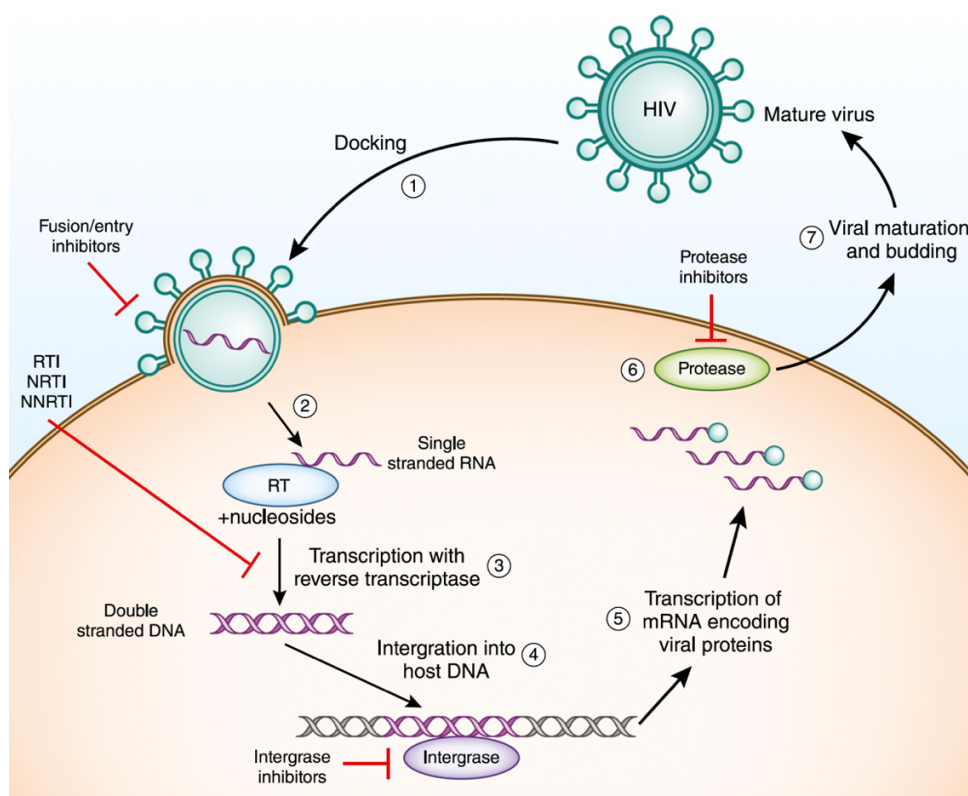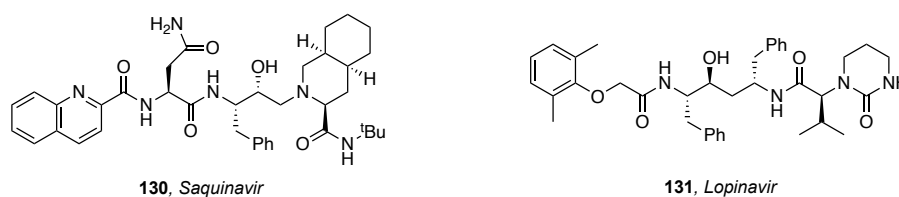

Figure 2. Typical life cycle of the *Human Immunodeficiency Virus* (HIV) Type-1 (Reprinted with permission from reference 96. Copyright © 2019, American Society of Nephrology).[96]
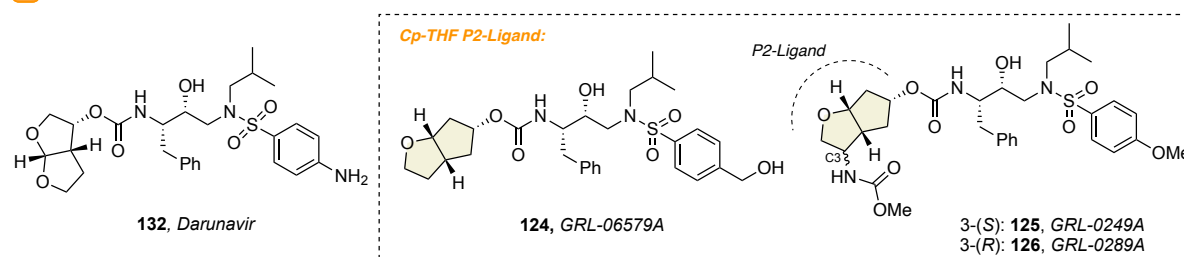
After binding and entry of virions into the host cell (step 1), the uncoating process occurs in which the virus core "uncoats" and releases viral RNA into the cytoplasm (step 2). Subsequent transcription of RNA by reverse transcriptase, a possible inhibition attacking point of reverse transcriptase inhibitors, to proviral DNA concludes step 3 and leads to the provirus integration to the host DNA through translocation to the nucleus (step 4). Afterwards, transcription of proviral DNA into mRNA occurs (step 5), thus initiating translation, the synthesis of structural proteins of new virions with post-translational cleavage by HIV protease (step 6).[90,96] During this stage of the viral life cycle, HIV protease inhibitors have the ability to interfere and stop the process of viral replication by efficient inhibition of the protease responsible for the selective cleavage of viral polyproteins into structural proteins and viral enzymes, thus preventing the production of infectious virions and leading to immature, non-infectious viral particles.[90,97,98] A closing viral mutation with "budding" of infectious particles through the host cell membrane concludes a successful viral life cycle, which is prevented by the presence of suitable HIV-1 protease inhibitors.[96]

During the last decades, numerous HIV-1 protease inhibitors with different structural properties were developed, significantly contributing to the dramatic increase of quality of life and survival of AIDS patients (Scheme 30).[97] Protease inhibitors of the first generation, approved for treatment before the year 2000, were mainly composed of peptidomimetic structure elements (Scheme 30, A), with examples being Saquinavir (**130**) and Lopinavir (**131**).[97] However, their structural rigidity limited their inhibition capability after the appearance of various mutations, leaving them unable to adapt the structural changes of mutated protease species and thus leading to the emergence of drug resistances.[98]

Scheme 30. Representative examples of HIV-1 Protease Inhibitors.[78,95,97]

These issues were accompanied by debilitating side effects, toxicity, low drug availability, the need for high therapeutic doses and expensive syntheses of peptidal inhibitors, leading to high treatment costs which is especially concerning considering that most of the HIV infections occur in developing countries with poor medicinal infrastructure.[97]

The discovery and development of second-generation, non-peptidal protease inhibitors helped to circumvent a lot of the prior mentioned drawbacks (Scheme 30, B). Improved pharmacokinetic properties and structural variability increased the drug efficiency and led to more effective therapeutic approaches, with Darunavir (**132**), FDA-approved since 2006, being the main representative of this class of inhibitors (IC$_{50}$ = 0.003 μM).[77,99] Nevertheless, effective long-term antiretroviral therapy for the treatment of AIDS patients remains a complex issue due to recurrent emergence of drug resistances wherefore it is a special concern to continuously develop new and effective PIs.[97]

A recent and promising variation of HIV-protease inhibitors are compounds containing a cyclopentanyl-fused tetrahydrofuran (Cp-THF) moiety as the respective P2-ligand, exhibiting remarkable biological activities. Representative examples of these types of inhibitors are the C3-substituted Cp-THF inhibitors **125** and **126** along with unsubstituted derivative **124**, being highly active inhibition agents due to their elevated number of backbone binding interactions with the protease active site through hydrogen bonding, possibly helping the respective inhibitors to retain their potency against various mutant strains (Scheme 30, B).[78,100] In this context, C3-substituted, diastereomeric GRL-0249A (**125**, IC$_{50}$ = 1.6 nM, K$_i$ = 1.8 pM) and GRL-0289A (**126**, IC$_{50}$ = 4.6 nM, K$_i$ = 4.0 pM) enable further backbone binding capabilities with the protease active site through the introduction of additional carbamate groups at C3, allowing for extensive hydrogen bonding due to the carbamates` hydrogen bonding donor and acceptor capabilities, resulting in impressive antiviral activity and a superb resistance profile.[78]

Typically, due to their commonality of similar structural properties, non-peptidal HIV-1 protease inhibitors are synthesized via fragment combination (Scheme 31).

Typical protease inhibitor synthesis via fragment combination

3-(*S*): **125**, GRL-0249A
3-(*R*): **126**, GRL-0289A

133
P2-Ligand

134
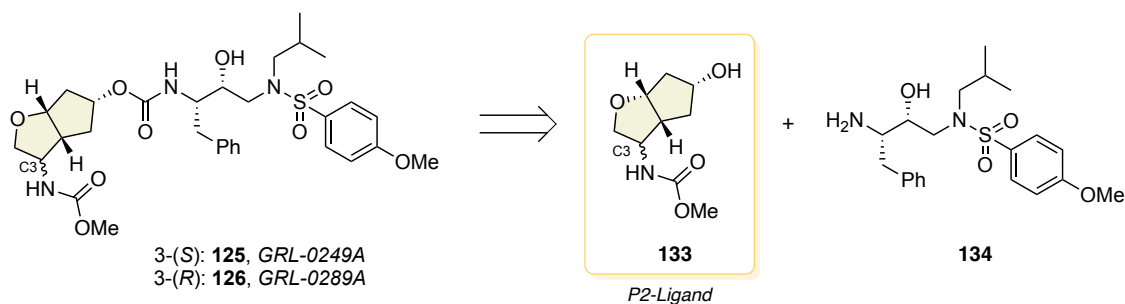
Scheme 31. Protease inhibitor synthesis via fragment combining.[78,79,101]

During this method, the bicyclic P2-ligand (bis-THF moiety for Darunavir (**132**) or Cp-THF moiety for Inhibitors **124-126**) is coupled with the respective sulfonamide-based residue **134** with varying substitution patterns on the aromatic ring after activation of the alcohol functionality.[78,79,101] An exemplary retrosynthetic visualization of a fragment combination of diastereomeric GRL-0249A (**125**) or GRL-0289A (**126**) is illustrated in Scheme 31.

While sulfonamide-derived fragment **134** can be easily obtained in a one-pot reaction starting from a commercially available epoxide,[101] the respective bicyclic Cp-THF motifs representing the P2-ligand in highly active inhibitors **124-126** is quite challenging, requiring extensive multistep synthetic routes. Two exemplary synthetic approaches by the working groups of Ghosh and Shibasaki are presented in Scheme 32.[79,102]
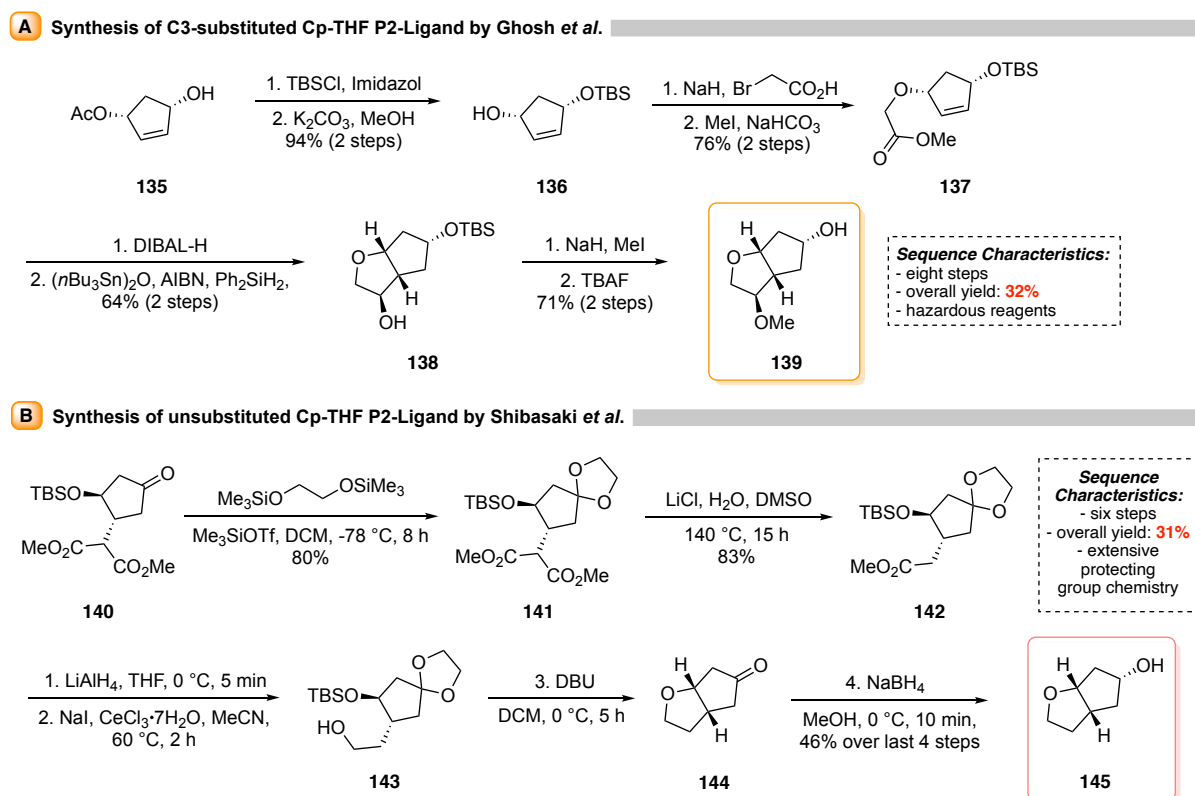
Scheme 32. Synthetic sequences to Cp-THF-based P2-Ligands.[79,102]

Both sequences require multiple steps, resulting in low overall yields of the desired bicyclic frameworks, accompanied by time- and work-intensive procedures and the use of partially hazardous and toxic substances, resulting in cost-inefficient synthetic approaches. A sustainable and efficient alternative starting preferably from renewable-resources derived and cheap substrates to provide expedient access to these valuable motifs is strongly desirable, especially considering their importance for the convenient synthesis and development of highly biological and medicinal relevant HIV-1 protease inhibitors.

1.3 Envisioned approach for the sustainable synthesis of CpO- and Cp-THF motifs

The envisioned synthetic approach towards a sustainable and efficient synthesis of valuable CpO- and, consequently, Cp-THF motifs is based on the specific photochemical behavior of Boc-protected 4-hydroxy-2-cyclopentenone **118**, which was discussed earlier in this present work under chapter 1.3 of the introduction part. The observed addition-elimination pathway regenerates the initial enone structure and should possibly allow for a rapid construction of the prolific CpO-THF motifs by utilization of suitable carboxylic acids **146** bearing a pendant hydroxyalkyl group. After the initial proposed visible-light mediated <u>D</u>ecarboxylative <u>R</u>adical <u>C</u>onjugate <u>A</u>ddition-<u>E</u>limination (*DcRCAE*), a subsequent intramolecular oxa-Michael addition of intermediate **147** can occur, thus closing the fused cyclic system and yielding the desired CpO-THF structures **148** in an highly efficient and inexpensive manner. The usage of renewable-resources derived 4-hydroxy-2-cyclopentenone derivatives along with abundant, cheap and non-toxic carboxylic acids as radical precursors catalyzed by visible-light mediated processes highlights the sustainable character of this proposed methodology to valuable structural motifs. An additional reduction of CpO-THF motif **148** would immediately give rise to the respective P2-ligands **149**, thus opening access to the synthesis of a variety of HIV-1 protease inhibitors upon a few steps of simple synthetic manipulations.
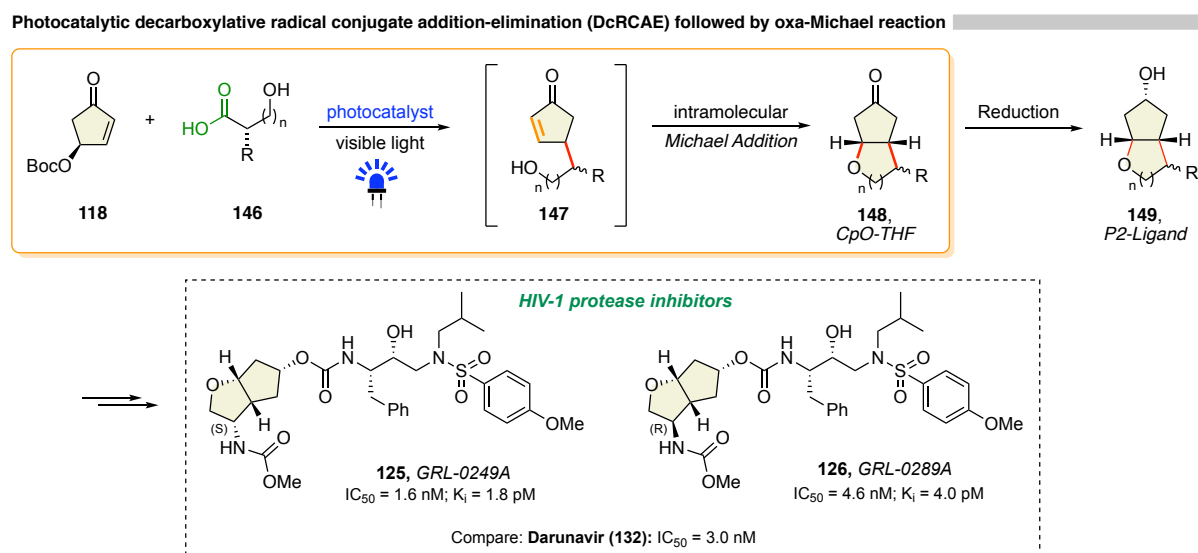
**Scheme 33.** Envisioned approach towards valuable CpO- and Cp-THF motifs.

In summary, this envisaged approach would allow to expeditiously access the highly desired CpO- and Cp-THF moieties and to streamline the synthetic blueprint to construct the stereoisomerically enriched molecular frameworks of C3-substituted Cp-THF-derived HIV-1 protease inhibitors in step-economic, time-saving, and high-yielding manner.

1.4 Development and implementation of the photocatalyzed DcRCAE-oxa Michael reaction cascade

1.4.1 Initial reaction optimization

With a view to develop a streamlined, economical and ecologically efficient synthetic process for constructing the pharmacologically significant 3-substituted tetrahydrofuran-fused cyclopentanone derivatives, the plausibility of the proposed photocatalytic decarboxylative radical conjugate addition-elimination (DcRCAE) of hydroxyalkyl-substituted carboxylic acids to cyclopentenones followed by an intramolecular oxa-Michael reaction under visible light irradiation was investigated.

Inspired by the impressive biological activity of protease inhibitors **125** and **126** bearing a 3-amino-substituted Cp-THF moiety, this study was commenced with *N*-Boc L-serine (**150**) as the employed initial model radical precursor, representing a highly desirable amino acid as starting material and allowing for the introduction of the required amino functionality into the bicyclic target structure. Following the reported photocatalytic protocol by MacMillan et al., which proved to be a suitable and efficient methodology for the conversion of the hydroxy-cyclopentenone system in our earlier studies,[60] the initial reaction of Boc-protected 4-hydroxy-2-cyclopentenone **118** with serin derivative **150** was carried out in the presence of 1 mol% of [Ir{dF(CF$_3$)ppy}$_2$(dtbbpy)]PF$_6$ (**18**; $E_{1/2}$(M*/M$^-$) = 1.21 V vs SCE)[103] and 1.2 equivalents of K$_2$HPO$_4$ in DMF (*c* = 0.5 M) while irradiating with a blue LED (λ = 455 nm) at room temperature (Scheme 34).[27]
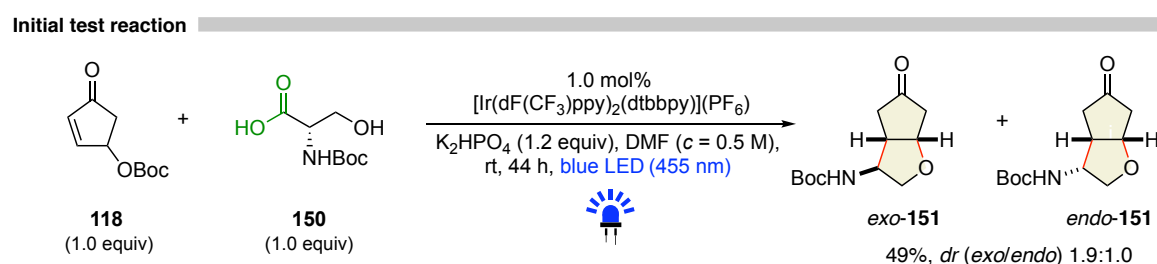
Scheme 34. Visible light-photocatalyzed decarboxylative radical conjugate addition–oxa-Michael reaction.

The validity of the proposed synthetic hypothesis was confirmed after observing the successful formation of the desired bicyclic motif **151** as a diastereomeric mixture of the *exo*- and *endo*-product in 49% yield by NMR analysis of the crude reaction mixture. Encouraged by this result, further optimization studies were subsequently conducted. However, rather than initially screening for additional photocatalysts other than the proven and employed photocatalyst **18**, the first set of exploration was dedicated to an optimization of the reaction environment including stoichiometry and concentration as an overall messy course of reaction was observed.

While a change of utilized equivalents of starting materials **118** and **150** did not result in any improvement of the yield, the reaction outcome was found to be highly dependent on the concentration of the coupling substrates present in the reaction mixture (Table 1).

Table 1. Photocatalytic DcRCAE-Oxa-Michael Reaction: Influence of substrate concentration.
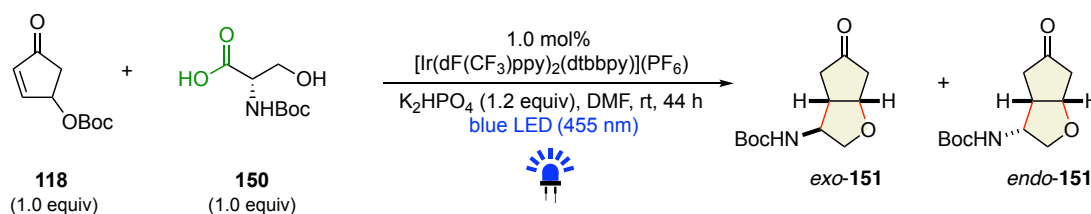
Entry	c [mol/L]	NMR yield (%)^a	dr 151 (exo:endo)
1	0.50	49%	1.9:1.0
2	0.25	**90%**	1.8:1.0
3^b	0.25	87%	1.8:1.0
4	0.10	86%	1.7:1.0

^{a}NMR yield using 1,1,2,2-tetrachloroethane as an internal standard. ^{b}Reaction time 20 h.

Interestingly, decreasing the concentration from 0.5 M to 0.25 M resulted in a dramatic enhancement in the efficiency of the transformation, affording the CpO-THF framework **151** in 90% yield with a diastereomeric ratio of 1.9:1.0 (entry 2), indicating solubility issues at concentrations higher or equal to 0.5 M. Reducing the reaction time under the present decreased concentration levels gave rise to **151** in a marginally decreased yield (entry 3), while additional dilution to a 0.1 M solution resulted in a similar effect on the reaction outcome (entry 4).

Having identified and optimized a major dependency of the transformation, it was subsequently proceeded to screen other transition-metal based photocatalysts with the aim of discovering even more efficient catalytic systems, possibly relying on more economical and ecological transition metals (Table 2).

Among the iridium-based photocatalysts screened, only initially utilized [Ir{dF(CF$_3$)ppy}$_2$(dtbbpy)]PF$_6$ (**18**; $E_{1/2}(M^*/M^-)$ = 1.21 V vs SCE)[103] induced an highly efficient transformation (90% NMR yield, entry 1), while iridium-photocatalysts with lower excited-state oxidation potentials such as [Ir(ppy)$_2$(dtbbpy)]PF$_6$ ($E_{1/2}(M^*/M^-)$ = 0.66 V vs SCE; entry 2)[104] or *fac*-[Ir(ppy}$_3$] ($E_{1/2}(M^*/M^-)$ = 0.31 V vs SCE; entry 3)[105] did not efficiently catalyze the process and the desired product **151** was either observed in very low yield or could not be obtained at all.

Table 2. Photocatalytic DcRCAE-Oxa-Michael Reaction: Testing of photocatalysts.
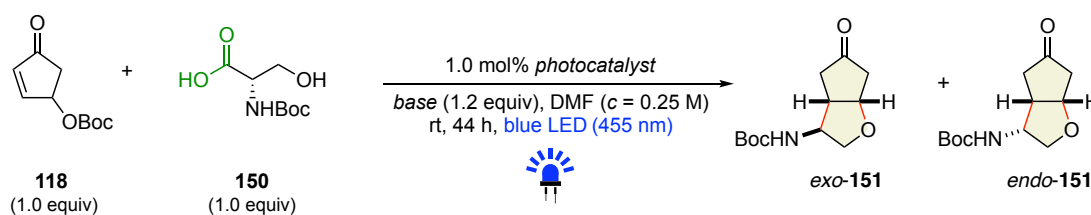
Entry	Photocatalyst	Base	NMR yield (%)[a]	dr 151 (exo:endo)
1	[Ir{dF(CF$_3$]ppy}$_2$(dtbbpy)]PF$_6$	K$_2$HPO$_4$	**90 (89[b])**	1.9:1.0
2	[Ir(ppy)$_2$(dtbbpy)]PF$_6$	K$_2$HPO$_4$	11	–
3	fac-[Ir(ppy)$_3$]	K$_2$HPO$_4$	0	–
4	[Ru(bpy)$_3$](PF$_6$)$_2$	K$_2$HPO$_4$	2	–
5	[Cu^I(dap)$_2$]Cl/[Cu^{II}(dap)]Cl$_2$	K$_2$HPO$_4$	0	–
6[c]	[Cu^I(dap)$_2$]Cl/[Cu^{II}(dap)]Cl$_2$	K$_2$HPO$_4$	0	–
7	[Fe(bpy)$_3$](NTf$_2$)$_2$	K$_2$HPO$_4$	0	–
8	none	K$_2$HPO$_4$	0	–
9	[Ir{dF(CF$_3$]ppy}$_2$(dtbbpy)]PF$_6$	none	0	–

[a]NMR yield using 1,1,2,2-tetrachloroethane as an internal standard. [b]Isolated yield. [c]The reaction mixture was irradiated with a 530 nm LED source.

When [Ru(bpy)$_3$](PF$_6$)$_2$ (E$_{1/2}$(M*/M$^-$) = 0.77 V vs SCE)[106] was used as the photocatalyst, only trace amounts were observed for the targeted compound (entry 4). Switching the catalyst's central atom to more abundant transition metals including copper and iron and thus utilizing [Cu(dap)$_2$]Cl/[Cu(dap)]Cl$_2$[107] (entry 5 and 6) or recently in the working group of Reiser designed iron-photocatalyst [Fe(bpy)$_3$](NTf$_2$)$_2$ (entry 7) did not result in any product formation. The transformation was proved to be a photoredox process as evidenced by no formation of the product in the absence of a photocatalyst (entry 8), while the indispensability of a base was recognized upon observing no reaction in its absence (entry 9).

The designed methodology was synthetically validated by isolation of the desired product **151** in 89% yield with a 1.9:1.0 diastereomeric ratio after the development of an optimized work-up and subsequent column chromatographic purification (table 2, entry 1). Column chromatographic separation of the *exo-* and *endo-*diastereomers remained a challenging task and was only partially achieved for a typical single column purification procedure, solely allowing for the isolation of a clean fraction of the major diastereomer and yielding a diastereomeric mixture in a second fraction.

Nevertheless, complete separation of both diastereomers was achieved after an extensive purification sequence consisting of six subsequent column chromatographic separations of the second fraction containing the diastereomeric mixture, stepwise concentrating the minor diasteromer by constant removal of the major.

Thorough in-depth 1-D and 2-D NMR analyses of the isolated major diastereomer supported the initial assumption that *exo*-**151** is the expected dominating stereochemical species, which was later confirmed by single crystal X-Ray analysis (Figure 3).
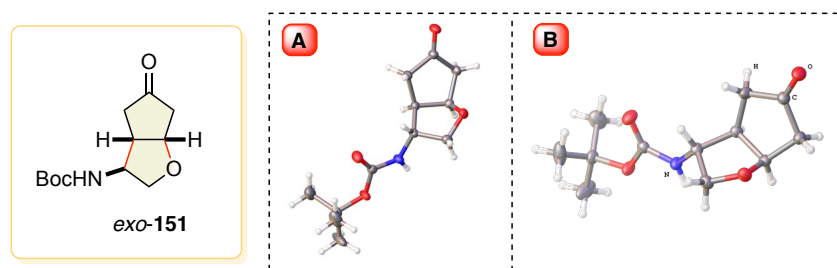
Figure 3. X-Ray crystallographic structure of *exo*-**151**.

1.4.2 Investigations regarding diastereoselectivity and exemplary synthetic manipulations

After the identification of an overall highly effective photocatalytic protocol for the synthesis of valuable CpO-THF moieties, the question arose whether the stereocontrol of the underlying transformation can be altered with the aim of achieving a higher level of diastereoselectivity. In anticipation of a temperature controlled radical addition mechanism, theoretically leading to a more selective addition orientation and thus higher stereoselectivity at lower temperatures, the temperature dependency of the diastereoselectivity was investigated (Table 3).

Table 3. Temperature dependency of diastereoselectivity.
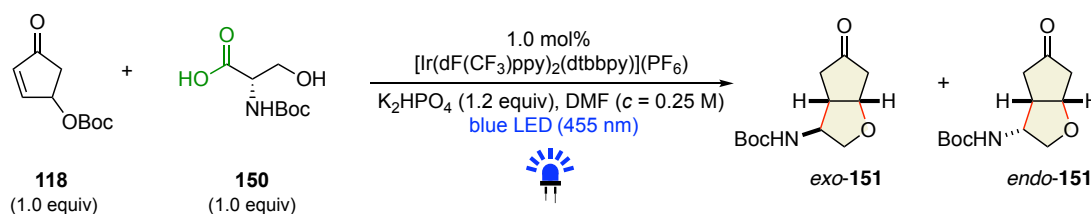
Entry	Temperature	Reaction time	NMR yield (%)[a]	dr 151 (exo:endo)
1	rt	20 h	87%	1.9:1.0
2	40 °C	6 h	82%	1.8:1.0
3[b]	0 °C	68 h	88%	1.8:1.0

[a]NMR yield using 1,1,2,2-tetrachloroethane as an internal standard.

Interestingly, the diastereomeric ratios remained basically unchanged at both elevated (40 °C) and significantly decreased temperatures (0 °C) in comparison to the standard conditions at room temperature (entry 1), thus invalidating a temperature controlled stereochemical outcome. However, a significant influence of the temperature on the underlying reaction time was observed, resulting in a full conversion of both starting materials after only six hours at 40 °C (entry 2), while lowering of the temperature dramatically decelerated the reaction progress, resulting in a tenfold increase of the reaction time compared to the temperature assisted approach (entry 3).

Next, a possible influence of the protecting group of the employed model radical precursor L-serine on the diastereochemical outcome of the photocatazed DcRCAE-oxa Michael reaction was investigated, testing for various L-serine derivatives as coupling partners (Scheme 35).
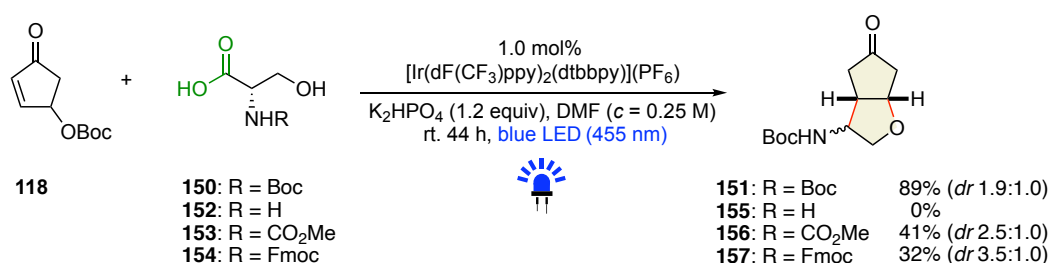
Scheme 35. Visible light-photocatalyzed decarboxylative radical conjugate addition–oxa-Michael reaction.

Remarkably, when carbamate-protected L-serine (**153**) was employed as substrate, a moderately improved diastereoselectivity was observed for the corresponding addition product **156**, already bearing the exact desired *N*-methyl carbamate group in C3-position for the envisioned synthesis of potent HIV-1 protease inhibitors **125** and **126**. However, the increase in diastereomeric ratio compared to the model reaction with Boc-protected L-serine **150** from 1.9:1.0 to 2.5:1.0 was counterbalanced by the significant reduction in yield, dropping from 89% to 41%. Similar results were obtained when Fmoc-protected serine **154** was subjected to the present reaction conditions, affording the bicyclic motif **157** in a diastereomeric ratio of 3.5:1.0, but in merely 32% yield. For both carbamate- and Fmoc protected products **156** and **157**, the diastereomeric mixtures remained completely inseparable. The necessity of a protecting group on the employed radical precursor was substantiated by observing no product formation when unprotected L-serine (**152**) was utilized as the coupling partner.

The significant reduction of yield when employing serine derivatives other than Boc-protected serine **150** as radical precursor generates the need for an alternative strategy to efficiently derivatize the amino functionality in the C3-position of the CpO-THF motif, especially bearing a later synthesis of various 3-aminosubstituted protease inhibitors in mind.

The formation of Boc-protected bicycle **151** in high yields along with the possibility of a complete separation of both diastereomers, although challenging, make it a desirable starting point for further synthetic manipulations, particularly considering the typically easy removal of a Boc-protecting group. Rather than changing the protection on the employed serine substrates, an efficient deprotection/reprotection methodology of Boc-protected Michael adduct **151** would be desirable for the introduction of various residues onto the amino-functionality. For this purpose, various deprotection techniques of the Boc-protecting group present in **151** were examined (Table 4).

Table 4. Screening of Boc-deprotection conditions.
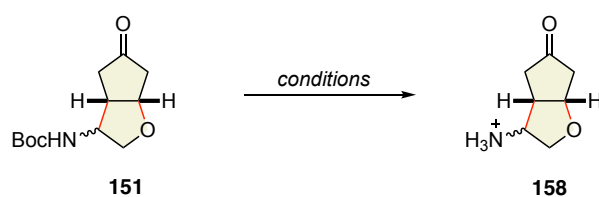
Entry	Conditions	Observation
1	TFA (5.0 equiv), DCM, rt, 20 h	partial conversion
2	TFA (25.0 equiv), DCM, rt, 20 h	partial conversion
3	HCl (aq., 25%), rt, 30 min	full conversion
4	HCl (aq., 25%), reflux, 30 min	complex mixture
5	HCl (1 M) in EA, rt, 20 h	partial conversion

The cleavage of a Boc-protecting group requires an acidic medium and is typically performed with an excess of TFA as the deprotecting agent.[108] Consequently, initial experiments involved the usage of TFA in excess amounts of 5.0 equivalents (entry 1) and 25.0 equivalents (entry 2), respectively, with both approaches resulting only in a partial conversion and deprotection of the starting material **151** after 20 h. Changing the strategy by employing an aqueous solution of HCl as the deprotecting medium improved the outcome of the reaction and led to a full deprotection after 30 min at room temperature to give rise to liberated amine **158** (entry 3), while heating under reflux resulted in a complex mixture of products (entry 4). Switching to a 1 M-solution of HCl in ethyl acetate (EA), which would enable an easier workup of the reaction mixture compared to an aqueous reaction environment, did not efficiently induce the desired protection.

After identification of the suitable deprotection technique, it was subsequently proceeded to refunctionalize the liberated amine salt. An overview of the obtained, amino-refunctionalized products is illustrated in Scheme 36.
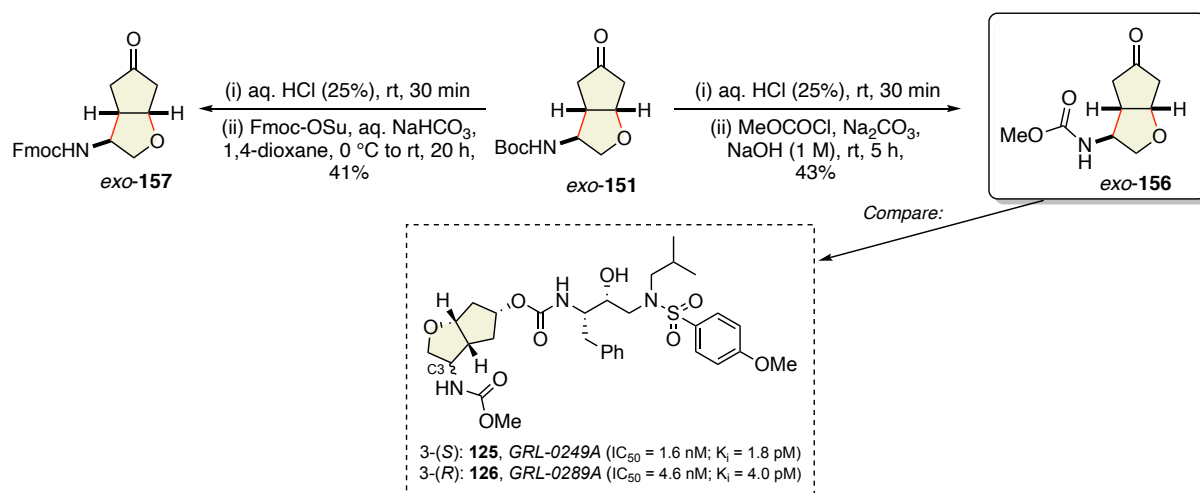
Scheme 36. Various refunctionalization approaches after Boc-deprotection.

N-Boc-protected Cp-THF derivative *exo*-**151** was converted to the corresponding *N*-methyl carbamate *exo*-**156** upon deprotection under acidic conditions followed by reprotection of the free amine group with methyl chloroformate in 43% yield over two steps, already generating the desired C3-substitution pattern for the synthesis of potent HIV-1 protease inhibitors **125** and **126**.[109] Optimized reprotection approaches involving Fmoc-succinimid ester as introducing agent led to the formation of the corresponding Fmoc-protected motif *exo*-**157** in 41% yield.[110,111]

Although a few synthetic manipulations of the amino-functionality in C3-position of the CpO-THF framework were successfully developed, a further optimization of the obtained yields for the corresponding deprotection/reprotection (31–43%) protocol is highly desirable, especially considering the aim of a highly efficient sequence towards potent HIV-1 protease inhibitors **125** and **126**, which will be discussed at a later point in this present thesis.

1.4.3 Further optimization of reaction conditions and improvement of sustainable character of the developed methodology

Although a highly efficient protocol for the visible-light mediated decarboxylative radical conjugate addition-elimination-oxa-Michael reaction cascade was already developed and introduced, at this stage of the study the desire for an even higher sustainable character of the present transformation became apparent. A main goal in this context was the examination of organic photocatalysts, recently emerging as a viable alternative to commonly employed

transition metal based photocatalysts and offering significant advantages compared to their typically employed iridium- and ruthenium derived counterparts including lower synthetic costs and reduced environmental impacts.[112]

With this principle in mind, a broad set of various organophotocatalysts was explored in order to identify a suitable and prolific substitution for the earlier utilized, highly efficient [Ir{dF(CF$_3$)ppy}$_2$(dtbbpy)]PF$_6$ (**18**) and to provide a metal-free approach towards valuable CpO-THF motifs (Table 5).

Table 5. Photocatalytic DcRCAE-Oxa-Michael reaction: Screening of organic photocatalysts.
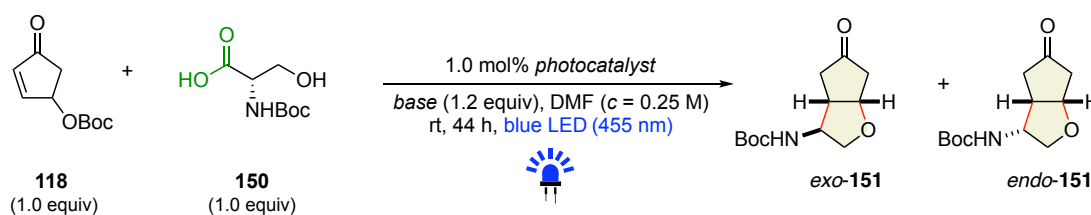
Entry	Photocatalyst	Base	NMR yield (%)^a	dr 151 (exo:endo)
1	[Ir{dF(CF$_3$]ppy}$_2$(dtbbpy)]PF$_6$	K$_2$HPO$_4$	90	1.9:1.0
2	[MesAcr]ClO$_4$	K$_2$HPO$_4$	14	-
3	TPT	K$_2$HPO$_4$	0	-
4	Eosin Y	K$_2$HPO$_4$	0	-
5^b	Eosin Y	K$_2$HPO$_4$	0	-
6^b	Rose Bengal	K$_2$HPO$_4$	2	-
7	DCA	K$_2$HPO$_4$	8	-
8^b	Rhodamine 6G	K$_2$HPO$_4$	59	1.8:1.0
9^b	Rhodamine B	K$_2$HPO$_4$	0	-
10	4CzIPN	K$_2$HPO$_4$	**92**	1.9:1.0

^{a}NMR yield using 1,1,2,2-tetrachloroethane as an internal standard. ^{b}The reaction mixture was irradiated with a 530 nm LED source.

For reference purposes, the initial optimized conditions with iridium-photocatalyst **18** are listed in entry 1, which gave rise to Michael adduct **151** in 90% NMR yield with a diastereomeric ratio of 1.9:1.0 starting from Boc-protected cyclopentenone **118** and *N*-Boc L-serine (**150**).

The study of organic photocatalysts for the photocatalytic DcRCAE-oxa-Michael addition sequence commenced with the test of Fukuzumi's catalyst ([MesAcr]ClO$_4$, E$_{1/2}$(PC*/PC$^-$) = 2.08 V vs SCE),[113] resulting in the formation of the desired product in 14% yield by NMR

analysis of the crude reaction mixture after 44 h (entry 2). Encouraged by this result, it was subsequently proceeded to screen other organic photocatalysts for the underlying transformation.

Utilizing photocatalysts with higher excited-state oxidation potential such as 2,4,6-triphenylpyrylium-BF$_4$ (TPT, $E_{1/2}$(PC*/PC$^-$) = 2.55 V vs SCE; entry 3)[114] and with much lower excited-state oxidation potentials such as Eosin Y (EY-Na$_2$, $E_{1/2}$(M$^+$/M*) = 0.83 V vs SCE; entries 4 and 5)[115] or Rose Bengal (RB, $E_{1/2}$(PC*/PC$^-$) = 0.81 V vs SCE; entry 6)[115] did not efficiently induce the transformation under both blue or green light irradiation and the desired product could not be obtained at all or formed only in trace amount. When 9,10-dicyanoanthracene (DCA, $E_{1/2}$(PC*/PC$^-$) = 1.99 V vs SCE) was employed as the photocatalyst, only 8% NMR yield was observed for the targeted compound (entry 7).[114]

A significant formation of target compound **151** was noticed when Rhodamine 6G (Rh6G, $E_{1/2}$(PC*/PC$^-$) = 1.18 V vs SCE)[116] was used in the reaction under green light irradiation, resulting in a yield of 59% with a 1.8:1.0 diastereomeric ratio (entry 8). However, Rhodamine B (RhB, $E_{1/2}$(PC*/PC$^-$) = 1.26 V vs SCE)[115] failed to furnish any desired product under the same irradiation source (entry 9). Remarkably, dramatic enhancement in the efficiency of the transformation was observed when 1,2,3,5-tetrakis(carbazole-9-yl)-4,6-dicyanobenzene (4CzIPN (**36**), $E_{1/2}$(PC*/PC$^-$) = 1.35 V vs SCE)[117] was employed as the photocatalyst under blue light irradiation, giving rise to desired product **151** in 92% yield with a diastereomeric ratio of 1.9:1.0 (entry 10), thus even outperforming the present iridium-based benchmark catalyst **18**. This surprising result concluded the search for a more ecological photocatalytic alternative, opening the pathway for an overall highly sustainable approach towards valuable bicyclic motifs considering the employed organo-photocatalyzed process and both utilized, renewable resources derived coupling partners.

With these exciting findings and a new organic photocatalyst in hands, it was subsequently proceeded to perform additional control experiments to possibly further optimize the underlying protocol by examination of various parameters (Table 6).

A change of the blue light-source to a green LED with a λ_{max} of 530 nm did not induce any product formation (entry 2). However, when a near-UV light-source was used (λ_{max} = 403 nm), the desired product was obtained in 78% yield with a diastereomeric ratio of 1.9:1.0 (entry 3). Having identified the optimal combination of photocatalyst and light source, it was next ventured into exploring the scope of the inorganic base used in the reaction. Replacing the employed base K$_2$HPO$_4$ with either Cs$_2$CO$_3$ (entry 4) or K$_2$CO$_3$ (entry 5) resulted in significant drops in both yield and diastereoselectivity of the transformation (45%, *dr* 1.1:1.0 and 36%, *dr*

1.0:1.0, respectively). Likewise, the use of K_3PO_4 also deteriorated the yield (57%, *dr* 1.1:1.0, entry 6).

Table 6. Organo-photocatalyzed DcRCAE-Oxa-Michael Reaction: Optimization and control experiments.
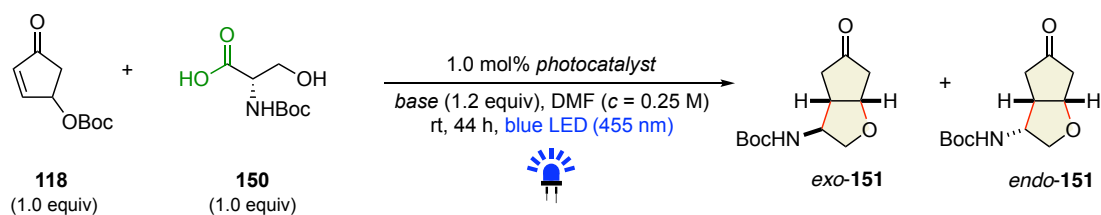
Entry	Photocatalyst	Base	NMR yield (%)[a]	*dr* 3a (*exo:endo*)
1	4CzIPN	K_2HPO_4	92	1.9:1.0
2[b]	4CzIPN	K_2HPO_4	0	-
3[c]	4CzIPN	K_2HPO_4	78	1.9:1.0
4	4CzIPN	Cs_2CO_3	45	1.1:1.0
5	4CzIPN	K_2CO_3	36	1.1:1.0
6	4CzIPN	K_3PO_4	57	1.0:1.0
7	4CzIPN	KF	85	2.0:1.0
8	4CzIPN	none	0	-
9	none	K_2HPO_4	0	-
10[d]	4CzIPN	K_2HPO_4	0	-
11[e]	4CzIPN	K_2HPO_4	82	2.0:1.0
12[f]	4CzIPN	K_2HPO_4	**95 (92[g])**	2.0:1.0
13[h]	4CzIPN	K_2HPO_4	91	1.8:1.0
14[i]	4CzIPN	K_2HPO_4	58	2.0:1.0
15[j]	4CzIPN	K_2HPO_4	88	2.1:1.0

[a]NMR yield using 1,1,2,2-tetrachloroethane as an internal standard. [b]The reaction mixture was irradiated with a 530 nm LED source. [c]The reaction mixture was irradiated with a 403 nm LED source. [d]The reaction was performed in the absence of light. [e]The reaction was performed under air. [f]Reaction time 68 h. [g]Isolated yield. [h]Concentration 0.1 M (0.5 mmol scale, 5 mL of DMF). [i]Concentration 0.5 M (1.0 mmol scale, 2 mL of DMF). [j]Catalyst loading 2.0 mol%, reaction time 20 h.

When KF was used as the base, the desired products were obtained in 85% yield with a 2.0:1.0 diastereomeric ratio (entry 7). The indispensability of a base was recognized upon observing no reaction in its absence (entry 8). Therefore, K_2HPO_4 was selected as the base of choice (see entry 1).
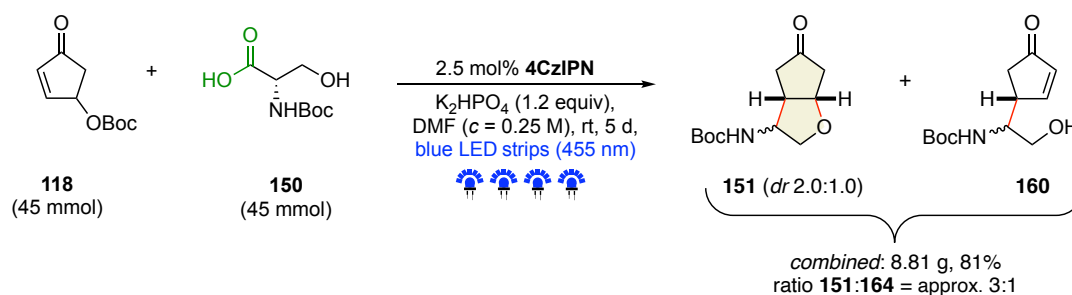
Once more, the transformation was proved to be a photoredox process as evidenced by no formation of the product in the absence of a photocatalyst (entry 9) or the absence of light irradiation with a present photocatalyst (entry 10). When the same reaction was performed with 4CzIPN under air instead of an inert nitrogen atmosphere, the desired product was obtained in 82% yield with a diastereomeric ratio of 2.0:1.0 (entry 11).

Increasing the reaction time from 44 h (entry 1) to 68 h led to a marginally elevated yield of 95% (entry 12). While changing the substrate concentration to 0.1 M in DMF resulted in 91% product formation and a marginal decrease in the diastereoselectivity (entry 13), concentrating the reaction mixture had an adverse effect on the efficiency of the transformation and the product was obtained in only 58% yield with 2.0:1.0, supporting aforementioned findings (entry 14). Lastly, the effect of an increase in catalyst-loading of 4CzIPN was studied and a diastereomeric mixture of *exo*-**151** and *endo*-**151** in a 2.1:1.0 ratio was obtained in 88% yield after 20 h (entry 15). Having analyzed the best NMR yield under the conditions described, the reaction was synthetically validated by isolation of the desired 3-amino-CpO-THF-derivatives *exo*-**151** and *endo*-**151** in 92% yield with 2.0:1.0 diastereomeric ratio after column chromatographic purification (entry 12). With these optimized, highly efficient and overly sustainable conditions in hands, it was afterwards proceeded to exemplify the synthetic strategy in the next phases of the titular study.

1.5 Upscaling approach: Multigram-scale synthesis of the CpO-THF framework

In order to show the practicality of the developed synthetic methodology and with a view to synthesize the requisite synthetic precursor for the pharmacologically significant drug candidates **125** and **126** in large quantity for a multistep synthetic route, the benchmark reaction between Boc-protected cyclopentenone **118** and *N*-Boc L-serine (**150**) was performed in multigram-scale (Scheme 37).

118
(45 mmol)

150
(45 mmol)

2.5 mol% **4CzIPN**
K$_2$HPO$_4$ (1.2 equiv),
DMF (*c* = 0.25 M), rt, 5 d,
blue LED strips (455 nm)

151 (*dr* 2.0:1.0)   **160**

combined: 8.81 g, 81%
ratio **151**:**164** = approx. 3:1

Scheme 37. Multigram-scale experiment for the photocatalytic DcRCAE-oxa-Michael reaction.

Accordingly, an equimolar mixture of **118** and **150** was reacted in a 45 mmol scale in the presence of a slightly higher loading of the photocatalyst (2.5 mol % 4CzIPN) under the optimized reaction conditions in a specially-designed large-scale photocatalytic reaction set-up with blue LED strips as the irradiation source (Figure 4).
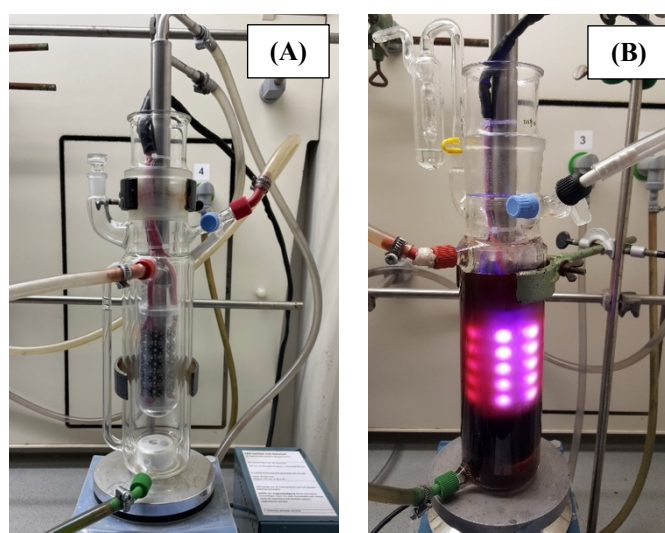

Figure 4. Reaction upscaling: (**A**) Big-Scale irradiation setup (200 mL) with 30 OSLON SSL 80 deep blue LEDs (each: 1 W, 700 mA, λ_{max} = 455 nm) for 45 mmol scale. (**B**) Big-scale irradiation setup (200 mL) after irradiating the reaction mixture for 5 d.

After a prolonged reaction time in the big-scale photoapparatus for five days, most likely being a consequence of a more inefficient light penetration through the dark solution due to a comparably thicker solution layer surrounding the centrally located LED strips,

the formation of target compound **151** was observed along with an unexpected uncyclized derivative **160** in a combined yield of 81%, referring to 8.81 g of product (Scheme 37). While the decarboxylative radical conjugate addition still proceeded in an efficient manner, the subsequent oxa-Michael addition proceeded significantly slower in the upscaled set-up, resulting in an inseparable mixture of the desired bicycle **151** and uncyclized cylopentenone **160** in a ratio of approximately 3:1.

Consequently, with the aim of a full conversion of the uncyclized intermediate to the bicyclic target structure, several cyclization approaches assisting the undergoing oxa-Michael addition were investigated (Table 7).

Table 7. Cyclization studies towards desired bicyclic motif **151**.

starting ratio **151**:**164** = 1.0:2.0
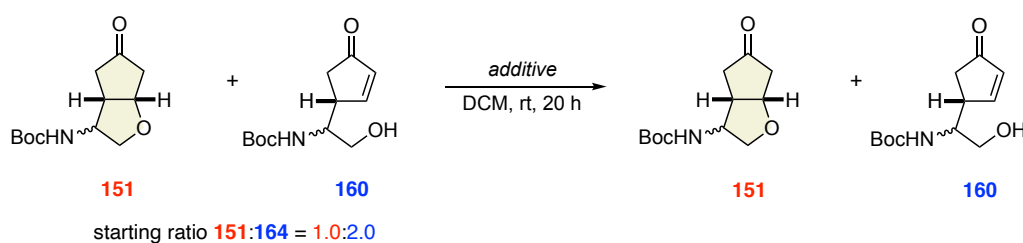
Entry	Additive [equiv]	Ratio 151:160
1	-	1.3:1.0
2	DMAP [0.2]	4.2:1.0
3	KF/Al$_2$O$_3$ [1.2]	quant. (>20.0:1.0)
4	Sc(OTf)$_3$ [1.2]	7.0:1.0
5	BF$_3$OEt$_2$ [1.2]	3.1:1.0

Starting with a mixture of CpO-THF framework **151** with an excess of uncyclized product **164** in a ratio of 1:2, only stirring the mixture in DCM without the addition of any external reagents for 20 hours led to a significant decrease in uncyclized intermediate **164**, giving rise to the respective product mixture with an excess of cyclized motif **151** in a ratio of 1.3:1.0 (entry 1). To further assist the spontaneously favored oxa-Michael reaction, numerous Lewis acids and base catalysts were further investigated. Among the additives tested, including potent Lewis acids Sc(OTf)$_3$ (entry 4) and BF$_3$OEt$_2$ (entry 5) or activating agent DMAP (entry 2), an equimolar combination of KF and Al$_2$O$_3$ in a slight excess of 1.2 equivalents was found to induce the desired cyclization in a highly efficient manner, affording the cyclized product **151** in quantitative amounts (entry 3).[118]

Implementation of the developed cyclization protocol into the aforementioned big-scale synthetic approach led to the exclusive formation of CpO-THF moiety **151** after a subsequent treatment of the corresponding mixture of both partially cyclized and uncyclized (**160**) cyclopentenone derivatives with KF and Al_2O_3, thus enabling the prevention of otherwise inevitable extensive separation procedures (Scheme 38).
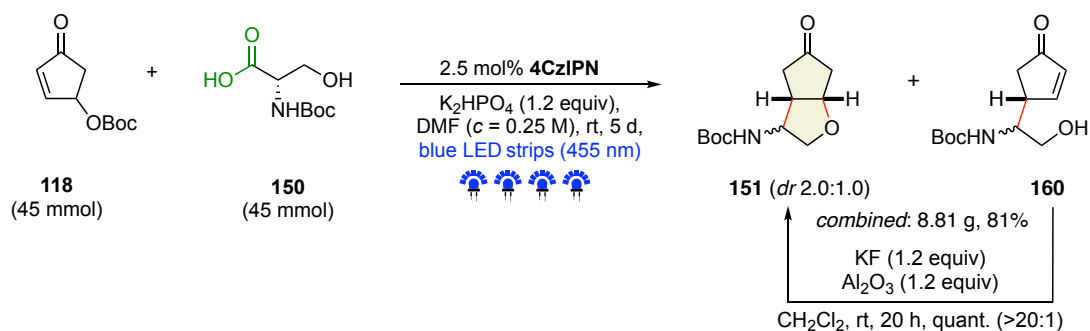
Scheme 38. Multigram-scale decarboxylative coupling with subsequent cyclization of the product mixture.[118]

## 1.6 Expansion of the developed methodology: Substrate scope

Having optimized the reaction protocol towards a highly sustainable process for the sequential photocatalytic DcRCAE–Oxa-Michael reaction of hydroxyalkylated amino acids with cyclopentenones including a suitable multigram-scale approach for future derivatizations, it was subsequently proceeded to explore the substrate scope and functional group tolerance of the developed synthetic methodology. With the aim of a further expansion of the scope of carboxylic acids as the radical precursors and thereby probing the generality of the methodology, several hydroxyalkylated carboxylic acids were synthesized following established procedures. While the employed amino-acids were typically commercially available, most of the alkyl- and alkoxy substituted carboxylic acids had to be synthesized individually, which turned out be a challenging task and required testing of various different protocols. The successfully performed procedures and the corresponding carboxylic acid products are illustrated in Scheme 39.[119,120]
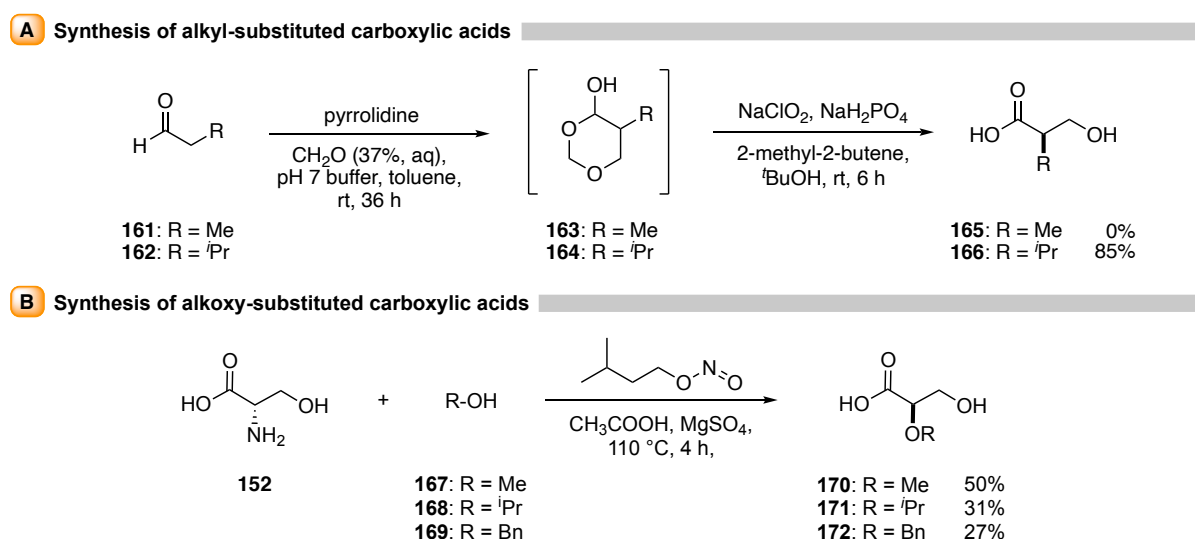
Scheme 39. Synthetic procedures towards various alkyl- and alkoxy-substituted carboxylic acids.[119,120]

Among alkyl-substituted carboxylic acids, besides commercially available tropic acid (**174a**, phenyl-substitution in α-position), the introduction of other alkyl substituents including methyl- or isopropyl-groups was examined. However, efficient product formation of acid **166** was only observed from starting from isovaleraldehyde (**162**), while the corresponding methyl-substituted aldehyde **161** failed to furnish the desired carboxylic acid (Scheme 39, A).[119] Syntheses of alkoxy-substituted carboxylic acids **170-172** were more successful, giving rise to the respective products in 27-50% yield after deamination of free L-serine (**152**) followed by nucleophilic trapping by the corresponding employed alcohols **167-169** (Scheme 39, B).

With various carboxylic acids in hands, it was subsequently proceeded to generate a broad scope of the underlying transformation (Scheme 40). In order to introduce substitutional variability into the synthesized products, it was intended to use various cyclopentenone derivatives bearing alkyl appendages around its core. Therefore, when 5-methyl-substituted cyclopentenone **173a** was reacted with *N*-Boc L-serine (**150**) in the presence of 1 mol % 4CzIPN under the optimized reaction conditions, the exclusive formation of the radical-coupled cyclopentenone derivative **176a** in its uncyclized form was observed in 91% yield as a mixture of diastereomers with a 1.9:1.0 ratio. Likewise, when 5-isopropyl substituted cyclopentenone **173b** was employed as the substrate, the corresponding uncyclized cyclopentenone derivative **176b** was obtained in 62% yield (*dr* 2.1:1.0). Subjecting uncyclized products **176a** and **176b** to the aforementioned assisted cyclization protocol by further treatment with KF and Al_2O_3 did not result in a successful cyclization towards the desired bicyclic motif.
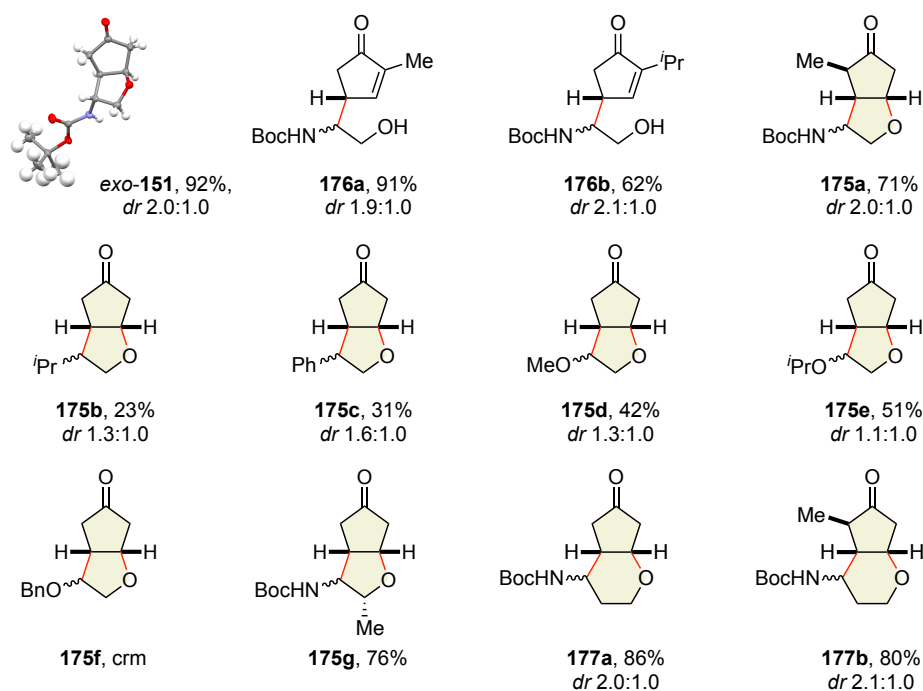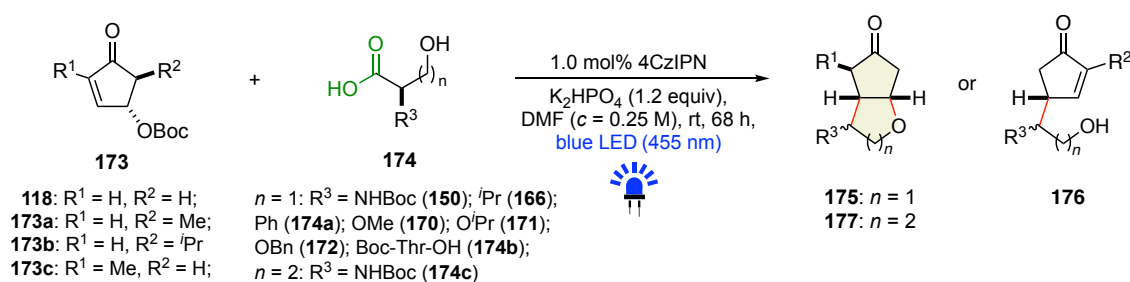
Scheme 40. Substrate scope for the photocatalyzed DcRCAE-oxa-Michael reaction.

The inability of substrates **173a** and **173b** to furnish the corresponding desired bicyclic 3-amino-CpTHF derivatives is most likely a consequence of a combination of the sterically more

hindered and electronically less activated α,β-enone moiety, thus preventing the subsequent oxa-Michael addition step. This hypothesis was further supported by the observation from the experiment wherein 2-methyl-substituted cyclopentenone derivative **173c** was engaged with **150**, affording the corresponding completely cyclized and methylated bicycle **175a** in 71% yield as a mixture of diastereomers in a ratio of 2.0:1.0. Next, the scope of carboxylic acids was expanded, testing the prior synthesized alkyl- and alkoxy-substituted acids instead of an α-amino acid. Carboxylic acids with an isopropyl (**166**) or phenyl (**174a**) substituent in α-position as radical precursors proved to be significantly less effective, giving rise to the corresponding bicyclic and volatile adducts **175b** and **175c** in merely 23% and 31% yield, respectively. The observation could be explained by the significantly decreased stability and nucleophilicity of the photogenerated incipient alkyl radicals, thus impeding the process of radical conjugate addition. This reasoning is also in line with the lower *exo*-preference observed (1.3-1.6:1.0), pointing to an early transition state. Additional experiments with a higher catalyst loading for acids **166** and **174a** did not lead to any improvement in yield.

With a view to enhance the nucleophilicity of the incipient radical and also to broaden the substitutional variability of the products, the scope of α-alkoxy radical precursors was investigated in a next step. Accordingly, when 3-hydroxy-2-methoxypropanoic acid (**170**) was used as the radical precursor and reacted with **118**, the corresponding bicyclic fused cyclopentanone derivative **175d** was obtained in 42% yield with a 1.3:1.0 diastereomeric ratio. Likewise, 2-isopropoxyl- and 2-benzyloxyl-substituted 3-hydroxypropanoic acids **171** and **172**, respectively, were employed in a next set of experiments. While in the case of **171** the corresponding CpO-THF moiety **175e** was obtained in 51% yield (*dr* 1.1:1.0), the reaction of **172** failed to furnished the desired product. Nevertheless, the slightly improved yields in case of carboxylic acids **170** and **171** could be attributed to the enhanced nucleophilicity of the incipient radical due to the presence of the adjacent oxygen-heteroatom. Furthermore, the introduction of an alkyl substituent in a different position on the desired bicyclic motif was tested by subjecting *N*-Boc L-threonine (**174b**) to the present photocatalytic conditions, which gave rise to the expected product **175g** in 76% yield albeit as a mixture of multiple inseparable diastereomers.

In a next step of this study, the question arose whether the same principle could be exploited to synthesize one-carbon higher homologues of 3-aminotetrahydrofuran-fused cyclopentanone derivatives. To examine this hypothesis, commercially available *N*-Boc L-homoserine (**174c**) was employed as the radical precursor and reacted with **118** in the presence of 1 mol % 4CzIPN under the optimized reaction conditions.

Accordingly, the corresponding 4-aminotetrahydropyran-fused cyclopentanone derivative **177a** was obtained in 86% yield with a diastereomeric ratio of 2.0:1.0. Encouraged by this result, 2-methyl-substituted cyclopentenone derivative **173c** was subsequently employed as the substrate and led to the formation of 5-methyl-substituted bicyclic tetrahydropyran-fused cyclopentanone **177b** in 80% yield (*dr* 2.1:1.0).

It should be noted that numerous additional attempts for the synthesis of a higher number of carboxylic acid derivatives were performed, including several approaches towards carboxylic acids which would afford 7-membered fused cyclic ethers or substrates bearing various different substitution patterns; however, these syntheses turned out to be quite challenging and extensive, often requiring multistep synthetic sequences and exotic reaction set-ups, wherefore it was refrained to synthesize a broader set of carboxylic acids as radical precursors.

After the extensive exemplification of the developed methodology, it was subsequently pursued to construct comparatively more structurally intricate molecular frameworks by exploiting the established strategy to obtain heretofore unprecedented fused polyheterocyclic compounds which might nonetheless possess interesting and beneficial pharmacological activities. To achieve this, in a first set of experiments, commercially-available (2*S*,4*R*)-4-hydroxy-*N*-Boc proline (**178**) was reacted with **118** under the aforementioned optimized reaction conditions (Scheme 41).

Synthesis of cyclopentanone-fused 2,5-methanooxazepines
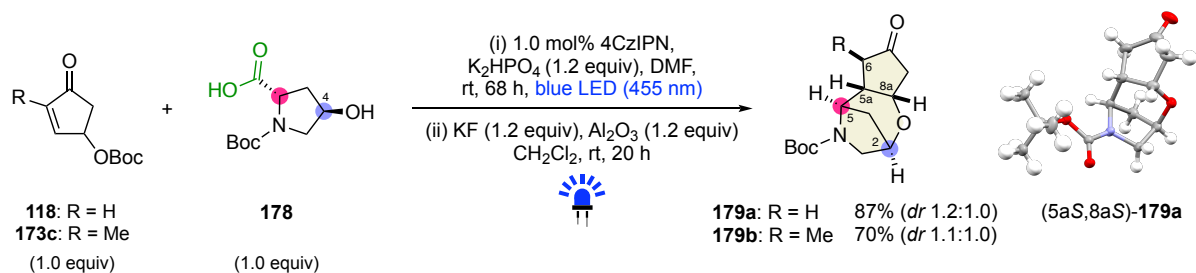
Scheme 41. Synthesis of a bridged homomorpholine system.

Gratifyingly, a prolific photocatalytic reaction was observed, giving rise to a mixture of the desired cyclized product **179a** and the corresponding uncyclized derivative, being a consequence of a less efficient Michael addition due to the resulting formation of a 7-membered ring system. Following the earlier developed assisted cyclization protocol by further treatment with KF and Al$_2$O$_3$ in dichloromethane at room temperature, the exotic bridged homo-morpholine framework **179a** was exclusively obtained in 87% yield with a diastereomeric ratio of 1.2:1.0.[118]

The structure of **179a** was unambiguously confirmed by spectroscopic and single-crystal X-ray analyses. Likewise, when proline derivative **178** was reacted with methyl-substituted cyclopentenone **173c** following the same photocatalytic procedure and cyclization protocol, the corresponding methylated bridged moiety **179b** was formed in 70% yield. Interestingly, cyclic motif **179** formed as a mixture of only two diastereomers, being a consequence of the rigid framework that compels the two hydrogen substituents at the bridgehead positions to orient themselves on the same specific side determined by the stereochemistry at C-4 in hydroxyproline **178**.

1.7 Mechanistic picture of the photocatalyzed DcRCAE-oxa-Michael Reaction

On the basis of the experimental observations, a probable mechanism for the organic photocatalyzed decarboxylative radical conjugate addition-elimination (DcRCAE) Oxa-Michael reaction cascade of hydroxyalkylated carboxylic acids **174** to various hydroxycyclopentenones **173** was postulated and the mechanistic steps are depicted in Scheme 42 in detail. The reaction initiates with the deprotonation of carboxylic acid **174** by the base present in the reaction medium. Upon irradiation with a blue LED (λ_{max} = 455 nm), the excited photocatalyst **PC*** oxidizes the newly-formed carboxylate anion **A** via a single-electron transfer process which after subsequent extrusion of CO_2 leads to the formation of radical **B**, being an α-amino, α-oxy- or α-alkyl radical, depending on the employed carboxylic acid as the radical precursor. Addition to cyclopentenone **173** furnishes the open-shell intermediate **C** which is in a next step reduced to the corresponding carbanion species **D** by the reduced photocatalyst (**PC***⁻), thereby closing the photocatalytic cycle via reductive termination with concurrent triggering of the anellation sequence: tautomeric conversion of anion **D** to intermediate **E** expels the OBoc-leaving group to generate the uncyclized cyclopentenone **176** which, depending on the substitution pattern at the C5-position (R^2), undergoes an intramolecular oxa-Michael reaction by the pendant hydroxy group under basic conditions and ultimately furnishes the cyclopentanonyl-fused cyclic ether frameworks **175** or **177**.

Proposed catalytic cycle
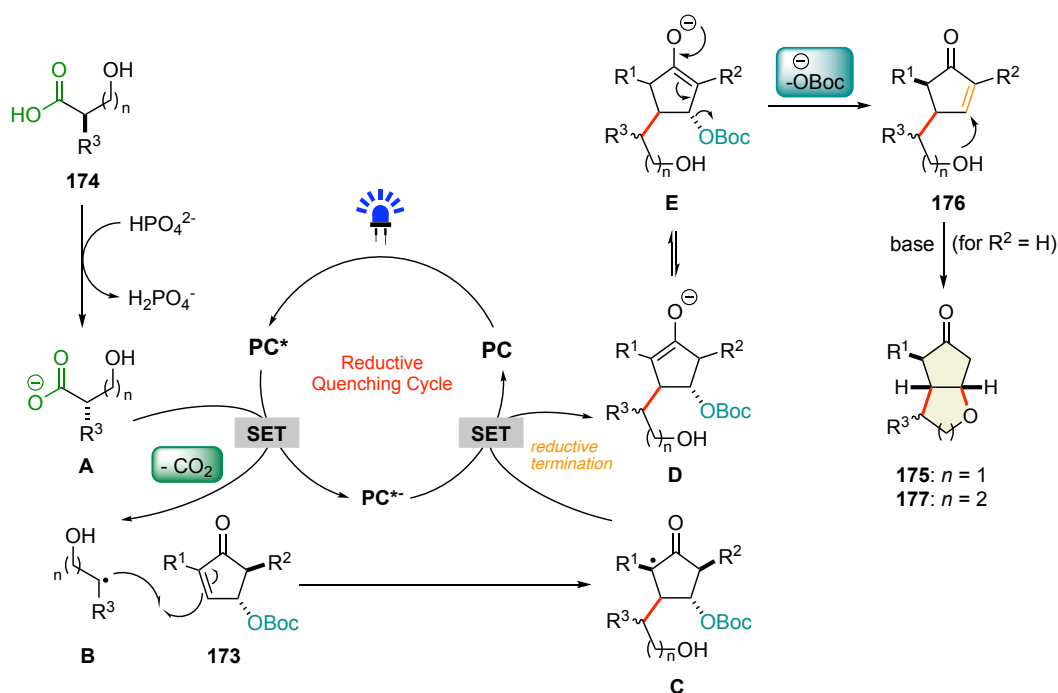
Scheme 42. Plausible reaction mechanism for the organic photocatalyzed decarboxylative radical conjugate addition-elimination (DcRCAE) Oxa-Michael reaction cascade.

1.8 Stereochemical outcome of the developed methodology

With the vision of synthesizing the C3-amino cyclopentyltetrahydrofuranyl-derived HIV-1 protease inhibitors **125** and **126** in their enantioenriched forms, it was intended in the next phase of the ongoing study to investigate the prospect of conducting the developed photocatalytic DcRCAE-oxa-Michael reaction with an enantiopure substrate in a stereoselective fashion.
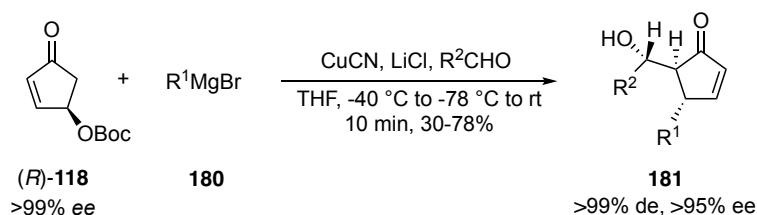

Scheme 43. Nucleophilic conjugate addition to enantiopure hydroxycyclopentenone.

In this context, Reiser and co-workers previously introduced an enantiopure synthetic route to substituted 2-cyclopentenones from enantiopure Boc-protected 4-hydroxy-2-cyclopentenone (*R*)-**118** by the reaction of Grignard reagents **180** in the presence of copper, which proceeded with high stereoselectivity initiated by the nucleophilic, conjugate addition *anti* to the *O*Boc group giving rise to diastereo- and enantiomerically pure products of type **181** (Scheme 43).[121]
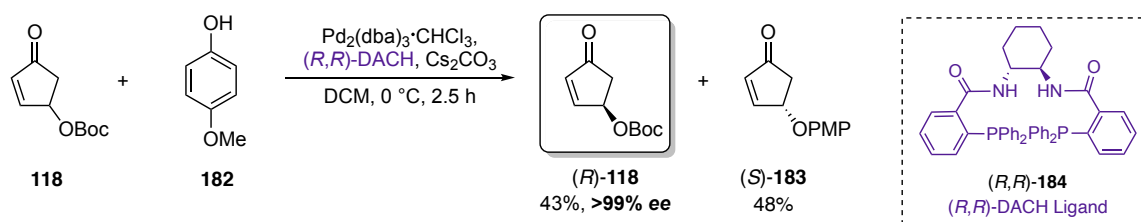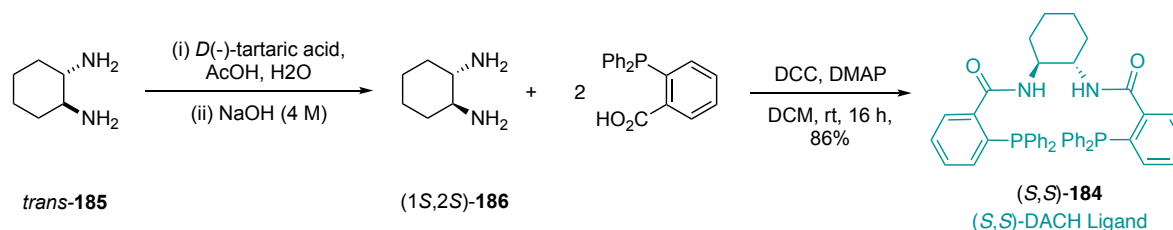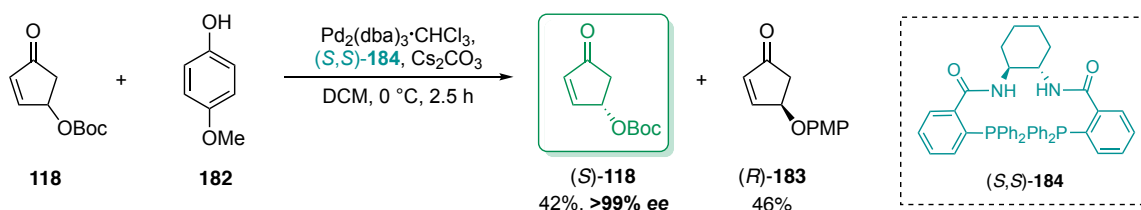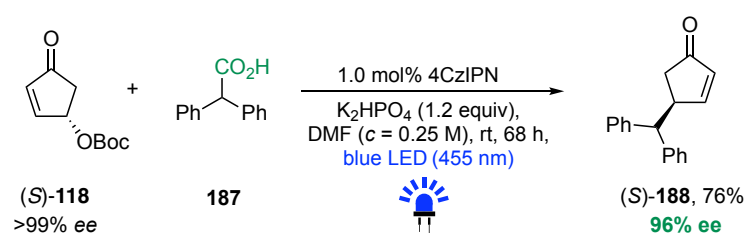

Scheme 44. Enantiopure synthesis of Boc-protected hydroxycyclopentenone **118**.[121,122]

For the examination regarding the stereochemical outcome of the developed present methodology, the additional synthesis of enantiomer (S)-**118** is necessary, which in contrast to (R)-**118** has the right stereochemical orientation for the later envisioned synthesis of enantioenriched protease inhibitors **125** and **126**. Accordingly, besides (R)-**118**, remaining enantiomer (S)-**118** was produced after successful synthesis of the required (S,S)-DACH Trost ligand ((S,S)-**184**) following the literature-known procedure reported by Reiser et al., affording both enantiomers (R)-**118** and (S)-**118** in enantiopure form (>99% *ee*) (Scheme 44).[121,122]

Consequently, when enantiopure (S)-**118** was reacted with diphenylacetic acid (**187**) as a stable radical precursor under the present conditions, the formation of the corresponding benzhydryl-substituted cyclopentenone derivative (S)-**188** was observed in 76% yield with a remarkable enantiomeric excess of 96% *ee*, given that in contrast to the aforementioned ionic process to 2-substituted cyclopentenones **181** (see Scheme 43) the radical addition to (S)-**188** was assumed to proceed via an earlier, thus less selective transition state (Scheme 45).


Scheme 45. Stereoselectivity of the photocatalyzed DcRCAE-oxa-Michael reaction.

With these promising results in hands, the stereochemical outcome towards the desired bicyclic CpO-THF motifs was examined as well. Hence, when enantiopure (R)-**118** was reacted with N-Boc L-serine (**150**), the corresponding enantioenriched adduct (3S/3R)-**151** was formed as a mixture of two diastereomers in 87% yield (Scheme 46).

In order to introduce an UV-active functional group onto the otherwise UV-inactive CpO-THF moiety, being a requirement for a successful stereochemical analysis via chiral HPLC-chromatography, the purified and separated *exo*-diastereomer (3S)-**151** was converted to its corresponding UV-active Fmoc-protected derivative (3S)-**157** by the earlier developed deprotection/reprotection approach. Subsequent HPLC-chromatographic analysis revealed an enantiomeric excess of 84% *ee*, a moderately lower value compared to the aforementioned addition product (S)-**188** (see Scheme 45 for reference)**,** but still representing a remarkable outcome for a radical conjugate addition process.

**Stereoselective radical conjugate addition to desired CpO-THF motif**
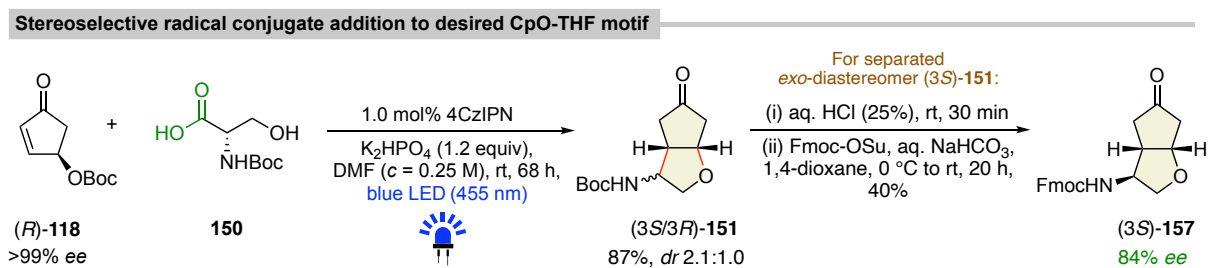
Scheme 46: Stereochemical information present in the desired CpO-THF framework.

## 1.9 Synthetic sequence to highly potent HIV-1 Protease Inhibitors

From the successful upscaling of the photocatalytic DcRCAE-oxa-Michael reaction strategy with racemic substrate **118** as well as the exemplary enantioselective photocatalytic radical conjugate addition, subsequent efforts were directed to accomplish the targeted total syntheses of the 3-amino substituted, Cp-THF derived potent HIV-1 protease inhibitors **125** and **126** in diastereo- and enantiomerically enriched forms (Scheme 47).[78]
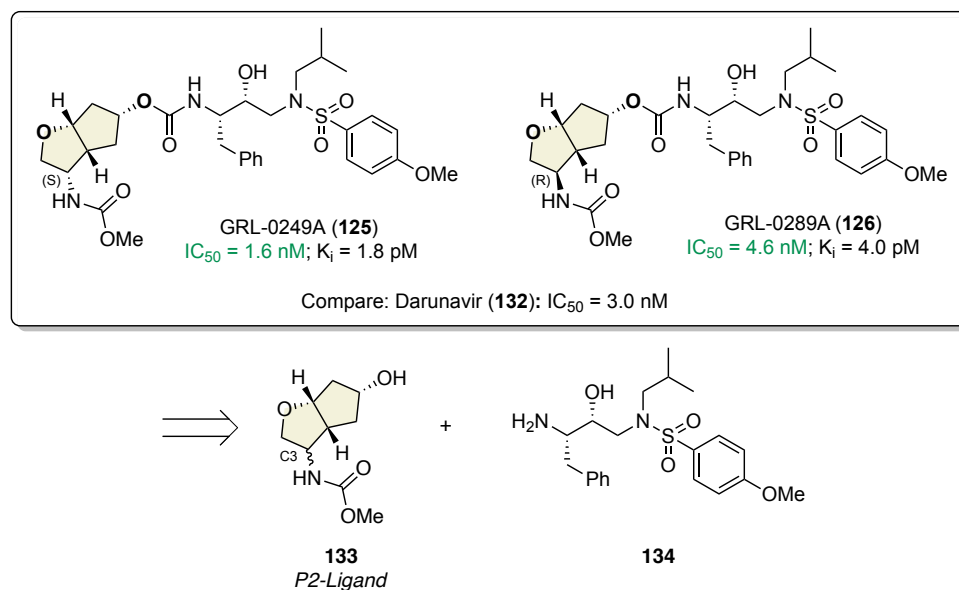
Scheme 47. Total synthesis of desired HIV-1 protease inhibitors.[78]

The key to a highly efficient synthetic sequence towards the desired drug candidates is the rapid and high-yielding construction of P2-Ligand **133**, which requires only a few steps of synthetic manipulations starting from the generated CpO-THF derivative **151**. First investigations towards the necessary amino-functionalization present in bicycle **151** were reported under chapter 1.4.2 of the main part, describing a deprotection/reprotection protocol towards *N*-methyl carbamate protected derivative **156** (Scheme 48).
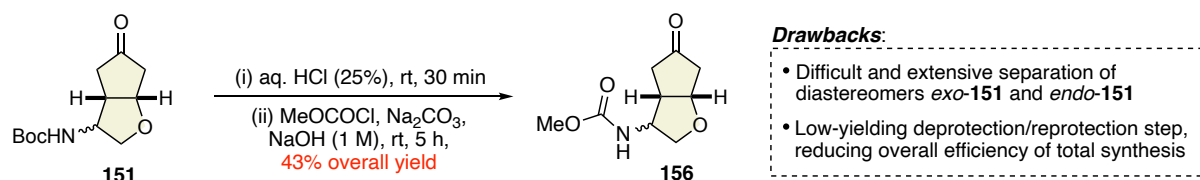

Scheme 48. Earlier developed amino-functionalization approach.

Simple subsequent reduction of the carbonyl moiety in **156** would readily afford the required, racemic P2-ligand **133**. However, despite the successful introduction of the required *N*-methyl carbamate group, this procedure suffers from operational drawbacks.

In order to achieve a diastereoselective synthesis of the targeted drug candidates **125** and **126**, a diastereopure CpO-THF precursor is essential. Derivatization product **156** was isolated earlier as a mixture of inseparable diastereomers. Furthermore, a complete separation of both *exo-* and *endo*-diastereomers present in Boc-protected bicycle **151** requires, like mentioned under chapter 1.4.2 of the main part, an extensive purification procedure of six subsequent columns for a typical small-scale reaction, which is not suitable in terms of chemical waste generation and time intensity especially for the synthesis and complete isolation of larger amounts of the respective diastereomers. Secondly, the rather low-yielding process of the deprotection/reprotection sequence to **156** significantly decreased the overall efficiency of the envisioned total synthetic route. Therefore, an alternative strategy for this synthetic manipulation is highly desirable.

A solution for the aforementioned issue of challenging diastereomer separation was found by a rather simple alteration of the underlying procedure. Instead of a derivatization of the amino-functionality in racemic substrate **151** in an initial step of the sequence, the reduction of the carbonyl group was carried out at first, affording the corresponding alcoholic Cp-THF moieties **189** in good yields of 80–81% (Scheme 49). The reduction via NaBH$_4$ proved to proceed diastereoselectively, affording exclusively one diastereomer as the product when a diastereopure starting material was employed (Scheme 49, A).
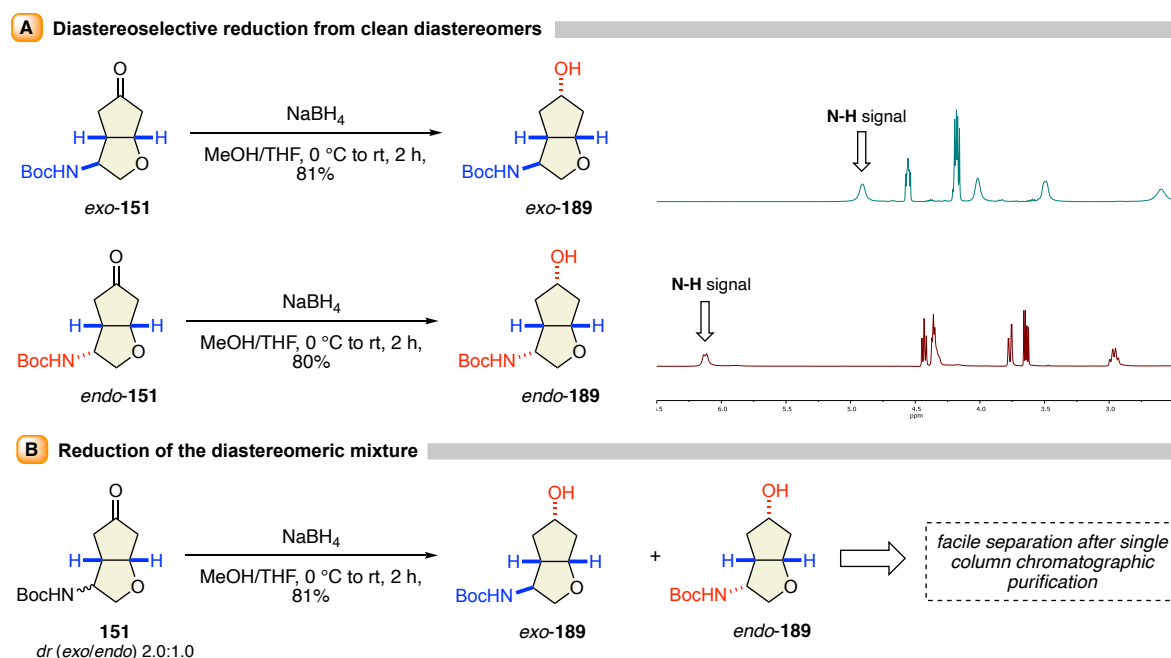
Scheme 49. Diastereoselective reduction of **151.**

Interestingly, NMR-analysis of alcohol *endo*-**189** revealed a significant downfield-shift of the signal assigned to the proton located on the amino-group (N–H) compared to *exo*-**189**, possibly originating from the occurrence of hydrogen-bonding effects between the hydroxyl- and amino-group being located on the same side of the fused cyclic framework. Subsequently, a mixture of both diastereomers of **151** was subjected to the same reducing conditions, resulting in a mixture of both *exo*-**189** and *endo*-**189**. Gratifyingly, the reduction to the corresponding alcohols led to a facile separation of the stereoisomers after a single column chromatographic purification procedure, thus circumventing extensive separation techniques for the isolation of diastereopure intermediates (Scheme 49, B).

Subsequently, the deprotection of the Boc-group of alcohol **189** was examined. A short screening of deprotection techniques revealed that a 1 M-solution of HCl in ethyl acetate (EA) was the most effective approach for the underlying novel system, which after reprotection with methyl chloroformate gave rise to carbamates *exo*-**190** and *endo*-**190** in 82% and 77% yield, respectively (Scheme 50).
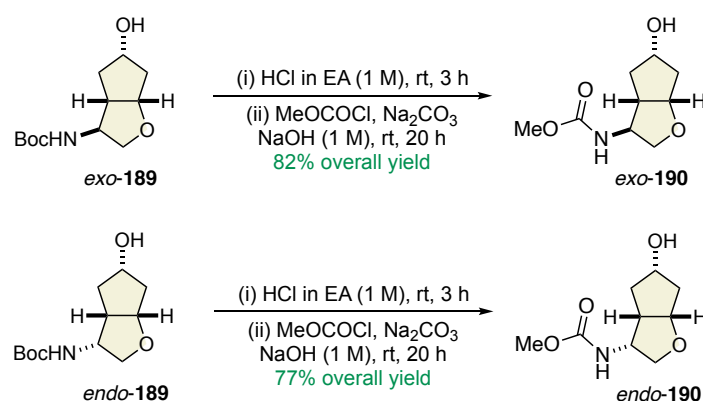

Scheme 50. C3-amino-derivatization of alcohol **189**.

Compared to the earlier deprotection/reprotection approach starting from cyclic ketone **151** (see Scheme 48 for reference) which gave rise to *N*-methyl carbamate protected derivative **156** in merely 43% yield, the amino-derivatization of alcohol **189** proceeded smoothly in yields from 77–82%. Reversing the order of deprotection/reprotection and reduction resulted in a significantly increased overall efficiency of the sequence, accompanied by a resolution of the thus far challenging and extensive separation of diastereomers.

At this stage, the two racemic P2-ligands *exo*-**190** and *endo*-**190** were readily synthesized in a highly efficient manner in overall three steps starting from racemic Boc-protected 4-hydroxy-2-cyclopentenone **118**, representing a significant improvement to earlier reported procedures[79,102] and thus highlighting the synthetic utility of the developed, highly efficient and sustainable methodology.

In a next step of the overall sequence towards targeted HIV-1 protease inhibitors **125** and **126**, the respective alcohols *exo*-**190** and *endo*-**190** were converted to their corresponding activated carbonates for the concluding fragment combination reaction. Treatment with 4-nitrophenyl chloroformate in the presence of pyridine afforded the corresponding activated fused cyclic ethers *exo*-**191** and *endo*-**191** in 81% and 85% yield, respectively (Scheme 51).[123]

Activation of P2-Ligands
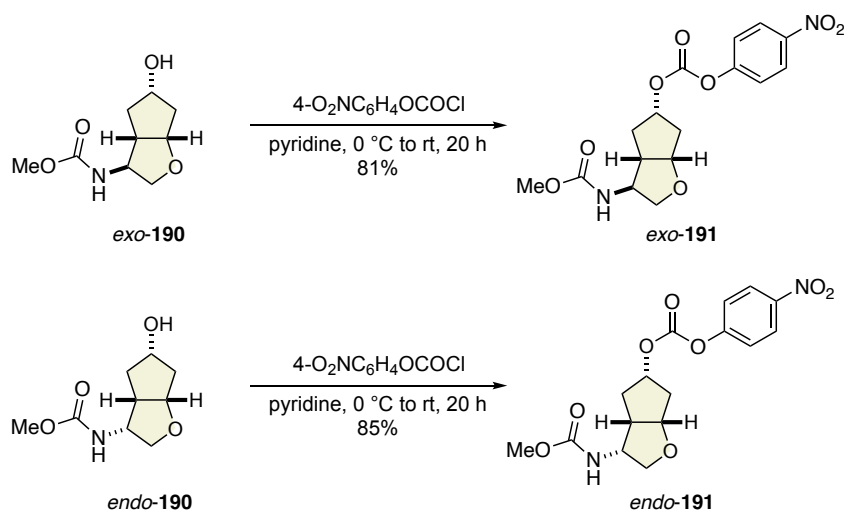
Scheme 51. Conversion of alcohols **190** to activated carbonates.[123]

Conducively, the introduction of the UV-active 4-nitrophenyl group into the bicyclic Cp-THF motif enables a detailed stereochemical analysis via chiral HPLC-chromatography, thus circumventing the need of an additional introduction of a Fmoc-group solely for analytical purposes. The obtained stereochemical results will be discussed at a later point when the synthetic pathway starting from enantiopure hydroxycyclopentenone (*S*)-**118** is described.

Afterwards, the other required fragment of the targeted inhibitors was synthesized by following methods as established by Ghosh and co-workers (Scheme 52).[124] The commercially available epoxide **192** was reacted with *iso*–butylamine (**193**) to furnish the corresponding ring-opened amino alcohol, which was later protected with 4-methoxybenzenesulfonylchloride to form intermediate **194** in 87% overall yield over two steps. The *N*-Boc group was subsequently deprotected in the presence of trifluoroacetic acid to obtain the free amine **134** in 91% yield.

Synthesis of coupling fragment
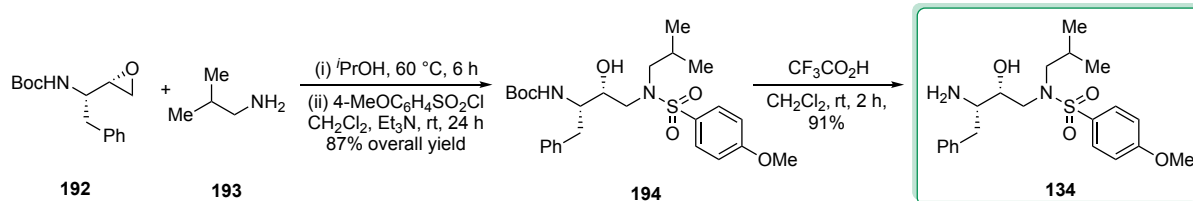
Scheme 52. Fragment synthesis established by Ghosh and co-workers.[124]

With both required fragments in hands, the last step of the synthetic sequence was performed. Fragment coupling between racemic and activated P2-ligands *exo*-**191** and *endo*-**191** with enantiomerically pure amine **134** afforded the P2-racemic HIV-1 protease inhibitors (*rac*)-**126** and (*rac*)-**125** in 87% and 89%, respectively (Scheme 53).[78]

Fragment combination to P2-racemic inhibitors
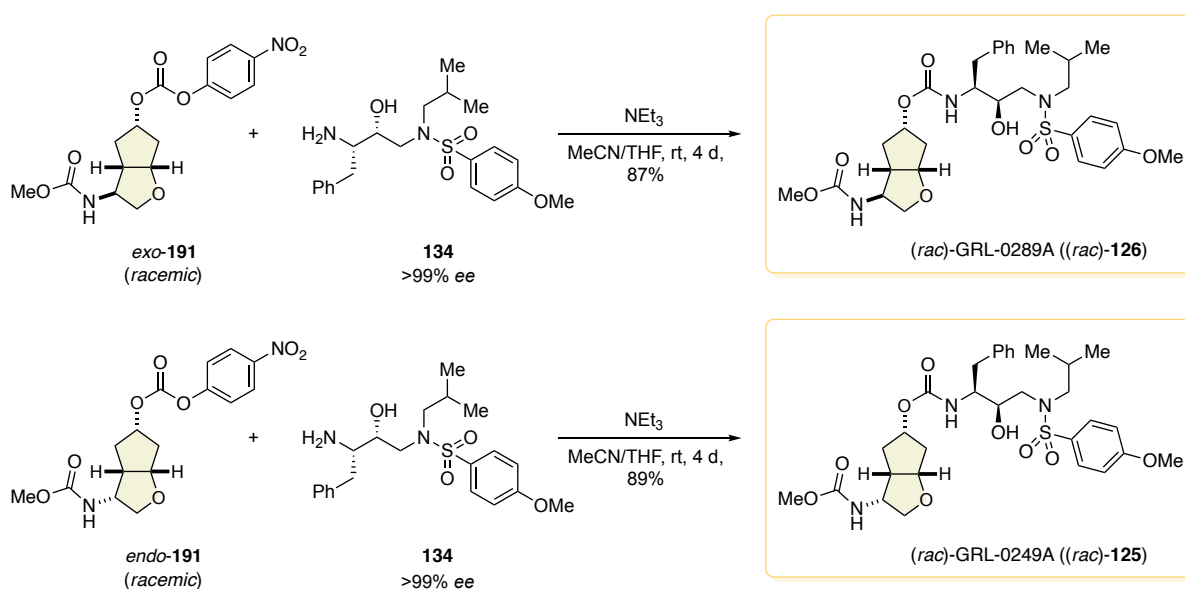

Scheme 53. Synthesis of P2-racemic HIV protease inhibitors.

Having completed, optimized and tested the respective steps of the synthetic sequence towards the targeted drug candidates starting from racemic Boc-protected 4-hydroxy-2-cyclopentenone **118,** the direct synthesis of biologically highly potent, enantioenriched HIV-1 protease inhibitors was conducted and the summarized synthetic steps are delineated in Scheme 54.

For this purpose, enantiomerically pure Boc-protected 4-hydroxy-2-cyclopentenone (*S*)-**118** was employed as the chiral starting material carrying the stereochemical information. Firstly, an asymmetric photocatalytic decarboxylative radical coupling between (*S*)-**118** and protected serine **150** was carried out in a 5 mmol scale in the presence of 1 mol % of 4CzIPN under the optimized photocatalytic reaction conditions in a large-sized pressure tube, which afforded the corresponding enantioenriched decarboxylative radical adduct (*ent*)-**151** in 86% yield as a diastereomeric mixture of *exo*-(3*R*)-**151** and *endo*-(3*R*)-**151** in a 2.2:1.0 ratio.

**Enantioselective total syntheses of potent HIV-1 protease inhibitors**
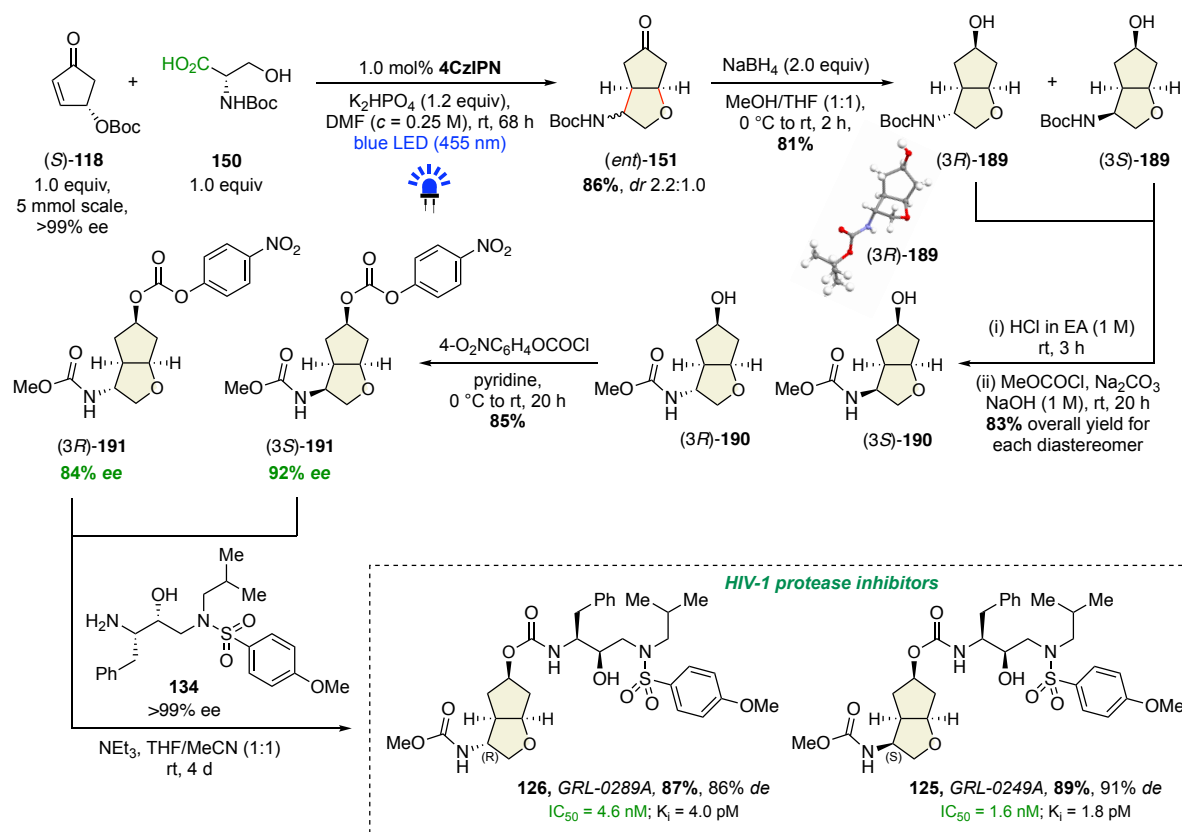
Scheme 54. Total synthesis of enantioenriched HIV-1 protease inhibitors **125** and **126**.

The carbonyl moieties of the cyclopentanone derivatives *exo*-(3*R*)-**151** and *endo*-(3*R*)-**151** were subsequently reduced by the treatment of the diastereomeric mixture with sodium borohydride in a 1:1 mixture of MeOH and THF and the corresponding diastereomers of the alcohol derivatives (3*R*)-**189** and (3*S*)-**189** were obtained in 81% yield. Gratifyingly, as reported above, the two diastereomers could be separated easily at this stage by column chromatographic purification and the subsequent synthetic steps were carried out with diastereopure compounds. The relative stereochemistry of the functional groups in (3*R*)-**189** was confirmed by single crystal X-ray analysis, which allows to unambiguously assign the stereochemistry of all further products along the synthetic route. Afterwards, diastereopure alcohols (3*R*)-**189** and (3*S*)-**189** were converted to their corresponding *N*-methyl carbamate derivatives (3*R*)-**190** and (3*S*)-**190**, respectively, upon deprotection of the *N*-Boc groups under acidic conditions and reprotection of the free amine groups with methyl chloroformate under basic conditions in 83% yield over two steps for each diastereomer. In a next step, these two diastereomers were treated separately with 4-nitrophenyl chloroformate in the presence of pyridine and the corresponding activated carbonates (3*R*)-**191** and (3*S*)-**191** were obtained in 85% yield in both cases.[78] Having synthesized the racemic reference compounds for chiral HPLC analysis during the aforementioned test reactions for this sequence, the enantiomeric excesses of these

enantioenriched diastereomers were determined at this stage and found to be 84% and 92% *ee*, respectively, representing a remarkable outcome and being in line with earlier described results in the present work. The endgame of the total synthesis was carried out with the coupling of enantiopure and free amine **134** with activated P2-ligands (3*R*)-**191** and (3*S*)-**191** in two sets of experiments in the presence of triethylamine in a mixture of THF and MeOH to furnish the Cp-THF derived HIV-1 protease inhibitors GRL-0289A (**126**; IC_{50} = 4.6 nM, K_i = 4.0 pm) and GRL-0249A (**125**; IC_{50} = 1.6 nM, K_i = 1.8 pm) in 87% and 89% yield, respectively, in diastereo- and enantiomerically enriched forms (86% and 91% *de*).[78,124]

Interestingly, the developed approach allows for the synthesis of all four possible stereoisomers of the Cp-THF derived P2-ligand, solely depending on the stereochemical orientation of the Boc-group in the respective 4-hydroxy-2-cyclopentenone (Scheme 55).
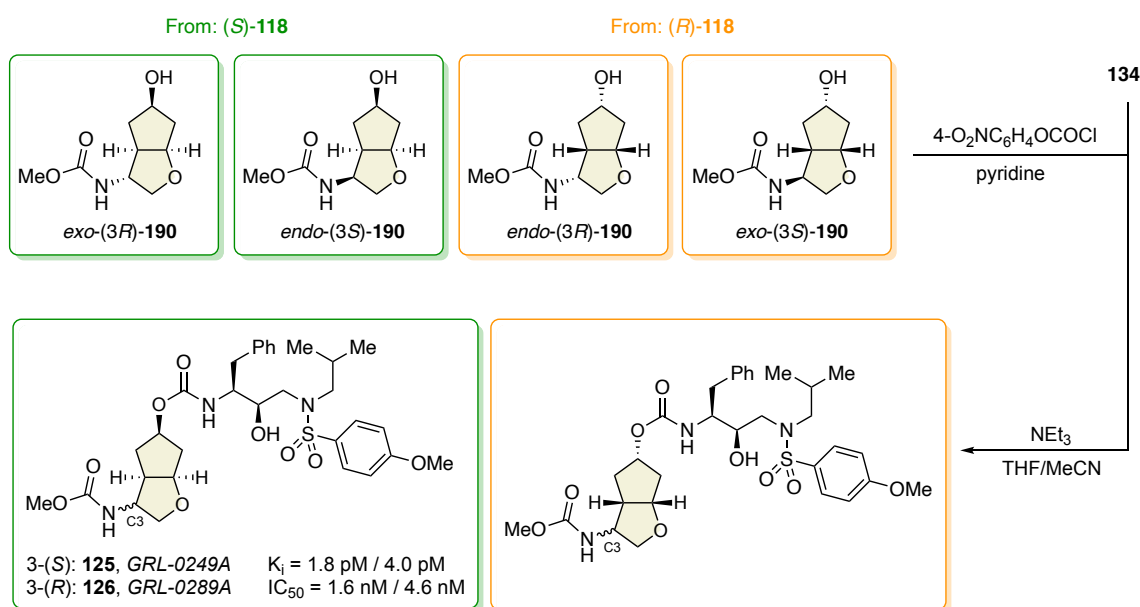

Scheme 55. Possible synthesis of additional potent protease inhibitors.

In addition to the executed total synthesis towards inhibitors **125** and **126** from enantiopure (*S*)-**118**, a synthetic approach towards new PIs with an inverted stereochemistry on the P2-ligand is practicable by utilizing enantiopure hydroxycyclopentenone (*R*)-**118**, thus opening access to another set of possibly potent target structures.

To conclude, a novel visible-light mediated synthetic route to access a wide panoply of structurally-variegated cyclopentanonyl-fused functionalized cyclic ether derivatives in the presence of an inexpensive organic photocatalyst was developed. In addition, a highly efficient total synthesis of the two diastereomers of a potent HIV-1 protease inhibitor from easily obtainable renewable resources-derived starting materials was achieved, underlining the high sustainable character and synthetic utility of the designed methodology.

1.10 Possible future approaches and outlook towards new target structures

The efficiency and flexibility of the developed photocatalyzed DcRCAE-oxa-Michael reaction cascade offers a wide range of possible approaches towards other pharmacologically relevant compounds and target structures, which can be exploited in future studies following the established methods in this present work. One of these potentially desirable synthetic targets are analogs of the naturally occurring prostacyclin (PGI_2), a representative of the prostaglandin family, which can be obtained by a simple change of the nucleophile present in the carboxylic acid (Scheme 56).[125,126]
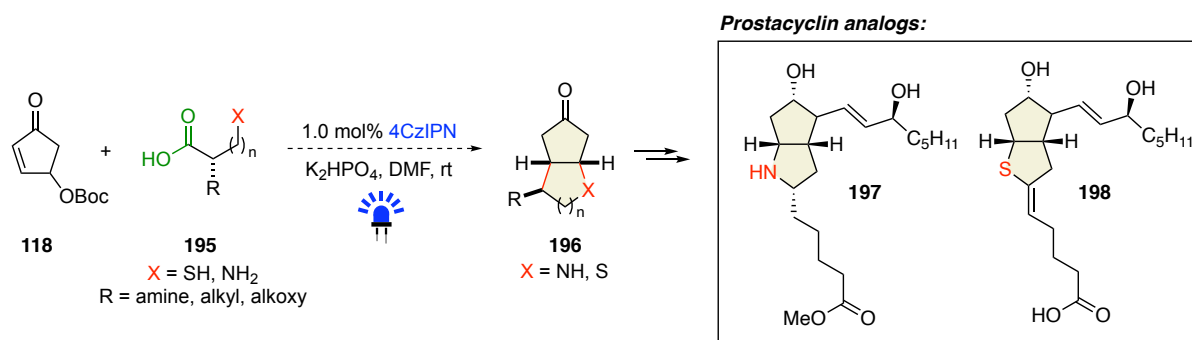
Scheme 56. Accessible structures by change of nucleophile.

Instead of the utilization of serine derivatives as the main coupling partner, a switch towards cysteine derivatives and their corresponding nitrogen containing analogs as radical precursors potentially gives rise to attractive thia- and aza-Cp-THF motifs **197** and **198**.[125,126] First studies for the utilization of cysteine derivatives were already carried out and revealed that a different approach is necessary when sulfur-nucleophiles are employed under the present photocatalytic reaction conditions (Scheme 57).
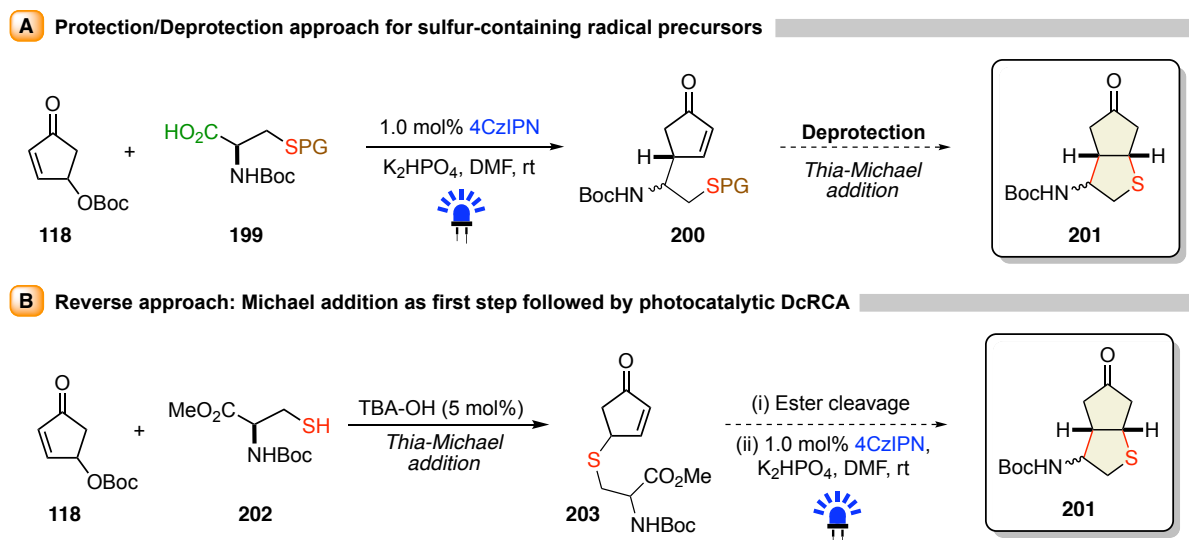

Scheme 57. Two-step approach towards thia-CpO-THF moieties.

The instability of a free SH-group during a photochemical process, thus leading to complex product mixtures during the examined test reactions, prevents the utilization of sulfur-unprotected cysteine derivatives. Nevertheless, one potentially successful alternative approach involves the usage of a *S*-protected carboxylic acid **199**, affording radical addition product **200** after decarboxylative coupling. Subsequent deprotection potentially induces the required thia-Michael addition to the envisioned framework **201**.

Another possibility is a reversed approach, proceeding via the thia-Michael addition in a first step, followed by the visible-light mediated decarboxylative ring closure to afford the desired fused thia-ether **201**. Preliminary performed studies revealed that a free carboxylic acid impedes the initial thia-Michael addition, which can be circumvented by the utilization of ester protected cysteine derivative **202**, making a subsequent ester cleavage step of intermediate **203** essential prior to the envisioned photocatalytic cyclization step.[127]

A further extension potentially carrying synthetical value is the derivatization of the existing CpO-THF and the envisioned thia- and aza-CpO-THF fused ethers. Besides the described synthetic manipulations resulting in potent HIV-1 protease inhibitors, further derivatization approaches towards a variety of new bicyclic motifs seems desirable, thus potentially expanding the scope for suitable P2-ligands in the field of protease inhibitor research (Scheme 58).
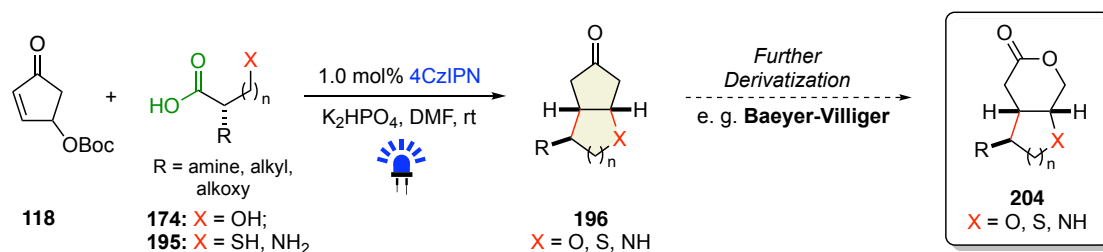
Scheme 58. Possible derivatizations of existing and envisioned fused ethers.

The developed methodology can also be utilized in future works to access novel, so far unknown cyclic frameworks, thus enabling a possible route towards a new class of fused cyclic compounds (Scheme 59, A). Whereas 4-hydroxy-proline **178** as employed radical precursor resulted in the formation of bridged homo-morpholine system **179** (see Scheme 41 for reference), the utilization of the corresponding isomer 3-hydroxy-proline **205** potentially enables the synthesis of tricyclic fused systems **206**, which in this composition hasn't been reported yet in literature. However, initial trials to synthesize the required precursor **205** for the desired transformation failed due to highly extensive and complex procedures.

A Photocatalytic DcRCAE: Synthesis of new tricyclic fused systems
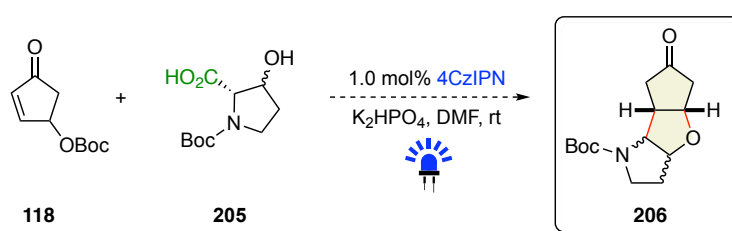
B Amines as radical precursors for the synthesis of bicyclic fused motifs
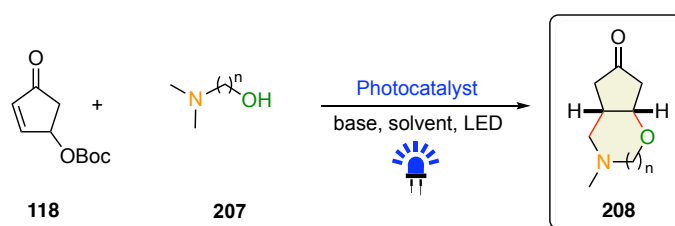
Scheme 59. Potentially accessible frameworks starting from **118**.

Besides utilizing the concept of photocatalytic decarboxylative radical couplings and carboxylic acids as radical precursors, other suitable starting materials may lead to the formation of fused cyclic ethers by exploiting the specific reactivity pattern of Boc-protected 4-hydroxy-2-cyclopentenone (**118**) under photocatalytic conditions (Scheme 59, B). Various hydroxy-substituted amines **207** may afford bicyclic motifs **208** after α-amino radical generation followed by conjugate addition with subsequent elimination-oxa-Michael reaction, thus potentially further expanding the synthetic utility of 4-hydroxy-2-cyclopentenone (**116**) and derivatives as valuable starting materials.

2 Envisioned photocatalytic carbanion trapping towards 4,5-dialkylsubstituted 2-cyclopentenones

Having developed the highly efficient and sustainable methodology for rapid construction of valuable CpO-THF frameworks via photocatalytic DcRCAE-oxa-Michael reaction, it was envisaged in a next step of the present study to expand the developed protocol to open access to another class of precious substrates by employing the concept of photoredox catalysis. Inspired by the proposed mechanism of the photocatalyzed DcRCAE-oxa-Michael reaction (see Scheme 42 for reference),[69] the question arose whether specific intermediates proposed in the present mechanistic picture can be functionalized in an alternative pathway to afford new types of interesting products. In this context, the carbanion species **D** generated after reductive termination by the reduced photocatalyst (**PC*⁻**) was targeted and envisioned to undergo an alternative reaction pathway by exploiting typical carbanion reactivity patterns (Scheme 60). Instead of triggering the anellation sequence towards the CpO-THF fused ethers **175** and **177**, the generated carbanion **D** can potentially be trapped by intermolecular addition to electrophiles, specifically aldehydes **209**, to afford valuable 4-alkyl-5-hydroxyalkyl substituted 2-cyclopentenones **210**.

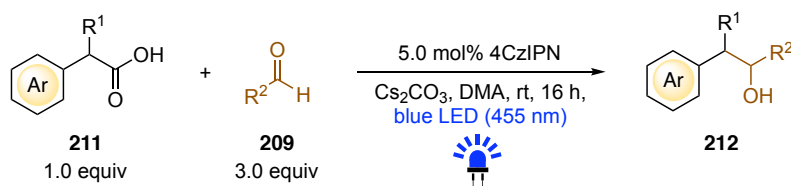**Proposed photocatalytic carbanion trapping**
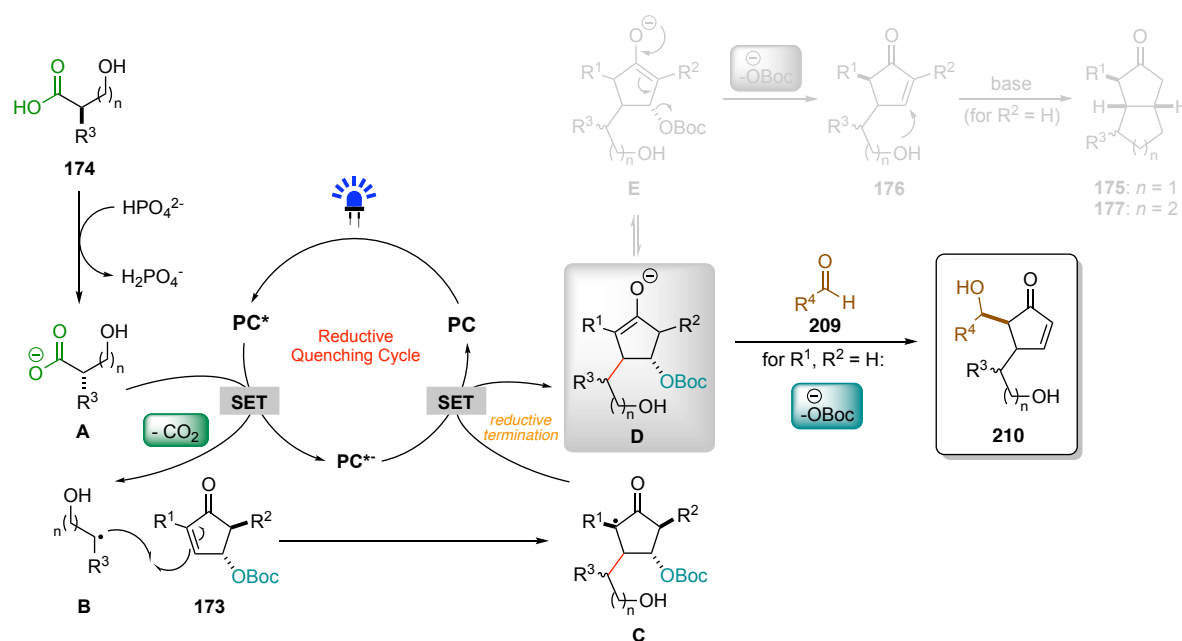
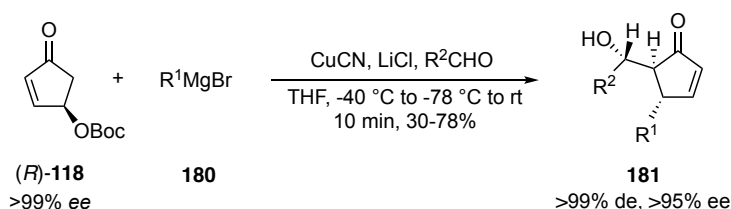**Scheme 60.** Envisioned addition of photogenerated carbanions to aldehydes.

The potential feasibility of this envisaged approach is underlined by literature reports by König *et al.*, wherein the photocatalytic carbanion generation followed by intermolecular addition to various aliphatic aldehydes **209** was described (Scheme 61, A).[128]

Interestingly, carbanions were only efficiently generated from numerous phenyl acetic acids **211**, illustrating the necessity of an adjacent stabilizing aromatic moiety assisting the benzyl-anion generation. Furthermore, Reiser and co-workers reported a nucleophilic conjugate addition approach towards substituted 2-cyclopentenones **181** starting from enantiopure Boc-protected hydroxy-cyclopentenone (R)-**118**, representing the nucleophilic counterpart to the envisioned radical conjugate addition to products of type **210** (Scheme 61, B).[121]


Scheme 61. Literature reports by König et al. and Reiser and co-workers.

Encouraged by the described literature reports, the feasibility of the envisaged transformation was examined by combination of both approaches and the obtained results are summarized in Table 8.

However, instead of the desired 4,5-disubstituted 2-cyclopentenone **214**, the corresponding and earlier described addition-elimination product **188** was observed as the exclusive product, irrespective of the employed parameters. An increase of equivalents of aldehyde **213** to up to a tenfold excess and thus highly encouraging an intermolecular nucleophilic addition did not result in any targeted product formation with Cs_2CO_3 as the base, following the optimized conditions from the report of König and co-workers (entries 1–3). The same outcome regarding the envisioned carbanion trapping was observed when K_2HPO_4 was utilized as the deprotonation system, irrespective of the tested stoichiometry, enone **188** was formed exclusively in an enhanced yield of up to 81% (entries 4–6). A change of the solvent from DMF to DMA with tenfold excess of aldehyde **213** did not have any effect on the examined reaction (entries 7 and 8). The exclusive formation of addition-elimination product **188** illustrates the strong driving force behind the expulsion of the OBoc-group which is triggered after carbanion formation during the photocatalytic process, making the anionic species inaccessible even in high excess amounts of the present electrophile.

Table 8. Screening of envisioned photocatalytic carbanion trapping.
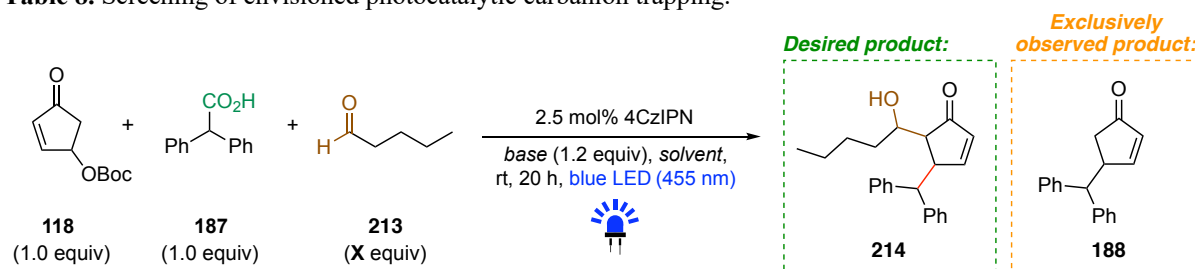
| Entry	213 (equiv)	Base	Solvent	NMR yield (%)^a 188
1	1.0	Cs_2CO_3	DMF	46
2	3.0	Cs_2CO_3	DMF	44
3	10.0	Cs_2CO_3	DMF	40
4	1.0	K_2HPO_4	DMF	81
5	3.0	K_2HPO_4	DMF	79
6	10.0	K_2HPO_4	DMF	74
7	10.0	Cs_2CO_3	DMA	42
8	10.0	K_2HPO_4	DMA	72

^{a}NMR yield using 1,1,2,2-tetrachloroethane as an internal standard.

Potentially, the generated carbanion species **D** (see Scheme 60 for reference) is not stabilized enough to undergo a conjugate intermolecular addition to aldehydes as original reports from König et al.[128] already outlined that efficient radical generation was only achieved from phenyl acetic acids, thus affording the corresponding stabilized benzyl anions, whereas aliphatic carboxylic acids did not lead to the desired product formation.

C Summary

The present thesis deals with the efficient and visible-light mediated conversion of renewable resources derived 4-hydroxy-2-cyclopentenone **116** and its corresponding derivatives towards valuable structural motifs. An envisioned approach towards precious cyclopentanonyl-fused tetrahydrofuran (CpO-THF) frameworks was realized after identifying a highly efficient protocol utilizing organic photocatalyst 4CzIPN (**36**) and *N*-Boc L-serine (**150**) as the model radical precursor, affording bicyclic fused ether **151** after visible-light induced Decarboxylative Radical Conjugate Addition-Elimination (*DcRCAE*)-oxa Michael reaction cascade (Scheme 62).

Model reaction with optimized conditions
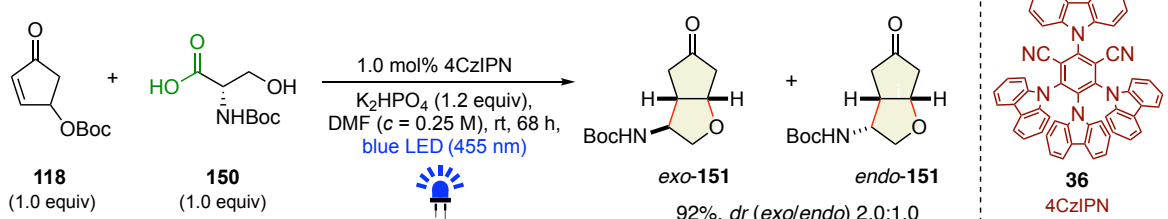
**Scheme 62.** Optimized reaction conditions for the photocatalzyed DcRCAE-oxa-Michael reaction cascade.

The practicality of the developed methodology was showcased via an upscaling approach, affording the CpO-THF motif **151** in a multigram-scale and thus making it accessible in larger amounts for future derivatizations. Interestingly, uncyclized radical addition product **160** was observed during these studies, which could be later successfully cyclized by applying an assisted cyclization approach (Scheme 63).

Upscaling experiment with developed cyclization protocol
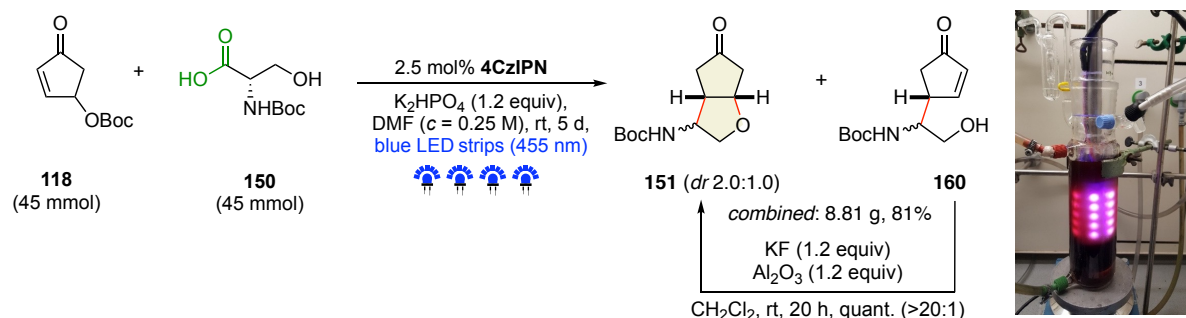
**Scheme 63.** Multigram-scale experiment followed by assisted cyclization of the product mixture.

The designed synthetic protocol was subsequently expanded to a variety of different types of carboxylic acids as radical precursors and substituted hydroxycyclopentenone derivatives to construct numerous structurally intricate molecular frameworks, showcasing the synthetic utility of the photocatalytic DcRCAE-oxa-Michael reaction (Scheme 64).
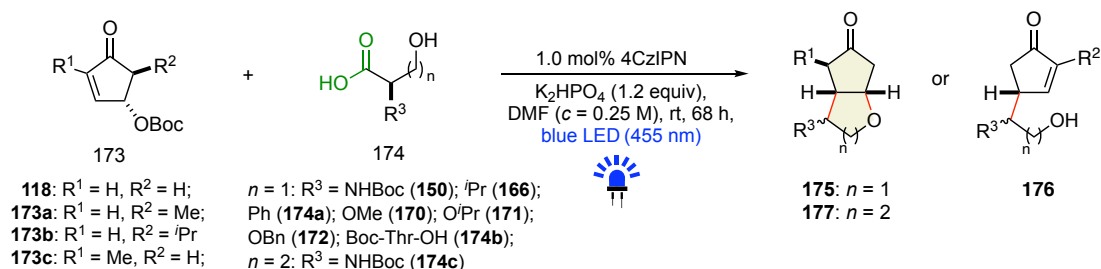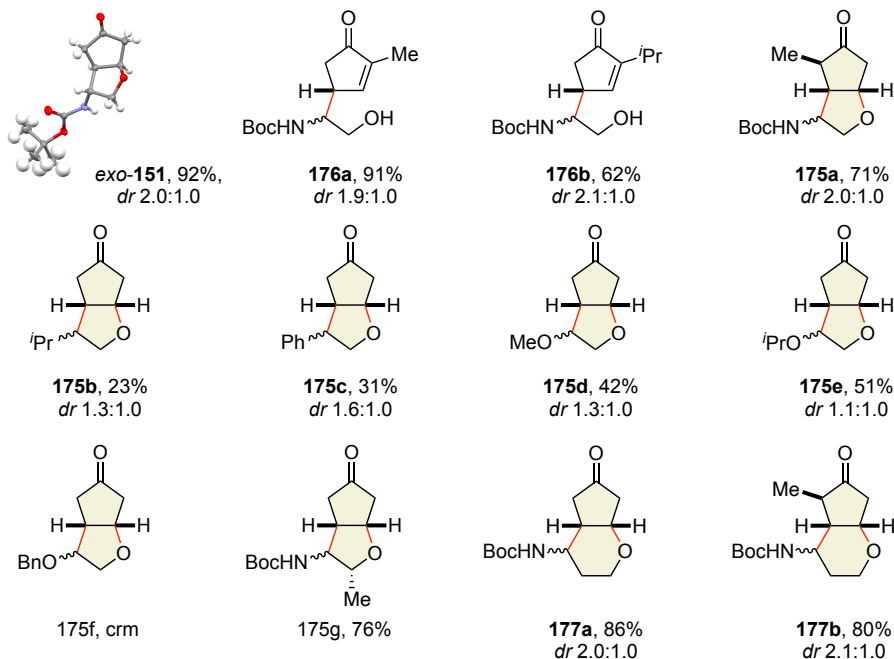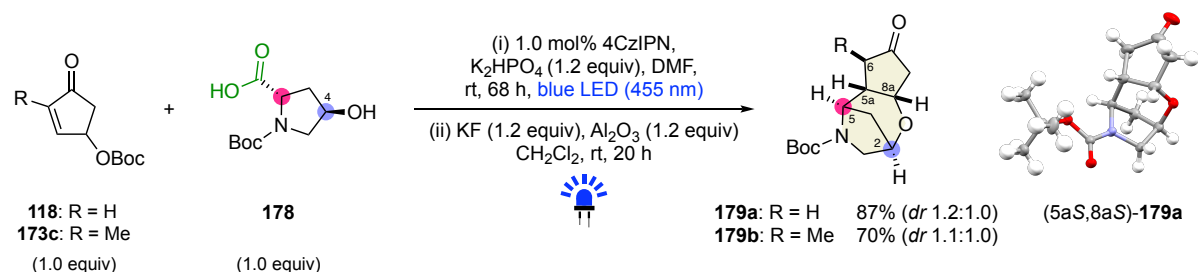
Scheme 64. Extended substrate scope of the developed methodology.

The rapid and facile construction of CpO-THF frameworks enabled by the developed methodology was exploited in a next step of this present work to expeditiously access highly potent and enantioenriched HIV-1 protease inhibitors **125** and **126** upon a few steps of synthetic manipulations. The efficient access towards the required P2-ligand starting from enantiopure (*S*)-**118** significantly streamlines the synthetic sequence towards these desirable drug candidates, considerably improving earlier reported approaches in terms of efficiency and sustainability (Scheme 65).

Enantioselective total syntheses of potent HIV-1 protease inhibitors
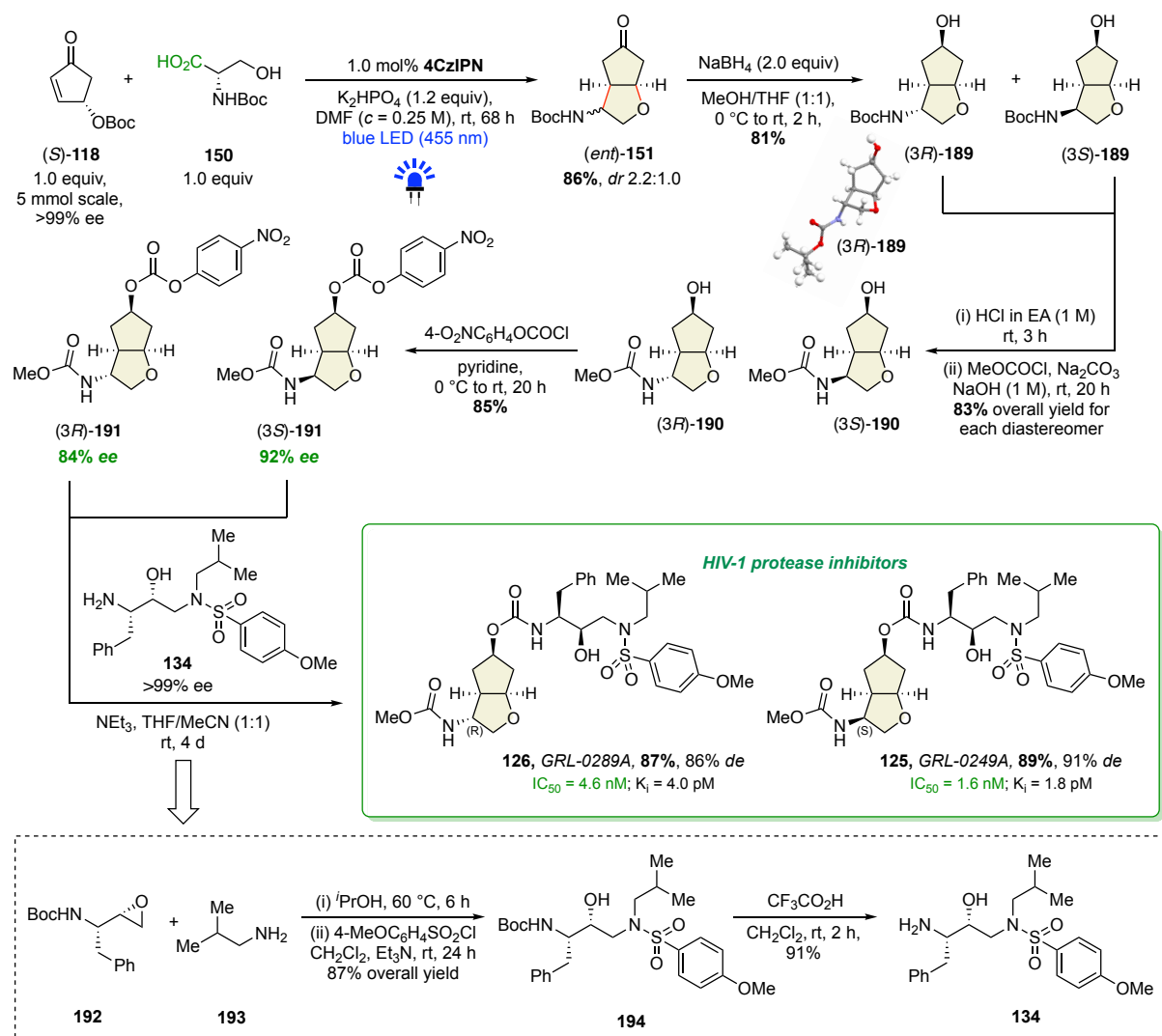
Scheme 65. Total synthesis of potent HIV-1 protease inhibitors **125** and **126**.

To conclude, a novel visible-light mediated, cost-effective and highly sustainable synthetic route to access structurally variegated cyclopentanonyl-fused functionalized cyclic ether derivatives was developed. With this strategy, the total syntheses of potent HIV-1 protease inhibitors in diastereo- and enantioenriched forms was achieved from easily obtainable, renewable resource-derived starting materials (Scheme 66).[69]
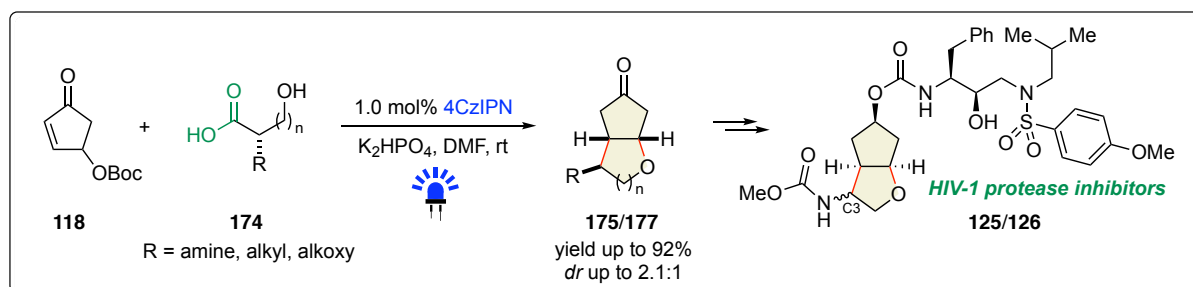

Scheme 66. Photocatalytic DcRCAE-oxa-Michael reaction and total synthesis of HIV-1 protease inhibitors.

D Zusammenfassung

Die vorliegende Arbeit befasst sich mit der effizienten, durch sichtbares Licht vermittelten Umwandlung von aus nachwachsenden Rohstoffen gewonnenem 4-Hydroxy-2-cyclopentenon (**116**) und seinen entsprechenden Derivaten zu wertvollen Strukturmotiven. Ein ins Auge gefasster Ansatz hin zu kostbaren Cyclopentanonyl-kondensierten Tetrahydrofuran-Gerüsten (CpO-THF) wurde nach Identifizierung eines hocheffizienten Protokolls unter Verwendung des organischen Photokatalysators 4CzIPN (**36**) und *N*-Boc L-Serin (**150**) als Modellradikalvorläufer realisiert, dass nach einer durch sichtbares Licht induzierten, decarboxylativen und konjugierten Radikal Addition-Eliminierungskaskade (*DcRCAE*) den bizyklischen kondensierten Ether **151** ergibt (Schema 1).
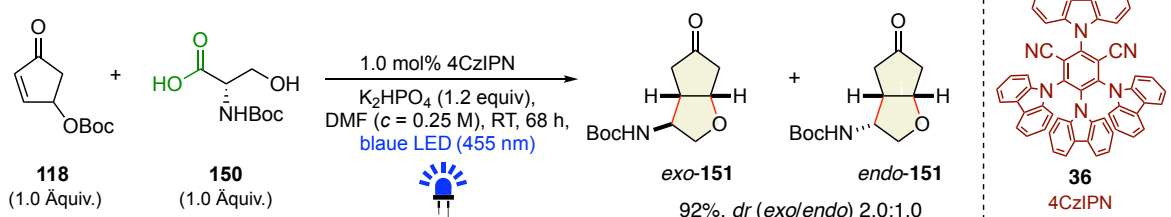
Schema 1. Optimierte Reaktionsbedingungen für die photokatalysierte DcRCAE-Oxa-Michael Reaktion.

Die Praktikabilität der entwickelten Methodik wurde durch einen Upscaling-Ansatz demonstriert, der das CpO-THF Strukturmotiv **151** im Multigramm-Maßstab bereitstellt und es somit in größeren Mengen für zukünftige Derivatisierungen zugänglich macht. Interessanterweise wurde während dieser Studien ein nicht zyklisiertes Radikal-additionsprodukt **160** beobachtet, dass später durch Anwendung eines assistierten Zyklisierungsansatzes erfolgreich zum Ringschluss gebracht werden konnte (Schema 2).
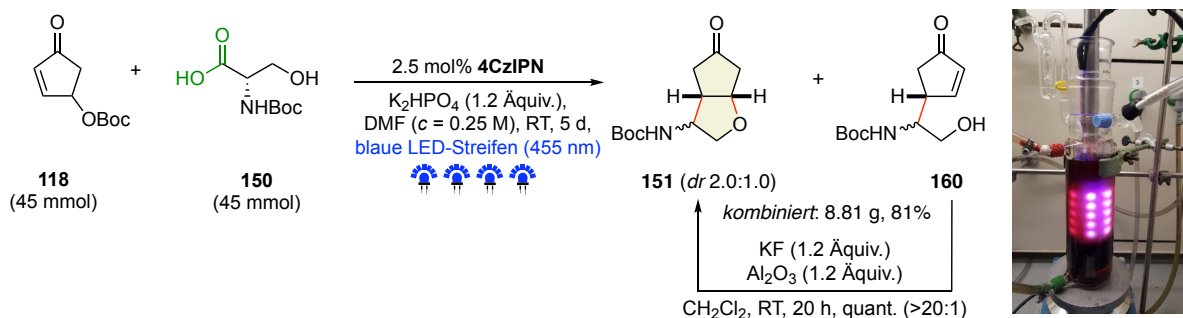
Schema 2. Multigramm-Maßstab-Experiment und anschließende unterstütze Zyklisierung des Produktgemisches.

Das entworfene Syntheseprotokoll wurde anschließend auf eine Vielzahl unterschiedlicher Arten von Carbonsäuren als Radikalvorläufer und weitere substituierte Hydroxycyclopentenon-Derivate ausgeweitet, um zahlreiche strukturell anspruchsvolle Molekülgerüste zu generieren, die den synthetischen Nutzen der photokatalytischen DcRCAE-Oxa-Michael Reaktion aufzeigen (Schema 3).
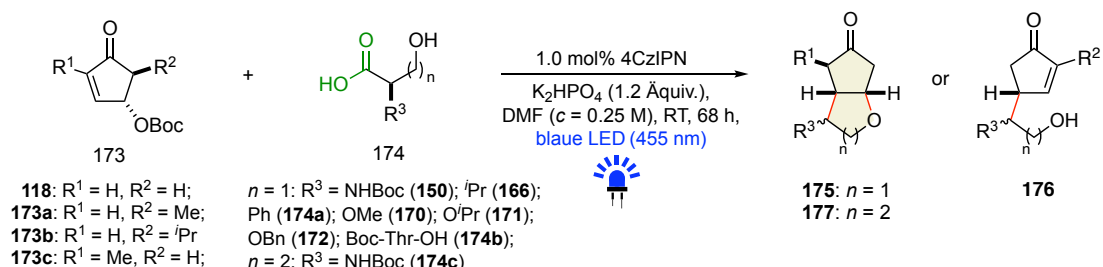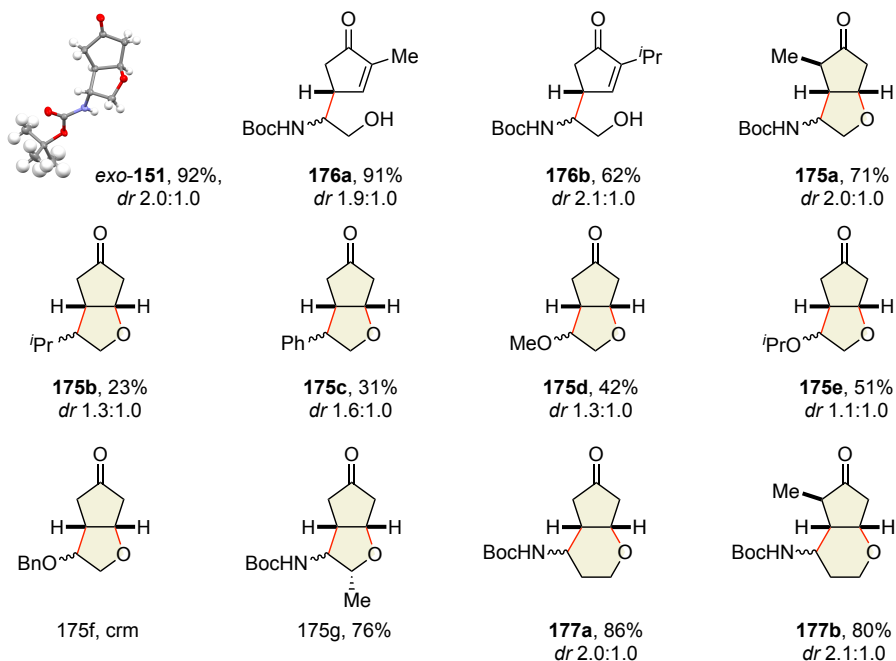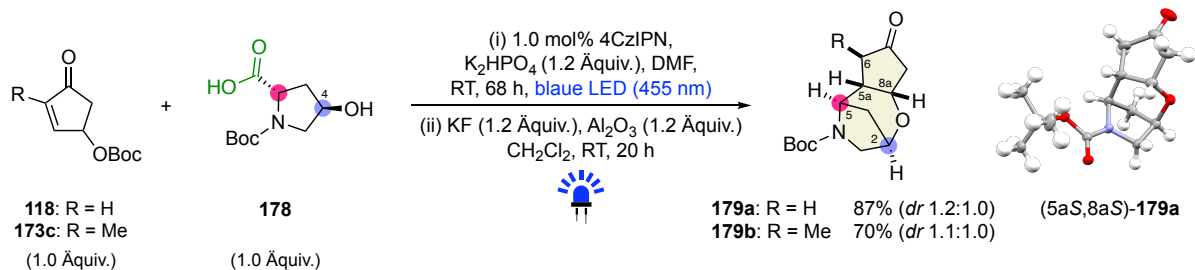
Schema 3. Erweiterter Substratumfang der entwickelten Methodik.

Die schnelle und einfache Konstruktion von CpO-THF-Gerüsten, die durch die entwickelte Methodik ermöglicht wird, wurde in einem nächsten Schritt dieser vorliegenden Arbeit genutzt, um mit wenigen synthetischen Manipulationen schnell zu den hochwirksamen und

enantiomerenangereicherten HIV-1-Proteaseinhibitoren **125** und **126** zu gelangen. Der effiziente Zugang zum erforderlichen P2-Liganden ausgehend von enantiomerenreinem (*S*)-**118** vereinfacht die Synthesesequenz für diese begehrten Wirkstoffkandidaten erheblich und verbessert frühere Ansätze deutlich in Bezug auf Effizienz und Nachhaltigkeit (Schema 4).

Schema 4. Totalsynthese der wirksamen HIV-1 Proteaseinhibitoren **125** und **126**.

Zusammenfassend lässt sich feststellen, dass ein neuartiger, durch sichtbares Licht vermittelter, kostengünstiger und äußerst nachhaltiger Syntheseweg für den Zugang zu strukturell vielfältigen Cyclopentanonyl-kondensierten zyklischen Etherderivaten entwickelt wurde. Mit Hilfe dieser Strategie wurde darüberhinaus die Totalsynthese von potenten HIV-1 Proteaseinhibitoren in diastereomeren- und enantiomerenangereicherter Form aus leicht erhältlichen und aus erneuerbaren Ressourcen stammenden Ausgangsmaterialien erreicht (Schema 5).[69]
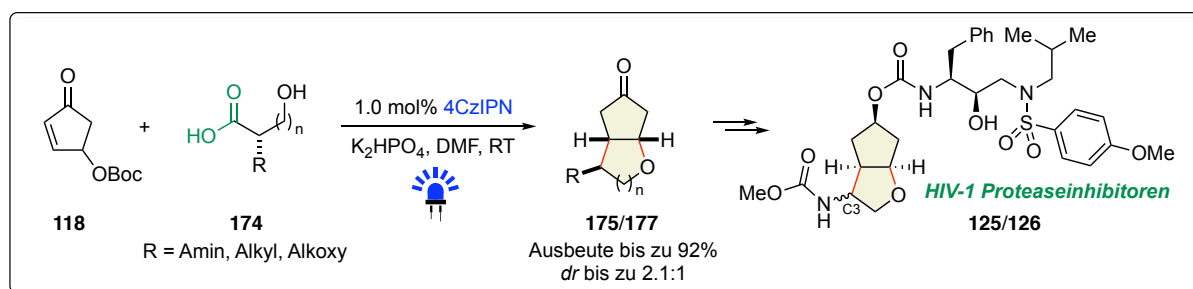
Schema 5. Photokatalytische DcRCAE-Oxa-Michael Reaktion und Totalsynthese von HIV-1 Proteaseinhibitoren.

E Experimental Part

1 General information

Solvents and Chemicals

Commercially available chemicals were employed without further purification if not stated otherwise. Reactions with moisture or oxygen sensitive reagents were carried out in flame-dried glass ware under an atmosphere of predried nitrogen. Hexanes (40-60 °C), EtOAc and DCM were distilled before use for column chromatography. Anhydrous solvents were prepared according to standard procedures.[129] Reported yields are referred to isolated compounds if not stated otherwise.

Thin Layer Chromatography (TLC)

TLC was performed on alumina plates coated with silica gel (Merck silica gel 60 F_{254}, d = 0.2 mm). Visualization was accomplished by irradiation with UV-light (λ = 254 nm) or staining with suitable reagents (potassium permanganate, vanillin/sulfuric acid).

Column Chromatography

(Flash-) Column chromatography was performed using Merck Geduran 60 (0.063–0.200 mm) or Merck flash silica gel 60 (0.040–0.063 mm).

NMR Spectroscopy

All NMR spectra were measured using a Bruker Avance 300 (^{1}H: 300 MHz, ^{13}C: 75 MHz, T = 300 K) or a Bruker Avance III HD 400 spectrometer (^{1}H: 400 MHz, ^{13}C: 101 MHz, T = 300 K). The chemical shifts are reported in δ [ppm] relative to an internal standard, represented by the solvent residual peak, while the coupling constants J are given in Hertz [Hz]. All spectra were analyzed by first order. Abbreviations used for signal multiplicities: s = singlet, br s = broad singlet, d = doublet, t = triplet, q = quartet, p = pentet, hept = heptet, m = multiplet, dd = doublet of doublets, td = triplet of doublets, qd = quartet of doublets, dt = doublet of triplets, ddd = doublet of doublet of doublets, ddt = doublet of doublet of triplets.

Mass Spectrometry

Mass spectrometry was performed by the Central Analytical Department of the University of Regensburg using a Jeol AccuTOF GCX, Agilent Q-TOF 6540 UHD, Finnigan MAT SSQ 710 A or a ThermoQuest Finnigan TSQ 7000. High-resolution mass spectra were measured using atmospheric pressure chemical ionization (APCI), electron ionization (EI) or electrospray ionization (ESI) with a quadrupole time-of-flight (Q-TOF) detector.

IR Spectroscopy

FTIR spectroscopy was carried out on an Agilent Technologies Cary 630 FTIR spectrometer. Solid and liquid compounds were measured neatly and wave numbers are reported in cm^{-1}.

X-Ray Crystallography

X-ray crystallographic analysis was performed by the Central Analytic Department of the University of Regensburg using an Agilent Technologies SuperNova, an Agilent Technologies Gemini R Ultra, an Agilent GV 50 or a Rigaku GV 50 diffractometer. Suitable crystals were mounted on a Lindemann tube oil and kept at a steady temperature of T = 123 K or T = 100 K during data collection. The structures were solved with the SheIXT (Scheldrick 2015) structure solution program using the Intrinsic Phasing solution method and by using Olex2 as the graphical interface.[130,131] The model was refined with SheIXL using Least Squares minimization.[132]

HPLC

HPLC was performed on a Varian 920-LC with a photodiode array (PDA) detector, using a specified chiral stationary phase.

Optical Rotation

The optical rotation was determined on an Anton Paar MCP 500 polarimeter at 589 nm wavelength (sodium-*d*-line) in a 1.0 dm measuring cell.

Melting Point

Measurements of melting point (mp) were carried out on a SRS MPA 100 – Automated melting point system by OptiMelt using a ramp rate of 1 K/min.

Light Source and Photographs

Photochemical reactions were performed using a LED-stick as irradiation source if not stated otherwise. For the detailed reaction setup see Figure 1 in section 2. Blue light irradiation was carried out using an OSLON 80 rb (3 W, 700 mA, λ_{max} = 455 nm) or OSLON SSL 80 (3 W, 700 mA, λ_{max} = 455 nm). Green light irradiation was carried out using an OSLON SSL 80 (3 W, 700 mA, λ_{max} = 530 nm).

2   Photochemical set-up
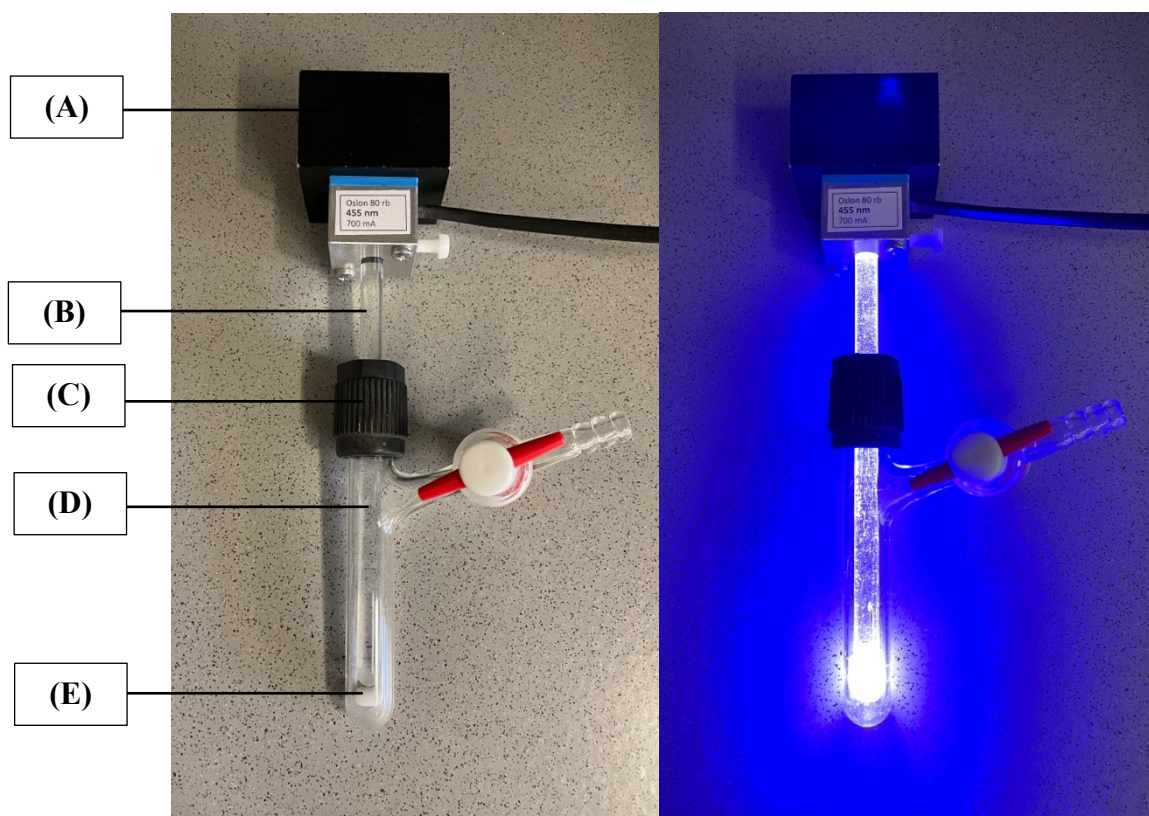
Figure S1. Standard irradiation setup for photochemical reactions (0.75 mmol scale): (**A**) 455 nm LED; (**B**) glass rod; (**C**) Teflon adapter; (**D**) Schlenk tube (10 mL size); (**E**) Teflon-coated stirring bar.

3 Synthesis of starting materials

3.1 Boc-protection of hydroxycyclopentenones

General Procedure I for the activation of hydroxycyclopentenones via Boc-protection

To a solution of hydroxycyclopentenone (25.0 mmol, 1.00 equiv) and Boc$_2$O (6.5 g, 30.0 mmol, 1.20 equiv) in 25 mL THF were added NEt$_3$ (3.04 g, 4.2 mL, 30.0 mmol, 1.20 equiv) and DMAP (61 mg, 0.50 mmol, 2.0 mol%). After stirring the reaction mixture for 30 min at ambient temperature, the solvent was removed under reduced pressure and the crude product was purified by column chromatography on silica gel (hexanes / EtOAc 10:1 to 5:1) to afford protected hydroxycyclopentenone **1**.

***Tert*-butyl (4-oxocyclopent-2-en-1-yl) carbonate (118)**[121]
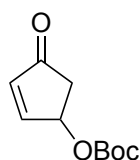
According to general procedure **I**, 4-hydroxycyclopent-2-en-1-one (2.45 g, 25.0 mmol, 1.00 equiv) was reacted with Boc$_2$O to yield protected hydroxycyclopentenone **118** (4.00 g, 20.2 mmol, 81%) as a white solid. The spectroscopic data is in accordance with those reported in literature.[121]

^{1}H-NMR (300 MHz, CDCl$_3$) δ 7.60 (dd, J = 5.7, 2.4 Hz, 1H), 6.33 (dd, J = 5.7, 1.2 Hz, 1H), 5.72 (ddt, J = 3.5, 2.2, 1.8 Hz, 1H), 2.83 (dd, J = 18.7, 6.4 Hz, 1H), 2.41 (dd, J = 18.7, 2.2 Hz, 1H), 1.50 (s, 9H).

^{13}C-NMR (75 MHz, CDCl$_3$) δ 204.7, 158.8, 152.8, 137.3, 83.4, 74.3, 41.1, 27.8.

(S)-Tert-butyl (4-oxocyclopent-2-en-1-yl) carbonate ((S)-118)[121]
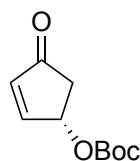
(R)-Tert-butyl (4-oxocyclopent-2-en-1-yl) carbonate ((R)-118)[121]
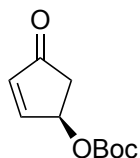
A flame dried reaction vessel was charged with racemic **118** (6.34 g, 32.0 mmol, 2.00 equiv), 4-methoxyphenol (1.99 g, 16.0 mmol, 1.00 equiv) and Cs_2CO_3 (1.54 g, 4.75 mmol, 0.30 equiv) in anhydrous DCM (140 mL). The resulting solution was cooled to 0 °C and the catalyst solution, being separately prepared by stirring $Pd_2dba_3 \cdot CHCl_3$ (166 mg, 0.16 mmol, 1.0 mol%) with either (S,S)- or (R,R)-DACH-phenyl Trost ligand (387 mg, 0.56 mmol, 3.5 mol%) in anhydrous DCM (70 mL) until the color of the solution changes from initially purple to yellow-brown (4–5 min), was added under nitrogen atmosphere. After stirring the reaction mixture for 4 h at 0 °C, the solvent was removed under reduced pressure without any external heat and the crude product was purified by column chromatography on silica gel (PE:EA 7:1 to 3:1) to afford enantiomerically pure (S)-**118** (2.68 g, 13.8 mmol, 42%, >99% ee) or (R)-**118** (2.73 g, 13.8 mmol, 43%, >99% ee) as a yellowish oil. The spectroscopic data is in accordance with those reported in literature.[121]

(S)-Tert-butyl (4-oxocyclopent-2-en-1-yl) carbonate ((S)-**118**):

$[\alpha]_D^{20}$ = - 91.4 ° (c = 1.0, $CHCl_3$).

HPLC (OJ-H, i-propanol/n-heptane = 1/99, flow rate = 1.0 mL/min, I = 215 nm): t_R = 14.63 min (major), >99% ee.

(R)-Tert-butyl (4-oxocyclopent-2-en-1-yl) carbonate ((R)-**118**):

$[\alpha]_D^{20}$ = + 92.3 ° (c = 1.0, $CHCl_3$).

HPLC (OJ-H, i-propanol/n-heptane = 1/99, flow rate = 1.0 mL/min, I = 215 nm): t_R = 13.27 min (major), >99% ee.
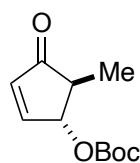
(±)-*Tert*-butyl ((1*R*,5*S*)-5-methyl-4-oxocyclopent-2-en-1-yl) carbonate (173a)

According to general procedure **I**, (±)-4-hydroxy-5-methylcyclopent-2-en-1-one (2.80 g, 25.0 mmol, 1.00 equiv) was reacted with Boc$_2$O to yield the protected hydroxycyclopentenone **173a** (4.37 g, 20.6 mmol, 82%) as a white solid.

R_f (hexanes / EtOAc 3:1 on silica) = 0.50.

mp: 36–38 °C.

^{1}H-NMR (300 MHz, CDCl$_3$) δ 7.49 (dd, J = 5.8, 2.3 Hz, 1H), 6.26 (dd, J = 5.8, 1.3 Hz, 1H), 5.31–5.22 (m, 1H), 2.38 (qd, J = 7.6, 2.6 Hz, 1H), 1.46 (s, 9H), 1.25 (d, J = 7.5 Hz, 3H).

^{13}C-NMR (75 MHz, CDCl$_3$) δ 206.8, 157.2, 153.0, 135.9, 83.2, 81.6, 47.0, 27.7, 13.3.

IR $\tilde{v}_{max}$ (neat, cm^{-1}) 2978, 2937, 2877, 1722, 1457, 1394, 1326, 1252, 1159, 1088, 1039, 1002, 957, 913, 853, 827, 793, 726.

HRMS (ESI): *m/z* calculated for C$_{11}$H$_{17}$O$_4$ (M+H)$^+$: 213.1121, found 213.1118.

(±)-*Tert*-butyl ((1*R*,5*S*)-5-isopropyl-4-oxocyclopent-2-en-1-yl) carbonate (173b)

According to general procedure **I**, (±)-(4*R*,5*S*)-4-hydroxy-5-isopropylcyclopent-2-en-1-one (3.50 g, 25.0 mmol, 1.00 equiv) was reacted with Boc$_2$O to yield the protected hydroxy-cyclopentenone **173b** (4.51 g, 18.8 mmol, 75%) as a white solid.

R_f (hexanes / EtOAc 3:1 on silica) = 0.60.

mp: 66–68 °C.

^{1}H-NMR (400 MHz, CDCl$_3$) δ 7.55 (dd, J = 5.8, 2.4 Hz, 1H), 6.28 (dd, J = 5.8, 1.2 Hz, 1H), 5.61 (td, J = 2.4, 1.2 Hz, 1H), 2.41 (dd, J = 4.1, 2.6 Hz, 1H), 2.36–2.27 (m, 1H), 1.51 (s, 9H), 1.03 (d, J = 7.0 Hz, 3H), 0.88 (d, J = 6.9 Hz, 3H).

^{13}**C-NMR** (101 MHz, CDCl$_3$) δ 206.4, 157.8, 152.9, 136.9, 83.2, 76.8, 56.9, 27.8, 27.2, 20.1, 18.2.

IR $\tilde{v}_{max}$ (neat, cm^{-1}) 2970, 2873, 1714, 1595, 1461, 1397, 1330, 1252, 1155, 1103, 950, 857.

HRMS (ESI): *m/z* calculated for C$_{13}$H$_{21}$O$_4$ (M+H)$^+$: 241.1434, found 241.1437.

***Tert*-butyl (3-methyl-4-oxocyclopent-2-en-1-yl) carbonate (173c)**
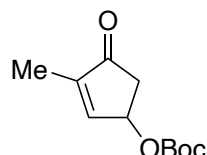
According to general procedure **I**, 4-hydroxy-2-methylcyclopent-2-en-1-one (2.80 g, 25.0 mmol, 1.00 equiv) was reacted with Boc$_2$O to yield the protected hydroxycyclopentenone **173c** (4.31 g, 20.3 mmol, 81%) as a white solid.
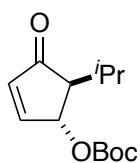
R$_f$ (hexanes / EtOAc 5:1 on silica) = 0.40.

mp: 59–61 °C.

^{1}**H-NMR** (400 MHz, CDCl$_3$) δ 7.22 (dt, J = 3.0, 1.5 Hz, 1H), 5.64–5.57 (m, 1H), 2.84 (dd, J = 18.8, 6.3 Hz, 1H), 2.42 (dd, J = 18.8, 2.0 Hz, 1H), 1.82 (t, J = 1.6 Hz, 3H), 1.50 (s, 9H).

^{13}**C-NMR** (101 MHz, CDCl$_3$) δ 204.8, 152.9, 152.1, 145.9, 83.0, 72.7, 41.1, 27.8, 10.0.

IR $\tilde{v}_{max}$ (neat, cm^{-1}) 2981, 2948, 2922, 2877, 1710, 1442, 1408, 1364, 1326, 1252, 1159, 1103, 991, 887, 790.

HRMS (ESI): *m/z* calculated for C$_{11}$H$_{17}$O$_4$ (M+H)$^+$: 213.1121, found 213.1120.

3.2 Synthesis of carboxylic acids as radical precursors

2-(Hydroxymethyl)-3-methylbutanoic acid (166)[119]
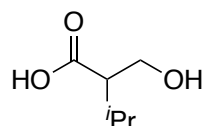
To a solution of pyrrolidine (71 mg, 82 μL, 1.00 mmol, 0.10 equiv), formaldehyde (37% solution in water, 2.24 mL, 30.0 mmol, 3.00 equiv) and pH 7 buffer (equimolar mixture of K$_2$HPO$_4$ and KH$_2$PO$_4$, 1.00 g) in toluene (20 mL) was added freshly distilled isovaleraldehyde

(**162**) (861 mg, 1.07 mL, 10.0 mmol, 1.00 equiv). After vigorous stirring for 36 h at ambient temperature, the reaction mixture was extracted with toluene (3 × 10 mL) and the combined organic layers were dried over Na_2SO_4 and concentrated in vacuo. In a second reaction step, the resulting residue is dissolved in *tert*-butanol (50 mL) followed by the addition of freshly distilled 2-methyl-2-butene (3.51 g, 5.31 mL, 50.0 mmol, 5.00 equiv). The resulting mixture was cooled to 0 °C and a separately prepared solution of sodium chlorite (3.62 g, 40.0 mmol, 4.00 equiv) and NaH_2PO_4 (4.80 g, 40.0 mmol, 4.00 equiv) in water (25 mL) was added dropwise. After stirring for 6 h at ambient temperature, *tert*-butanol was removed under reduced pressure and the resulting aqueous phase was diluted with EtOAc (40 mL), brine (15 mL) and aqueous hydrochloric acid solution (2.7 M, 15 mL). The phases were separated and the remaining aqueous phase was extracted with EtOAc (3 × 40 mL). After drying the combined organic layers over Na_2SO_4 and removal of the solvent in vacuo, the crude product was purified by column chromatography on silica gel (DCM / MeOH 9:1) to yield carboxylic acid **166** (1.12 g, 8.47 mmol, 85%) as a white solid. The spectroscopic data is in accordance with those reported in literature.[119]

^{1}H-NMR (400 MHz, CDCl$_3$) δ 6.35 (br s, 1H), 3.88 (dd, J = 11.2, 8.4 Hz, 1H), 3.80 (dd, J = 11.2, 4.0 Hz, 1H), 2.44 (ddd, J = 8.4, 7.1, 4.0 Hz, 1H), 2.06 (hept, J = 6.8 Hz, 1H), 1.01 (d, J = 4.4, 3H), 0.99 (d, J = 4.4 Hz, 3H).
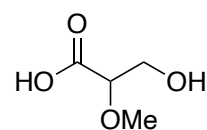
^{13}C-NMR (101 MHz, CDCl$_3$) δ 180.2, 61.4, 54.1, 27.7, 20.6, 20.1.

3-Hydroxy-2-methoxypropanoic acid (170)[120]

L-Serine (750 mg, 7.14 mmol, 1.00 equiv), isoamyl nitrite (927 mg, 1.06 mL, 7.92 mmol, 1.11 equiv), MgSO$_4$ (902 mg, 7.50 mmol, 1.05 equiv) and glacial acetic acid (270 mg, 0.26 mL, 4.5 mmol, 0.63 equiv) were dissolved in MeOH (**167**; 15 mL, 52.0 equiv) and heated to 110 °C for 4 h in a sealed pressure tube. The cooled mixture was filtered and evaporated under reduced pressure. The crude product was resolved in water and washed with CHCl$_3$ (3 × 20 mL) and EtOAc (3 × 20 mL) to yield carboxylic acid **170** (430 mg, 3.58 mmol, 50%) after evaporation of the aqueous phase as a colorless oil. The spectroscopic data is in accordance with those reported in literature.[120]

¹H-NMR (400 MHz, D$_2$O) δ 4.05 (dd, J = 5.2, 3.2 Hz, 1H), 3.93 (dd, J = 12.3, 3.2 Hz, 1H), 3.81 (dd, J = 12.2, 5.2 Hz, 1H), 3.45 (s, 3H).

¹³C-NMR (101 MHz, D$_2$O) δ 174.6, 81.0, 61.5, 57.7.

3-Hydroxy-2-isopropoxypropanoic acid (171)[120]
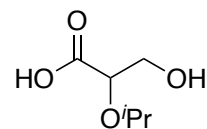
L-Serine (525 mg, 5.00 mmol, 1.00 equiv), isoamyl nitrite (650 mg, 0.75 mL, 5.55 mmol, 1.11 equiv), MgSO$_4$ (632 mg, 5.25 mmol, 1.05 equiv) and glacial acetic acid (189 mg, 0.18 mL, 3.15 mmol, 0.63 equiv) were dissolved in isopropanol (**168**; 20 mL, 52.0 equiv) and heated to 110 °C for 4 h in a sealed pressure tube. The cooled mixture was filtered and evaporated under reduced pressure. The residue was resolved in water and washed with CHCl$_3$ (3 × 15 mL) and EtOAc (3 × 15 mL). After evaporation of the aqueous phase, the resulting crude product was purified by column chromatography on silica gel (CHCl$_3$ / MeOH 9:1) to afford carboxylic acid **171** (231 mg, 1.56 mmol, 31%) as a yellowish oil.

R_f (CHCl$_3$ / MeOH 9:1 on silica) = 0.35.

¹H-NMR (400 MHz, D$_2$O) δ 4.19 (dd, J = 5.7, 3.6 Hz, 1H), 3.85–3.75 (m, 3H), 1.18 (dd, J = 6.2, 3.3 Hz, 6H).

¹³C-NMR (101 MHz, D$_2$O) δ 175.7, 77.3, 73.0, 62.4, 21.4, 20.9.

IR $\tilde{v}_{max}$ (neat, cm^{-1}) 3354, 2974, 2937, 2885, 1722, 1461, 1379, 1207, 1110, 1051, 965, 894, 816, 764, 726.

HRMS (ESI): m/z calculated for C$_6$H$_{11}$O$_4$ (M-H)$^-$: 147.0663, found 147.0663.

2-(Benzyloxy)-3-hydroxypropanoic acid (172)[120]
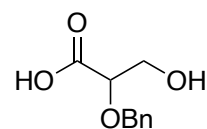
L-Serine (631 mg, 6.00 mmol, 1.00 equiv), isoamyl nitrite (780 mg, 0.89 mL, 6.66 mmol, 1.11 equiv), MgSO$_4$ (758 mg, 6.3 mmol, 1.05 equiv) and glacial acetic acid (227 mg, 0.22 mL, 3.78 mmol, 0.63 equiv) were dissolved in benzylalcohol (**169**; 32 mL, 52.0 equiv) and heated to 110 °C for 4 h in a sealed pressure tube. The cooled mixture was filtered and subsequently

distilled under reduced pressure to remove excess benzylalcohol. The resulting residue was purified by column chromatography on silica gel (CHCl$_3$ / MeOH 9:1) to afford carboxylic acid **172** (322 mg, 1.64 mmol, 27%) as a yellowish oil.

R_f (CHCl$_3$ / MeOH 9:1 on silica) = 0.30.

^{1}H-NMR (300 MHz, D$_2$O) δ 7.45–7.34 (m, 5H), 4.69 (d, J = 11.5 Hz, 1H), 4.55 (d, J = 11.5 Hz, 1H), 4.17–4.08 (m, 1H), 3.85 (dd, J = 12.1, 3.5 Hz, 1H), 3.78 (dd, J = 12.1, 5.4 Hz, 1H).

^{13}C-NMR (75 MHz, D$_2$O) δ 174.9, 136.7, 128.8, 128.7, 128.5, 79.0, 72.4, 62.0.

IR $\tilde{v}_{max}$ (neat, cm^{-1}) 3350, 3034, 2937, 2877, 2512, 1722, 1602, 1453, 1401, 1326, 1207, 1118, 1043, 909, 738, 697.

HRMS (ESI): m/z calculated for C$_{10}$H$_{11}$O$_4$ (M-H)$^-$: 195.0663, found 195.0667.

N-Boc L-threonine (174b)[133]
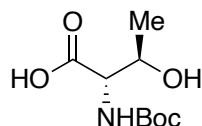
To a solution of L-threonine (595 mg, 5.0 mmol, 1.00 equiv) in water (8 mL) and dioxane (3 mL) was added DIPEA (969 mg, 1.28 mL, 1.50 mmol, 1.50 equiv) and a second solution of Boc$_2$O (1.36 g, 6.25 mmol, 1.25 equiv) in dioxane (3 mL). The mixture was acidified to pH = 3 after 24 h of stirring at ambient temperature using a 2 M HCl-solution and was subsequently extracted with EtOAc (3 × 15 mL). The combined organic layers were dried over Na$_2$SO$_4$ and the solvent was concentrated in vacuo to give rise to protected amino acid **174b** (868 mg, 3.96 mmol, 79%) as a white solid. The spectroscopic data is in accordance with those reported in literature.[133]

^{1}H-NMR (400 MHz, DMSO-d$_6$) δ 6.29 (d, J = 9.0 Hz, 1H), 4.07–3.99 (m, 1H), 3.86 (dd, J = 9.1, 3.3 Hz, 1H), 1.38 (s, 9H), 1.07 (d, J = 6.4 Hz, 3H).

^{13}C-NMR (101 MHz, DMSO-d$_6$) δ 172.5, 155.7, 78.3, 66.5, 59.4, 28.2, 20.4.

4 General procedure for the photocatalytic DcRCAE-oxa-Michael reaction

General Procedure II for the photocatalytic DcRCAE-Oxa-Michael Reaction

173   **174**   **175**: $n = 1$ **176**
     177: $n = 2$
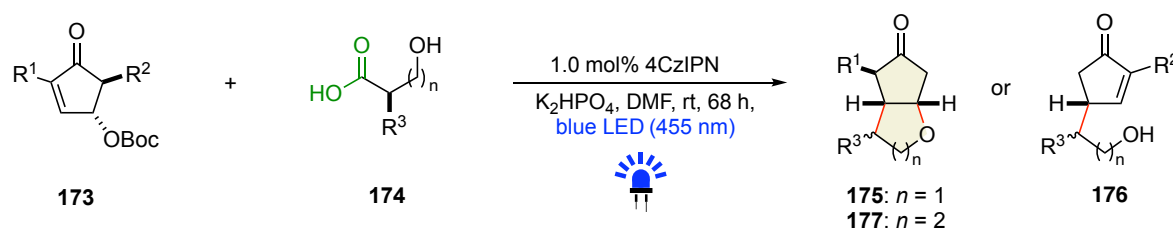
A flame-dried pressure tube was charged with protected hydroxycyclopentenone **173** (0.75 mmol, 1.00 equiv), carboxylic acid **174** (0.75 mmol, 1.00 equiv), K_2HPO_4 (157 mg, 0.90 mmol, 1.20 equiv), 4CzIPN (5.9 mg, 7.50 μmol, 1.0 mol%) and anhydrous DMF (3 mL, 0.25 M) under nitrogen atmosphere. The reaction vessel was sealed with a screw-cap and subsequently degassed by applying three cycles of freeze-pump-thaw-backfill. The screw-cap was replaced by a glass rod and the reaction mixture was placed under a nitrogen atmosphere. After irradiation using a 455 nm high power LED through the pre-installed glass rod (see figure S1) and stirring for 68 h at ambient temperature, the reaction mixture was worked up by two different procedures, depending on the employed carboxylic acid. For **A)** _alkoxy-_ and _amine-substituted_ carboxylic acids as coupling partners (**150**, **170**, **171**, **172**, **174b**, **174c**), the reaction was directly concentrated in vacuo by addition of _p_-xylene to facilitate the removal of DMF. For **B)** _alkyl-substituted_ carboxylic acids as radical precursors (**166**, **174a**), the reaction mixture was diluted with saturated $NaHCO_3$-solution (15 mL), extracted with Et_2O (3 × 40 mL), washed with water (15 mL) and brine (15 mL) and the resulting combined organic layers were dried over Na_2SO_4 and concentrated in vacuo. The crude product was purified for both work-up procedures **A)** and **B)** by flash column chromatography on silica gel with the solvent system indicated. Of note, partially uncyclized coupling products were observed in almost all cases in the crude NMR which, during work-up and purification, cyclized quantitatively unless stated otherwise.

(±)-*Tert*-butyl ((3*S*,3a*S*,6a*S*)-5-oxohexahydro-2*H*-cyclopenta[*b*]furan-3-yl)carbamate (*exo*-151)
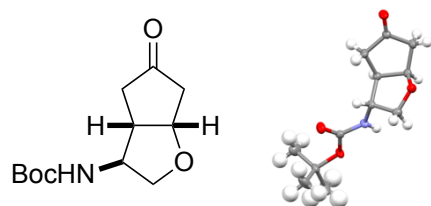
(±)-Tert-butyl ((3*R*,3a*S*,6a*S*)-5-oxohexahydro-2*H*-cyclopenta[*b*]furan-3-yl)carbamate (*endo*-151)
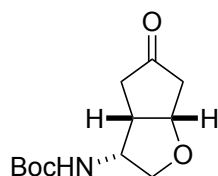
Following general procedure **II**, *tert*-butyl (4-oxocyclopent-2-en-1-yl) carbonate (**118**) (149 mg, 0.75 mmol, 1.00 equiv) was reacted with *N*-Boc L-serine (**150**) (154 mg, 0.75 mmol, 1.00 equiv) to yield bicycle **151** (166 mg, 688 μmol, 92%) as a mixture of two diastereomers *exo*-**151** (major) and *endo*-**151** (minor) in a diastereomeric ratio of 2.0:1.0 after purification by flash column chromatography (hexanes / EtOAc 1:1) on silica gel. Subsequent separation of both diastereomers was exclusively performed and achieved for **151** as the model substrate after a multiple column procedure, giving rise to *exo*-**151** as a white solid and *endo*-**151** as a yellowish oil.

(±)-*Tert*-butyl((3*S*,3a*S*,6a*S*)-5-oxohexahydro-2*H*-cyclopenta[*b*]furan3-yl)carbamate (*exo*-**151**):

R_f (hexanes / EtOAc 1:1 on silica) = 0.46.

mp: 81–83 °C.

^{1}H-NMR (300 MHz, CDCl$_3$) δ 5.37 (br s, 1H), 4.60 (dt, *J* = 6.3, 3.4 Hz, 1H), 4.07–4.00 (m, 1H), 3.99–3.87 (m, 1H), 3.55 (d, *J* = 9.5 Hz, 1H), 2.81–2.61 (m, 1H), 2.57–2.41 (m, 1H), 2.34 (d, *J* = 3.4 Hz, 2H), 1.92 (dd, *J* = 19.6, 7.7 Hz 1H), 1.30 (s, 9H).

^{13}C-NMR (75 MHz, CDCl$_3$) δ 216.6, 155.3, 79.5, 77.5, 72.7, 57.8, 46.8, 45.0, 41.0, 28.3.

IR $\tilde{v}_{max}$ (neat, cm^{-1}) 3325, 2967, 2922, 2870, 1729, 1699, 1524, 1394, 1345, 1297, 1244, 1159, 1095, 1058, 987, 961, 864, 812, 756, 711, 685.

HRMS (ESI): *m/z* calculated for C$_{12}$H$_{20}$NO$_4$ (M+H)$^+$: 242.1387, found 242.1386.

Suitable crystals for X-Ray analysis were obtained by slow evaporation of a Et$_2$O solution containing *exo*-**151**. The crystals obtained were colourless and prism-shaped (CCDC 2085697; see details in section 3 of this chapter).

(±)-*Tert*-butyl ((3*R*,3a*S*,6a*S*)-5-oxohexahydro-2*H*-cyclopenta[*b*]furan-3-yl)carbamate (*endo*-**151**):

R_f (hexanes / EtOAc 1:1 on silica) = 0.42.

^{1}H-NMR (300 MHz, CDCl$_3$) δ 4.83 (br s, 1H), 4.65–4.56 (m, 1H), 4.47–4.33 (m, 1H), 3.98 (dd, *J* = 9.4, 6.9 Hz, 1H), 3.64 (dd, *J* = 9.4, 5.4 Hz, 1H), 3.18–3.03 (m, 1H), 2.50–2.42 (m, 2H), 2.37–2.20 (m, 2H), 1.40 (s, 9H).

^{13}C-NMR (101 MHz, CDCl$_3$) δ 216.2, 155.5, 80.3, 80.1, 72.1, 53.9, 45.2, 43.4, 37.2, 28.3.

IR $\tilde{v}_{max}$ (neat, cm^{-1}) 3328, 2974, 2929, 1744, 1684, 1520, 1390, 1248, 1159, 1058, 1021, 905, 762.

HRMS (ESI): *m/z* calculated for C$_{12}$H$_{20}$NO$_4$ (M+H)$^+$: 242.1387, found 242.1384.

(±)-*Tert*-butyl (2-hydroxy-1-((*R*)-3-methyl-4-oxocyclopent-2-en-1-yl)ethyl)carbamate (176a*)*
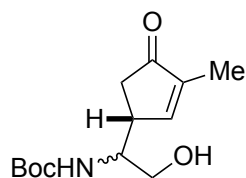
Following general procedure **II**, (±)-*tert*-butyl ((1*R*,5*S*)-5-methyl-4-oxocyclopent-2-en-1-yl) carbonate (**173a**) (159 mg, 0.75 mmol, 1.00 equiv) was reacted with *N*-Boc L-serine (**150**) (154 mg, 0.75 mmol, 1.00 equiv) to yield uncyclized product **176a** (175 mg, 685 μmol, 91%) as an inseparable mixture of two diastereomers (dr 1.9:1.0) as a yellowish oil after purification by flash column chromatography (hexanes / EtOAc 1:1) on silica gel.

R_f (hexanes / EtOAc 1:1 on silica) = 0.22.

^{1}H-NMR (300 MHz, CDCl$_3$, mixture of diastereomers) δ 7.34–7.26 (m, 1H, both), 5.08 (d, *J* = 8.2 Hz, 0.66H, major), 4.91 (d, *J* = 7.1 Hz, 0.34H, minor), 3.85–3.55 (m, 3H, both), 3.12 (br s, 2H, both), 2.58–2.37 (m, 1H, both), 2.31–2.09 (m, 1H, both), 1.79–1.75 (m, 1.05H, minor), 1.75–1.70 (m, 1.95H, major), 1.47–1.30 (m, 9H, both).

^{13}C-NMR (101 MHz, CDCl$_3$, mixture of diastereomers) δ 209.4, 208.9, 159.4, 158.0, 156.3, 156.2, 143.7, 142.8, 80.2, 80.0, 64.1, 63.9, 54.7, 54.5, 41.3, 40.5, 38.6, 37.2, 28.4, 28.4, 10.4, 10.2.

IR $\tilde{v}_{max}$ (neat, cm^{-1}) 3332, 2974, 2929, 1681, 1520, 1390, 1370, 1244, 1162, 1054, 943, 864, 767.

HRMS (ESI): *m/z* calculated for C$_{13}$H$_{21}$NNaO$_4$ (M+Na)$^+$: 278.1363, found 278.1365.

(±)-*Tert*-butyl   (2-hydroxy-1-((*R*)-3-isopropyl-4-oxocyclopent-2-en-1-yl)ethyl)carbamate (176b*)*
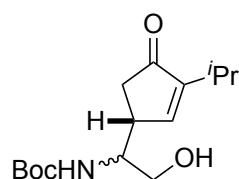
Following general procedure **II**, (±)-*tert*-butyl ((1*R*,5*S*)-5-isopropyl-4-oxocyclopent-2-en-1-yl) carbonate (**173b**) (180 mg, 0.75 mmol, 1.00 equiv) was reacted with *N*-Boc L-serine (**150**) (154 mg, 0.75 mmol, 1.00 equiv) to yield uncyclized product **176b** (132 mg, 466 μmol, 62%) as an inseparable mixture of two diastereomers (dr 2.1:1.0) as a yellowish oil after purification by flash column chromatography (hexanes / EtOAc 1:1) on silica gel.

R$_f$ (hexanes / EtOAc 1:1 on silica) = 0.31.

^{1}H-NMR (400 MHz, CDCl$_3$, mixture of diastereomers) δ 7.26–7.15 (m, 1H, both), 5.04 (d, *J* = 8.5 Hz, 0.68H, major), 4.90 (d, *J* = 8.4 Hz, 0.32H, minor), 3.88–3.56 (m, 3H, both), 3.10 (br s, 2H, both), 2.64–2.39 (m, 2H, both), 2.29–2.13 (m, 1H, both), 1.43–1.35 (m, 9H, both), 1.10–1.00 (m, 6H, both).

^{13}C-NMR (101 MHz, CDCl$_3$, mixture of diastereomers) δ 208.7, 208.1, 156.6, 156.2, 156.1, 155.2, 153.8, 153.1, 80.0, 79.8, 63.9, 54.8, 54.3, 41.0, 40.2, 39.3, 37.8, 28.3, 28.2, 24.8, 24.6, 21.3, 21.2.

IR $\tilde{v}_{max}$ (neat, cm^{-1}) 3343, 2967, 2933, 2877, 1684, 1520, 1364, 1248, 1162, 1054, 1006, 943, 868, 730.

HRMS (ESI): *m/z* calculated for C$_{15}$H$_{26}$NO$_4$ (M+H)$^+$: 284.1856, found 284.1855.

(±)-*Tert*-butyl ((3a*S*,4*R*,6a*S*)-4-methyl-5-oxohexahydro-2*H*-cyclopenta[*b*]furan-3-yl)carbamate (175a*)*
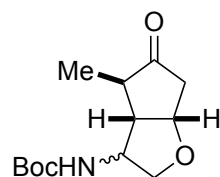
Following general procedure **II**, *tert*-butyl (3-methyl-4-oxocyclopent-2-en-1-yl) carbonate (**173c**) (159 mg, 0.75 mmol, 1.00 equiv) was reacted with *N*-Boc L-serine (**150**) (154 mg, 0.75 mmol, 1.00 equiv) to yield bicycle **175a** (136 mg, 533 μmol, 71%) as an inseparable mixture of two diastereomers (dr 2.0:1.0) as a yellowish oil after purification by flash column chromatography (hexanes / EtOAc 1:1) on silica gel.

R_f (hexanes / EtOAc 1:1 on silica) = 0.53.

^{1}H-NMR (300 MHz, CDCl$_3$, mixture of diastereomers) δ 5.03–4.69 (m, 1H, both), 4.66–4.52 (m, 1H, both), 4.33–3.97 (m, 2H, both), 3.68 (dd, J = 9.9, 2.8 Hz, 0.67H, major), 3.60 (dd, J = 9.4, 6.7 Hz, 0.33H, minor), 2.74–2.48 (m, 2H, both), 2.47–2.25 (m, 1H, both), 2.22–2.14 (m, 0.33H, minor), 2.08–1.92 (m, 0.67H, major), 1.50–1.35 (m, 9H, both), 1.20 (d, J = 7.1 Hz, 2H, major), 1.12 (d, J = 7.3 Hz, 1H, minor).

^{13}C-NMR (101 MHz, CDCl$_3$, mixture of diastereomers) δ 218.5, 218.1, 155.5, 155.3, 80.2, 79.0, 77.7, 73.8, 71.7, 57.0, 55.8, 53.8, 51.3, 46.3, 44.2, 43.9, 42.7, 28.5, 28.4, 15.2, 13.8.

IR $\tilde{v}_{max}$ (neat, cm^{-1}) 3355, 2974, 2933, 1740, 1677, 1520, 1457, 1364, 1159, 1039, 857, 782.

HRMS (ESI): *m/z* calculated for C$_{13}$H$_{22}$NO$_4$ (M+H)$^+$: 256.1543, found 256.1547.

(±)-(3a*S*,6a*S*)-3-Isopropylhexahydro-5*H*-cyclopenta[*b*]furan-5-one (175b*)*

Following general procedure **II**, *tert*-butyl (4-oxocyclopent-2-en-1-yl) carbonate (**118**) (149 mg, 0.75 mmol, 1.00 equiv) was reacted with 2-(hydroxymethyl)-3-methylbutanoic acid (**166**) (99 mg, 0.75 mmol, 1.00 equiv) to yield volatile bicycle **175b** (29 mg, 173 μmol, 23%) as an inseparable mixture of two diastereomers (dr 1.3:1.0) as a yellowish oil after purification by flash column chromatography (hexanes / EtOAc 1:1) on silica gel.
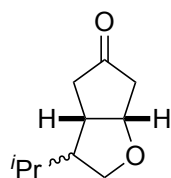
R_f (hexanes / EtOAc 1:1 on silica) = 0.49.

^{1}H-NMR (400 MHz, CDCl$_3$, mixture of diastereomers) δ 4.64 (t, J = 4.5 Hz, 0.57H, major), 4.57–4.50 (m, 0.43H, minor), 4.15–4.03 (m, 1H, both), 3.60 (dd, J = 10.3, 8.4 Hz, 0.57H, major), 3.49 (dd, J = 9.1, 8.1 Hz, 0.43H, minor), 2.65–2.50 (m, 1H, both), 2.50–2.45 (m, 1H, both), 2.44–2.17 (m, 2H, both), 2.17–2.07 (m, 1H, both), 1.69–1.41 (m, 2H, both), 1.00–0.96 (m, 3H, both), 0.92–0.86 (m, 3H, both).

^{13}C-NMR (101 MHz, CDCl$_3$, mixture of diastereomers) δ 216.8, 216.6, 80.8, 79.4, 71.7, 70.9, 54.9, 50.4, 44.5, 43.8, 43.6, 42.7, 42.0, 35.3, 30.3, 27.9, 21.2, 20.9, 20.4, 20.0.

IR $\tilde{v}_{max}$ (neat, cm^{-1}) 2959, 2873, 1744, 1464, 1259, 1121, 1028, 842, 797, 700.

HRMS (EI): m/z calculated for C$_{10}$H$_{16}$O$_2$ (M$^+$): 168.1145, found 168.1144.

(±)-(3a*S*,6a*S*)-3-Phenylhexahydro-5*H*-cyclopenta[*b*]furan-5-one (175c)
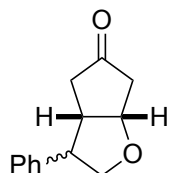
Following general procedure **II**, *tert*-butyl (4-oxocyclopent-2-en-1-yl) carbonate (**118**) (149 mg, 0.75 mmol, 1.00 equiv) was reacted with tropic acid (**174a**) (125 mg, 0.75 mmol, 1.00 equiv) to yield bicycle **175c** (29 mg, 232 μmol, 31%) as a mixture of two diastereomers (dr 1.6:1.0) as a yellowish oil after purification by flash column chromatography (hexanes / EtOAc 1:1) on silica gel. NMR spectra are reported only for the major diastereomer *exo*-**175c**.

R_f (hexanes / EtOAc 1:1 on silica) = 0.58.

^{1}H-NMR (300 MHz, CDCl$_3$, major diastereomer) δ 7.39–7.23 (m, 5H), 4.93–4.80 (m, 1H), 4.36 (dd, J = 9.1, 7.1 Hz, 1H), 3.90 (dd, J = 9.2, 7.2 Hz, 1H), 3.27–3.14 (m, 1H), 3.05–2.92 (m, 1H), 2.71–2.54 (m, 3H), 2.26 (dd, J = 19.1, 5.9 Hz, 1H).

^{13}C-NMR (101 MHz, CDCl$_3$, major diastereomer) δ 216.9, 141.4, 128.9, 127.3, 127.0, 80.5, 74.9, 53.4, 48.1, 45.3, 43.5.

IR $\tilde{v}_{max}$ (neat, cm^{-1}) 3030, 2826, 1736, 1602, 1494, 1453, 1394, 1341, 1159, 1043, 909, 756.

HRMS (EI): m/z calculated for C$_{13}$H$_{14}$O$_2$ (M$^+$): 202.0988, found 202.0984.

(±)-(3a*R*,6a*S*)-3-Methoxyhexahydro-5*H*-cyclopenta[*b*]furan-5-one (175d)
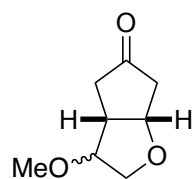
Following general procedure **II**, *tert*-butyl (4-oxocyclopent-2-en-1-yl) carbonate (**118**) (149 mg, 0.75 mmol, 1.00 equiv) was reacted with 3-hydroxy-2-methoxypropanoic acid (**170**) (90 mg, 0.75 mmol, 1.00 equiv) to yield bicycle **175d** (49 mg, 314 μmol, 42%) as an inseparable mixture of two diastereomers (dr 1.3:1.0) as a yellowish oil after purification by flash column chromatography (hexanes / EtOAc 1:2) on silica gel.

R_f (hexanes / EtOAc 1:2 on silica) = 0.34.

^{1}H-NMR (300 MHz, CDCl$_3$, mixture of diastereomers) δ 4.70–4.63 (m, 0.57H, major), 4.56 (td, J = 6.3, 4.4 Hz, 0.43H, minor), 4.14–3.99 (m, 1H, both), 3.90–3.74 (m, 2H, both), 3.30 (s, 1.7H, major), 3.25 (s, 1.3H, minor), 3.02–2.92 (m, 0.43H, minor), 2.89–2.78 (m, 0.57H, major), 2.63–2.32 (m, 3H, both), 2.21 (dd, J = 19.2, 9.9 Hz, 0.43H, minor), 1.85 (dd, J = 19.3, 9.1 Hz, 0.57H, major).

^{13}C-NMR (75 MHz, CDCl$_3$, mixture of diastereomers) δ 216.9, 216.6, 86.7, 81.9, 80.3, 79.9, 72.8, 71.9, 57.7, 57.0, 45.3, 45.0, 45.0, 43.1, 39.7, 36.3.

IR $\tilde{v}_{max}$ (neat, cm^{-1}) 3440, 2929, 2829, 1736, 1461, 1394, 1338, 1159, 1099, 1051, 939, 902, 834, 790, 752.

HRMS (EI): *m/z* calculated for C$_8$H$_{12}$O$_3$ (M$^+$): 156.0781, found 156.0781.

(±)-(3a*R*,6a*S*)-3-Isopropoxyhexahydro-5*H*-cyclopenta[*b*]furan-5-one (175e)
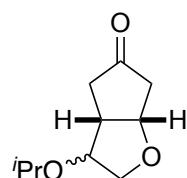
Following general procedure **II**, *tert*-butyl (4-oxocyclopent-2-en-1-yl) carbonate (**118**) (149 mg, 0.75 mmol, 1.00 equiv) was reacted with 3-hydroxy-2-isopropoxypropanoic acid (**171**) (111 mg, 0.75 mmol, 1.00 equiv) to yield bicycle **175e** (71 mg, 385 μmol, 51%) as an inseparable mixture of two diastereomers (dr 1.1:1.0) as a yellowish oil after purification by flash column chromatography (hexanes / EtOAc 1:1) on silica gel.

R_f (hexanes / EtOAc 1:1 on silica) = 0.47.

¹H-NMR (400 MHz, CDCl₃, mixture of diastereomers) δ 4.79–4.70 (m, 0.52H, major), 4.63 (dt, J = 6.4, 4.6 Hz, 0.48H, minor), 4.31–4.22 (m, 0.48H, minor), 4.17 (dd, J = 10.0, 5.0 Hz, 0.52H, major), 4.05–3.75 (m, 2H, both), 3.68–3.52 (m, 1H, both), 3.03–2.93 (m, 0.52H, major), 2.85–2.75 (m, 0.48H, minor), 2.69–2.38 (m, 3H, both), 2.25 (dd, J = 19.1, 9.8 Hz, 0.48H, minor), 1.93 (dd, J = 19.3, 8.7 Hz, 0.52H, major), 1.21–1.09 (m, 6H, both).

¹³C-NMR (75 MHz, CDCl₃, mixture of diastereomers) δ 217.2, 217.0, 86.7, 82.4, 80.2, 80.0, 74.0, 73.0, 71.2, 70.6, 46.6, 45.3, 45.0, 43.6, 40.0, 37.1, 22.6, 22.5, 22.3, 22.3.

IR $\tilde{v}_{max}$ (neat, cm^{-1}) 2970, 2929, 1740, 1468, 1379, 1330, 1155, 1118, 1043, 961, 928, 812.

HRMS (EI): m/z calculated for C₁₀H₁₆O₃ (M⁺): 184.1094, found 184.1095.

(±)-*Tert*-butyl ((2*R*,3a*S*,6a*S*)-2-methyl-5-oxohexahydro-2*H*-cyclopenta[*b*]furan-3-yl)carbamate (175g)
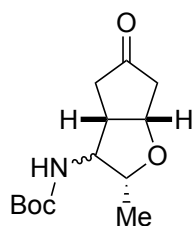
Following general procedure **II**, *tert*-butyl (4-oxocyclopent-2-en-1-yl) carbonate (**118**) (149 mg, 0.75 mmol, 1.00 equiv) was reacted with *N*-Boc L-threonine (**174b**) (164 mg, 0.75 mmol, 1.00 equiv) to yield bicycle **175g** (145 mg, 568 μmol, 76%) as an inseparable mixture of diastereomers as a yellowish oil after purification by flash column chromatography (hexanes / EtOAc 1:1) on silica gel.

R_f (hexanes / EtOAc 1:1 on silica) = 0.44.

¹H-NMR (300 MHz, CDCl₃, mixture of diastereomers) δ 4.96–4.43 (m, 2H), 4.20–3.85 (m, 1H), 3.77–3.43 (m, 1H), 2.73–2.41 (m, 3H), 2.39–1.90 (m, 2H), 1.43–1.36 (m, 9H), 1.33–1.11 (m, 3H).

¹³C-NMR (75 MHz, CDCl₃, mixture of diastereomers) δ 216.8, 216.7, 216.6, 155.9, 155.5, 81.5, 79.9, 79.3, 78.7, 78.1, 78.0, 77.6, 75.2, 65.1, 59.9, 56.0, 47.7, 47.0, 45.9, 45.8, 44.7, 44.7, 44.0, 43.2, 42.6, 41.6, 38.1, 37.2, 28.4, 28.3, 28.3, 19.3, 19.0, 14.8, 14.6.

IR $\tilde{v}_{max}$ (neat, cm^{-1}) 3332, 2974, 2933, 1740, 1688, 1520, 1453, 1390, 1244, 1159, 1043, 916, 868, 732.

HRMS (ESI): *m/z* calculated for C$_{13}$H$_{21}$NNaO$_4$ (M+Na)$^+$: 278.1363, found 278.1365.

(±)-*Tert*-butyl ((4a*S*,7a*S*)-6-oxooctahydrocyclopenta[*b*]pyran-4-yl)carbamate (177a)
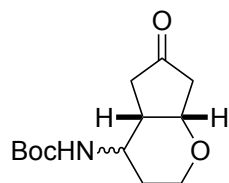
Following general procedure **II**, *tert*-butyl (4-oxocyclopent-2-en-1-yl) carbonate (**118**) (149 mg, 0.75 mmol, 1.00 equiv) was reacted with *N*-Boc L-homoserine (**174c**) (164 mg, 0.75 mmol, 1.00 equiv) to yield bicycle **177a** (164 mg, 642 μmol, 86%) as an inseparable mixture of two diastereomers (dr 2.0:1.0) as a yellowish oil after purification by flash column chromatography (hexanes / EtOAc 1:1) on silica gel.

R$_f$ (hexanes / EtOAc 1:1 on silica) = 0.46.

^{1}H-NMR (300 MHz, CDCl$_3$, mixture of diastereomers) δ 5.01–4.41 (m, 1H, both), 4.28–4.05 (m, 1H, both), 4.04–3.66 (m, 2H, both), 3.57 (dt, *J* = 12.3, 2.0 Hz, 0.67H, major), 3.42 (dt, *J* = 12.0, 2.1 Hz, 0.33H, minor), 2.69 (br s, 1H, both), 2.38–2.13 (m, 4H, both), 2.12–1.93 (m, 1H, both), 1.69–1.43 (m, 1H, both), 1.41–1.27 (m, 9H, both).

^{13}C-NMR (75 MHz, CDCl$_3$, mixture of diastereomers) δ 215.7, 215.5, 155.3, 155.2, 76.1, 72.7, 66.2, 61.9, 47.3, 46.7, 40.7, 40.4, 38.4, 34.8, 28.5, 28.5, 26.4, 25.4.

IR $\tilde{v}_{max}$ (neat, cm^{-1}) 3343, 2974, 2929, 1781, 1740, 1688, 1513, 1453, 1390, 1244, 1155, 1066, 1013, 928, 857, 752.

HRMS (APCI): *m/z* calculated for C$_{13}$H$_{22}$NO$_4$ (M+H)$^+$: 256.1543, found 256.1544.

(±)-*Tert*-butyl ((4a*S*,5*R*,7a*S*)-5-methyl-6-oxooctahydrocyclopenta[*b*]pyran-4-yl)carbamate (177b)
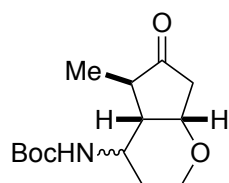
Following general procedure **II**, *tert*-butyl (3-methyl-4-oxocyclopent-2-en-1-yl) carbonate (**173c**) (159 mg, 0.75 mmol, 1.00 equiv) was reacted with *N*-Boc L-homoserine (**174c**) (164 mg, 0.75 mmol, 1.00 equiv) to yield bicycle **177b** (162 mg, 601 μmol, 80%) as an inseparable mixture of of two diastereomers (dr 2.1:1.0) as a yellowish solid after purification by flash column chromatography (hexanes / EtOAc 1:1) on silica gel.

R_f (hexanes / EtOAc 1:1 on silica) = 0.54.

mp: 123–125 °C.

^{1}H-NMR (400 MHz, CDCl$_3$, mixture of diastereomers) δ 4.97 (br s, 0.68H, major), 4.54 (br s, 0.32H, minor), 4.26–3.69 (m, 3H, both), 3.64–3.55 (m, 0.68H, major), 3.49–3.40 (m, 0.32H, minor), 2.40–2.22 (m, 3H, both), 2.05–1.47 (m, 3H, both), 1.46–1.31 (m, 9H, both), 1.13–1.07 (m, 3H, both).

^{13}C-NMR (101 MHz, CDCl$_3$, mixture of diastereomers) δ 218.7, 217.7, 155.1, 79.8, 74.7, 71.1, 66.3, 62.2, 48.4, 48.3, 47.1, 45.9, 45.6, 44.0, 42.7, 40.2, 28.5, 28.5, 26.6, 25.4, 16.0, 12.9.

IR $\tilde{v}_{max}$ (neat, cm^{-1}) 3358, 3265, 3123, 2974, 2929, 1736, 1692, 1524, 1390, 1248, 1162, 1114, 1058, 1013, 980, 838, 782, 745.

HRMS (ESI): *m/z* calculated for C$_{14}$H$_{24}$NO$_4$ (M+H)$^+$: 270.1700, found 270.1706.

Tert-butyl (2*R*,5*R*,5a*R*,8a*R*)-7-oxooctahydro-4*H*-2,5-methanocyclopenta[*f*][1,4]-oxazepine-4-carboxylate and **tert-butyl (2*R*,5*R*,5a*S*,8a*S*)-7-oxooctahydro-4*H*-2,5-methanocyclopenta[*f*][1,4]oxazepine-4-carboxylate (179a)**
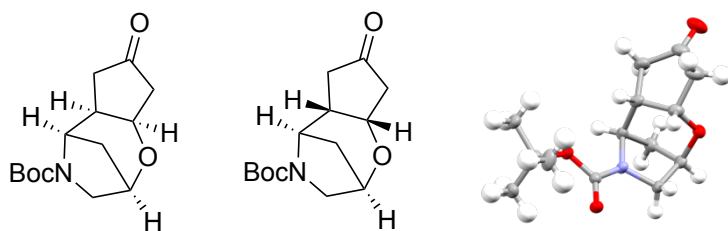
Following general procedure **II**, *tert*-butyl (4-oxocyclopent-2-en-1-yl) carbonate (**118**) (149 mg, 0.75 mmol, 1.00 equiv) was reacted with (2*S*,4*R*)-1-(*tert*-butoxycarbonyl)-4-hydroxypyrrolidine-2-carboxylic acid (**178**) (173 mg, 0.75 mmol, 1.00 equiv) to yield bridged bicycle **179a** and the corresponding uncyclized cyclopentenone derivative in a ratio of approximately 1:3 (combined yield: 179 mg, 670 μmol, 89%) after purification by flash column chromatography (hexanes / EtOAc 1:1) on silica gel. Subsequently, the purified mixture of both cyclized and uncyclized adducts was resolved in DCM (3 mL) and KF (47 mg, 804 μmol, 1.20

equiv) and Al_2O_3 (82 mg, 804 μmol, 1.20 equiv) were added.[118] The suspension was stirred for 20 h at ambient temperature, followed by a filtration over a pad of celite. The solvent was removed in vacuo and the crude product was purified by flash column chromatography (hexanes / EtOAc 1:1) on silica gel to yield **179a** (175 mg, 654 μmol, 87%) as an inseparable mixture of two diastereomers (dr 1.2:1.0) as a white solid.

R_f (hexanes / EtOAc 1:1 on silica) = 0.45.

mp: 99–101 °C.

^{1}H-NMR (400 MHz, CDCl$_3$, mixture of diastereomers) δ 4.54–4.21 (m, 3H, both), 3.76–3.58 (m, 1H, both), 3.55–3.39 (m, 1H, both), 2.74–2.59 (m, 0.55H, major), 2.57–2.46 (m, 0.45H, minor), 2.44–2.37 (m, 1H, both), 2.36–1.98 (m, 4H, both), 1.65–1.52 (m, 1H, both), 1.48 (s, 9H, both).

^{13}C-NMR (101 MHz, CDCl$_3$, mixture of diastereomers) δ 216.6, 216.5, 153.7, 80.0, 74.1, 73.3, 71.2, 71.1, 55.0, 54.3, 50.3, 49.8, 46.6, 40.6, 39.9, 37.7, 37.6, 31.5, 31.0, 28.7, 28.6.

IR $\tilde{v}_{max}$ (neat, cm^{-1}) 2985, 2922, 1740, 1677, 1476, 1449, 1394, 1293, 1207, 1177, 1110, 1032, 980, 916, 879, 756.

HRMS (ESI): m/z calculated for $C_{14}H_{22}NO_4$ (M+H)$^+$: 268.1543, found 268.1543.

Suitable crystals for X-Ray analysis were obtained by slow evaporation of a Et$_2$O solution containing a mixture of both diastereomers of **179a**. The crystals obtained were colourless and prism-shaped (CCDC 2085792; see details in section 3 of this chapter).

***Tert*-butyl (2*R*,5*R*,5a*R*,6*S*,8a*R*)-6-methyl-7-oxooctahydro-4*H*-2,5-methano-cyclopenta[*f*][1,4]oxazepine-4-carboxylate** and ***tert*-butyl (2*R*,5*R*,5a*S*,6*R*,8a*S*)-6-methyl-7-oxooctahydro-4*H*-2,5-methanocyclopenta[*f*][1,4]oxazepine-4-carboxylate (179b)**
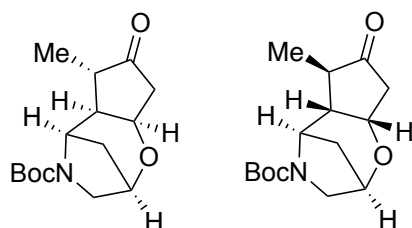
Following general procedure **II**, *tert*-butyl (3-methyl-4-oxocyclopent-2-en-1-yl) carbonate (**173c**) (159 mg, 0.75 mmol, 1.00 equiv) was reacted with (2*S*,4*R*)-1-(*tert*-butoxycarbonyl)-4-hydroxypyrrolidine-2-carboxylic acid (**178**) (173 mg, 0.75 mmol, 1.00 equiv) to yield bridged

bicycle **179b** and the corresponding uncyclized cyclopentenone derivative in a ratio of approximately 1:3 (combined yield: 153 mg, 544 μmol, 73%) after purification by flash column chromatography (hexanes / EtOAc 1:1) on silica gel. Subsequently, the purified mixture of both cyclized and uncyclized adducts was resolved in DCM (3 mL) and KF (38 mg, 653 μmol, 1.20 equiv) and Al$_2$O$_3$ (67 mg, 653 μmol, 1.20 equiv) were added.[118] The suspension was stirred for 20 h at ambient temperature, followed by a filtration over a pad of celite. The solvent was removed in vacuo and the crude product was purified by flash column chromatography (hexanes / EtOAc 1:1) on silica gel to yield **179b** (148 mg, 526 μmol, 70%) as an inseparable mixture of two diastereomers (dr 1.1:1.0) as a yellowish oil.

$\boldsymbol{R_f}$ (hexanes / EtOAc 1:1 on silica) = 0.55.

^{1}H-NMR (400 MHz, CDCl$_3$, mixture of diastereomers) δ 4.51–4.22 (m, 3H, both), 3.77–3.60 (m, 1H, both), 3.55–3.41 (m, 1H, both), 2.49–2.21 (m, 3H, both), 2.20–1.94 (m, 2H, both), 1.67–1.53 (m, 1H, both), 1.52–1.42 (m, 9H, both), 1.17–1.05 (m, 3H, both).

^{13}C-NMR (101 MHz, CDCl$_3$, mixture of diastereomers) δ 218.5, 218.3, 153.7, 80.0, 74.5, 73.7, 69.4, 69.1, 54.5, 53.8, 50.3, 49.7, 48.9, 47.9, 44.9, 43.1, 42.9, 32.0, 31.4, 28.6, 13.5.

IR $\tilde{v}_{max}$ (neat, cm^{-1}) 2967, 2929, 1744, 1688, 1476, 1394, 1259, 1162, 1107, 1028, 1006, 920, 868, 793, 734.

HRMS (ESI): m/z calculated for C$_{15}$H$_{24}$NO$_4$ (M+H)$^+$: 282.1700, found 282.1696.

(*S*)-4-Benzhydrylcyclopent-2-en-1-one ((*S*)-188)
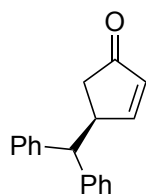
Following general procedure **II**, (*S*)-*tert*-butyl (4-oxocyclopent-2-en-1-yl) carbonate ((*S*)-**118**) (149 mg, 0.75 mmol, 1.00 equiv) was reacted with diphenylacetic acid (**187**) (164 mg, 0.75 mmol, 1.00 equiv) to yield coupling product (*S*)-**188** (141 mg, 568 μmol, 76%, 96% ee) as a white solid after purification by flash column chromatography (hexanes / EtOAc 4:1) on silica gel. In order to determine the enantiomeric excess by chiral HPLC analysis, the same reaction was performed using racemic **118** as starting material.

R_f (hexanes / EtOAc 4:1 on silica) = 0.49.

mp: 79–81 °C.

$[\alpha]_D^{20}$ = - 158.4 ° (c = 1.0, CHCl$_3$).

^{1}H-NMR (400 MHz, CDCl$_3$) δ 7.39 (dd, J = 5.8, 2.4 Hz, 1H), 7.33–7.22 (m, 8H), 7.22–7.14 (m, 2H), 6.14 (dd, J = 5.7, 1.9 Hz, 1H), 3.84–3.73 (m, 1H), 3.68 (d, J = 11.4 Hz, 1H), 2.50 (dd, J = 19.0, 6.2 Hz, 1H), 2.03 (dd, J = 19.0, 2.2 Hz, 1H).

^{13}C-NMR (101 MHz, CDCl$_3$) δ 209.2, 167.0, 142.9, 142.7, 134.6, 129.0, 128.9, 128.0, 127.8, 127.0, 126.9, 57.2, 45.9, 41.0.

IR $\tilde{v}_{max}$ (neat, cm^{-1}) 3026, 2914, 1707, 1584, 1490, 1449, 1408, 1341, 1233, 1185, 1080, 1028, 943, 782, 749, 704.

HRMS (EI): m/z calculated for C$_{18}$H$_{16}$O (M$^+$): 248.1196, found 248.1193.

HPLC (Amylose-1, i-propanol/n-heptane = 20/80, flow rate = 1.0 mL/min, I = 215 nm): t_R = 27.38 min (major), t_R = 54.81 min (minor), 96% *ee*.

(9*H*-fluoren-9-yl)Methyl ((3*S*,3a*S*,6a*S*)-5-oxohexahydro-2*H*-cyclopenta[*b*]furan-3-yl)carbamate ((3*S*)-157)
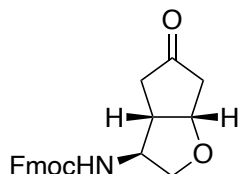
Diastereopure and enantioenriched (3*S*/3*R*)-**151** (69 mg, 286 μmol, 1.00 equiv) was dissolved in an aqueous HCl-solution (25%; 5 mL) and stirred for one hour at ambient temperature. The solvent was removed in vacuo and the residue was redissolved in water (3.5 mL) followed by an addition of NaHCO$_3$ (48 mg, 571 μmol, 2.00 equiv) with subsequent cooling to 0 °C. A solution of Fmoc-succinimid ester (116 mg, 343 μmol, 1.20 equiv) in 1,4-dioxane (2 mL) was added to the cooled reaction mixture and stirred for 20 h at ambient temperature. After acidifying the suspension to a pH of 3 with an aqueous HCl-solution (10%), the mixture was extracted with EtOAc (3 × 20 mL). The combined organic layers were dried over Na$_2$SO$_4$ and concentrated in vacuo. The crude product was purified via flash column chromatography (hexanes / EtOAc 1:1) on silica gel and gave rise to Fmoc-protected derivative (3*S*)-**157** (41 mg, 113 μmol, 40%) as a colorless sticky oil. The same reaction was performed from racemic *exo*-**151** in order to generate the reference sample *exo*-**157** for chiral HPLC analysis.

R_f (hexanes / EtOAc 1:1 on silica) = 0.38.

$[\alpha]_D^{20} = -61.5°$ (c = 1.0, CHCl$_3$).

¹H-NMR (300 MHz, CDCl$_3$) δ 7.77 (dt, J = 7.6, 1.0 Hz, 2H), 7.63–7.50 (m, 2H), 7.46–7.37 (m, 2H), 7.32 (td, J = 7.4, 1.3 Hz, 2H), 5.18–4.93 (m, 1H), 4.79–4.65 (m, 1H), 4.48 (d, J = 6.6 Hz, 2H), 4.29–4.01 (m, 3H), 3.67 (d, J = 8.1 Hz, 1H), 2.90–2.75 (m, 1H), 2.75–2.53 (m, 1H), 2.53–2.28 (m, 2H), 2.16–1.95 (m, 1H).

¹³C-NMR (75 MHz, CDCl$_3$) δ 216.2, 155.7, 143.7, 141.4, 127.8, 127.1, 124.9, 120.1, 79.6, 72.6, 66.6, 58.4, 47.3, 46.8, 45.1, 41.0.

IR $\tilde{v}_{max}$ (neat, cm^{-1}) 3321, 2972, 2861, 1751, 1732, 1714, 1628, 1520, 1489, 1463, 1339, 1256, 1155, 1117, 1084, 1039, 924, 877, 862, 772, 683.

HRMS (ESI): m/z calculated for C$_{22}$H$_{22}$NO$_4$ (M+H)$^+$: 364.1543, found 364.1544.

HPLC (AS-H, i-propanol/n-heptane = 20/80, flow rate = 0.5 mL/min, I = 254 nm): t_R = 53.84 min (major), t_R = 72.76 min (minor), 84% *ee*.

(±)-Methyl ((3S,3aS,6aS)-5-oxohexahydro-2H-cyclopenta[b]furan-3-yl)carbamate (exo-156)
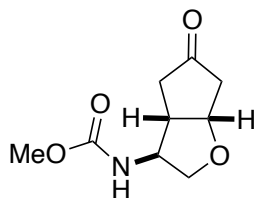
Diastereopure *exo*-**151** (121 mg, 500 μmol, 1.00 equiv) was dissolved in an aqueous HCl-solution (25%; 5 mL) and stirred for one hour at ambient temperature. The solvent was removed under reduced pressure and the residue was dissolved in an aqueous NaOH-solution (1 M, 0.5 mL, 1.00 equiv) followed by an addition of Na$_2$CO$_3$ (27 mg, 250 μmol, 0.50 equiv). The resulting solution was cooled in an ice-water bath and methylchloroformate (52 mg, 43 μL, 550 μmol, 1.10 equiv) was added dropwise. The mixture was stirred for 5 h at ambient temperature and was subsequently extracted with EtOAc (5 × 50 mL). The combined organic layers were dried over Na$_2$SO$_4$ and concentrated in vacuo before the purification of the crude product via flash column chromatography (hexanes / EtOAc 1:3) on silica gel gave rise to carbamate *exo*-**156** (43 mg, 215 μmol, 43%) as a colorless oil.

R_f (hexanes / EtOAc 1:3 on silica) = 0.40.

¹H-NMR (400 MHz, CDCl₃) δ 4.97 (s, 1H), 4.75 (td, J = 5.3, 2.1 Hz, 1H), 4.25–3.99 (m, 2H), 3.83–3.51 (m, 4H), 2.92–2.78 (m, 1H), 2.71–2.59 (m, 1H), 2.57–2.40 (m, 2H), 2.13–2.01 (m, 1H).

¹³C-NMR (75 MHz, CDCl₃) δ 216.2, 156.4, 79.6, 72.7, 58.4, 52.3, 46.9, 45.1, 41.1.

IR $\tilde{v}_{max}$ (neat, cm⁻¹) 3297, 2954, 1711, 1687, 1562, 1435, 1268, 1189, 1137, 1080, 1042, 979, 940, 869, 771.

HRMS (APCI): *m/z* calculated for $C_9H_{14}NO_4$ (M+H)⁺: 200.0917, found 200.0920.

5 Synthesis of HIV-1 protease inhibitors

The following synthetic manipulations towards target inhibitors **125** and **126** were performed starting from enantioenriched **151**, synthesized by our developed photocatalytic DcRCAE-Oxa-Michael Reaction by employing enantiopure (*S*)-**118** (>99% ee) as Michael acceptor on a 5 mmol scale. The detailed setup and synthetic procedure towards enantioenriched **151** is described under section 6 of the experimental part.

In order to determine the enantiomeric excesses by chiral HPLC analysis, the racemic versions of the following compounds **189**-**191** were synthesized simultaneously starting from racemic **151**.

Tert*-butyl ((3*R*,3a*R*,5*R*,6a*R*)-5-hydroxyhexahydro-2*H*-cyclopenta[*b*]furan-3-yl)carbamate ((*3R*)-189)
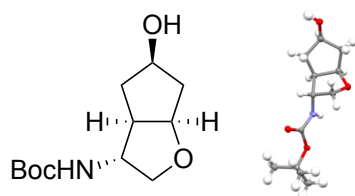
Tert*-butyl ((3*S*,3a*R*,5*R*,6a*R*)-5-hydroxyhexahydro-2*H*-cyclopenta[*b*]furan-3-yl)carbamate ((*3S*)-189)
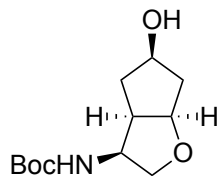
To a solution of enantioenriched **151** (*exo:endo* 2.2:1.0, 256 mg, 1.06 mmol, 1.00 equiv) in MeOH (2.5 mL) and THF (2.5 mL) was added $NaBH_4$ (80.3 mg, 2.12 mmol, 2.00 equiv) in small portions at 0 °C. The mixture was stirred for 2 h at ambient temperature and afterwards diluted with EtOAc (5 mL). The organic phase was washed with saturated NH_4Cl-solution (10 mL) and brine (10 mL), dried over Na_2SO_4 and concentrated in vacuo. The crude product was purified by flash column chromatography (hexanes / EtOAc 1:3) on silica gel to yield the separated diastereomers (*3R*)-**189** (148 mg, 608 μmol, 57%) and (*3S*)-**189** (61 mg, 251 μmol, 24%) as white solids.

Tert-butyl ((3*R*,3a*R*,5*R*,6a*R*)-5-hydroxyhexahydro-2*H*-cyclopenta[*b*]furan-3-yl)carbamate ((*3R*)-**189**)

R_f (hexanes / EtOAc 1:3 on silica) = 0.23.

mp: 92–94 °C.

$[\alpha]_D^{20} = + 11.5$ ° (c = 1.0, CHCl$_3$).

¹H-NMR (400 MHz, CDCl$_3$) δ 4.91 (br s, 1H), 4.60–4.51 (m, 1H), 4.23–4.14 (m, 2H), 4.02 (br s, 1H), 3.56–3.42 (m, 1H), 2.60 (br s, 1H), 2.48–2.37 (m, 1H), 2.20–2.05 (m, 1H), 1.97–1.82 (m, 2H), 1.72–1.60 (m, 1H), 1.41 (s, 9H).

¹³C-NMR (101 MHz, CDCl$_3$) δ 155.4, 83.9, 79.6, 73.2, 72.0, 58.5, 49.7, 41.8, 40.2, 28.4.

IR $\tilde{v}_{max}$ (neat, cm^{-1}) 3447, 3358, 2967, 2933, 2885, 2855, 1684, 1528, 1390, 1289, 1244, 1166, 1039, 1010, 872, 808, 775.

HRMS (ESI): *m/z* calculated for C$_{12}$H$_{22}$NO$_4$ (M+H)$^+$: 244.1543, found 244.1546.

Suitable crystals for X-Ray analysis were obtained by slow evaporation of a EtOAc solution containing (*3R*)-**189**. The crystals obtained were colourless and prism-shaped (CCDC 2085696; see details in section 3 of this chapter).

Tert-butyl ((3*S*,3a*R*,5*R*,6a*R*)-5-hydroxyhexahydro-2*H*-cyclopenta[*b*]furan-3-yl)carbamate ((*3S*)-**189**)

R_f (hexanes / EtOAc 1:1 on silica) = 0.30.

mp: 81–83 °C.

$[\alpha]_D^{20} = - 8.0$ ° (c = 1.0, CHCl$_3$).

¹H-NMR (400 MHz, CDCl$_3$) δ 6.23 (br s, 1H), 4.38 (t, J = 6.8 Hz, 1H), 4.33–4.18 (m, 2H), 3.70 (dd, J = 9.4, 2.3 Hz, 1H), 3.58 (dd, J = 9.4, 4.9 Hz, 1H), 3.08–2.67 (m, 2H), 1.98–1.90 (m, 1H), 1.89–1.73 (m, 2H), 1.66 (ddd, J = 14.8, 10.3, 4.7 Hz, 1H), 1.37 (s, 9H).

¹³C-NMR (101 MHz, CDCl$_3$) δ 156.1, 86.0, 79.2, 75.4, 74.0, 53.4, 45.6, 42.2, 34.9, 28.6.

IR $\tilde{v}_{max}$ (neat, cm^{-1}) 3395, 3343, 3250, 2978, 2937, 2855, 1707, 1677, 1531, 1453, 1274, 1248, 1162, 1051, 924, 857, 771, 700.

HRMS (ESI): *m/z* calculated for C$_{12}$H$_{22}$NO$_4$ (M+H)$^+$: 244.1543, found 244.1545.

Methyl ((3R,3aR,5R,6aR)-5-hydroxyhexahydro-2H-cyclopenta[b]furan-3-yl)carbamate ((3R)-190)
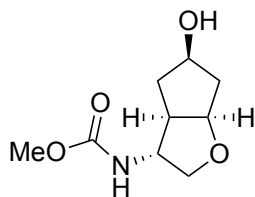
Diastereopure alcohol (3R)-**189** (96 mg, 394 μmol, 1.00 equiv) was dissolved in a 1 M-solution of HCl in EtOAC (20 mL). After stirring for 3 h at ambient temperature, the solvent was removed under reduced pressure. The residue was resolved in water (5 mL) and an aqueous NaOH-solution (1 M, 789 μL, 2.00 equiv) was added followed by the addition of Na_2CO_3 (21 mg, 197 μmol, 0.50 equiv). The resulting solution was cooled in an ice-water bath and methylchloroformate (93 mg, 76 μL, 986 μmol, 2.50 equiv) was added dropwise. The mixture was stirred for 20 h at ambient temperature and subsequently extracted with EtOAc (5 × 20 mL). The combined organic layers were dried over Na_2SO_4 and concentrated in vacuo before the purification of the crude product via flash column chromatography (hexanes / EtOAc 1:3) on silica gel gave rise to carbamate (3R)-**190** (66 mg, 328 μmol, 83%) as a colorless sticky oil.

R_f (hexanes / EtOAc 1:3 on silica) = 0.15.

$[\alpha]_D^{20}$ = + 11.6 ° (c = 1.0, CHCl$_3$).

^{1}H-NMR (400 MHz, CDCl$_3$) δ 5.20 (br s, 1H), 4.58 (td, J = 6.4, 3.3 Hz, 1H), 4.26–4.14 (m, 2H), 4.08 (br s, 1H), 3.63 (s, 3H), 3.56–3.43 (m, 1H), 2.54–2.41 (m, 2H), 2.18–2.04 (m, 1H), 1.99–1.83 (m, 2H), 1.69 (dt, J = 14.2, 4.5 Hz, 1H).

^{13}C-NMR (101 MHz, CDCl$_3$) δ 156.7, 84.2, 73.4, 71.9, 59.0, 52.2, 49.8, 41.8, 40.2.

IR $\tilde{v}_{max}$ (neat, cm^{-1}) 3302, 2952, 1692, 1535, 1457, 1349, 1259, 1192, 1136, 1069, 1032, 976, 920, 779.

HRMS (ESI): m/z calculated for $C_9H_{16}NO_4$ (M+H)$^+$: 202.1074, found 202.1074.

Methyl ((3*S*,3a*R*,5*R*,6a*R*)-5-hydroxyhexahydro-2*H*-cyclopenta[*b*]furan-3-yl)carbamate ((*3S*)-190)
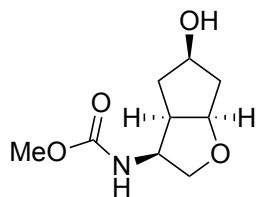
Diastereopure alcohol (*3S*)-**189** (48 mg, 197 μmol, 1.00 equiv) was dissolved in a 1 M-solution of HCl in EtOAC (10 mL). After stirring for 3 h at ambient temperature, the solvent was removed under reduced pressure. The residue was resolved in water (2 mL) and an aqueous NaOH-solution (1 M, 394 μL, 2.00 equiv) was added followed by the addition of Na_2CO_3 (10 mg, 99 μmol, 0.50 equiv). The resulting solution was cooled in an ice-water bath and methylchloroformate (47 mg, 38 μL, 493 μmol, 2.50 equiv) was added dropwise. The mixture was stirred for 20 h at ambient temperature and subsequently extracted with EtOAc (5 × 10 mL). The combined organic layers were dried over Na_2SO_4 and concentrated in vacuo before the purification of the crude product via flash column chromatography (hexanes / EtOAc 1:3) on silica gel gave rise to carbamate (*3S*)-**190** (33 mg, 166 μmol, 83%) as a colorless oil.

R_f (hexanes / EtOAc 1:3 on silica) = 0.24.

$[\alpha]_D^{20}$ = - 17.2 ° (*c* = 1.0, CHCl$_3$).

^{1}H-NMR (300 MHz, CDCl$_3$) δ 6.61 (br s, 1H), 4.52–4.25 (m, 3H), 3.79 (d, *J* = 9.5 Hz, 1H), 3.72–3.53 (m, 4H), 2.99 (q, *J* = 8.9 Hz, 1H), 2.30 (br s, 1H), 2.07–1.89 (m, 2H), 1.84 (ddd, *J* = 15.3, 6.2, 4.5 Hz, 1H), 1.72 (ddd, *J* = 14.9, 10.3, 4.6 Hz, 1H).

^{13}C-NMR (101 MHz, CDCl$_3$) δ 157.1, 85.8, 75.3, 73.5, 53.6, 52.0, 45.8, 41.9, 34.6.

IR $\tilde{v}_{max}$ (neat, cm^{-1}) 3287, 2952, 1692, 1531, 1461, 1349, 1252, 1192, 1140, 1077, 954, 924, 846, 775, 726.

HRMS (ESI): *m/z* calculated for C$_9$H$_{16}$NO$_4$ (M+H)$^+$: 202.1074, found 202.1073.

Methyl ((3*R*,3a*R*,5*R*,6a*R*)-5-(((4-nitrophenoxy)carbonyl)oxy)hexahydro-2*H*-cyclopenta[*b*]furan-3-yl)carbamate ((3*R*)-191)[78]
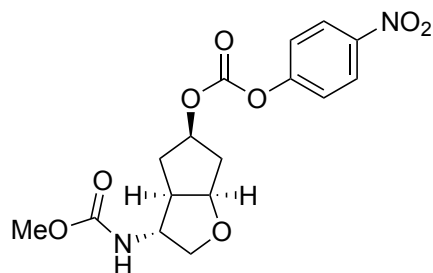
To a solution of carbamate (3*R*)-**190** (51 mg, 253 μmol, 1.00 equiv) in DCM (3 mL) was added pyridine (80 mg, 82 μL, 1.01 mmol, 4.00 equiv) and the resulting mixture was cooled to 0 °C. After addition of 4-nitrophenyl chloroformate (102 mg, 507 μmol, 2.00 equiv) in one portion and stirring the solution at ambient temperature for 20 h, the solvent was removed under reduced pressure. The crude product was purified by flash column chromatography (hexanes / EtOAc 1:2) on silica gel to afford the activated carbonate (3*R*)-**191** (79 mg, 216 μmol, 85%, 84% *ee*) as a white solid.

R_f (hexanes / EtOAc 1:2 on silica) = 0.36.

mp: 87–89 °C.

$[\alpha]_D^{20}$ = + 33.5 ° (*c* = 1.0, CHCl$_3$).

^{1}H-NMR (400 MHz, CDCl$_3$) δ 8.30–8.21 (m, 2H), 7.42–7.31 (m, 2H), 5.18–5.09 (m, 1H), 5.03 (d, *J* = 7.6 Hz, 1H), 4.67 (ddd, *J* = 6.8, 5.3, 2.9 Hz, 1H), 4.17 (dd, *J* = 9.4, 5.3 Hz, 1H), 4.10 (br s, 1H), 3.66 (s, 3H), 3.58 (dd, *J* = 9.5, 3.9 Hz, 1H), 2.61 (br s, 1H), 2.33 (ddd, *J* = 15.4, 9.8, 5.9 Hz, 1H), 2.22–2.07 (m, 2H), 1.97 (dt, *J* = 15.3, 4.3 Hz, 1H).

^{13}C-NMR (101 MHz, CDCl$_3$) δ 156.6, 155.6, 152.0, 145.5, 125.4, 121.9, 83.0, 81.2, 71.9, 58.7, 52.3, 49.9, 39.5, 36.7.

IR $\tilde{v}_{max}$ (neat, cm^{-1}) 3339, 2952, 2862, 1751, 1714, 1520, 1349, 1256, 1192, 1114, 1039, 972, 924, 857, 775, 678.

HRMS (ESI): *m/z* calculated for C$_{16}$H$_{19}$N$_2$O$_8$ (M+H)$^+$: 367.1136, found 367.1141.

HPLC (Cellulose-1, *i*-propanol/*n*-heptane = 40/60, flow rate = 0.5 mL/min, I = 254 nm): t_R = 19.36 min (minor), t_R = 23.05 min (major), 84% *ee*.

Methyl ((3*S*,3a*R*,5*R*,6a*R*)-5-(((4-nitrophenoxy)carbonyl)oxy)hexahydro-2*H*-cyclopenta[*b*]furan-3-yl)carbamate ((*3S*)-191)[78]
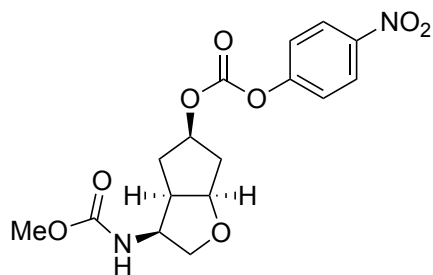
To a solution of carbamate (*3S*)-**190** (31 mg, 154 μmol, 1.00 equiv) in DCM (2 mL) was added pyridine (49 mg, 50 μL, 616 μmol, 4.00 equiv) and the resulting mixture was cooled to 0 °C. After addition of 4-nitrophenyl chloroformate (62 mg, 308 μmol, 2.00 equiv) in one portion and stirring the solution at ambient temperature for 20 h, the solvent was removed under reduced pressure. The crude product was purified by flash column chromatography (hexanes / EtOAc 1:2) on silica gel to afford the activated carbonate (*3S*)-**191** (48 mg, 131 μmol, 85%, 92% *ee*) as a white solid.

R_f (hexanes / EtOAc 1:2 on silica) = 0.34.

mp: 72–74 °C.

$[\alpha]_D^{20}$ = + 71.7 ° (*c* = 1.0, CHCl$_3$).

¹H-NMR (400 MHz, CDCl$_3$) δ 8.27–8.13 (m, 2H), 7.39–7.27 (m, 2H), 5.25 (d, *J* = 9.8 Hz, 1H), 5.19–5.12 (m, 1H), 4.45 (t, *J* = 6.7 Hz, 1H), 4.42–4.31 (m, 1H), 3.75–3.66 (m, 2H), 3.57 (s, 3H), 2.99 (p, *J* = 7.5 Hz, 1H), 2.22 (d, *J* = 15.8 Hz, 1H), 2.07–1.92 (m, 3H).

¹³C-NMR (101 MHz, CDCl$_3$) δ 156.7, 155.5, 151.6, 145.5, 125.3, 121.9, 84.7, 82.4, 73.8, 54.0, 52.3, 45.8, 39.1, 32.4.

IR $\tilde{v}_{max}$ (neat, cm^{-1}) 3421, 3324, 2952, 2870, 1759, 1718, 1595, 1520, 1349, 1196, 1084, 1036, 924, 857, 775, 726, 682.

HRMS (ESI): *m/z* calculated for C$_{16}$H$_{19}$N$_2$O$_8$ (M+H)$^+$: 367.1136, found 367.1132.

HPLC (Cellulose-1, *i*-propanol/*n*-heptane = 10/90, flow rate = 1.0 mL/min, I = 254 nm): t_R = 40.28 min (minor), t$_R$ = 43.68 min (major), 92% *ee*.

Tert-butyl ((2S,3R)-3-hydroxy-4-((N-isobutyl-4-methoxyphenyl)sulfonamido)-1-phenylbutan-2-yl)carbamate (194)[124]
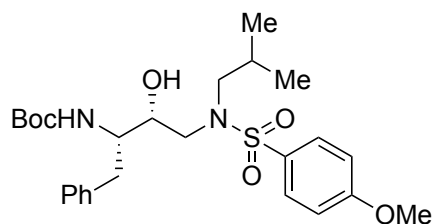
Commercially available and optically pure *tert*-butyl ((*S*)-1-((*S*)-oxiran-2-yl)-2-phenylethyl)carbamate (**192**; 1.05 g, 4.00 mmol, 1.00 equiv) was dissolved in isopropanol (20 mL) and *iso*-butylamine (**193**; 5.85 g, 7.95 mL, 80.0 mmol, 20.0 equiv) was added to the solution. The resulting mixture was stirred at 60 °C for 6 h before the solvent and the excess of amine was removed under reduced pressure. The residue was resolved in DCM (150 mL) followed by the addition of NEt$_3$ (992 mg, 1.37 mL, 10.0 mmol, 2.50 equiv) and 4-methoxybenzene sufonylchloride (972 mg, 4.80 mmol, 1.20 equiv). After stirring the mixture at ambient temperature for 24 h, the solution was quenched with aqueous H$_2$SO$_4$-solution (5%) and the organic layer was washed with saturated aqueous NaHCO$_3$-solution (50 mL) and brine (50 mL). The organic phase was dried over Na$_2$SO$_4$, concentrated in vacuo and subsequently purified by flash column chromatography (hexanes / EtOAc 3:1) on silica gel to afford optically pure coupling product **194** (1.76 g, 3.48 mmol, 87%, >99% *ee*) as a white solid. The spectroscopic data is in accordance with those reported in literature.[124]

^{1}H-NMR (400 MHz, CDCl$_3$) δ 7.78–7.66 (m, 2H), 7.36–7.16 (m, 5H), 7.03–6.91 (m, 2H), 4.64 (br s, 1H), 3.88 (s, 3H), 3.85–3.72 (m, 2H), 3.16–2.86 (m, 5H), 2.82 (dd, *J* = 13.4, 6.8 Hz, 1H), 1.85 (hept, *J* = 6.5 Hz, 1H), 1.35 (s, 9H), 0.91 (d, *J* = 6.6 Hz, 3H), 0.87 (d, *J* = 6.6 Hz, 3H).

^{13}C-NMR (101 MHz, CDCl$_3$) δ 163.1, 156.1, 138.0, 130.1, 129.7, 129.6, 128.6, 126.5, 114.4, 79.8, 72.9, 58.8, 55.7, 54.8, 53.9, 35.6, 28.4, 27.3, 20.3, 20.0.

HPLC (Cellulose-1, *i*-propanol/*n*-heptane = 40/60, flow rate = 0.5 mL/min, I = 215 nm): t_R = 8.65 min (major), >99% *ee*.

N-((*2R,3S*)-3-amino-2-hydroxy-4-phenylbutyl)-*N*-isobutyl-4-methoxybenzenesulfon-amide (134)[124]
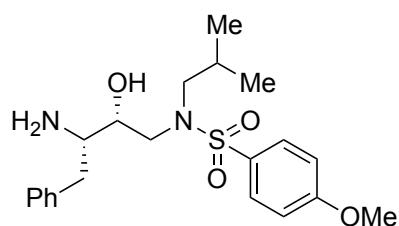
To a solution of alcohol **194** (1.50 g, 2.96 mmol, 1.00 equiv) in DCM (35 mL) was added TFA (15 mL) and the solution was stirred at ambient temperature for 2 h. The solvent was evaporated in vacuo followed by washing the remaining residue with toluene (3 × 20 mL). The organic phase was concentrated under reduced pressure and the crude product was purified by flash column chromatography (CHCl$_3$ / MeOH 9:1) on silica gel to afford optically pure free amine **134** (1.09 g, 2.68 mmol, 91%) as a white solid. The spectroscopic data is in accordance with those reported in literature.[13]

1H-NMR (400 MHz, CDCl$_3$) δ 7.74–7.64 (m, 2H), 7.28–7.17 (m, 5H), 6.99–6.87 (m, 2H), 5.67 (br s, 3H), 4.11–3.99 (m, 1H), 3.83 (s, 3H), 3.59–3.47 (m, 1H), 3.26–3.08 (m, 2H), 3.03 (dd, *J* = 14.1, 5.7 Hz, 1H), 2.88–2.67 (m, 3H), 1.73 (hept, *J* = 6.7 Hz, 1H), 0.82–0.70 (m, 6H).

13C-NMR (101 MHz, CDCl$_3$) δ 163.1, 136.7, 130.0, 129.6, 129.4, 129.0, 127.1, 114.4, 70.0, 58.1, 55.6, 55.6, 51.7, 34.8, 27.0, 20.0, 19.9.

(*3R,3aR,5R,6aR*)-3-((Methoxycarbonyl)amino)hexahydro-2*H*-cyclopenta[*b*]furan-5-yl ((*2S,3R*)-3-hydroxy-4-((*N*-isobutyl-4-methoxyphenyl)sulfonamido)-1-phenylbutan-2-yl)carbamate (126)[78]
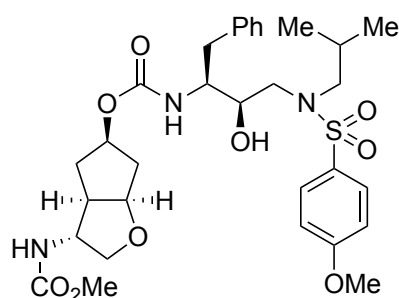
Optically pure Amine **134** (49 mg, 119 μmol, 1.25 equiv) was dissolved in MeCN (1 mL) and the solution was cooled to 0 °C. A separately prepared solution of activated carbonate (*3R*)-**191** (35 mg, 96 μmol, 1.00 equiv) in THF (1 mL) was added to the cooled mixture together with NEt$_3$ (48 mg, 67 μL, 478 μmol, 5.00 equiv). After stirring at ambient temperature for 4 d, the

solvent was removed in vacuo and the remaining residue was purified by flash column chromatography (hexanes / EtOAc 1:3) on silica gel to afford HIV-inhibitor **126** (53 mg, 84 μmol, 87%, 86% *de*) as a white solid.

$\textbf{\textit{R}_f}$ (hexanes / EtOAc 1:3 on silica) = 0.37.

mp: 62–64 °C.

$[\alpha]_D^{20} = +22.9\,°$ (*c* = 1.0, CHCl$_3$).

$\textbf{^1H-NMR}$ (400 MHz, CDCl$_3$) δ 7.74–7.67 (m, 2H), 7.32–7.26 (m, 2H), 7.25–7.17 (m, 3H), 7.01–6.94 (m, 2H), 5.01–4.70 (m, 3H), 4.57 (td, *J* = 6.0, 3.2 Hz, 1H), 4.05–3.89 (m, 2H), 3.89–3.73 (m, 6H), 3.67 (br s, 3H), 3.58–3.46 (m, 1H), 3.17–2.99 (m, 3H), 2.95 (dd, *J* = 13.4, 8.3 Hz, 1H), 2.89–2.74 (m, 2H), 2.47 (br s, 1H), 2.14 (ddd, *J* = 15.3, 9.7, 6.0 Hz, 1H), 1.99 (dt, *J* = 14.9, 6.2 Hz, 1H), 1.93–1.77 (m, 2H), 1.55–1.45 (m, 1H), 0.91 (d, *J* = 6.6 Hz, 3H), 0.86 (d, *J* = 6.6 Hz, 3H).

$\textbf{^{13}C-NMR}$ (101 MHz, CDCl$_3$) δ 163.2, 156.5, 156.2, 137.8, 130.0, 129.7, 129.6, 128.6, 126.7, 114.5, 83.2, 76.3, 72.7, 71.8, 58.9, 58.7, 55.8, 55.1, 53.9, 52.3, 49.6, 39.6, 37.1, 35.8, 27.4, 20.3, 20.0.

$\textbf{IR}\ \tilde{v}_{max}$ (neat, cm^{-1}) 3324, 2959, 2873, 1692, 1595, 1524, 1453, 1330, 1259, 1148, 1088, 1025, 920, 883, 834, 805, 749.

$\textbf{HRMS}$ (ESI): *m/z* calculated for C$_{31}$H$_{47}$N$_4$O$_9$S (M+NH$_4$)$^+$: 651.3058, found 651.3060.

$\textbf{HPLC}$ (Cellulose-1, *i*-propanol/*n*-heptane = 20/80, flow rate = 0.5 mL/min, I = 254 nm): t_R = 35.78 min (minor), t_R = 43.37 min (major), 86% *de*.

(3*S*,3a*R*,5*R*,6a*R*)-3-((Methoxycarbonyl)amino)hexahydro-2*H*-cyclopenta[*b*]furan-5-yl ((2*S*,3*R*)-3-hydroxy-4-((*N*-isobutyl-4-methoxyphenyl)sulfonamido)-1-phenylbutan-2-yl)carbamate (125)[78]
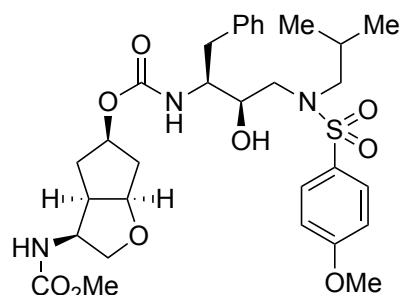
Optically pure Amine **134** (43 mg, 106 μmol, 1.25 equiv) was dissolved in MeCN (1 mL) and the solution was cooled to 0 °C. A separately prepared solution of activated carbonate (3*S*)-**191** (31 mg, 85 μmol, 1.00 equiv) in THF (1 mL) was added to the cooled mixture together with NEt$_3$ (43 mg, 59 μL, 423 μmol, 5.00 equiv). After stirring at ambient temperature for 4 d, the solvent was removed in vacuo and the remaining residue was purified by flash column chromatography (hexanes / EtOAc 1:3) on silica gel to afford HIV-inhibitor **125** (48 mg, 75 μmol, 89%, 91% *de*) as a white solid.

***R*$_f$** (hexanes / EtOAc 1:3 on silica) = 0.35.

mp: 91–93 °C.

$[\alpha]_D^{20}$ = + 38.8 ° (*c* = 1.0, CHCl$_3$).

¹H-NMR (400 MHz, CDCl$_3$) δ 7.75–7.64 (m, 2H), 7.30–7.19 (m, 5H), 7.01–6.91 (m, 2H), 5.28 (br s, 1H), 5.09–4.87 (m, 2H), 4.42 (dt, *J* = 7.5, 3.9 Hz, 1H), 4.36–4.26 (m, 1H), 3.91–3.62 (m, 10H), 3.62–3.55 (m, 1H), 3.15–2.97 (m, 3H), 2.96–2.85 (m, 3H), 2.79 (dd, *J* = 13.4, 6.8 Hz, 1H), 2.01–1.77 (m, 4H), 1.77–1.61 (m, 1H), 0.89 (d, *J* = 6.6 Hz, 3H), 0.85 (d, *J* = 6.6 Hz, 3H).

¹³C-NMR (101 MHz, CDCl$_3$) δ 163.1, 156.6, 155.6, 137.8, 129.9, 129.6, 129.5, 128.6, 126.6, 114.4, 84.8, 77.3, 73.2, 72.5, 58.8, 55.7, 55.2, 53.7, 52.2, 45.6, 39.5, 35.6, 32.4, 29.7, 27.2, 20.2, 19.9.

IR $\tilde{v}_{max}$ (neat, cm^{-1}) 3533, 3339, 2959, 2870, 1692, 1599, 1528, 1457, 1323, 1256, 1148, 1088, 1028, 991, 916, 879, 831, 752.

HRMS (ESI): *m/z* calculated for C$_{31}$H$_{47}$N$_4$O$_9$S (M+NH$_4$)$^+$: 651.3058, found 651.3058.

HPLC (Cellulose-1, *i*-propanol/*n*-heptane = 40/60, flow rate = 0.5 mL/min, I = 254 nm): t_R = 12.78 min (minor), t_R = 18.63 min (major), 91% *de*.

6 Gram-scale and multigram-scale synthesis of the CpO-THF moiety
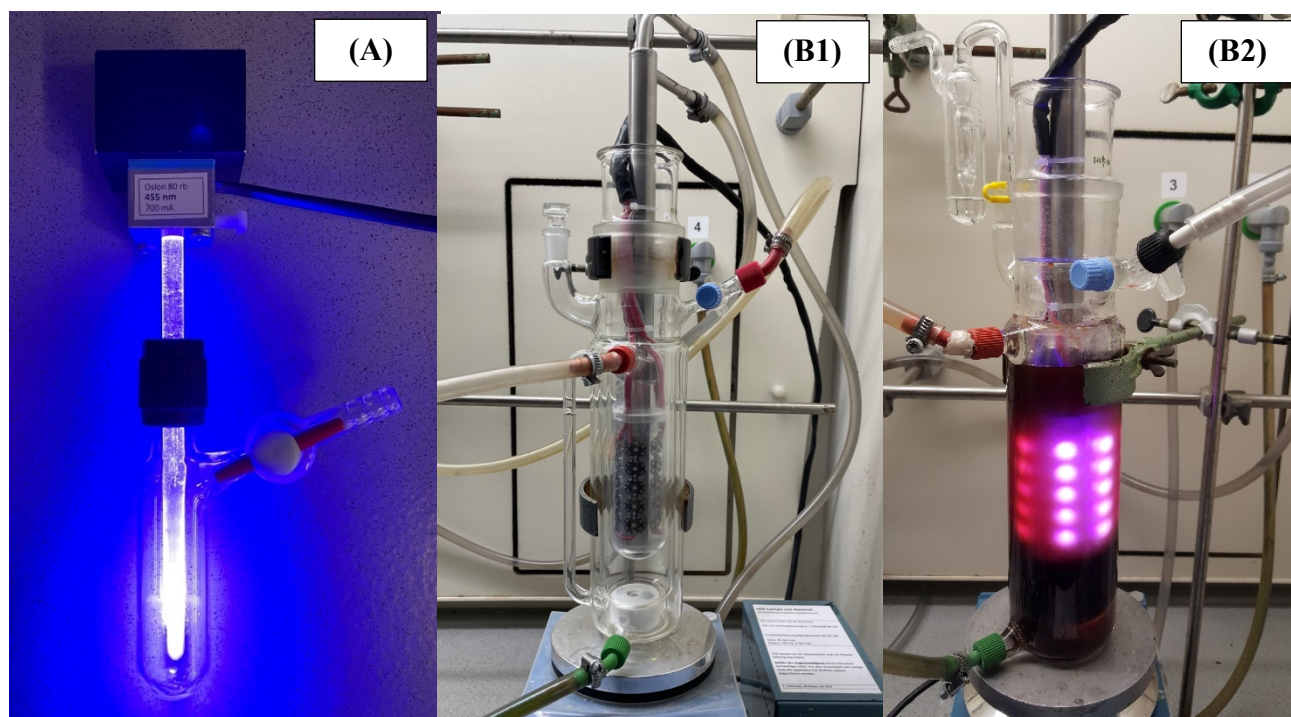
Figure S2. Reaction Upscaling: (**A**) Irradiation setup with large-sized Schlenk tube (30 mL size) for 5 mmol scale; (**B1**) Big-Scale irradiation setup (200 mL) with 30 OSLON SSL 80 deep blue LEDs (each: 1 W, 700 mA, λ_{max} = 455 nm) for 45 mmol scale. (**B2**) Big-Scale irradiation setup after irradiating the reaction mixture for 3 d.

Reaction Upscaling to gram (5 mmol) or multigram (45 mmol) quantities was performed by using specialized size-optimized photochemical setups (Figure S2, **(A)** and **(B1/B2)**).

Photocatalytic DcRCAE-Oxa-Michael Reaction in 5 mmol scale (Figure S2, Part **(A)**):

A flame-dried large-sized pressure tube was charged with *(S)-tert*-butyl (4-oxocyclopent-2-en-1-yl) carbonate ((*S*)-**118**) (991 mg, 5.00 mmol, 1.00 equiv), *N*-Boc L-serine (**150**) (1.03 g, 5.00 mmol, 1.00 equiv), K_2HPO_4 (1.05 g, 6.00 mmol, 1.20 equiv), 4CzIPN (39.4 mg, 50.0 μmol, 1.0 mol%) and anhydrous DMF (20 mL, 0.25 M) under nitrogen atmosphere. The reaction vessel was sealed with a screw-cap and subsequently degassed by applying three cycles of freeze-pump-thaw-backfill. The screw-cap was replaced by a glass rod and the reaction mixture was placed under a nitrogen atmosphere. After irradiation using a 455 nm high power LED through the pre-installed glass rod (see figure S2, part **A**) and stirring for 68 h at ambient temperature, the reaction mixture was directly concentrated in vacuo by the addition of *p*-xylene to facilitate the removal of DMF. The resulting crude product was purified by flash column chromatography (hexanes / EtOAc 1:1) on silica gel to yield enantioenriched bicycle (*ent*)-**151** (1.03 g, 4.28 mmol, 86%) as a mixture of two enantioenriched diastereomers *exo*-**151** and *endo*-**151** in a diastereomeric ratio of 2.2:1.0.

Photocatalytic DcRCAE-Oxa-Michael Reaction in 45 mmol scale (Figure S2, Part **(B1/B2)**):

A flame-dried specially designed big-scale photoapparatus (see Figure S2, Part **(B1/B2)**) was charged with *tert*-butyl (4-oxocyclopent-2-en-1-yl) carbonate (**118**) (8.92 g, 45.0 mmol, 1.00 equiv), *N*-Boc L-serine (**150**) (9.23 g, 45.0 mmol, 1.00 equiv), K_2HPO_4 (9.41 g, 54.0 mmol, 1.20 equiv), 4CzIPN (887 mg, 1.12 mmol, 2.5 mol%) and anhydrous, pre-degassed DMF (180 mL, 0.25 M) under nitrogen atmosphere. The photoapparatus was sealed and the irradiation was initiated using 30 OSLON SSL 80 deep blue LEDs (each: 1 W, 700 mA, λ_{max} = 455 nm). After stirring for 3 d at ambient temperature, the reaction mixture was directly concentrated in vacuo by the addition of *p*-xylene to facilitate the removal of DMF. The resulting crude product was purified by flash column chromatography (hexanes / EtOAc 1:1) on silica gel to yield bicycle **151** and the corresponding uncyclized cyclopentenone derivative **160** in a ratio of approximately 3:1 (combined yield: 9.03 g, 37.4 mmol, 83%). Subsequently, the purified mixture of both cyclized and uncyclized adducts was resolved in DCM (150 mL) and KF (2.61 g, 44.9 mmol, 1.20 equiv) and Al_2O_3 (4.58 g, 44.9 mmol, 1.20 equiv) were added.[118] The suspension was stirred for 20 h at ambient temperature, followed by a filtration over a pad of celite. The solvent was removed in vacuo and the crude product was purified by flash column chromatography (hexanes / EtOAc 1:1) on silica gel to give rise to **151** (8.81 g, 36.5 mmol, 81%) as a mixture of two diastereomers (*dr* 2.0:1.0) as a yellowish oil.

F Appendix

1 NMR-spectra

^{1}H NMR spectra   upper image

^{13}C NMR spectra   lower image

Solvent and frequency are given at the respective spectra.

Tert-butyl (4-oxocyclopent-2-en-1-yl) carbonate (118)
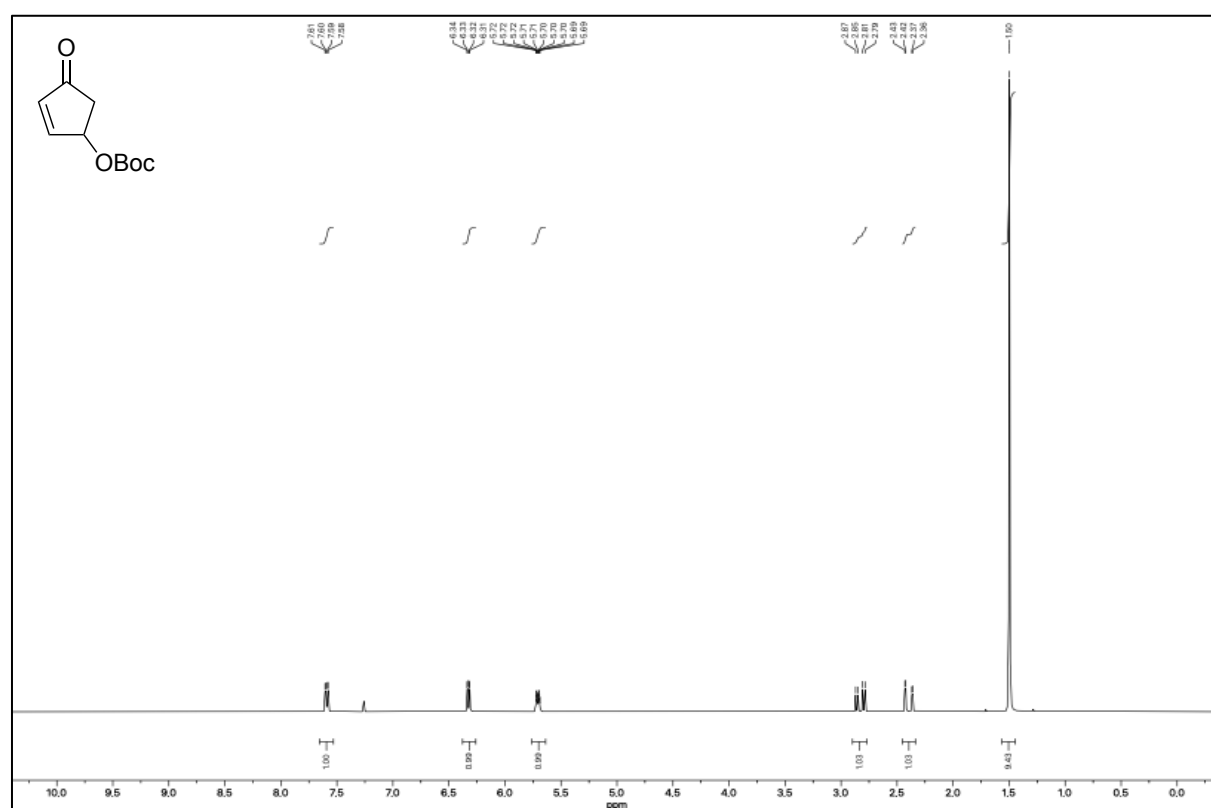
Figure S3. ¹H-NMR of **118** (300 MHz, CDCl₃).
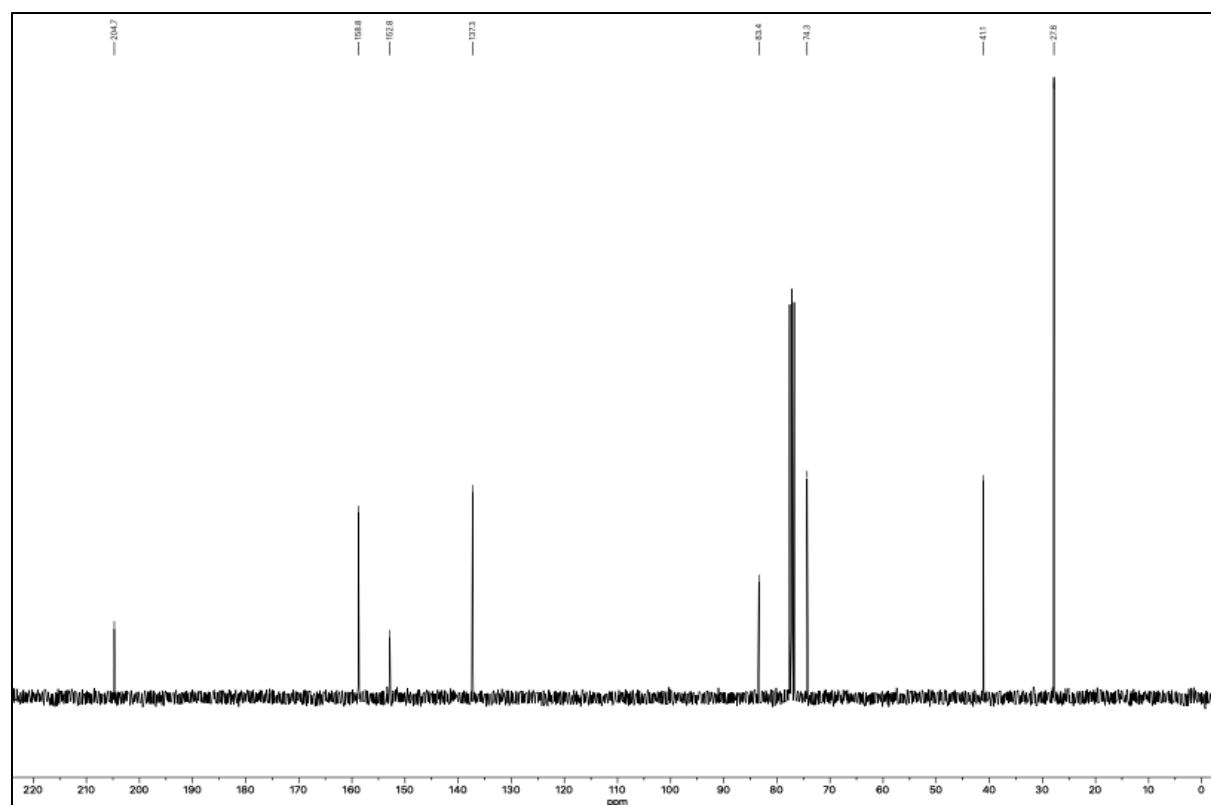
Figure S4. ¹³C-NMR of **118** (75 MHz, CDCl₃).

(±)-*Tert*-butyl ((1*R*,5*S*)-5-methyl-4-oxocyclopent-2-en-1-yl) carbonate (173a)
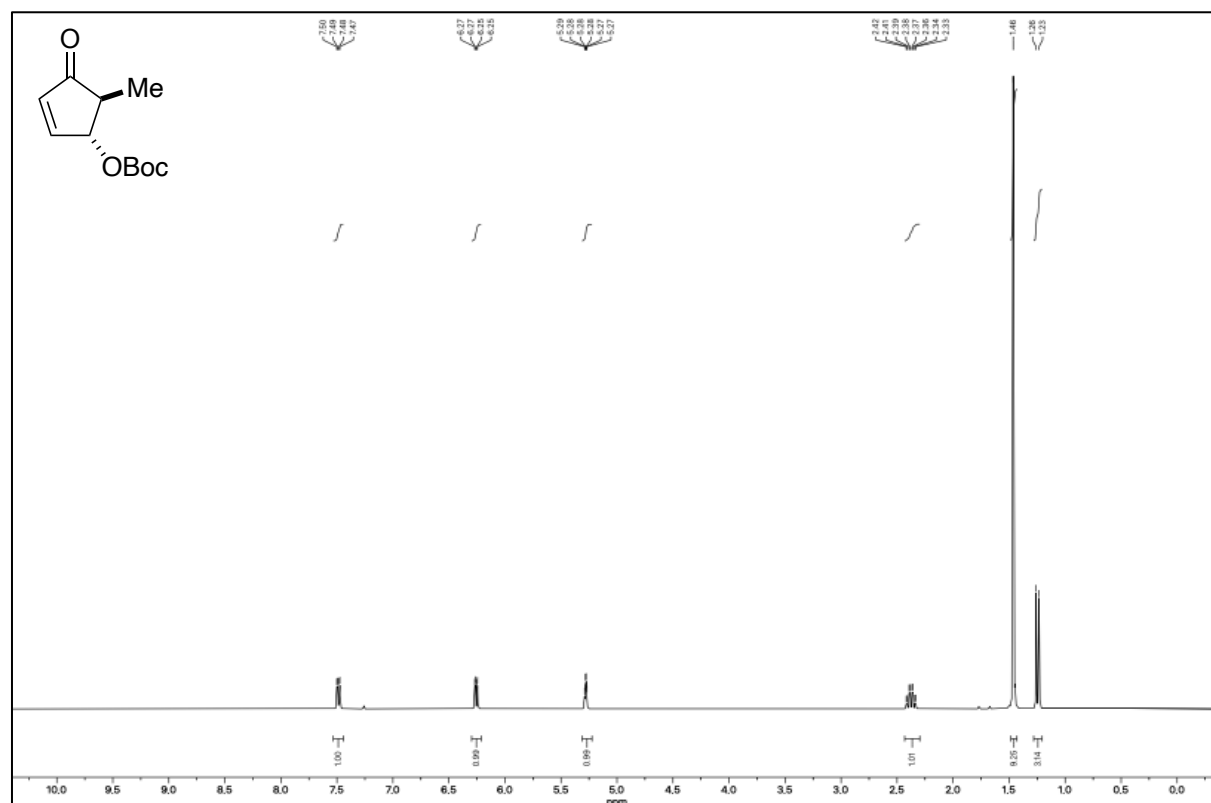
Figure S5. ^{1}H-NMR of **173a** (300 MHz, CDCl$_3$).
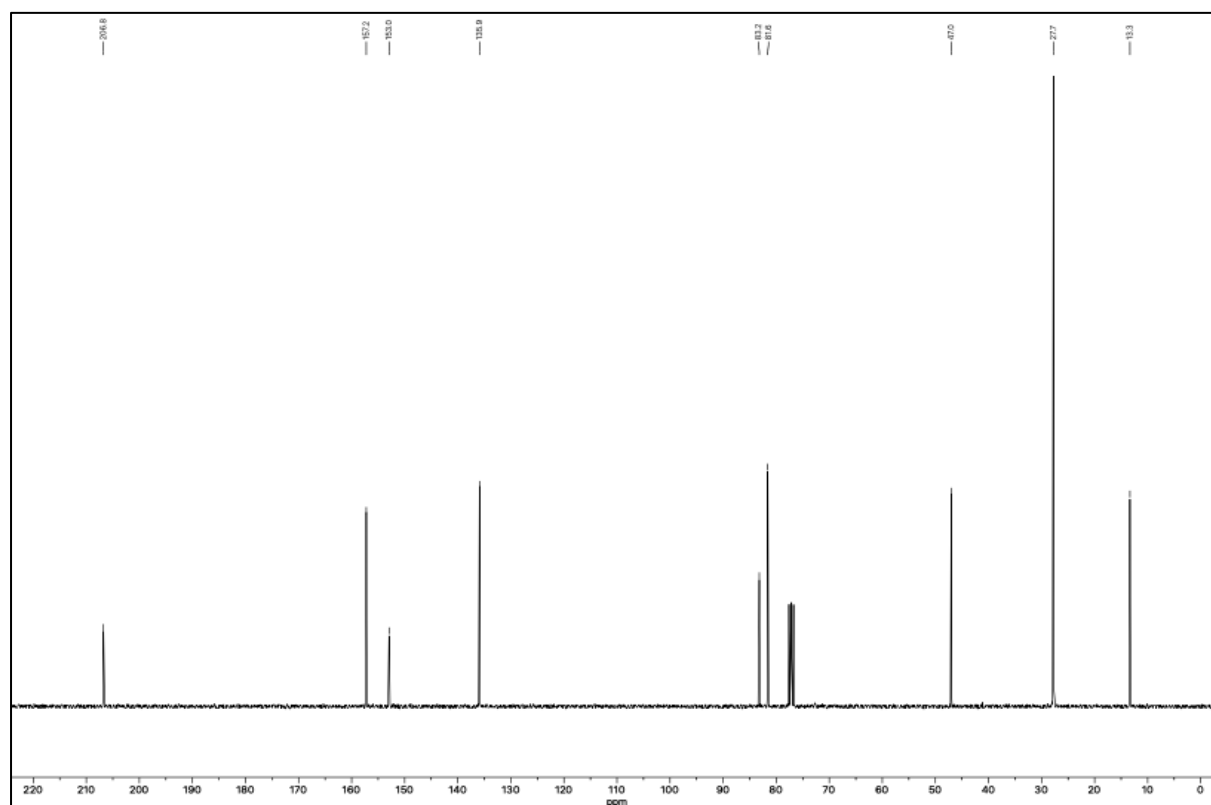
Figure S6. ^{13}C-NMR of **173a** (75 MHz, CDCl$_3$).

(±)-*Tert*-butyl ((1*R*,5*S*)-5-isopropyl-4-oxocyclopent-2-en-1-yl) carbonate (173b)
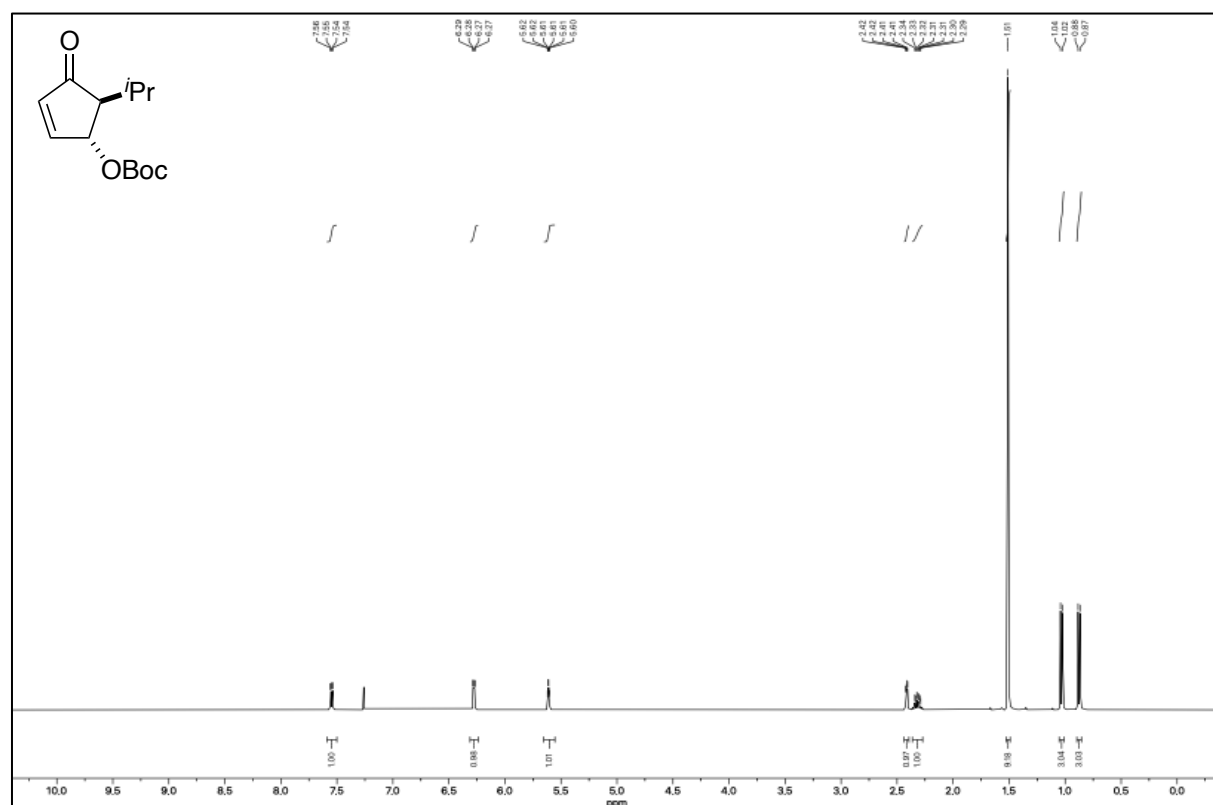
Figure S7. ^{1}H-NMR of **173b** (400 MHz, CDCl$_3$).
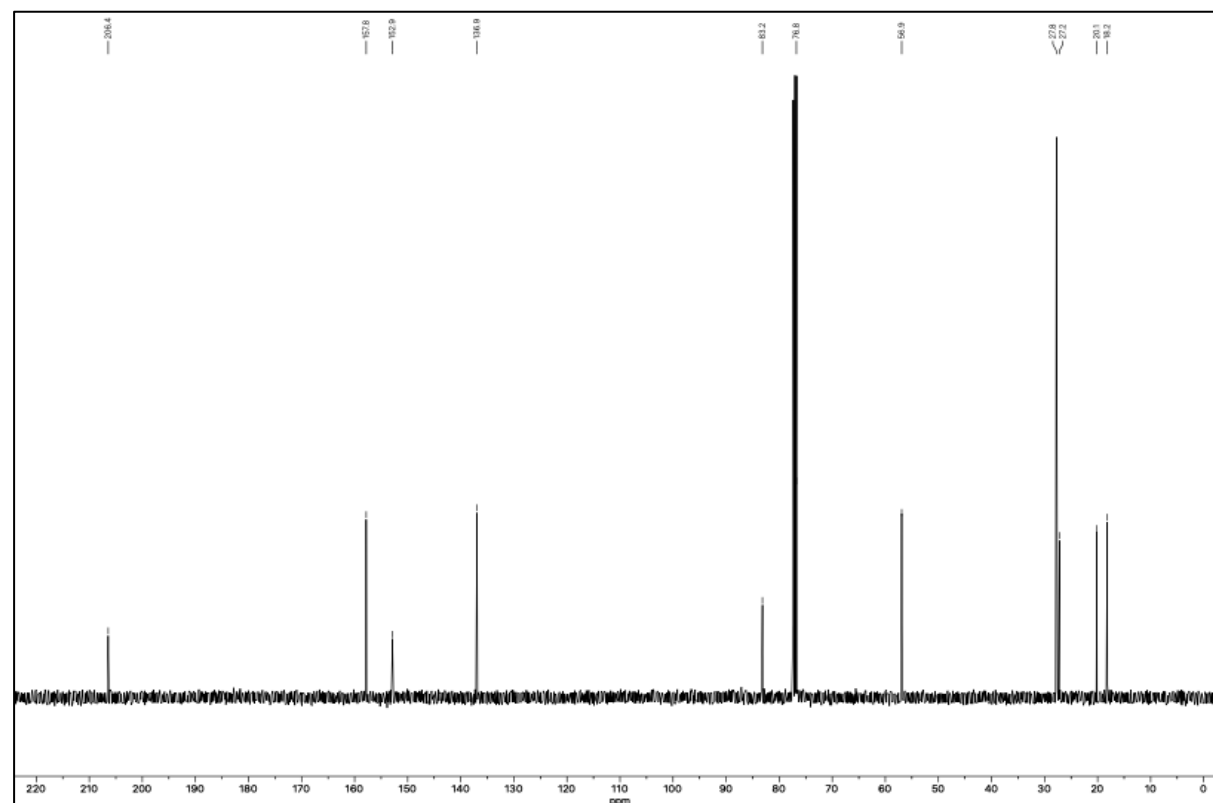
Figure S8. ^{13}C-NMR of **173b** (101 MHz, CDCl$_3$).

Tert-butyl (3-methyl-4-oxocyclopent-2-en-1-yl) carbonate (173c)
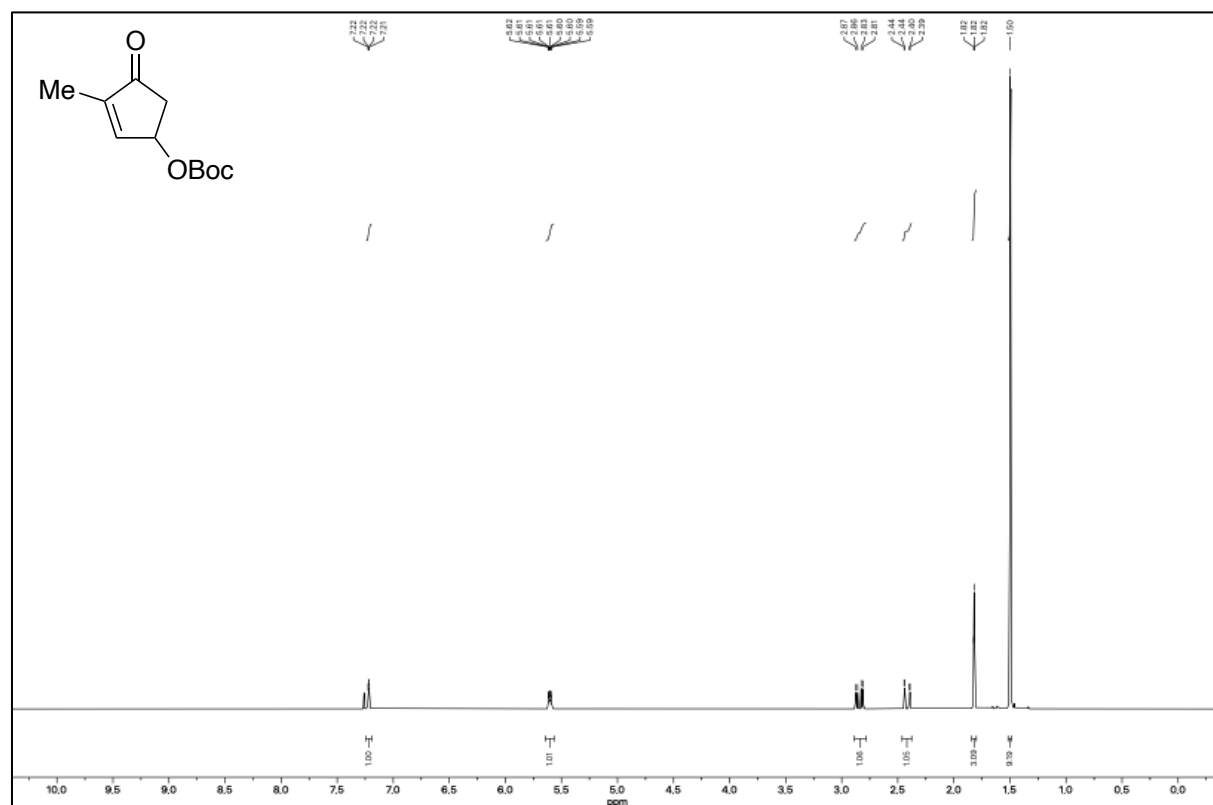
Figure S9. ^{1}H-NMR of **173c** (400 MHz, CDCl$_3$).
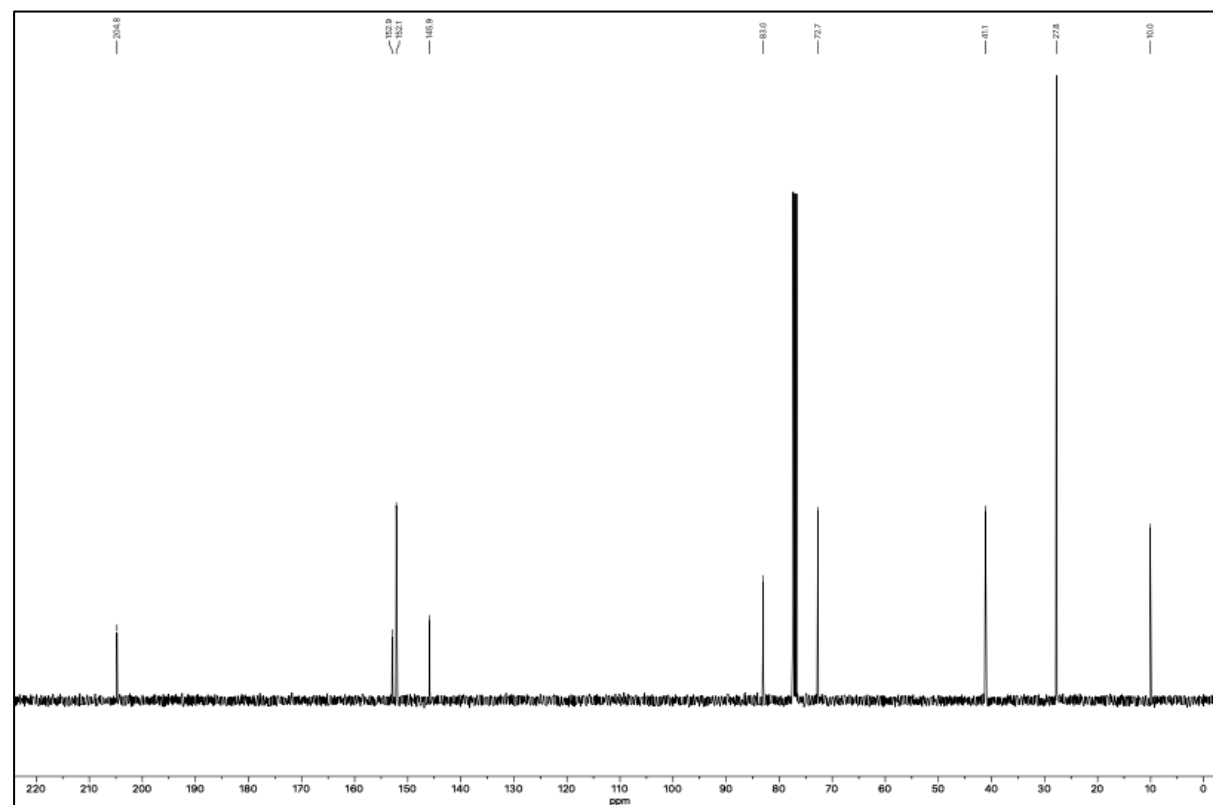
Figure S10. ^{13}C-NMR of **173c** (101 MHz, CDCl$_3$).

2-(Hydroxymethyl)-3-methylbutanoic acid (166)
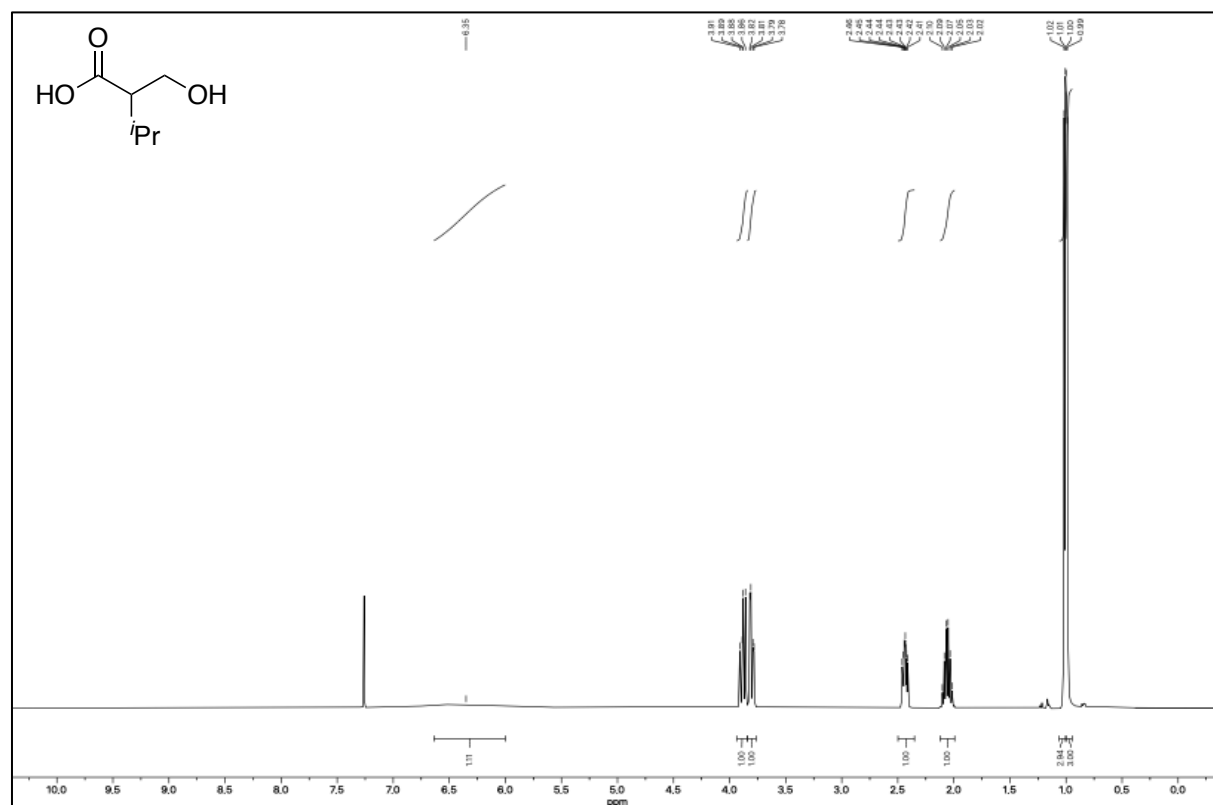
Figure S11. ^{1}H-NMR of **166** (400 MHz, CDCl3).
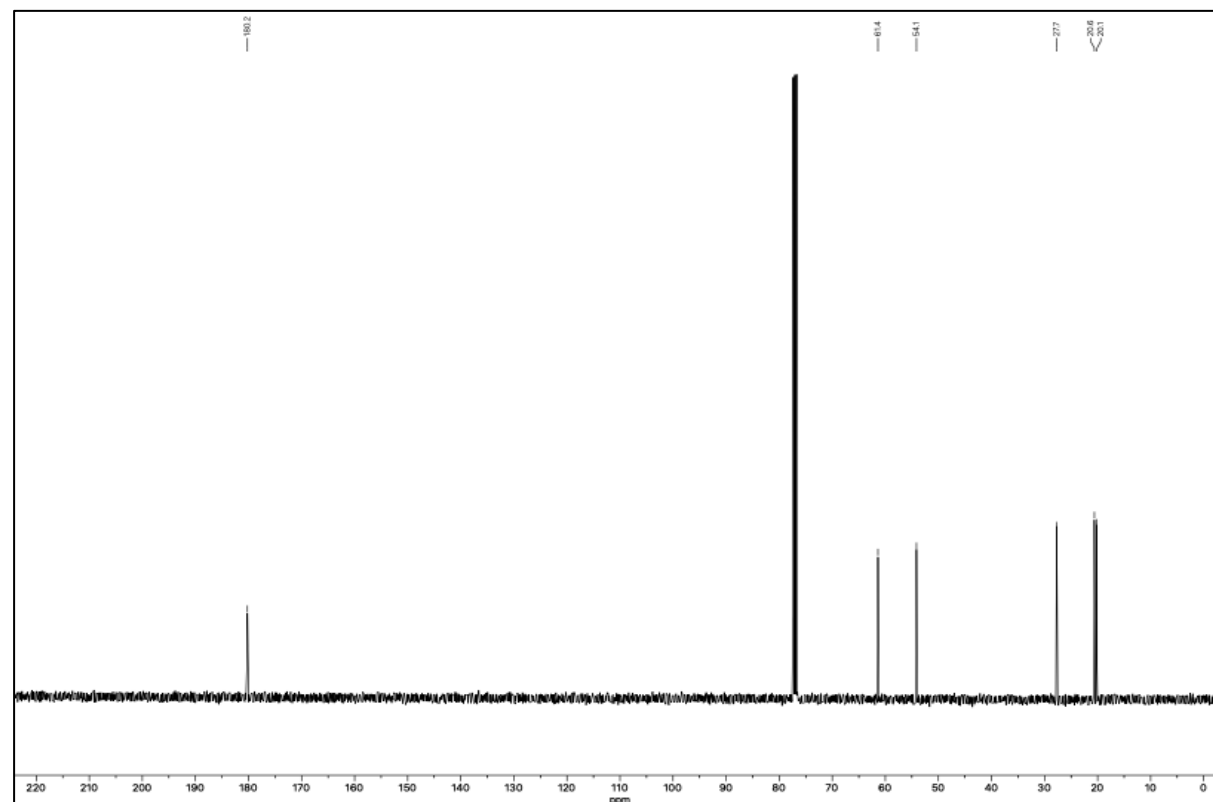
Figure S12. ^{13}C-NMR of **166** (101 MHz, CDCl3).

3-Hydroxy-2-methoxypropanoic acid (170)
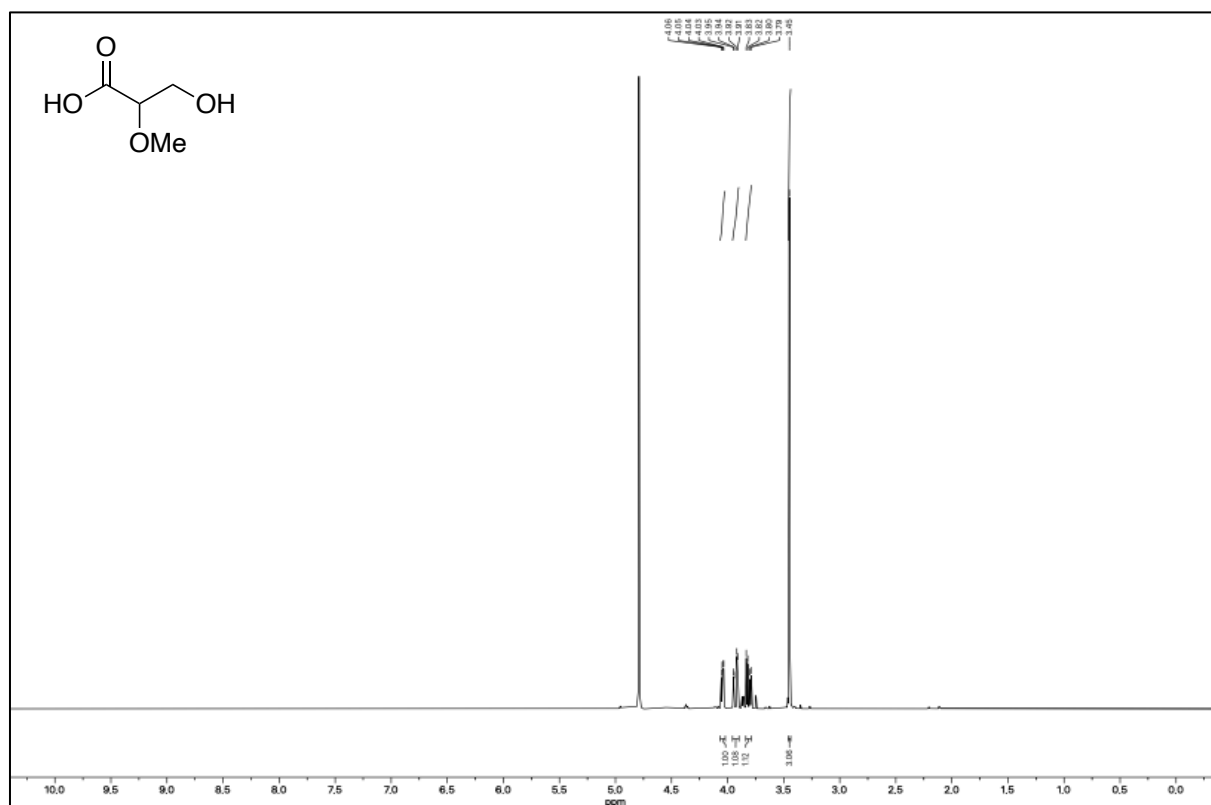
Figure S13. ^{1}H-NMR of **170** (400 MHz, D$_2$O).
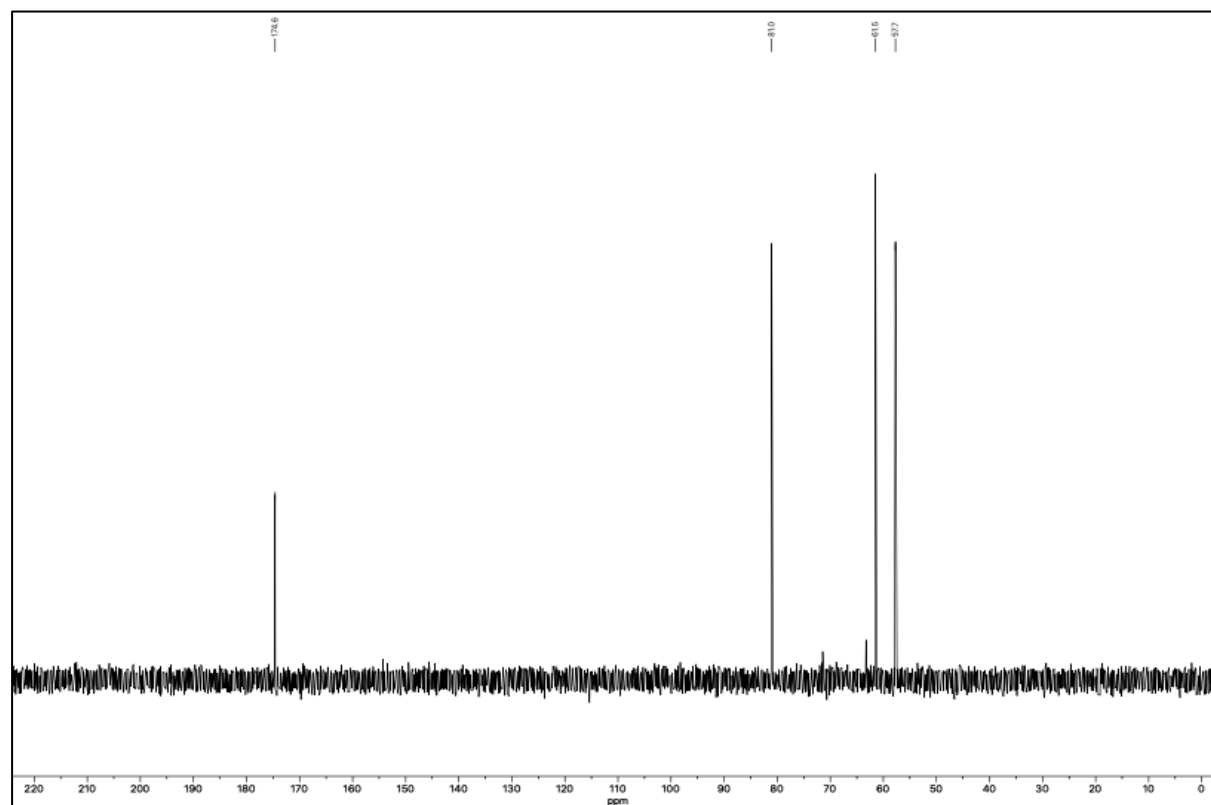
Figure S14. ^{13}C-NMR of **170** (101 MHz, D$_2$O).

3-Hydroxy-2-isopropoxypropanoic acid (171)
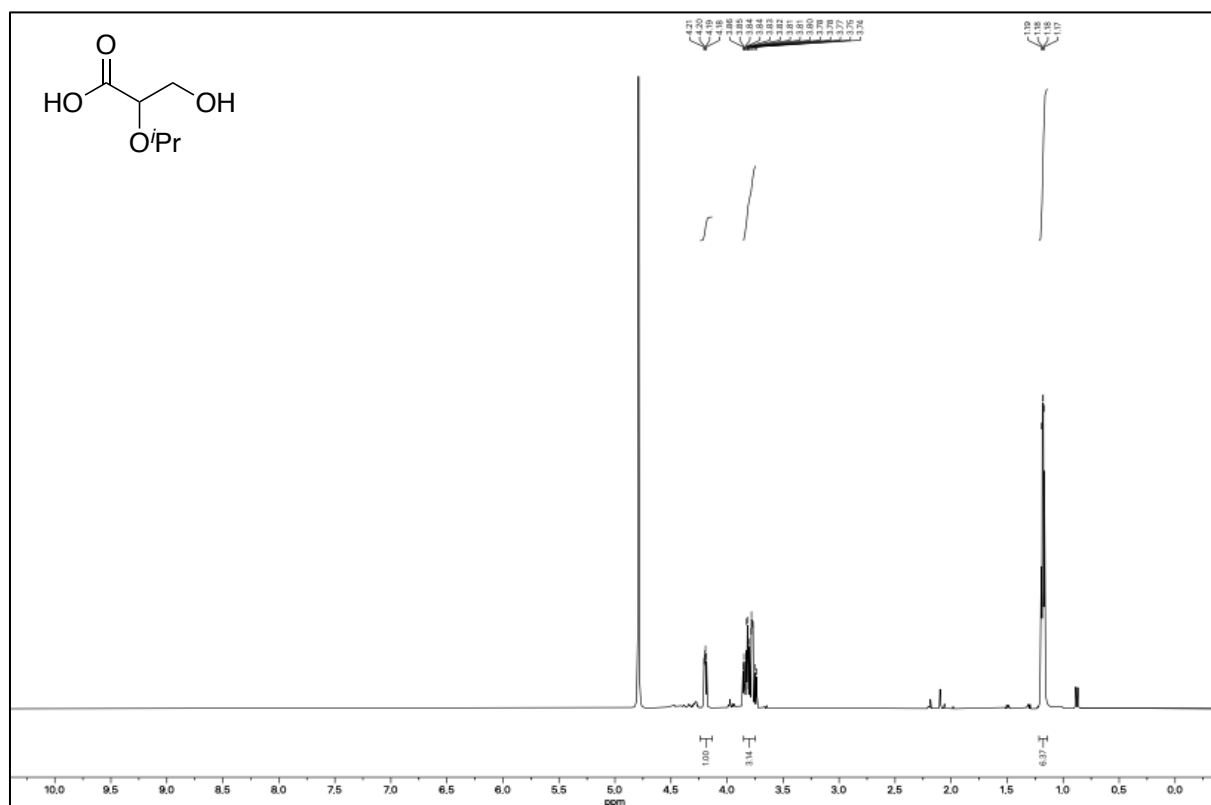
Figure S15. ^{1}H-NMR of **171** (400 MHz, D$_2$O).
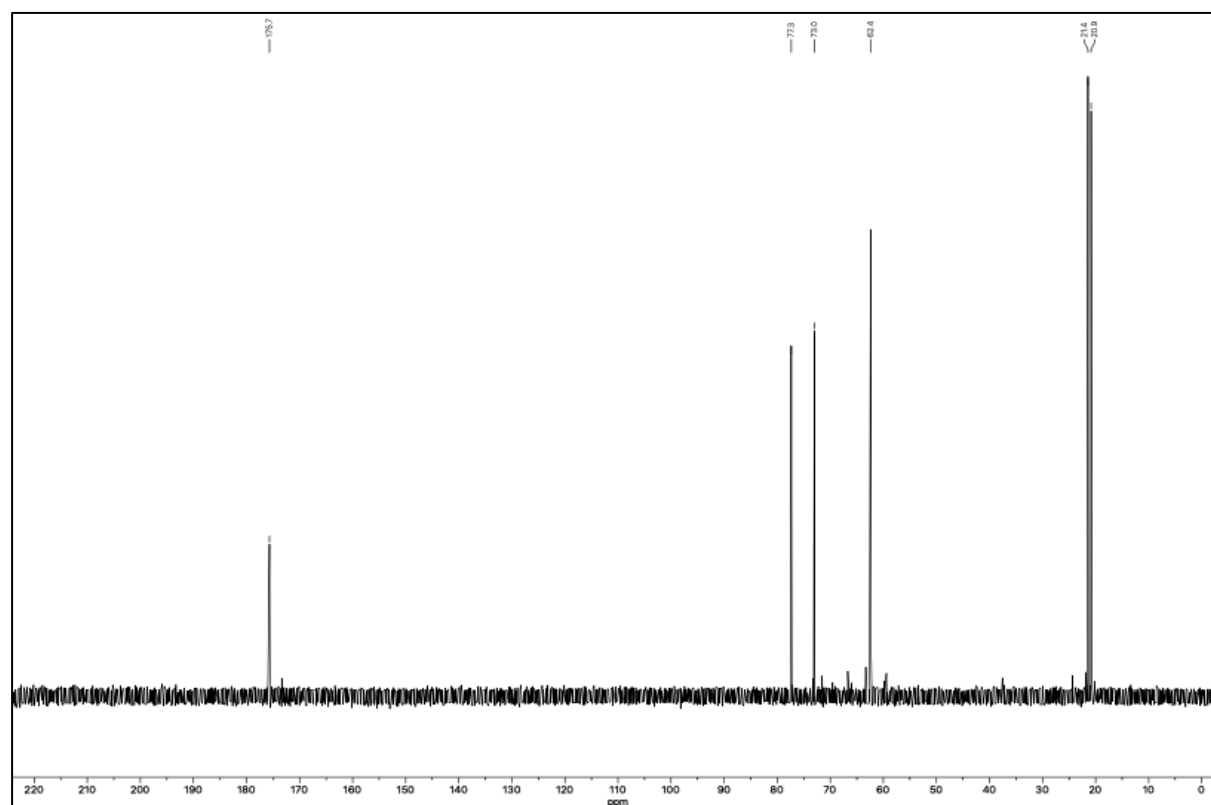
Figure S16. ^{13}C-NMR of **171** (101 MHz, D$_2$O).

2-(Benzyloxy)-3-hydroxypropanoic acid (172)
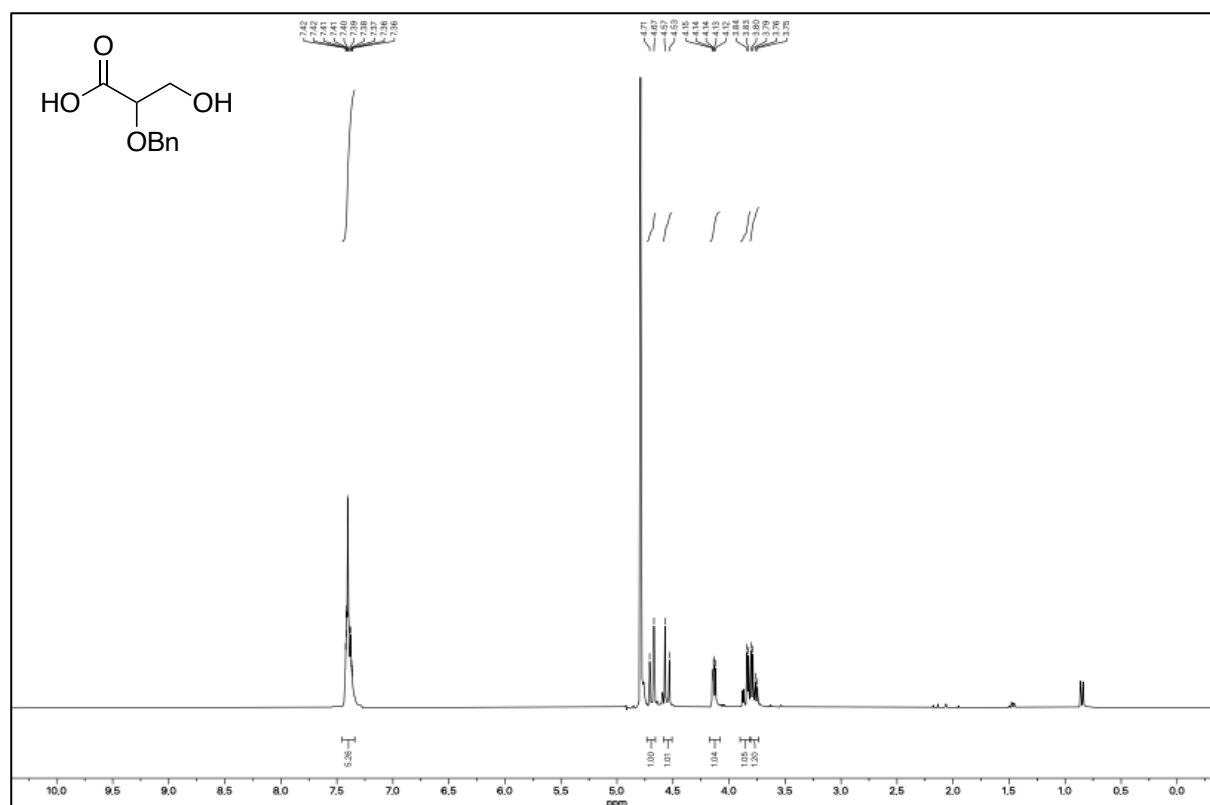
Figure S17. ^{1}H-NMR of **172** (300 MHz, D$_2$O).
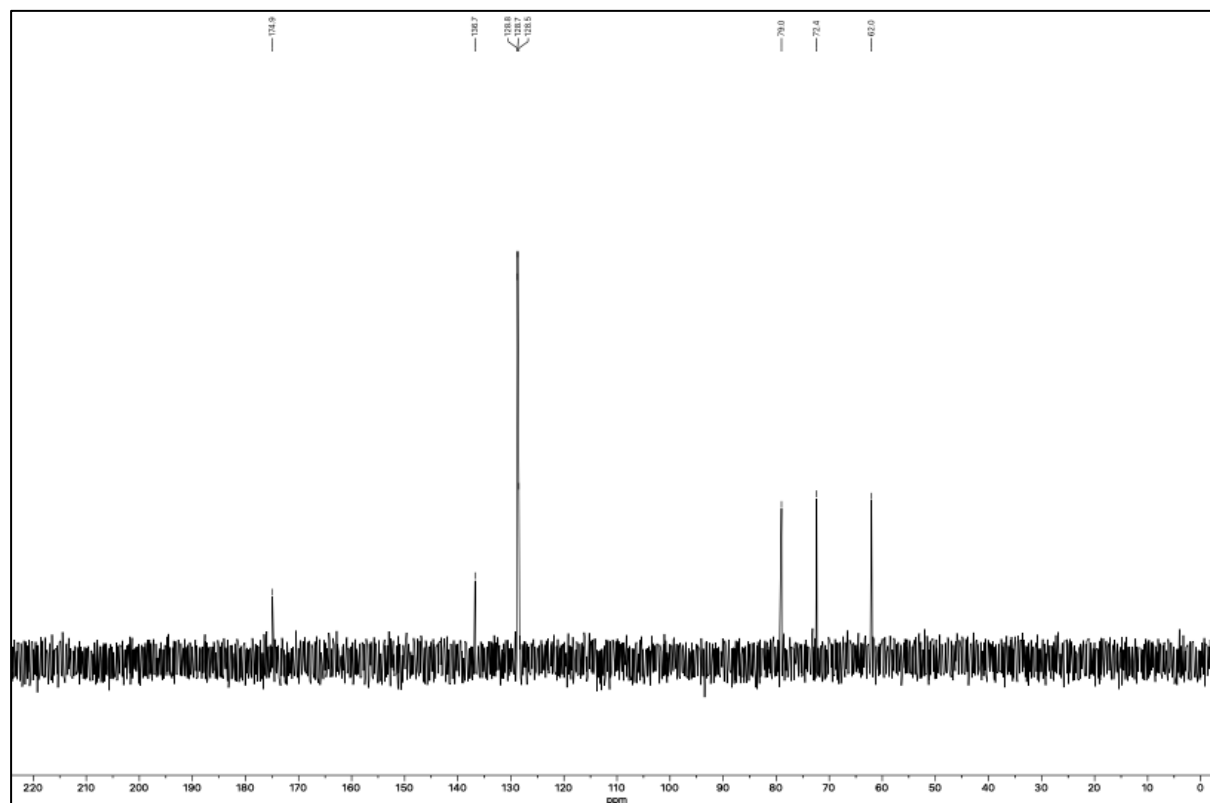
Figure S18. ^{13}C-NMR of **172** (75 MHz, D$_2$O).

N-Boc L-threonine (174b)
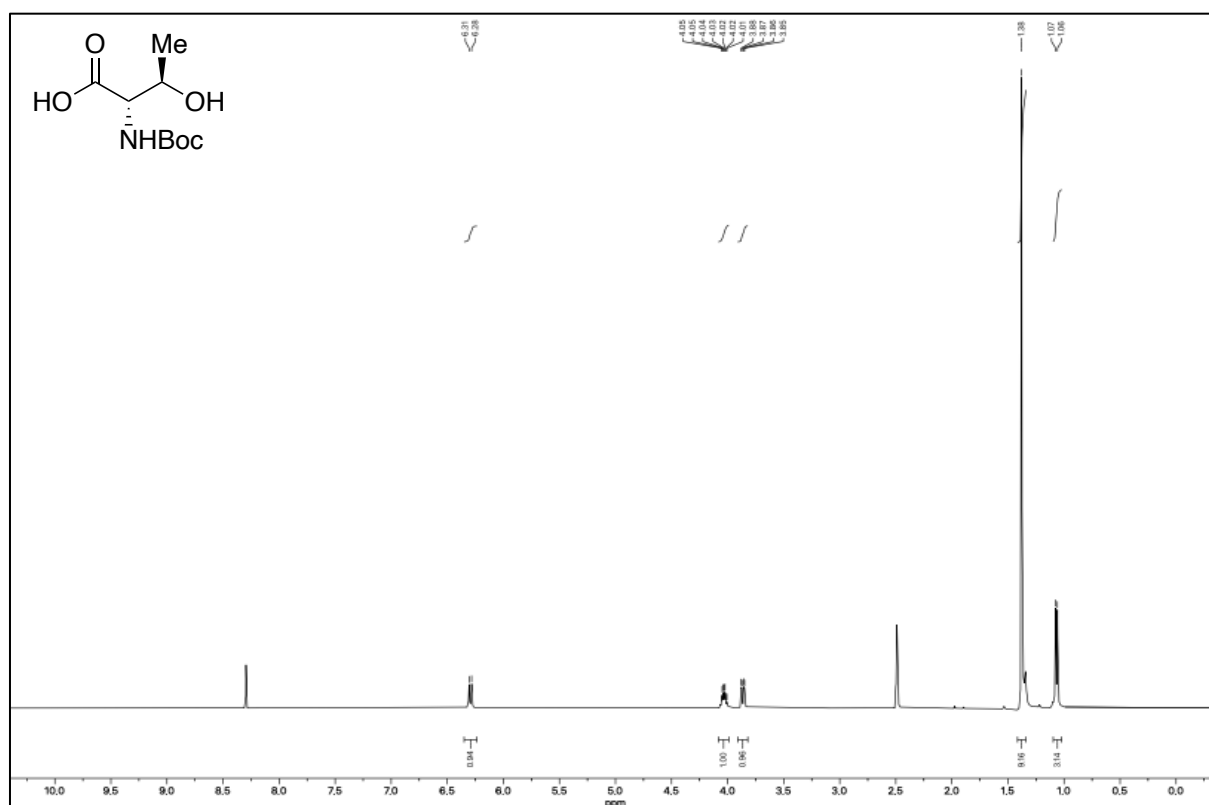
Figure S19. ^{1}H-NMR of **174b** (400 MHz, DMSO-d${}_6$).
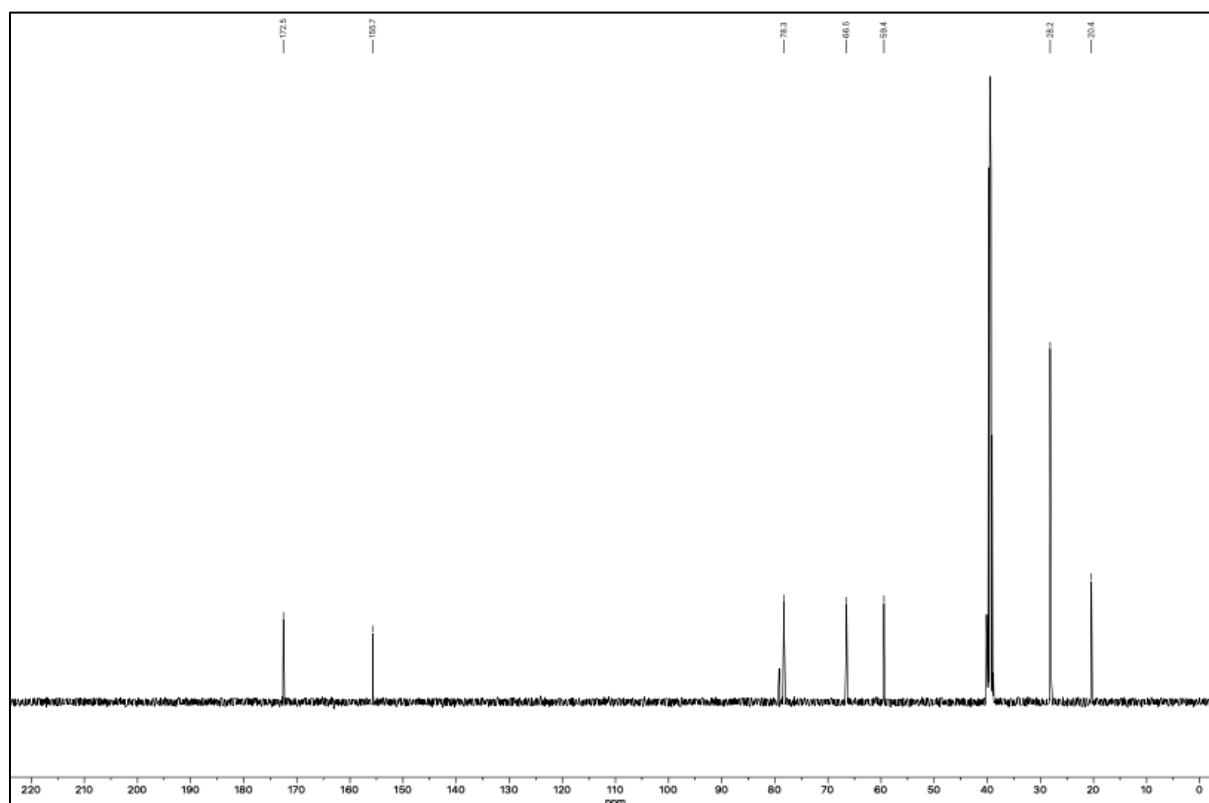
Figure S20. ^{13}C-NMR of **174b** (101 MHz, DMSO-d${}_6$).

(±)-*Tert*-butyl ((3*S*,3a*S*,6a*S*)-5-oxohexahydro-2*H*-cyclopenta[*b*]furan-3-yl)carbamate (*exo*-151)
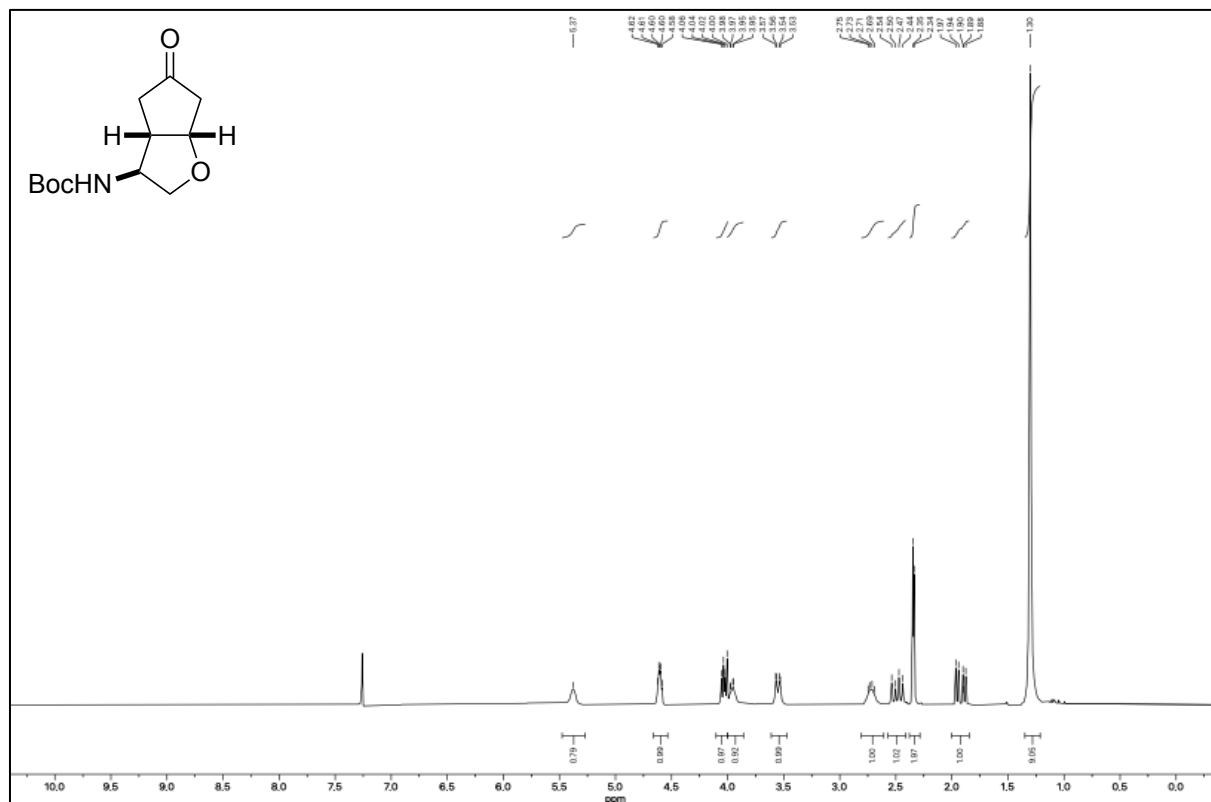
Figure S21. ^{1}H-NMR of *exo*–**151** (300 MHz, CDCl₃).
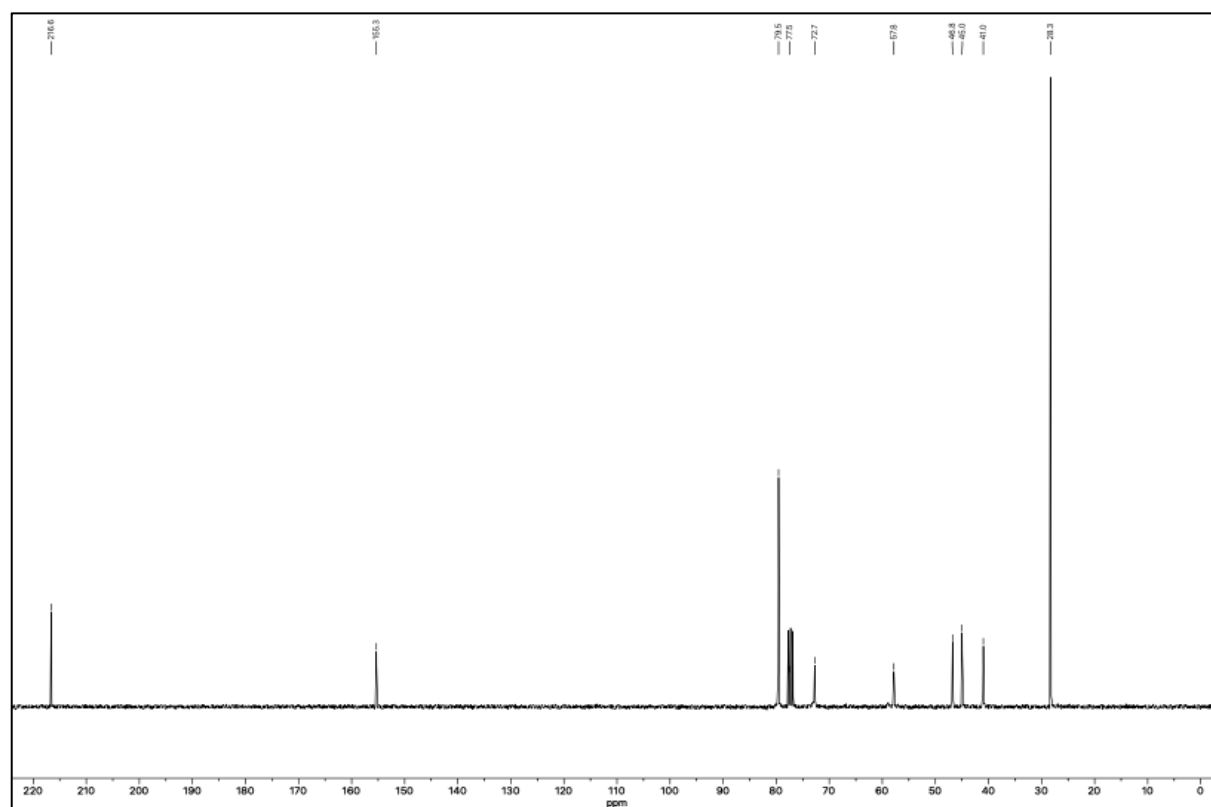
Figure S22. ^{13}C-NMR of *exo*–**151** (75 MHz, CDCl₃).

(±)-Tert-butyl ((3*R*,3a*S*,6a*S*)-5-oxohexahydro-2*H*-cyclopenta[*b*]furan-3-yl)carbamate (*endo*-151)
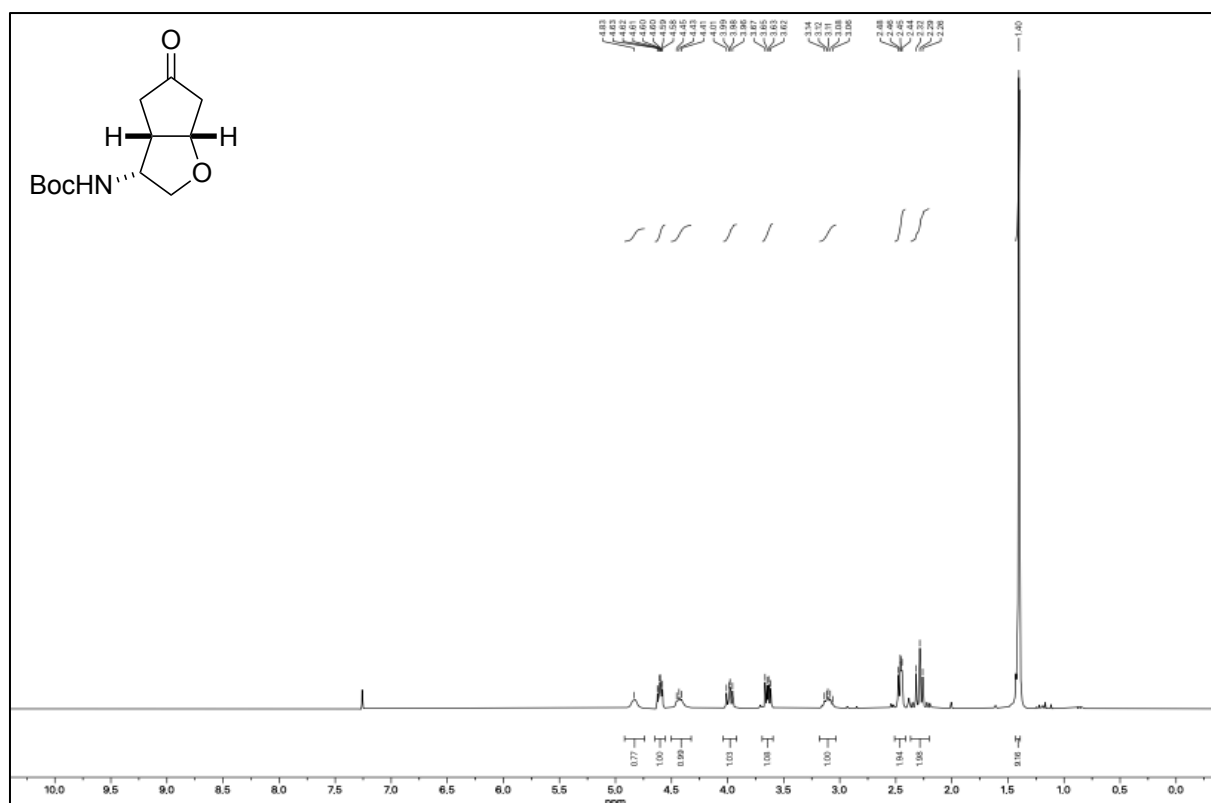
Figure S23. ^{1}H-NMR of *endo*–**151** (300 MHz, CDCl$_3$).
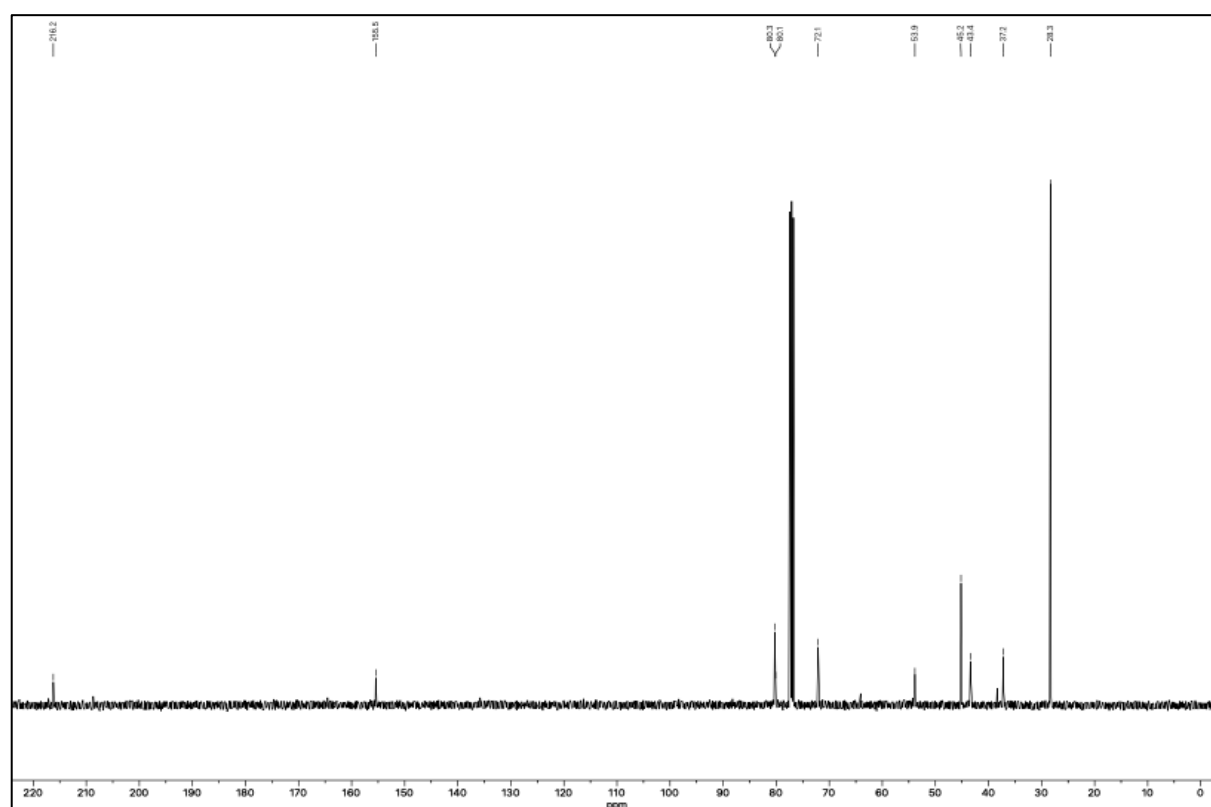
Figure S24. ^{13}C-NMR of *endo*–**151** (101 MHz, CDCl$_3$).

(±)-*Tert*-butyl (2-hydroxy-1-((*R*)-3-methyl-4-oxocyclopent-2-en-1-yl)ethyl)carbamate (176a)
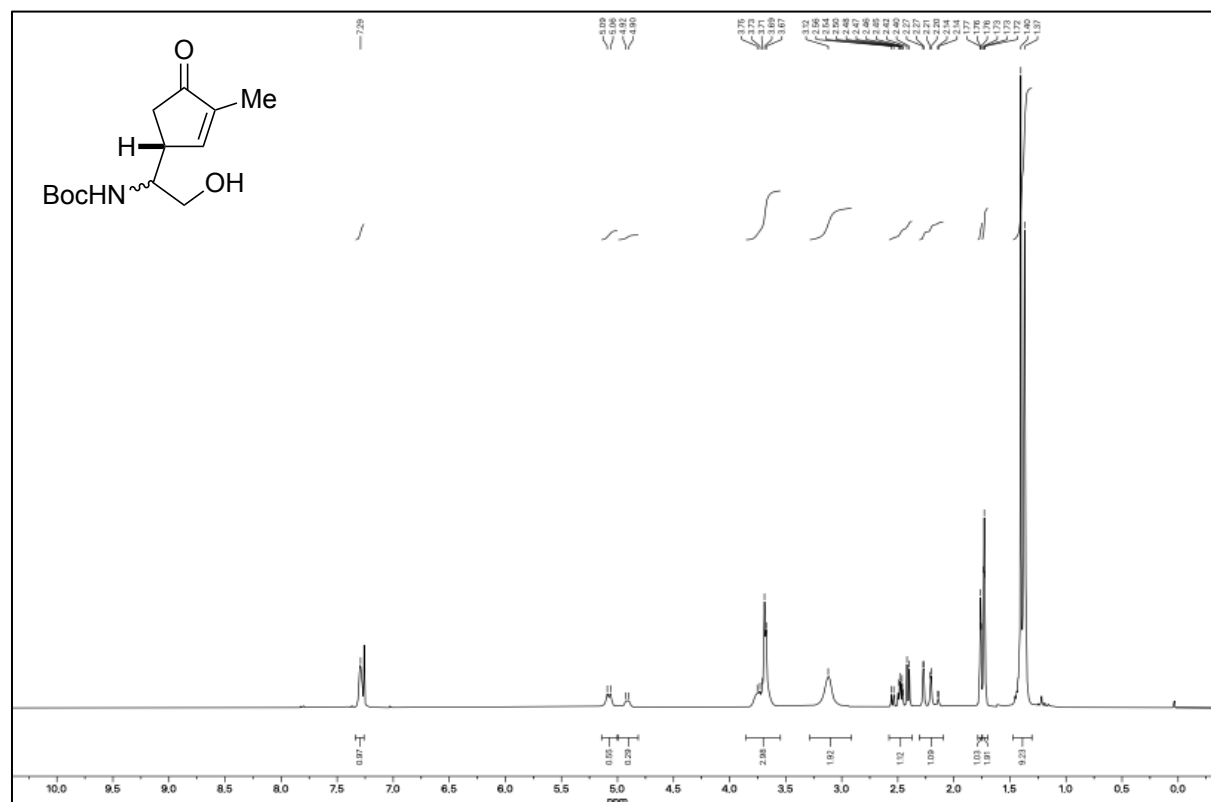
Figure S25. [^1]H-NMR of **176a** (300 MHz, CDCl₃).
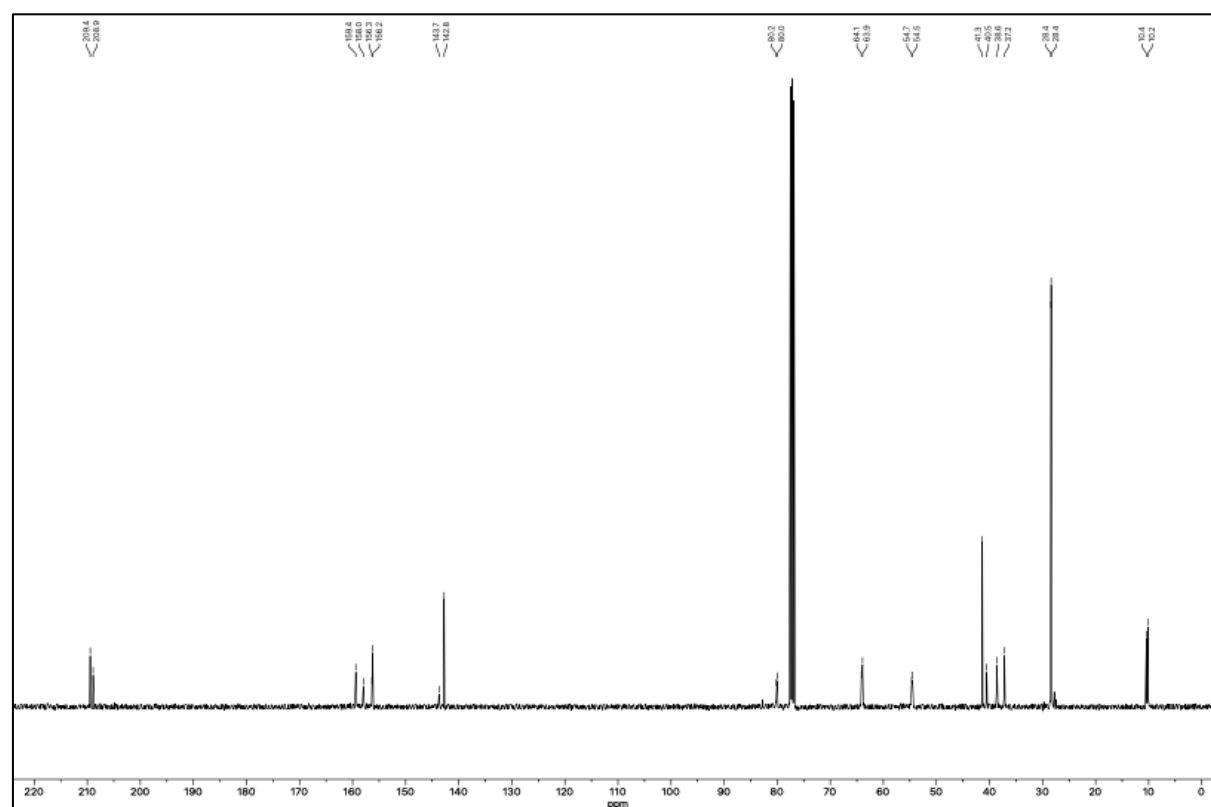
Figure S26. [^13]C-NMR of **176a** (101 MHz, CDCl₃).

127

(±)-*Tert*-butyl (2-hydroxy-1-((*R*)-3-isopropyl-4-oxocyclopent-2-en-1-yl)ethyl)carbamate (176b)

Figure S27. ^{1}H-NMR of **176b** (400 MHz, CDCl$_3$).

Figure S28. ^{13}C-NMR of **176b** (101 MHz, CDCl$_3$).

(±)-*Tert*-butyl ((3a*S*,4*R*,6a*S*)-4-methyl-5-oxohexahydro-2*H*-cyclopenta[*b*]furan-3-yl)carbamate (175a)

Figure S29. ^{1}H-NMR of **175a** (300 MHz, CDCl$_3$).

Figure S30. ^{13}C-NMR of **175a** (101 MHz, CDCl$_3$).
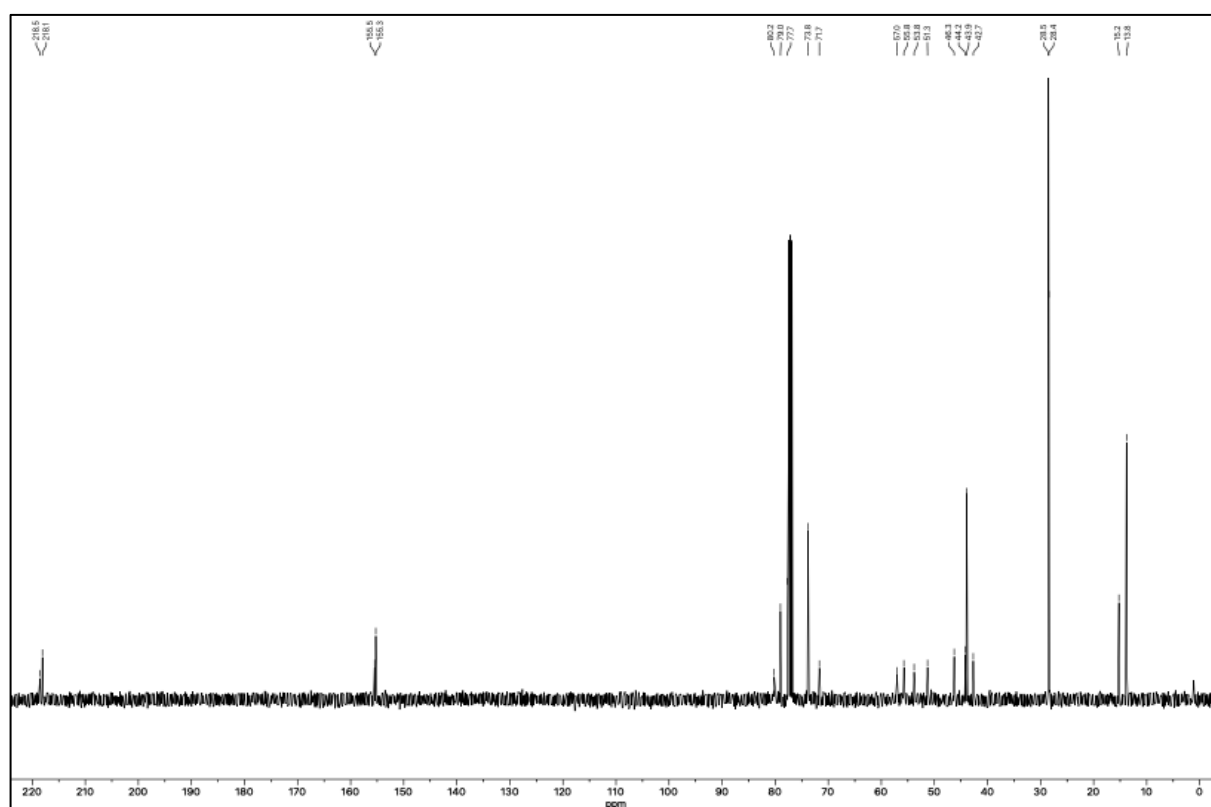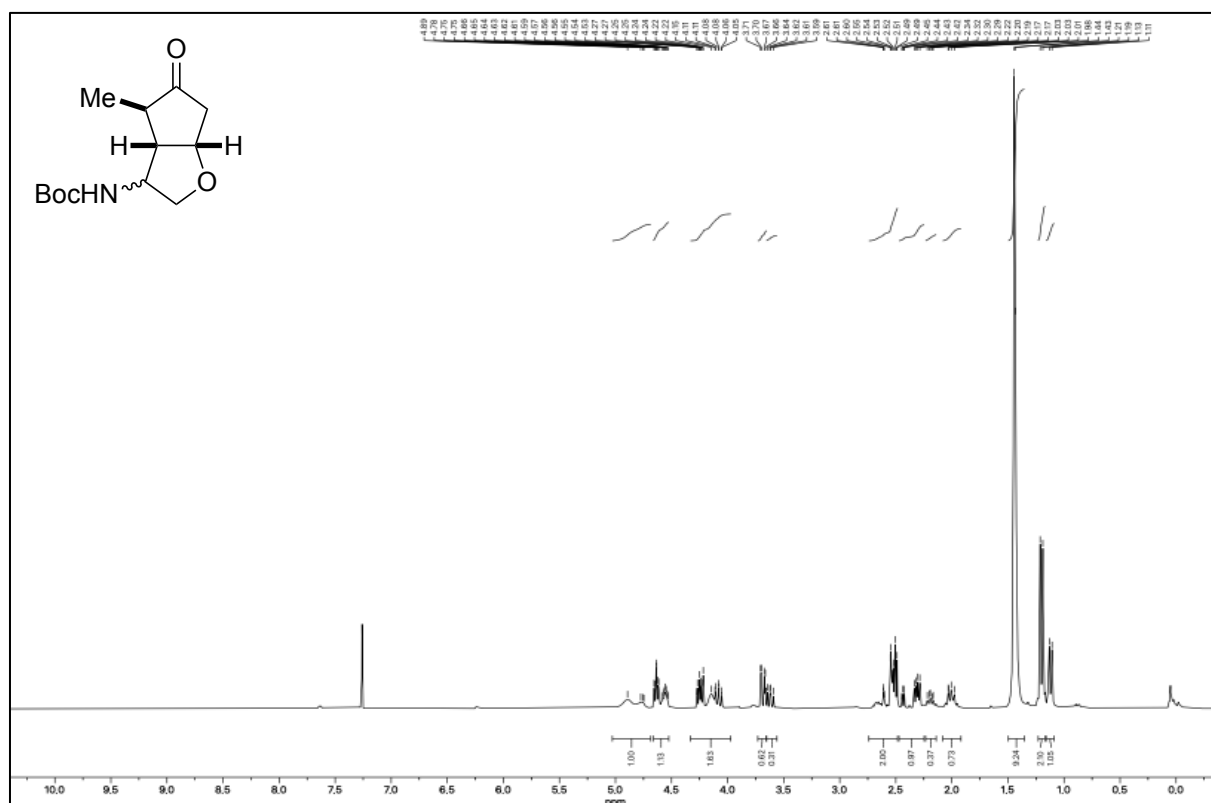
(±)-(3a*S*,6a*S*)-3-Isopropylhexahydro-5*H*-cyclopenta[*b*]furan-5-one (175b)
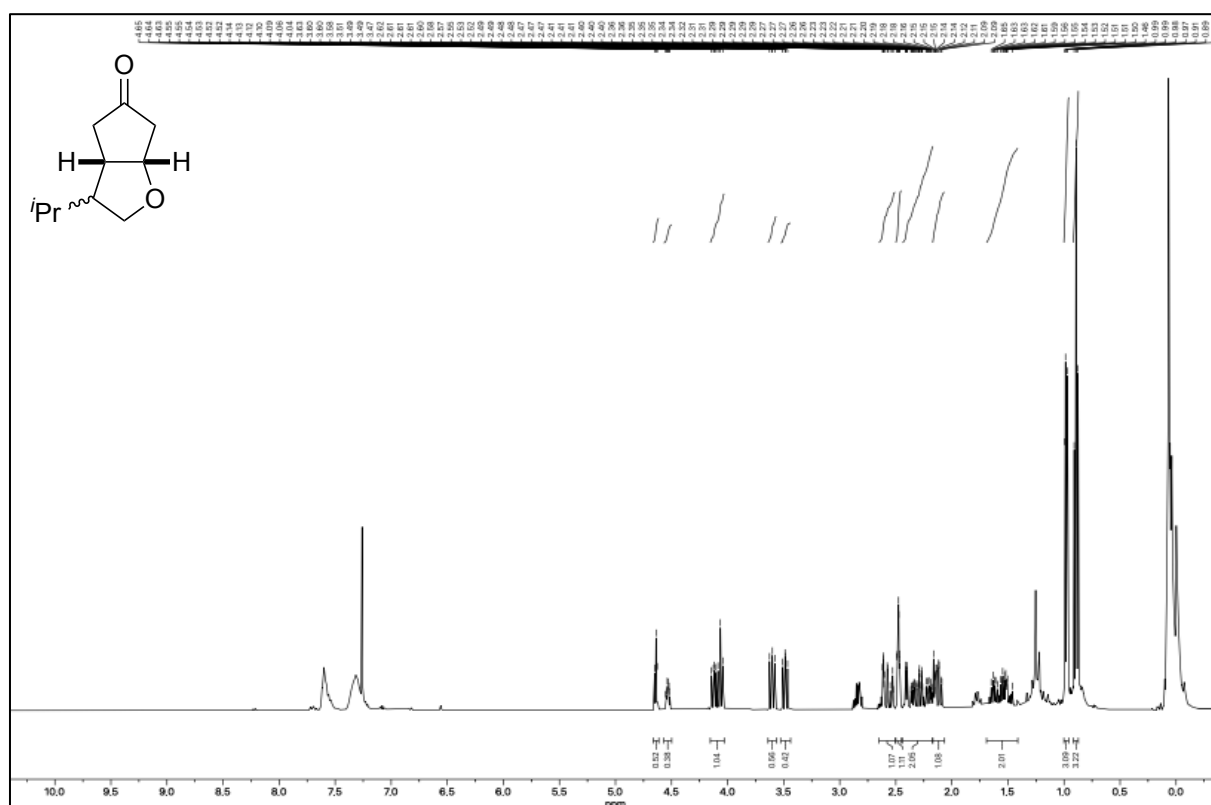
Figure S31. ^{1}H-NMR of **175b** (400 MHz, CDCl₃).
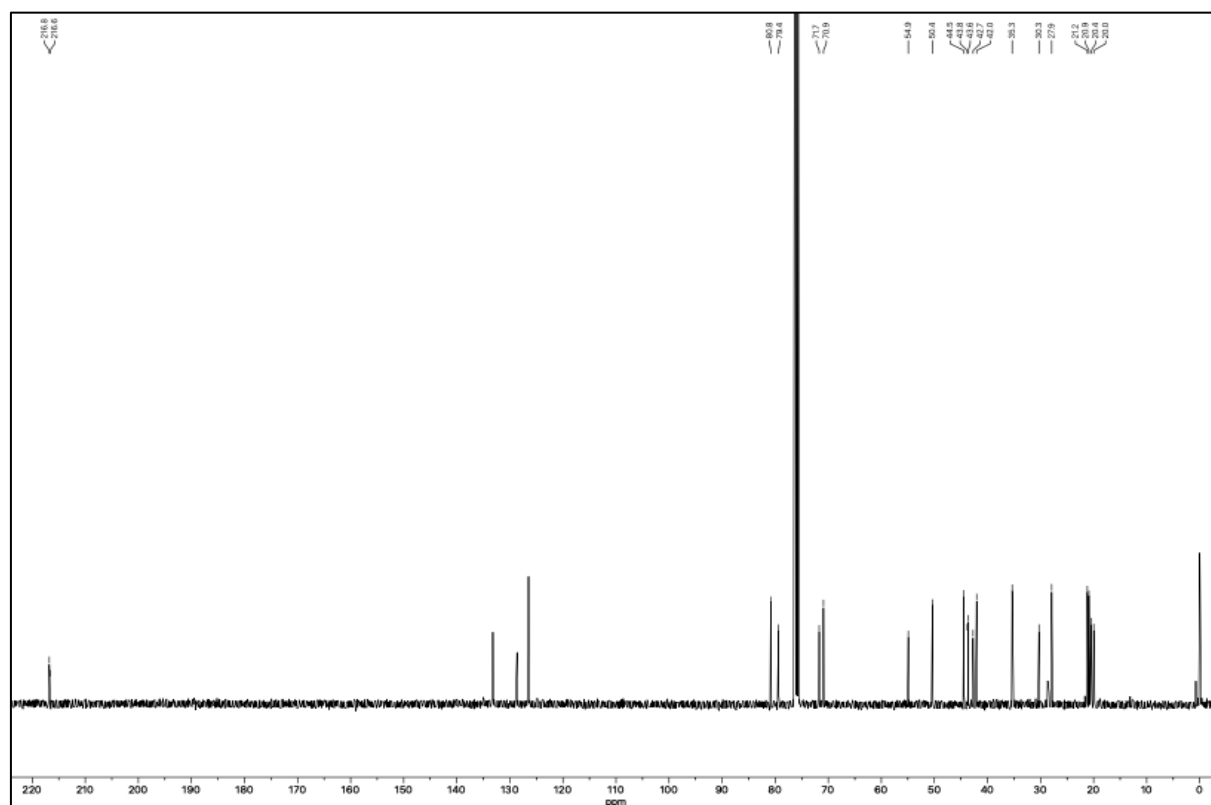
Figure S32. ^{13}C-NMR of **175b** (101 MHz, CDCl₃).

(±)-(3*R*,3a*S*,6a*S*)-3-Phenylhexahydro-5*H*-cyclopenta[*b*]furan-5-one (*exo*-175c)

Figure S33. ¹H-NMR of *exo*–**175c** (300 MHz, CDCl₃).

Figure S34. ¹³C-NMR of *exo*–**175c** (101 MHz, CDCl₃).
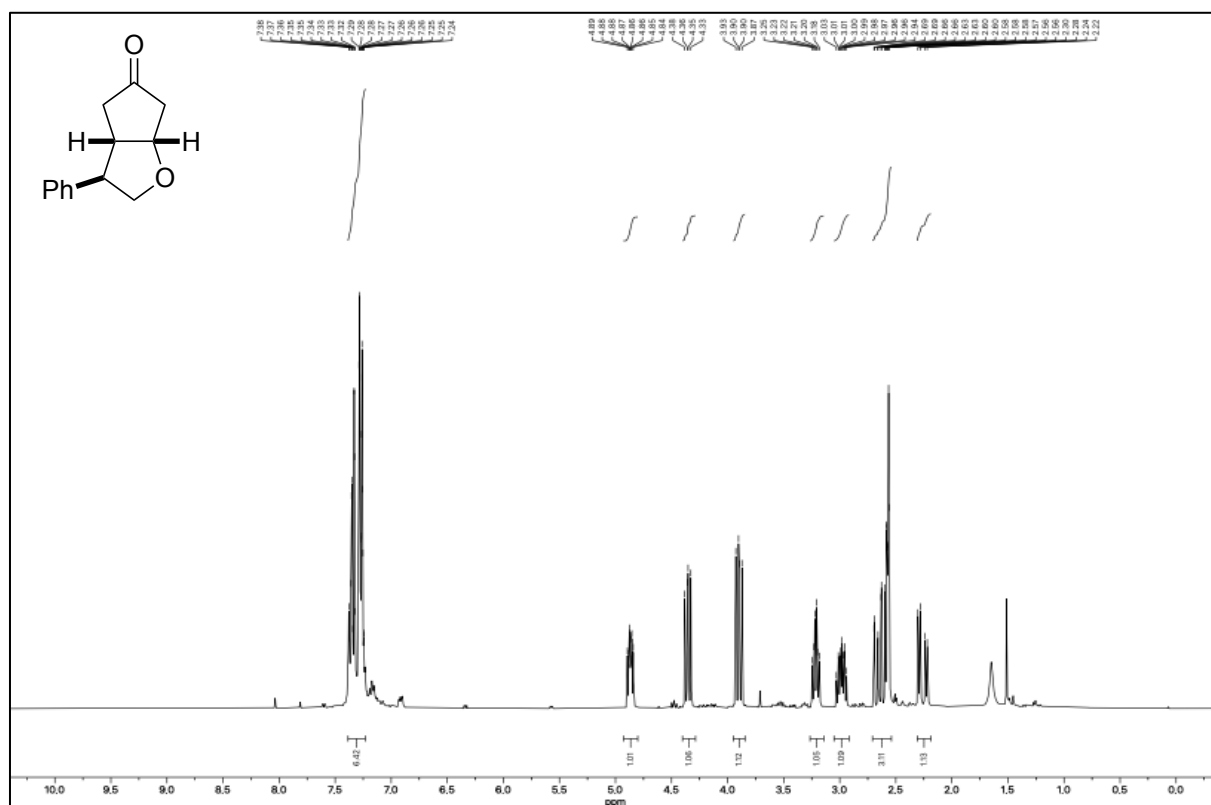
(±)-(3a*R*,6a*S*)-3-Methoxyhexahydro-5*H*-cyclopenta[*b*]furan-5-one (175d)
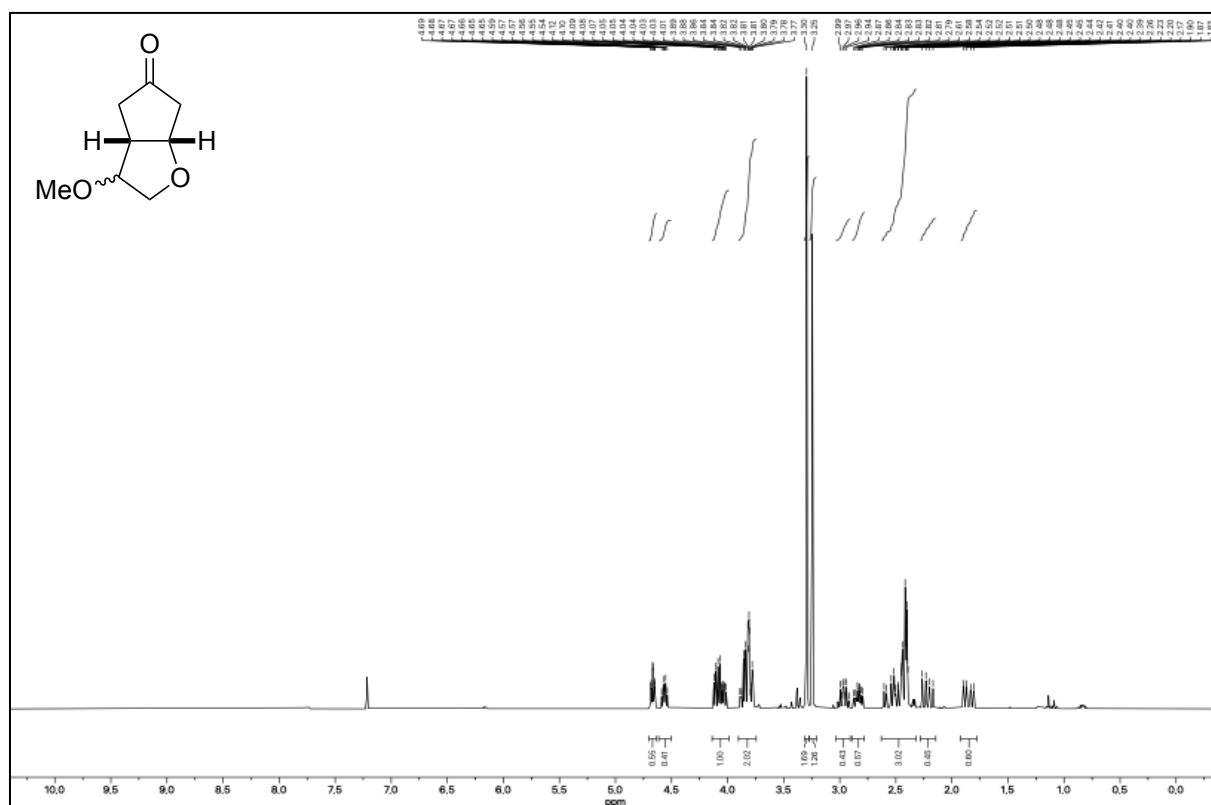
Figure S35. ¹H-NMR of **175d** (300 MHz, CDCl₃).
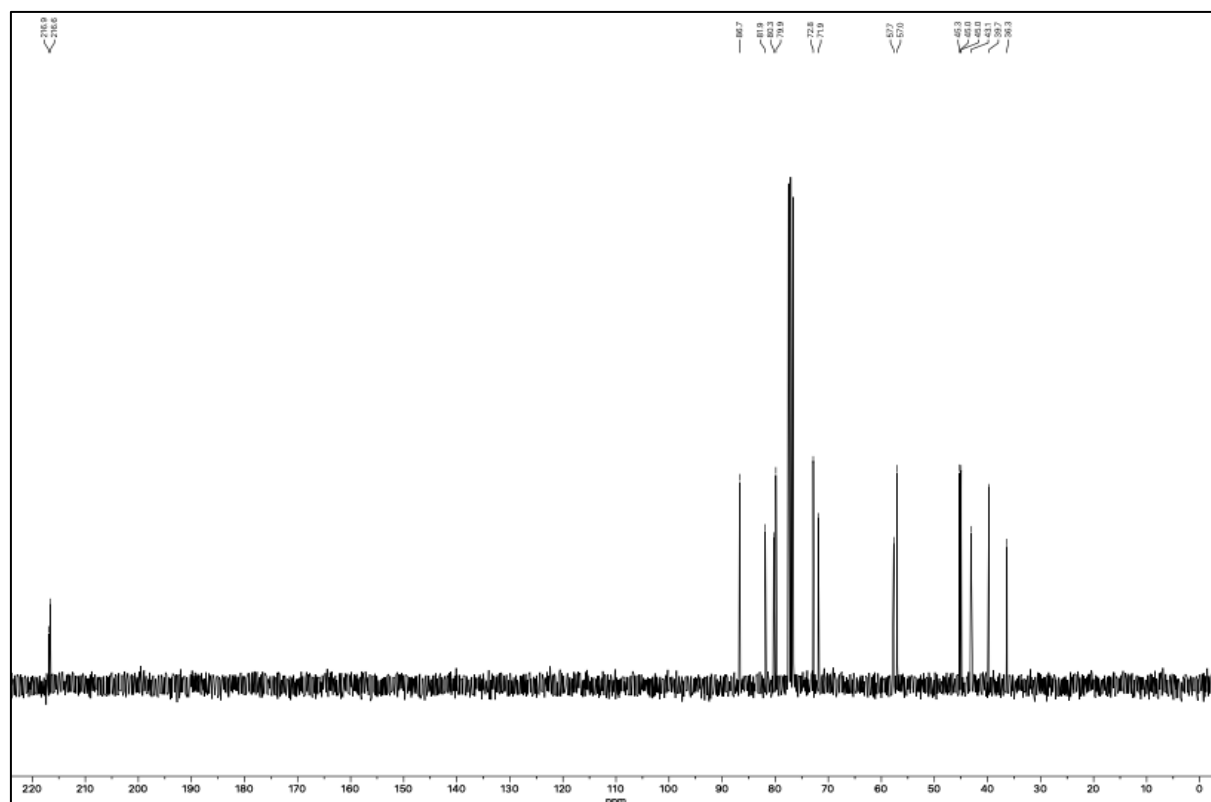
Figure S36. ¹³C-NMR of **175d** (75 MHz, CDCl₃).

(±)-(3a*R*,6a*S*)-3-Isopropoxyhexahydro-5*H*-cyclopenta[*b*]furan-5-one (175e)
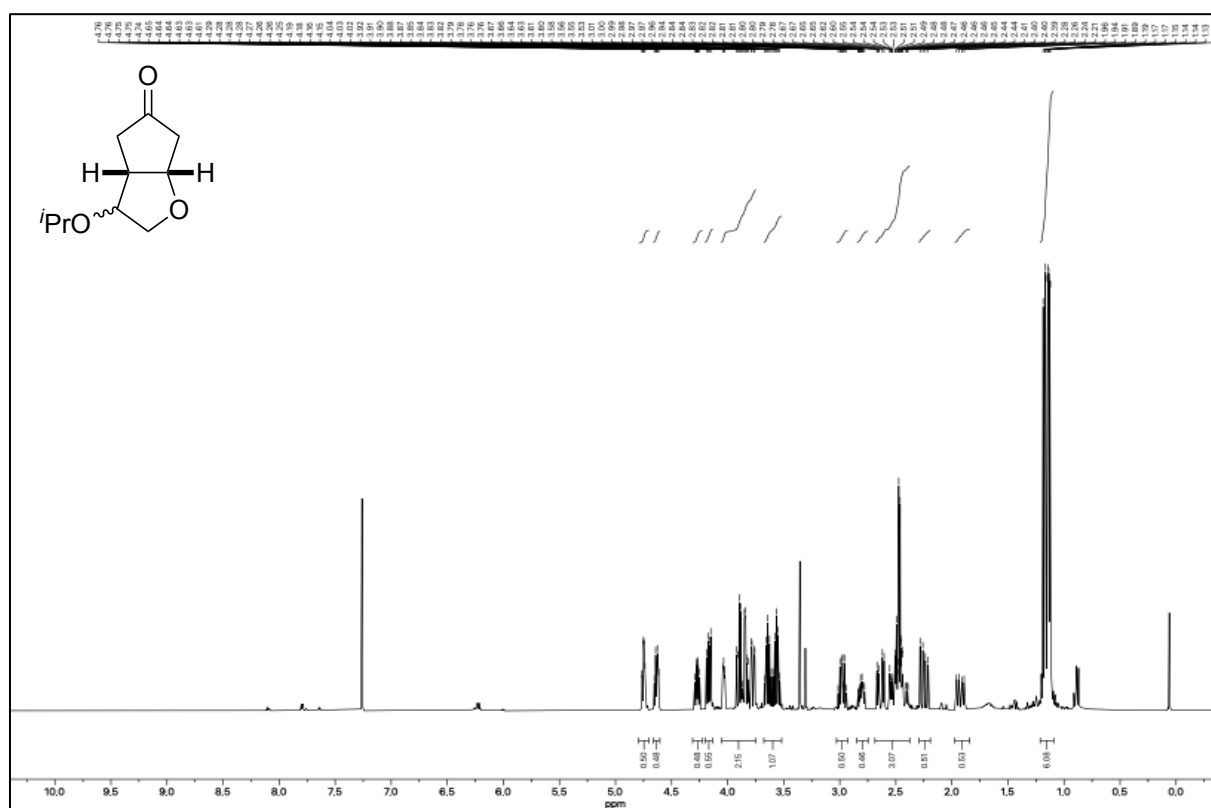
Figure S37. ^{1}H-NMR of **175e** (400 MHz, CDCl$_3$).
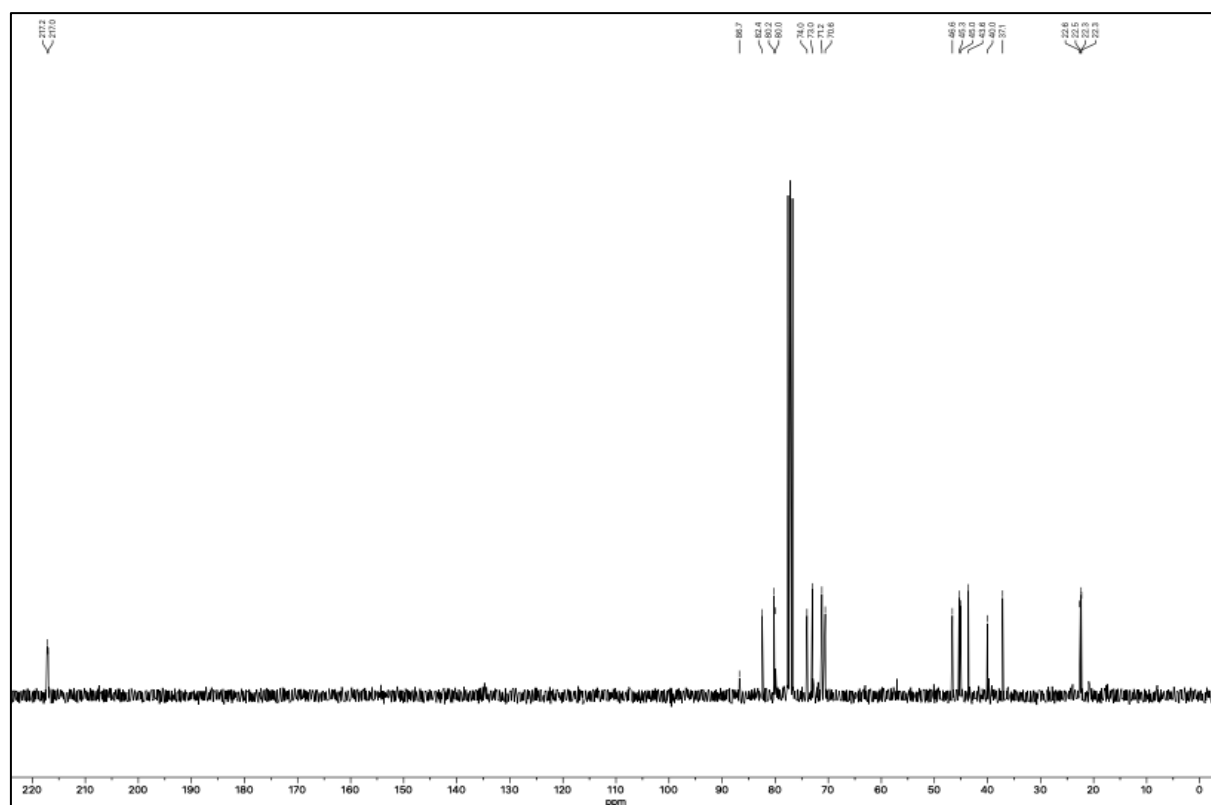
Figure S38. ^{13}C-NMR of **175e** (75 MHz, CDCl$_3$).

(±)-*Tert*-butyl ((2*R*,3a*S*,6a*S*)-2-methyl-5-oxohexahydro-2*H*-cyclopenta[*b*]furan-3-yl)carbamate (175g)
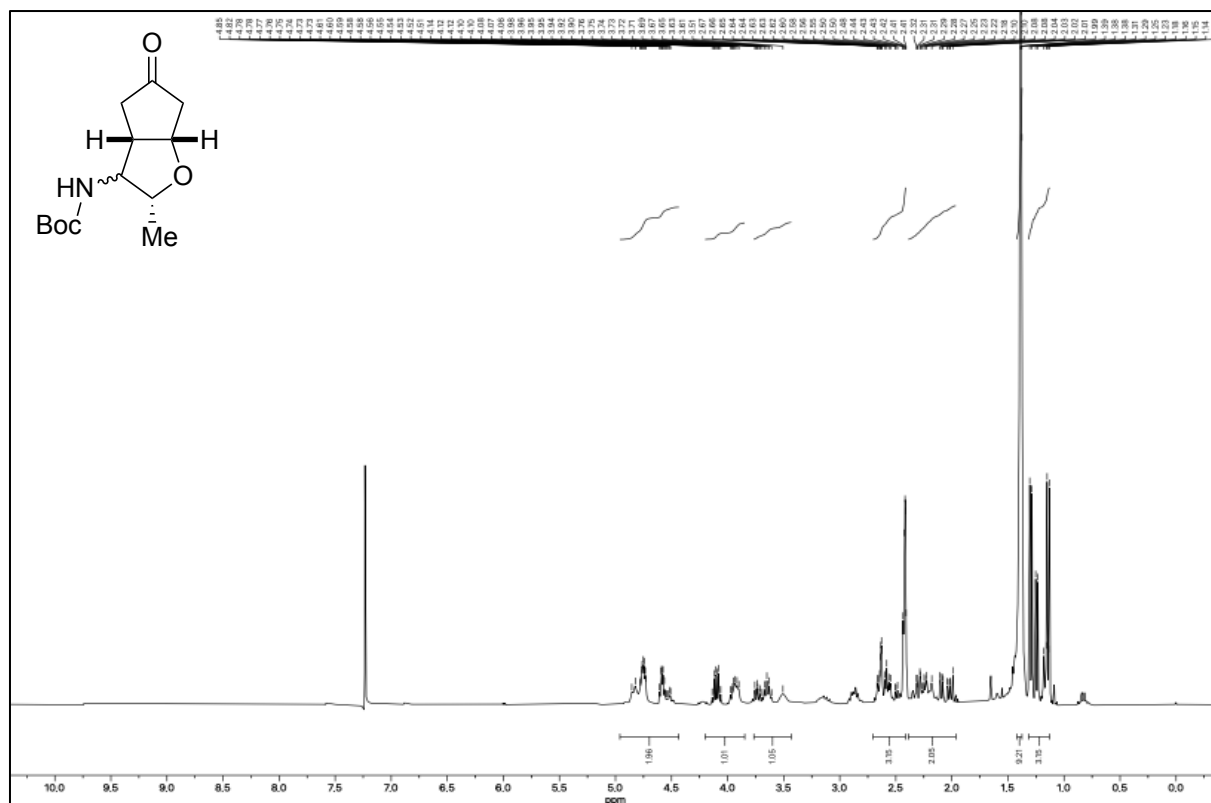
Figure S39. ^{1}H-NMR of **175g** (300 MHz, CDCl₃).
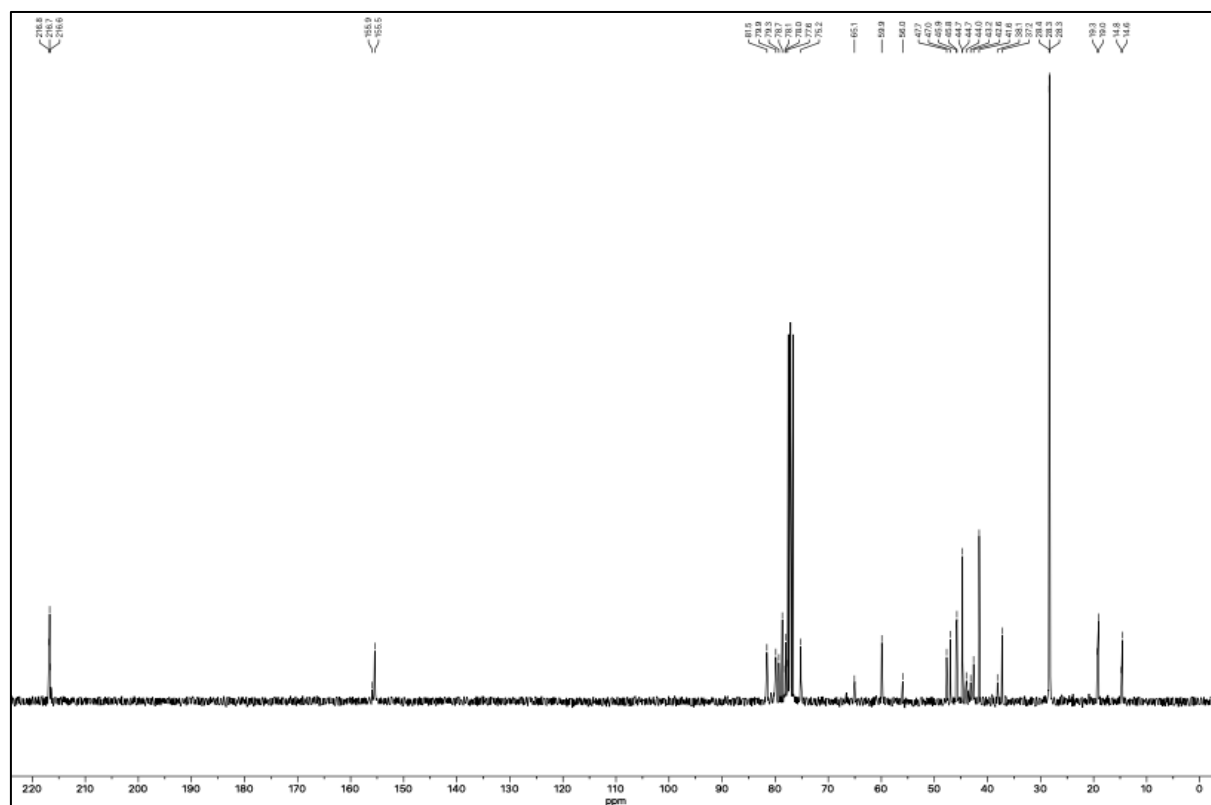
Figure S40. ^{13}C-NMR of **175g** (75 MHz, CDCl₃).

(±)-*Tert*-butyl ((4a*S*,7a*S*)-6-oxooctahydrocyclopenta[*b*]pyran-4-yl)carbamate (177a)

Figure S41. ^{1}H-NMR of **177a** (300 MHz, CDCl₃).

Figure S42. ^{13}C-NMR of **177a** (75 MHz, CDCl₃).

(±)-*Tert*-butyl ((4a*S*,5*R*,7a*S*)-5-methyl-6-oxooctahydrocyclopenta[*b*]pyran-4-yl)carbamate (177b)

Figure S43. ^{1}H-NMR of **177b** (400 MHz, CDCl₃).

Figure S44. ^{13}C-NMR of **177b** (101 MHz, CDCl₃).

***Tert*-butyl (2*R*,5*R*,5a*R*,8a*R*)-7-oxooctahydro-4*H*-2,5-methano-cyclopenta[*f*][1,4]-oxazepine-4-carboxylate and *tert*-butyl (2*R*,5*R*,5a*S*,8a*S*)-7-oxooctahydro-4*H*-2,5-methanocyclopenta[*f*][1,4]oxazepine-4-carboxylate (179a)**
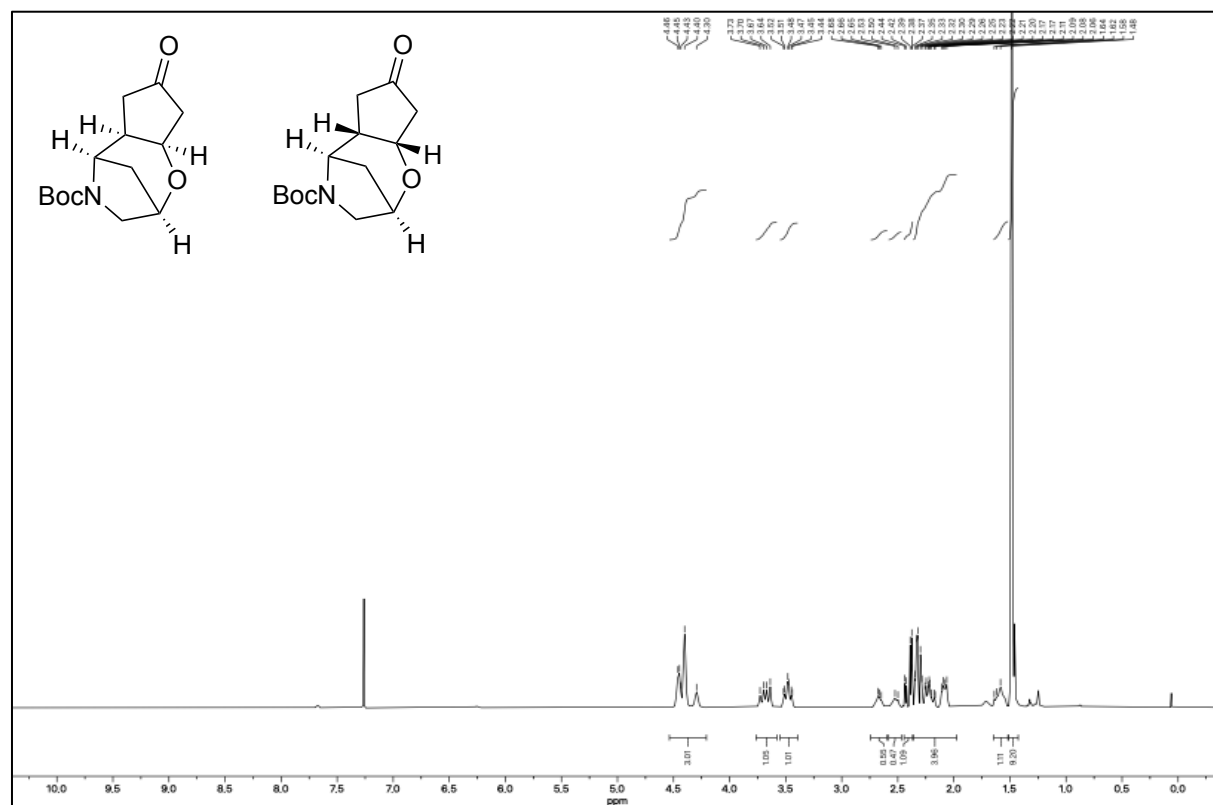
Figure S45. ¹H-NMR of **179a** (400 MHz, CDCl₃).
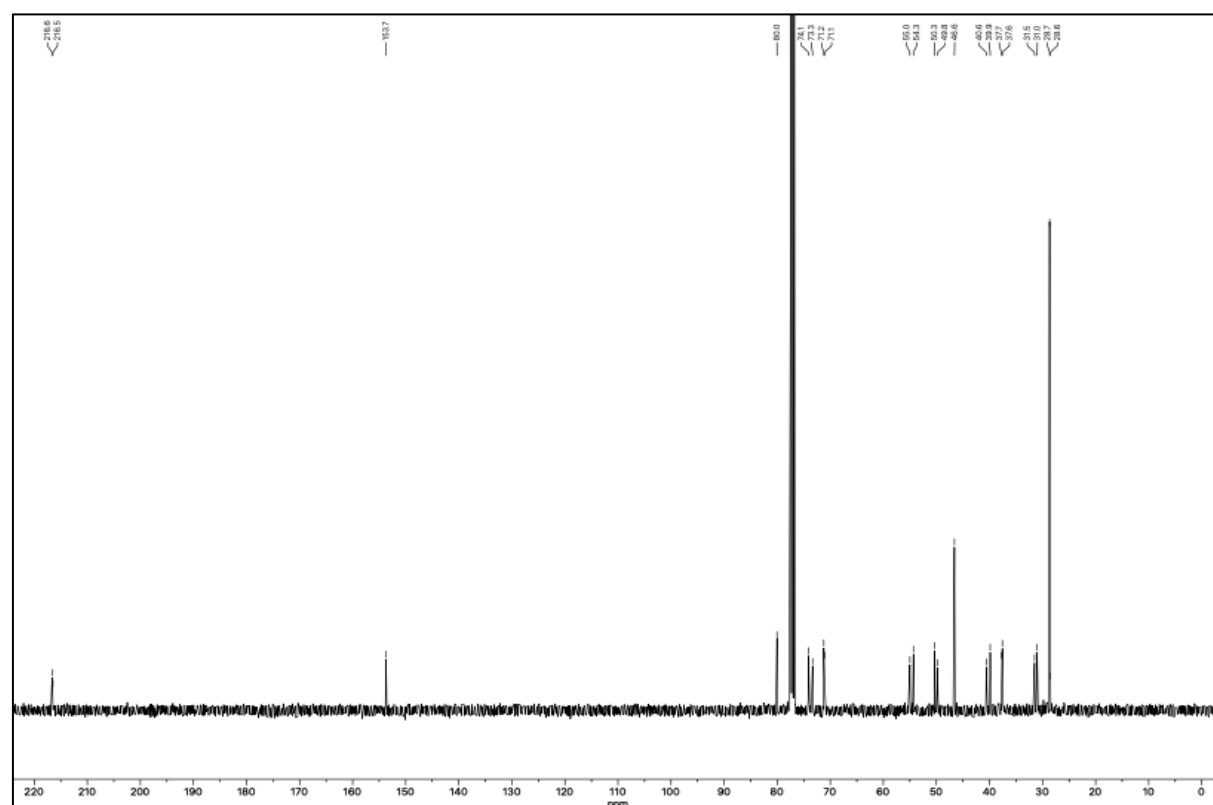
Figure S46. ¹³C-NMR of **179a** (101 MHz, CDCl₃).

137

***Tert*-butyl (2*R*,5*R*,5a*R*,6*S*,8a*R*)-6-methyl-7-oxooctahydro-4*H*-2,5-methanocyclopenta-[*f*][1,4]oxazepine-4-carboxylate** and ***tert*-butyl (2*R*,5*R*,5a*S*,6*R*,8a*S*)-6-methyl-7-oxooctahydro-4*H*-2,5-methanocyclopenta[*f*][1,4]oxazepine-4-carboxylate (179b)**

Figure S47. ^{1}H-NMR of **179b** (400 MHz, CDCl$_3$).

Figure S48. ^{13}C-NMR of **179b** (101 MHz, CDCl$_3$).

(*S*)-4-Benzhydrylcyclopent-2-en-1-one ((*S*)-188)

Figure S49. ^{1}H-NMR of (*S*)–**188** (400 MHz, CDCl₃).

Figure S50. ^{13}C-NMR of (*S*)–**188** (101 MHz, CDCl₃).
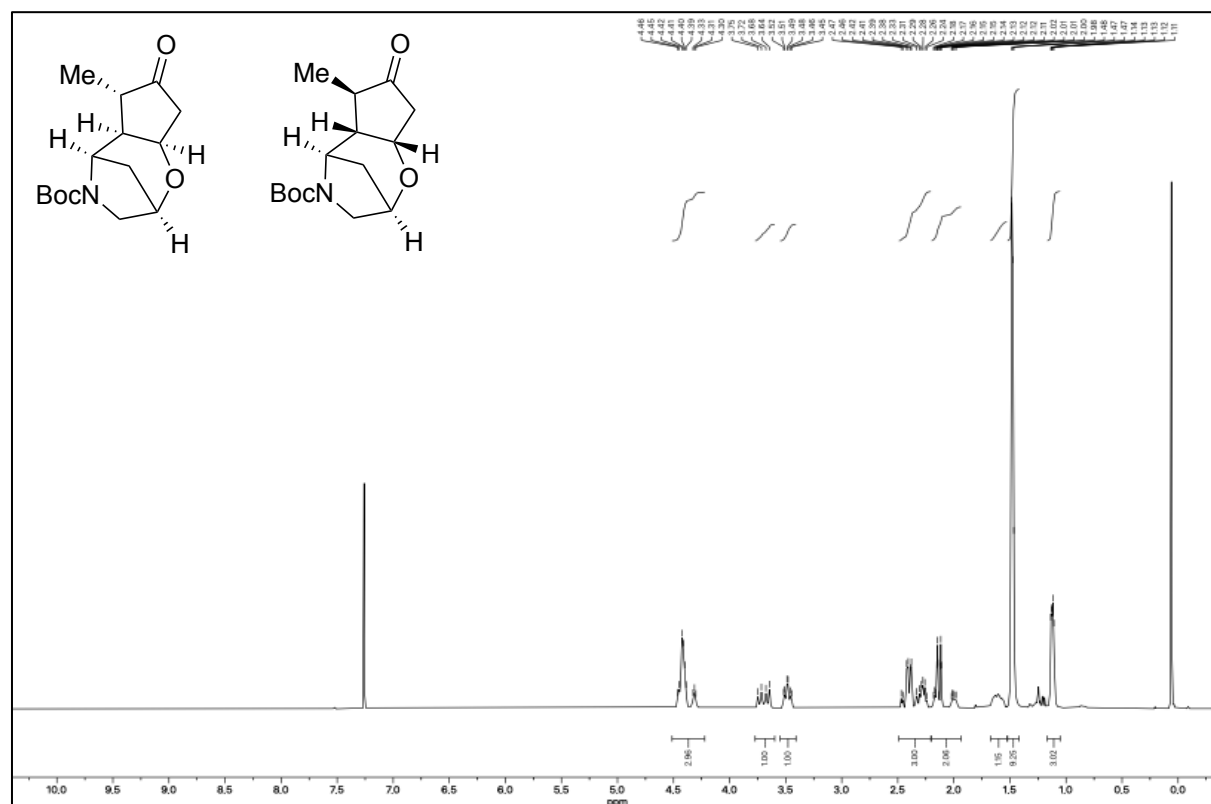
(9*H*-fluoren-9-yl)Methyl ((3*S*,3a*S*,6a*S*)-5-oxohexahydro-2*H*-cyclopenta[*b*]furan-3-yl)carbamate ((3*S*)-157)
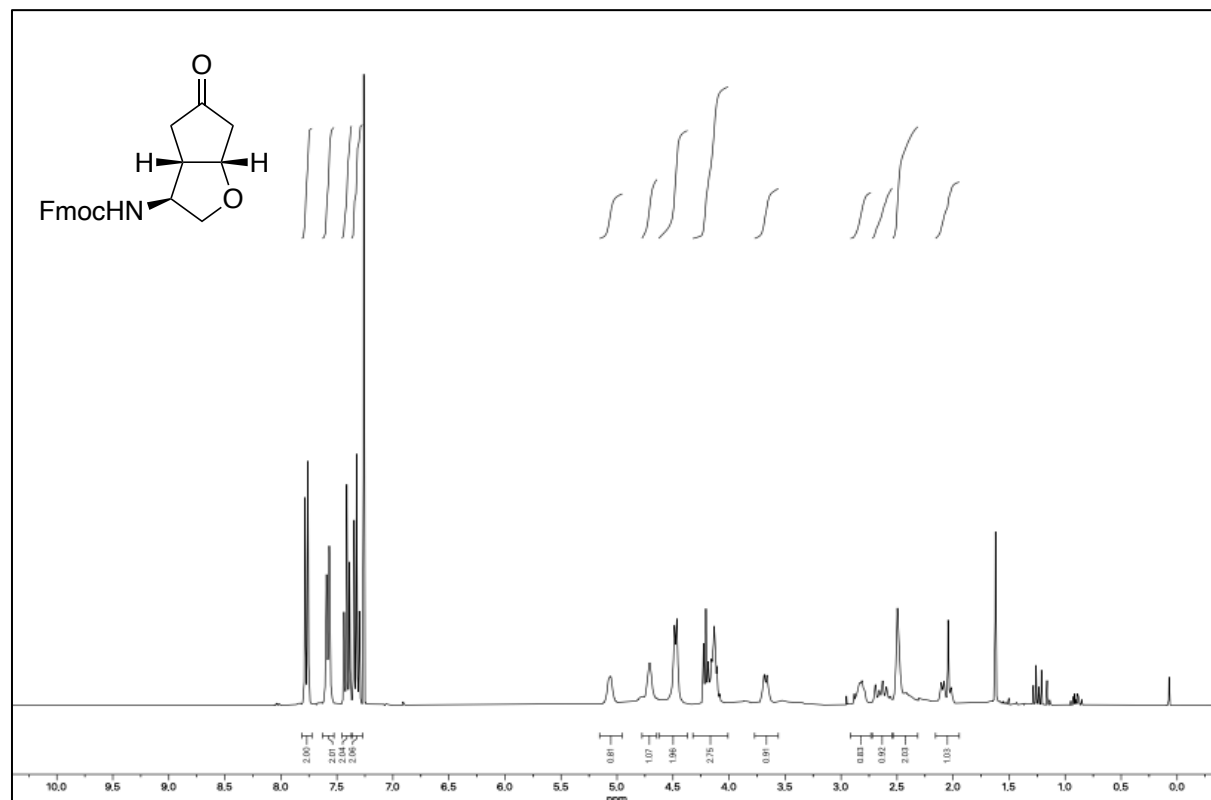
Figure S51. ^{1}H-NMR of (3*S*)–**157** (300 MHz, CDCl₃).
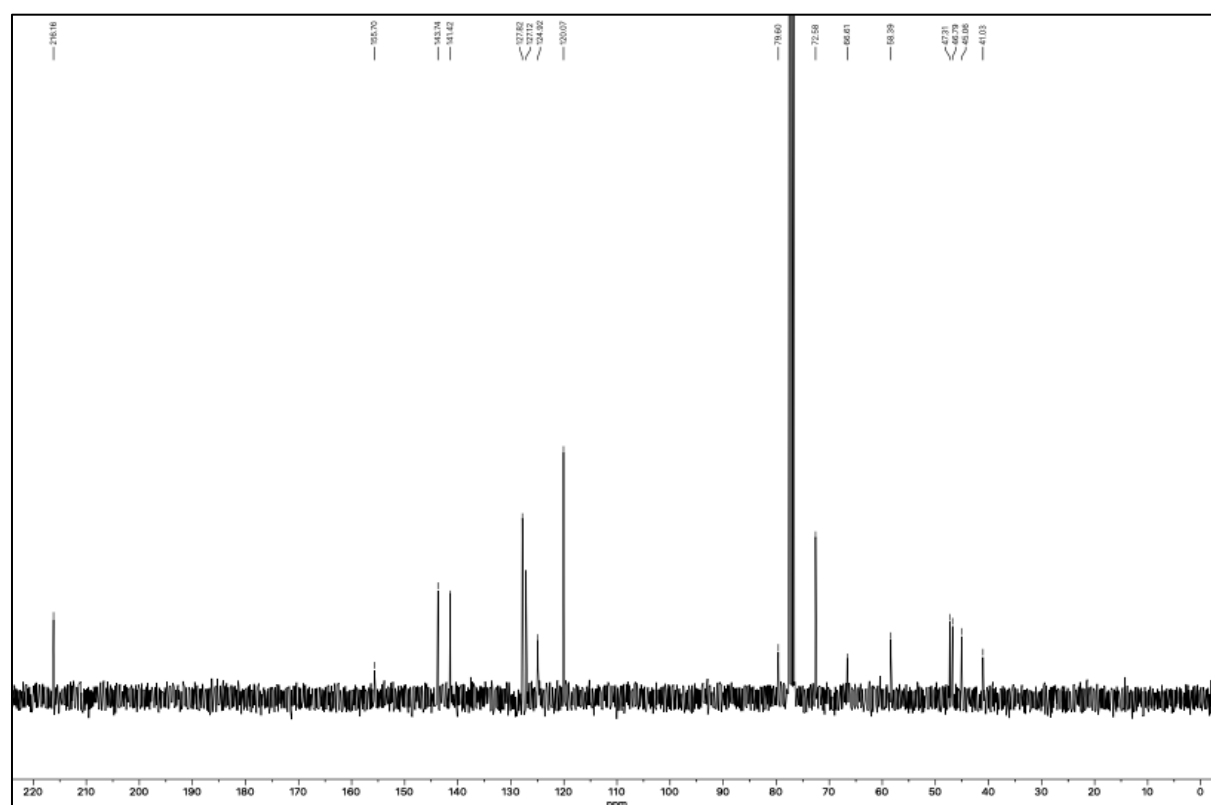
Figure S52. ^{13}C-NMR of (3*S*)–**157** (75 MHz, CDCl₃).

(±)-Methyl ((3S,3aS,6aS)-5-oxohexahydro-2H-cyclopenta[b]furan-3-yl)carbamate (*exo*-156)

Figure S53. ^{1}H-NMR of *exo*–**156** (400 MHz, CDCl$_3$).

Figure S54. ^{13}C-NMR of *exo*–**156** (101 MHz, CDCl$_3$).

Tert-butyl ((3*R*,3a*R*,5*R*,6a*R*)-5-hydroxyhexahydro-2*H*-cyclopenta[*b*]furan-3-yl)carbamate ((3*R*)-189)
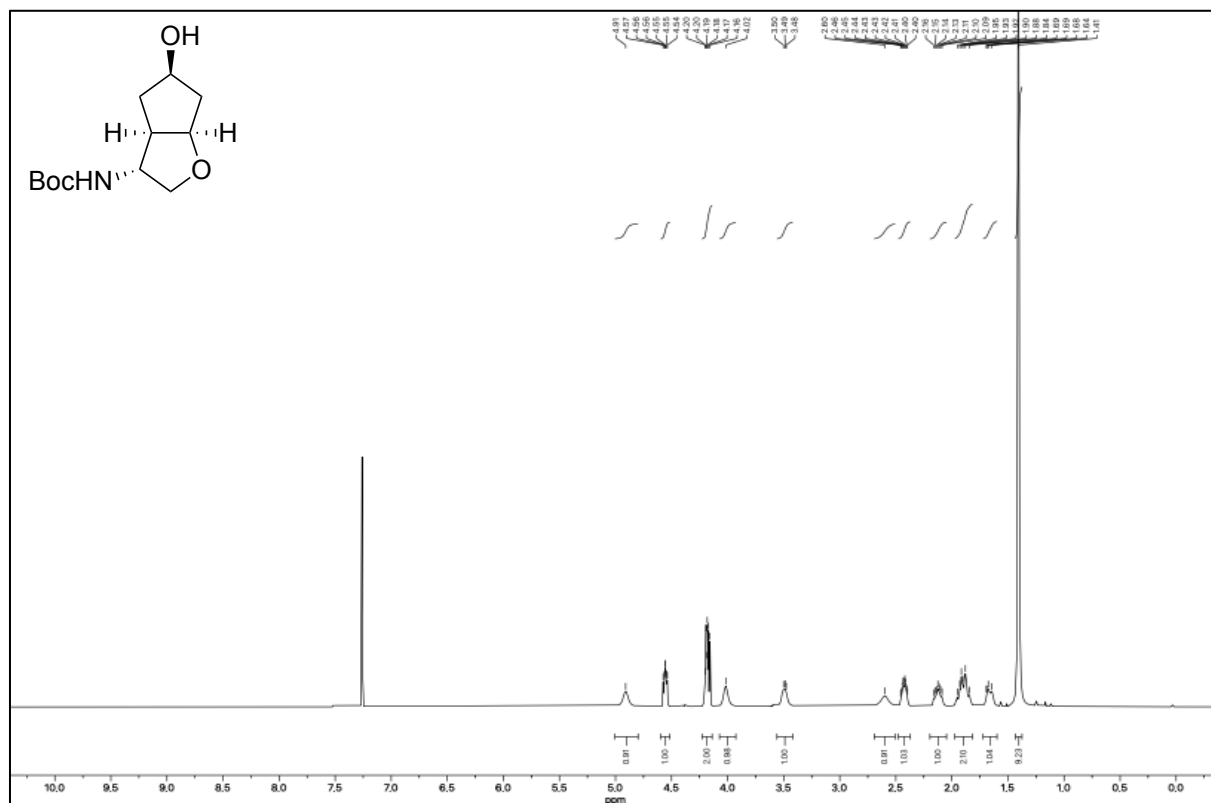
Figure S55. ^{1}H-NMR of (3*R*)–**189** (400 MHz, CDCl₃).
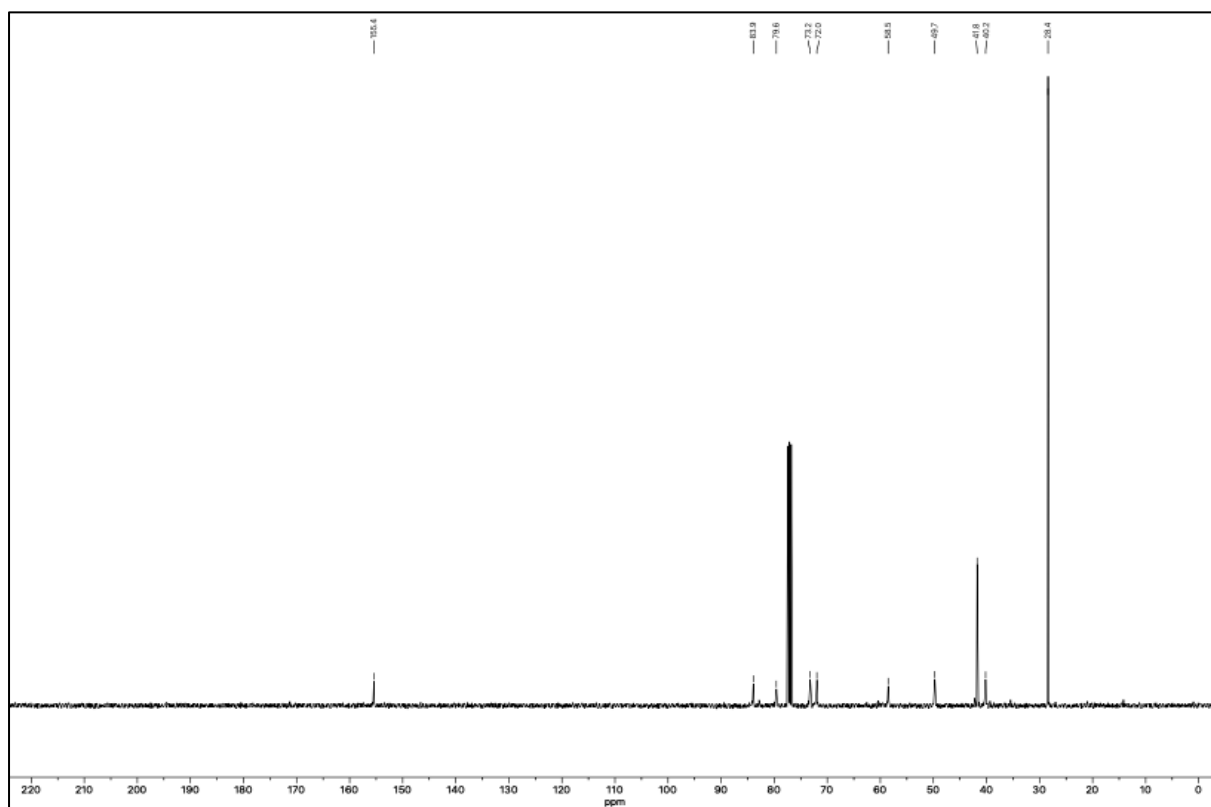
Figure S56. ^{13}C-NMR of (3*R*)–**189** (101 MHz, CDCl₃).

Tert-butyl ((3*S*,3a*R*,5*R*,6a*R*)-5-hydroxyhexahydro-2*H*-cyclopenta[*b*]furan-3-yl)carbamate ((3*S*)-189)

Figure S57. ^{1}H-NMR of (3*S*)–**189** (400 MHz, CDCl$_3$).

Figure S58. ^{13}C-NMR of (3*S*)–**189** (101 MHz, CDCl$_3$).

Methyl ((*3R,3aR,5R,6aR*)-5-hydroxyhexahydro-2*H*-cyclopenta[*b*]furan-3-yl)carbamate ((3*R*)-190)
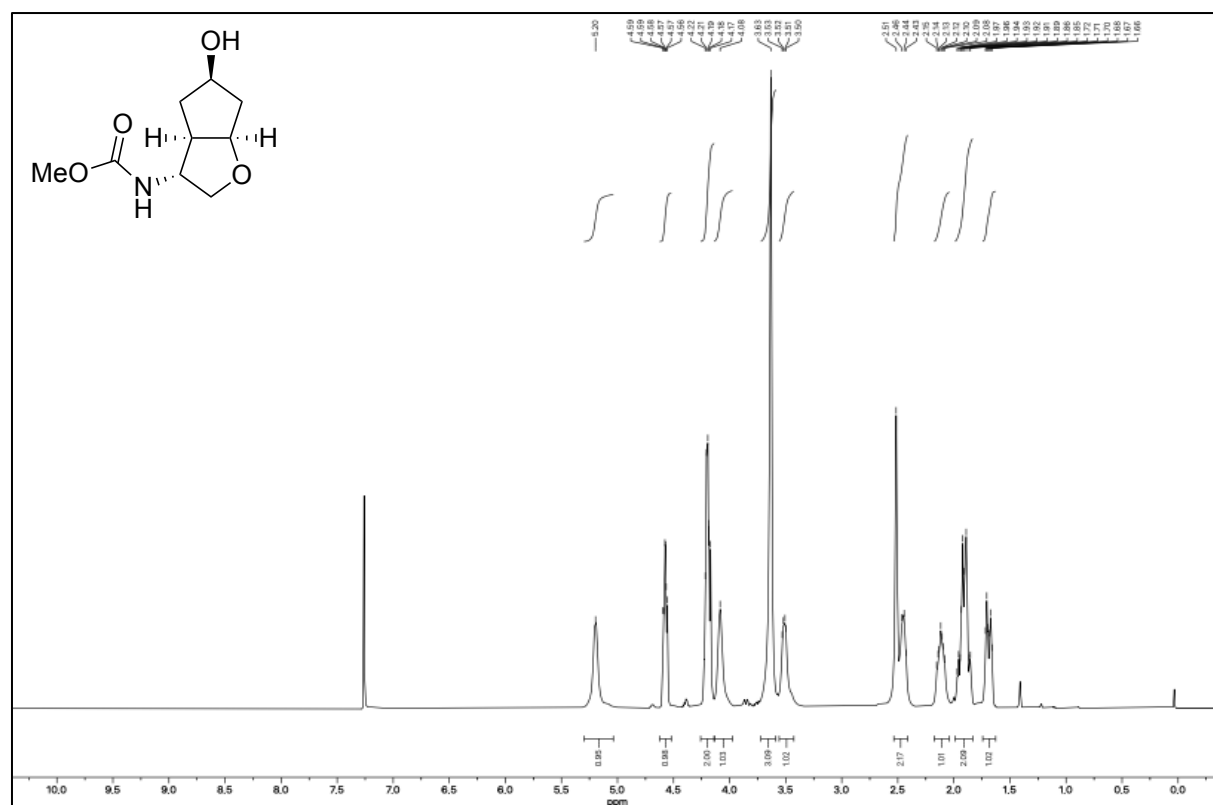
Figure S59. ^{1}H-NMR of (3*R*)–**190** (400 MHz, CDCl$_3$).
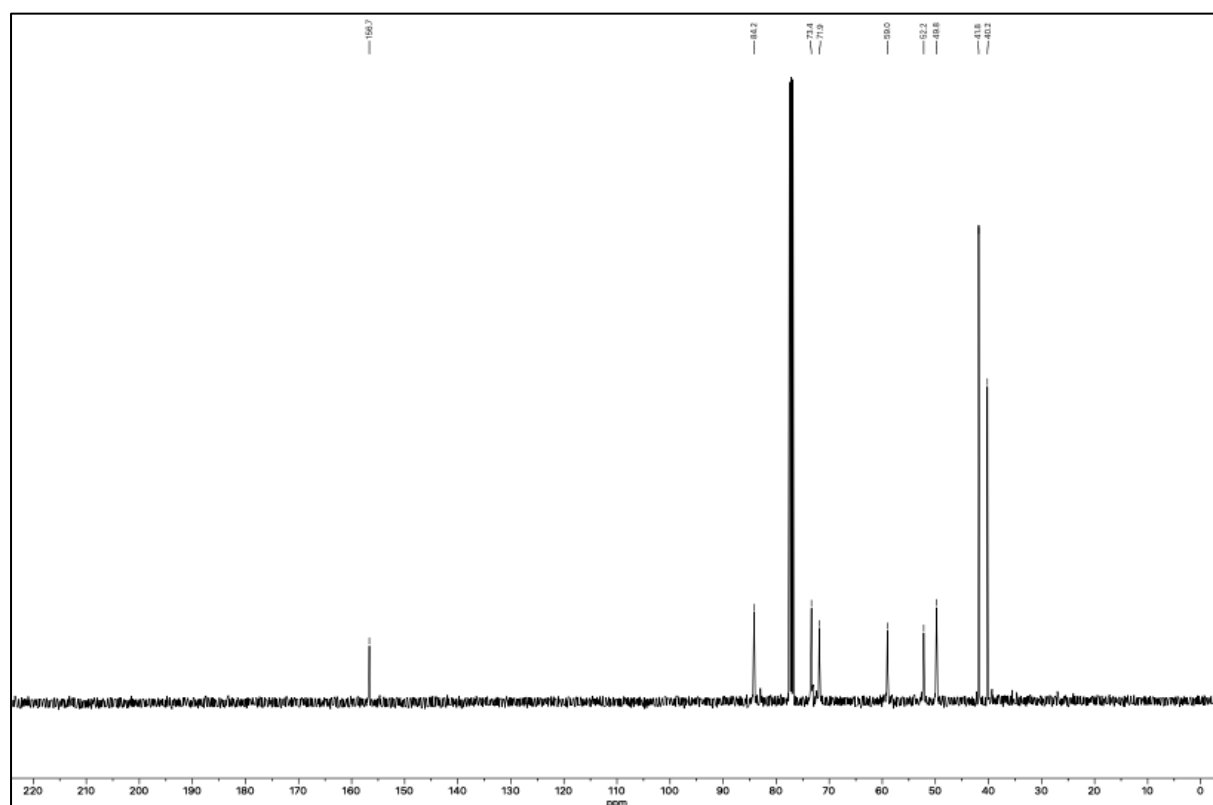
Figure S60. ^{13}C-NMR of (3*R*)–**190** (101 MHz, CDCl$_3$).

Methyl ((*3S,3aR,5R,6aR*)-5-hydroxyhexahydro-2*H*-cyclopenta[*b*]furan-3-yl)carbamate ((3*S*)-190)
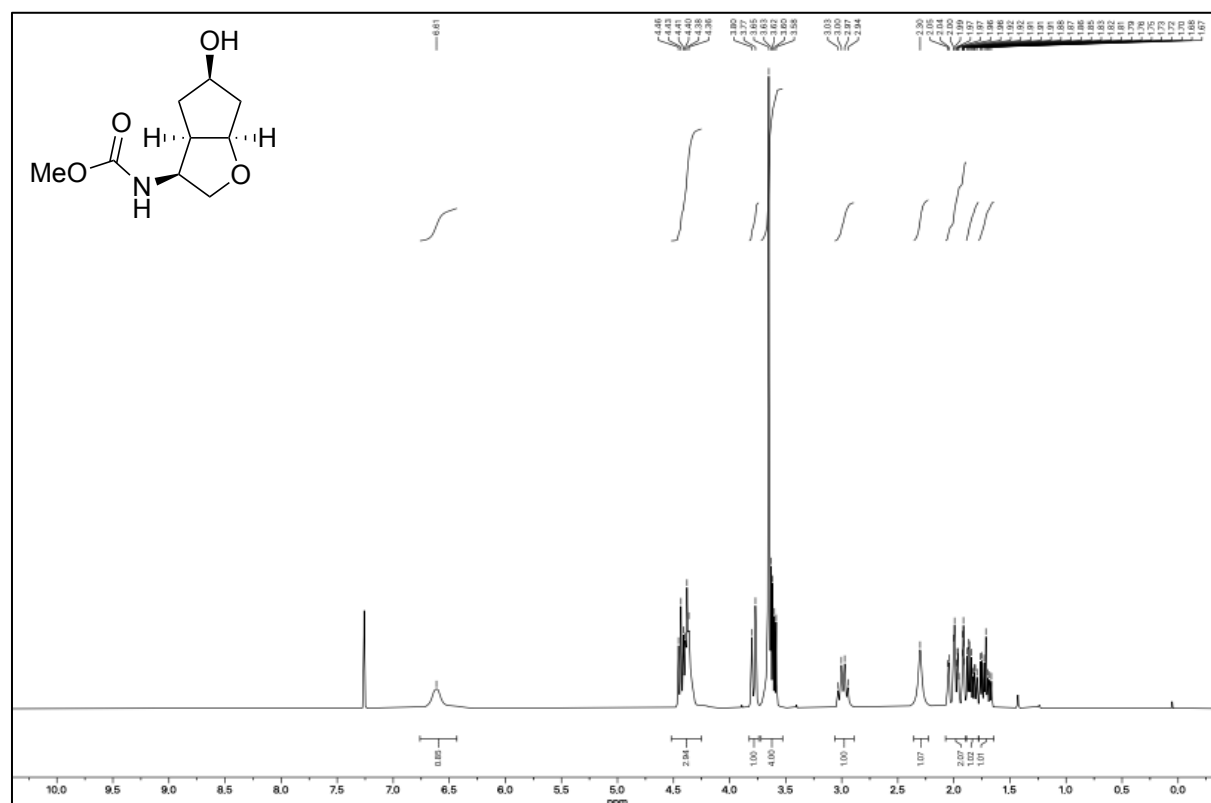
Figure S61. ^{1}H-NMR of (3*S*)-**190** (300 MHz, CDCl$_3$).
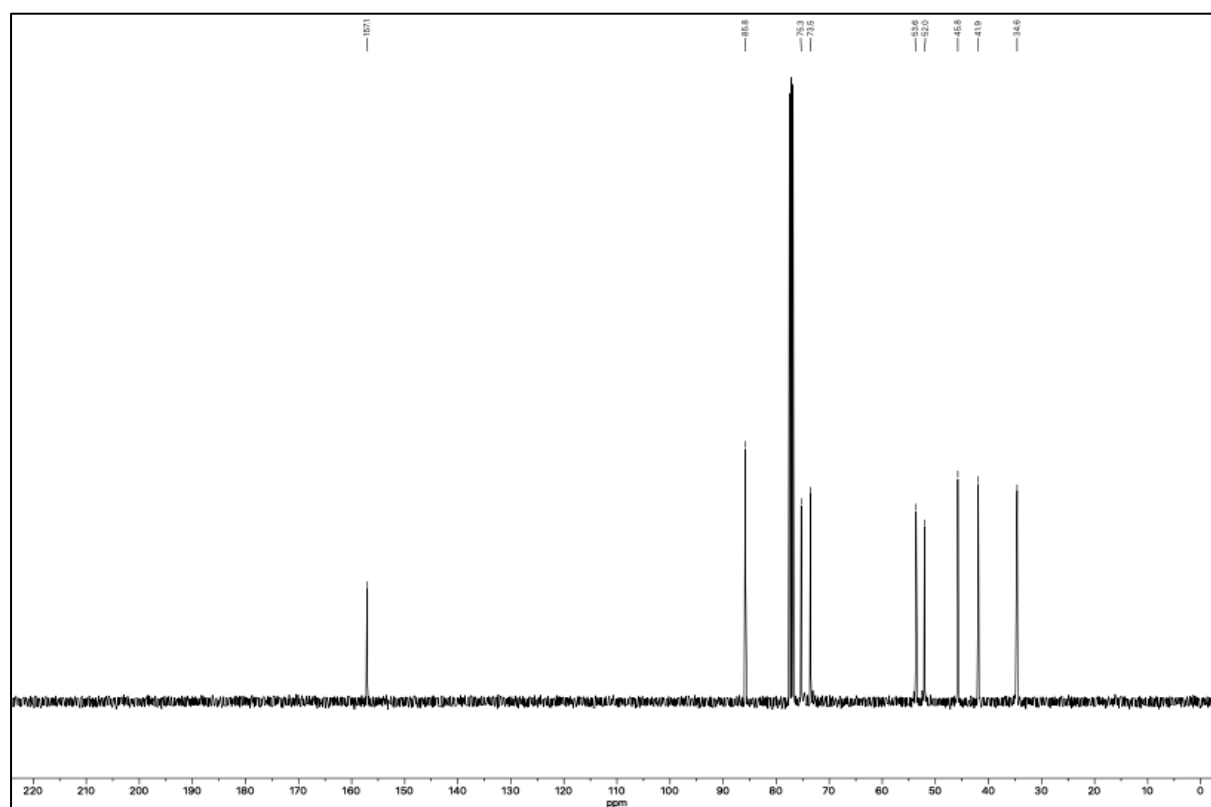
Figure S62. ^{13}C-NMR of (3*S*)-**190** (101 MHz, CDCl$_3$).

Methyl ((3*R*,3a*R*,5*R*,6a*R*)-5-(((4-nitrophenoxy)carbonyl)oxy)hexahydro-2*H*-cyclopenta[*b*]furan-3-yl)carbamate ((3*R*)-191)

Figure S63. ¹H-NMR of (3*R*)-**191** (400 MHz, CDCl₃).

Figure S64. ¹³C-NMR of (3*R*)-**191** (101 MHz, CDCl₃).
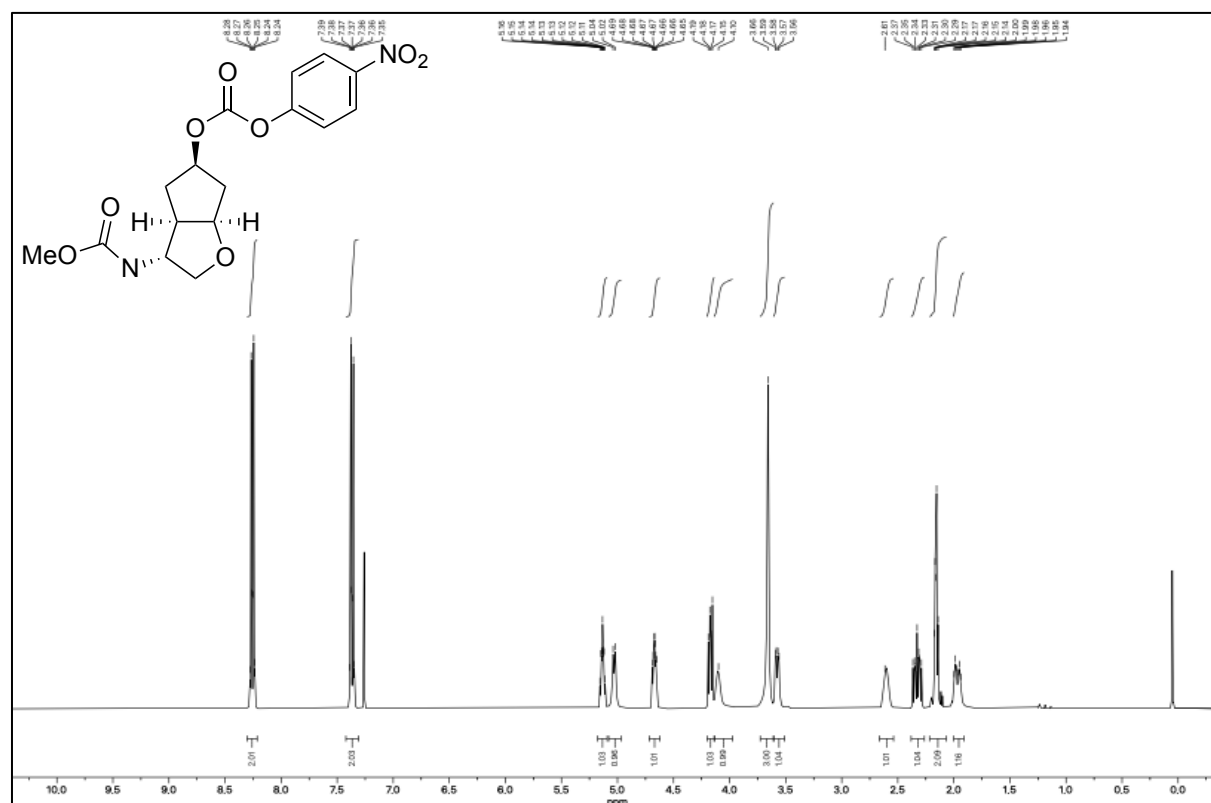
Methyl ((3*S*,3a*R*,5*R*,6a*R*)-5-(((4-nitrophenoxy)carbonyl)oxy)hexahydro-2*H*-cyclopenta[*b*]furan-3-yl)carbamate ((3*S*)-191)
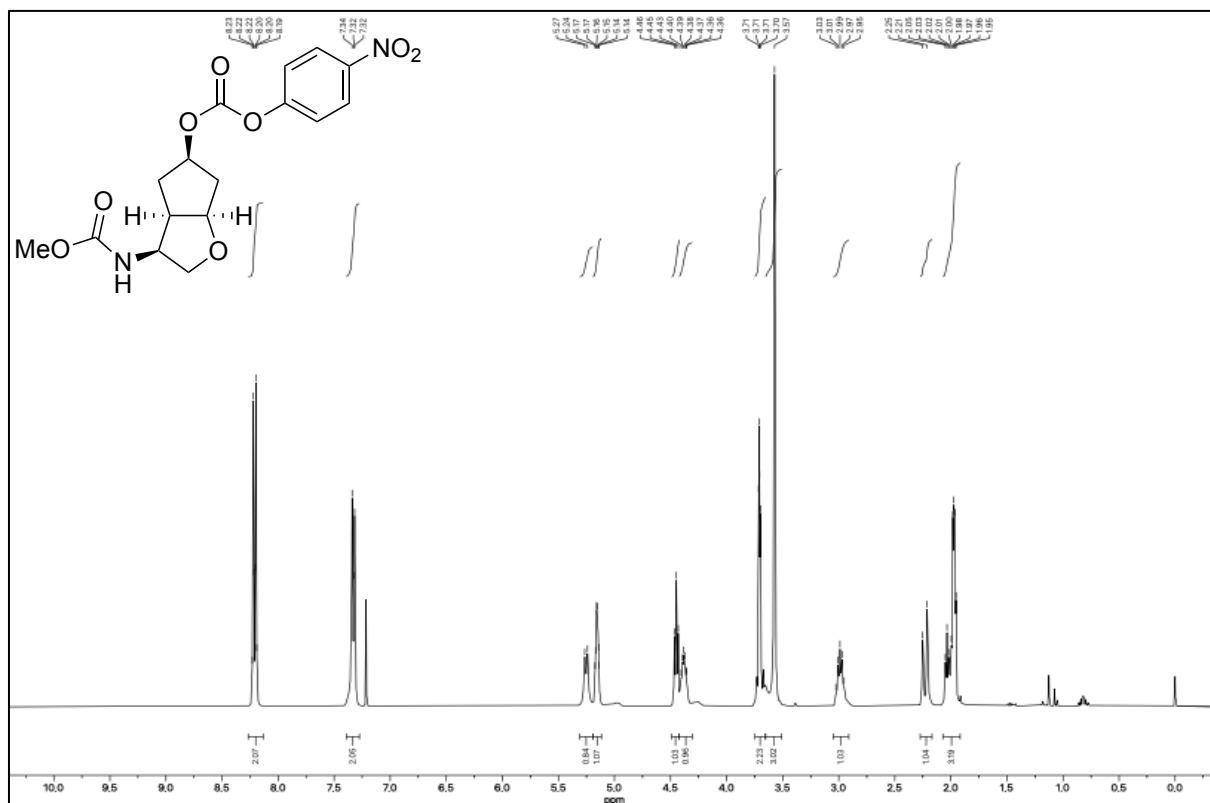
Figure S65. ^{1}H-NMR of (3*S*)-**191** (400 MHz, CDCl₃).
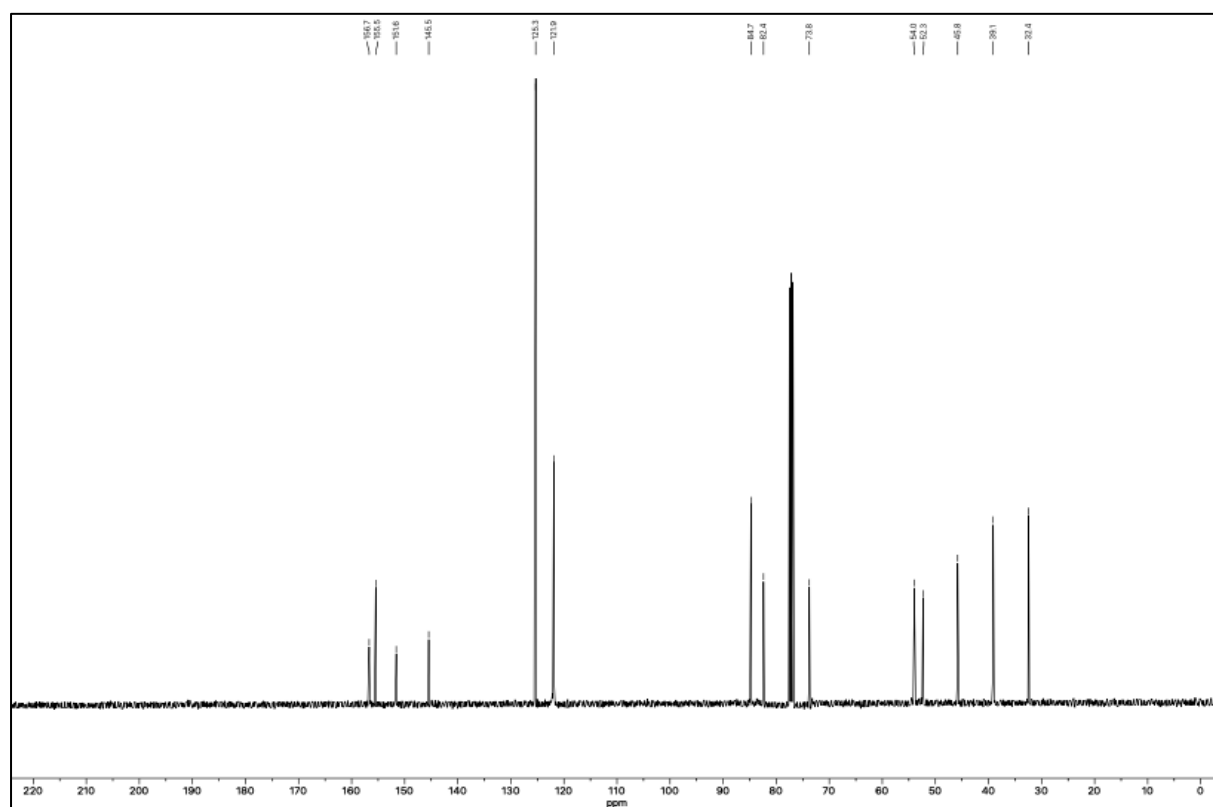
Figure S66. ^{13}C-NMR of (3*S*)-**191** (101 MHz, CDCl₃).

Tert-butyl ((2*S*,3*R*)-3-hydroxy-4-((*N*-isobutyl-4-methoxyphenyl)sulfonamido)-1-phenylbutan-2-yl)carbamate (194)
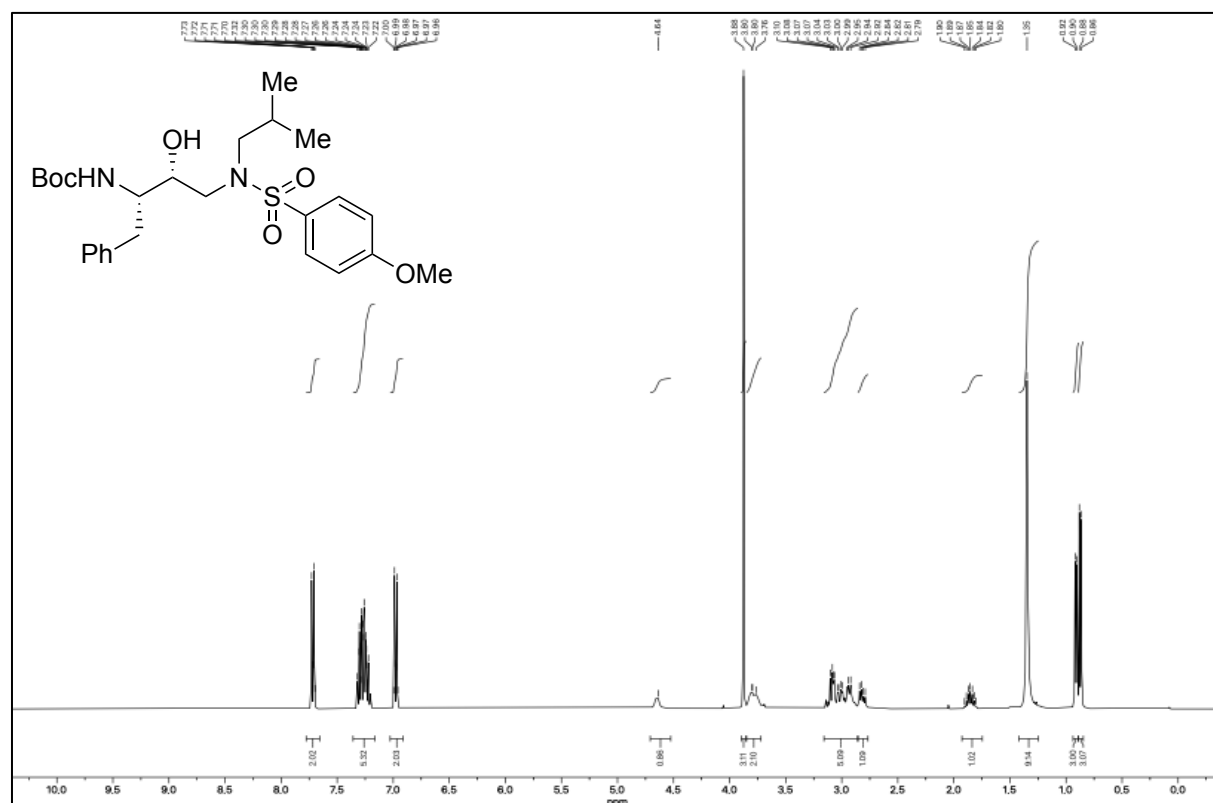
Figure S67. ^{1}H-NMR of **194** (400 MHz, CDCl₃).
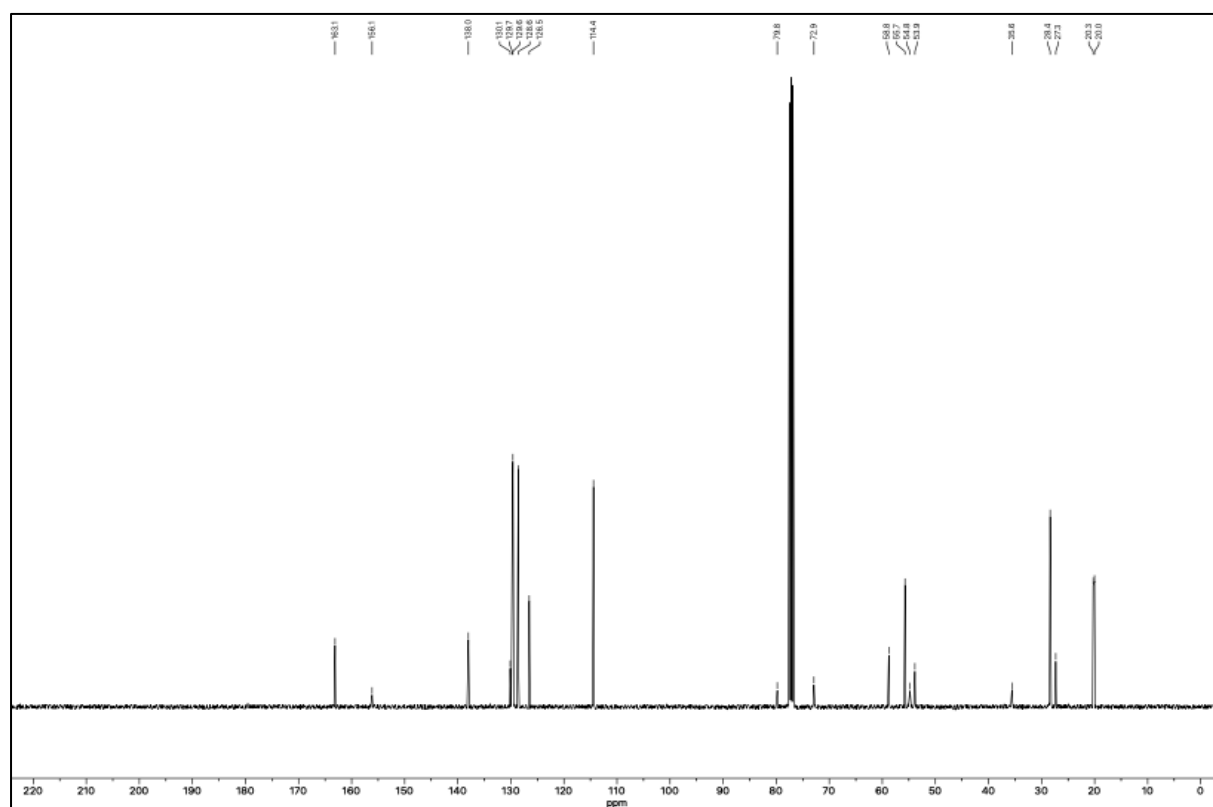
Figure S68. ^{13}C-NMR of **194** (101 MHz, CDCl₃).

N-((2R,3S)-3-amino-2-hydroxy-4-phenylbutyl)-N-isobutyl-4-methoxybenzene-sulfonamide (134)
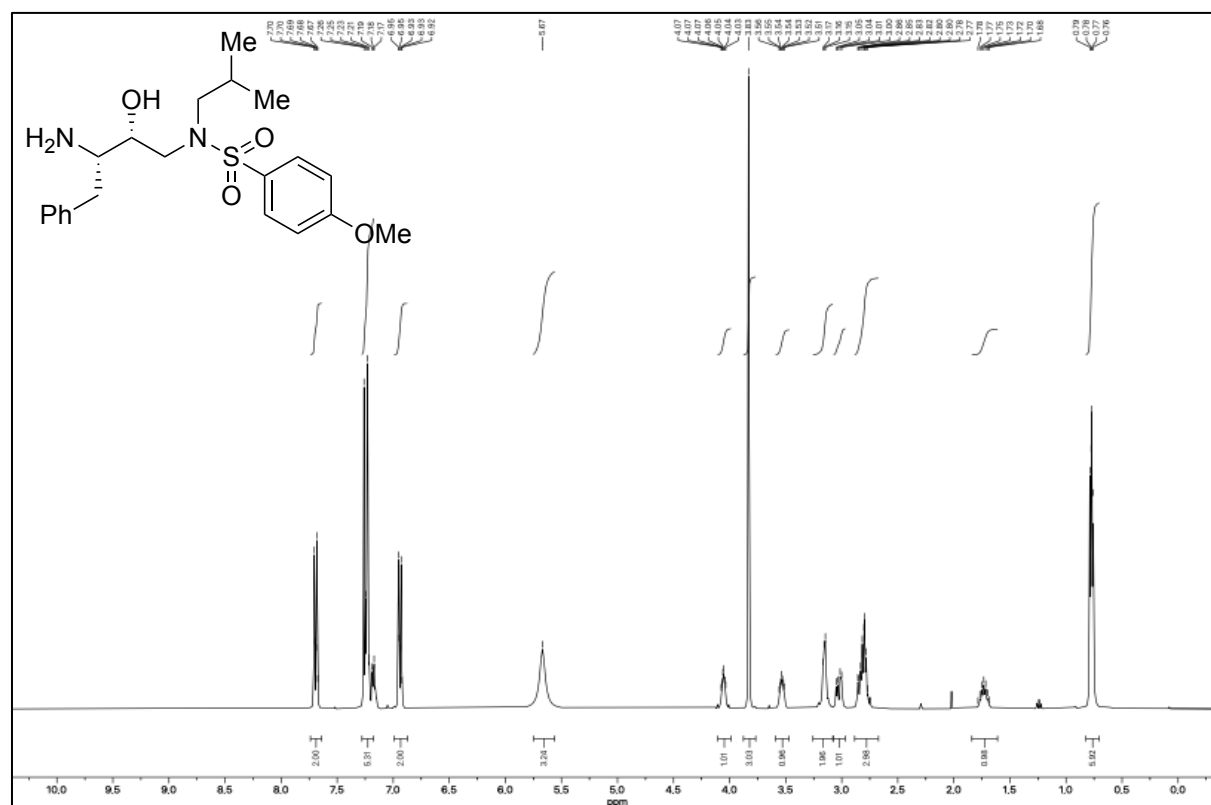
Figure S69. ^{1}H-NMR of **134** (400 MHz, CDCl$_3$).
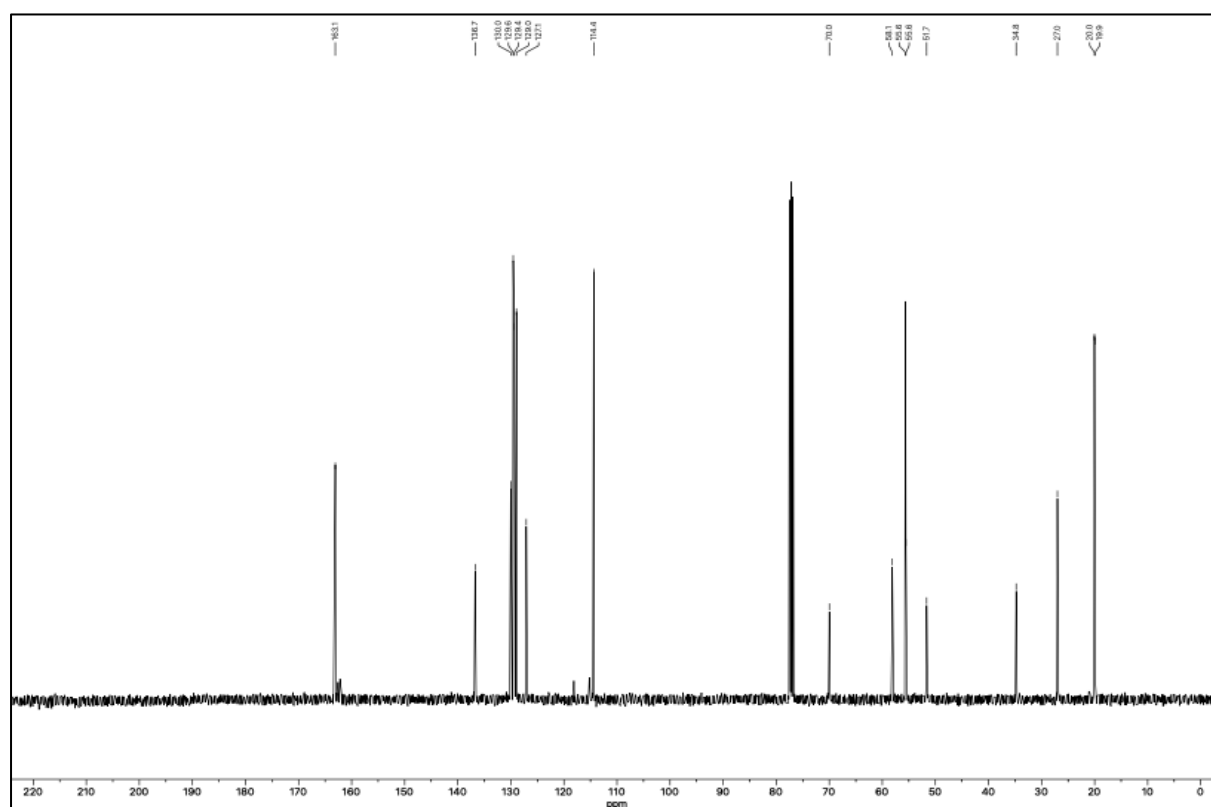
Figure S70. ^{13}C-NMR of **134** (101 MHz, CDCl$_3$).

(3R,3aR,5R,6aR)-3-((Methoxycarbonyl)amino)hexahydro-2H-cyclopenta[b]furan-5-yl ((2S,3R)-3-hydroxy-4-((N-isobutyl-4-methoxyphenyl)sulfonamido)-1-phenylbutan-2-yl)carbamate (126)

Figure S71. ^{1}H-NMR of **126** (400 MHz, CDCl$_3$).

Figure S72. ^{13}C-NMR of **126** (101 MHz, CDCl$_3$).

(3S,3aR,5R,6aR)-3-((Methoxycarbonyl)amino)hexahydro-2H-cyclopenta[b]furan-5-yl ((2S,3R)-3-hydroxy-4-((N-isobutyl-4-methoxyphenyl)sulfonamido)-1-phenylbutan-2-yl)carbamate (125)

Figure S73. ^{1}H-NMR of **125** (400 MHz, CDCl$_3$).

Figure S74. ^{13}C-NMR of **125** (101 MHz, CDCl$_3$).
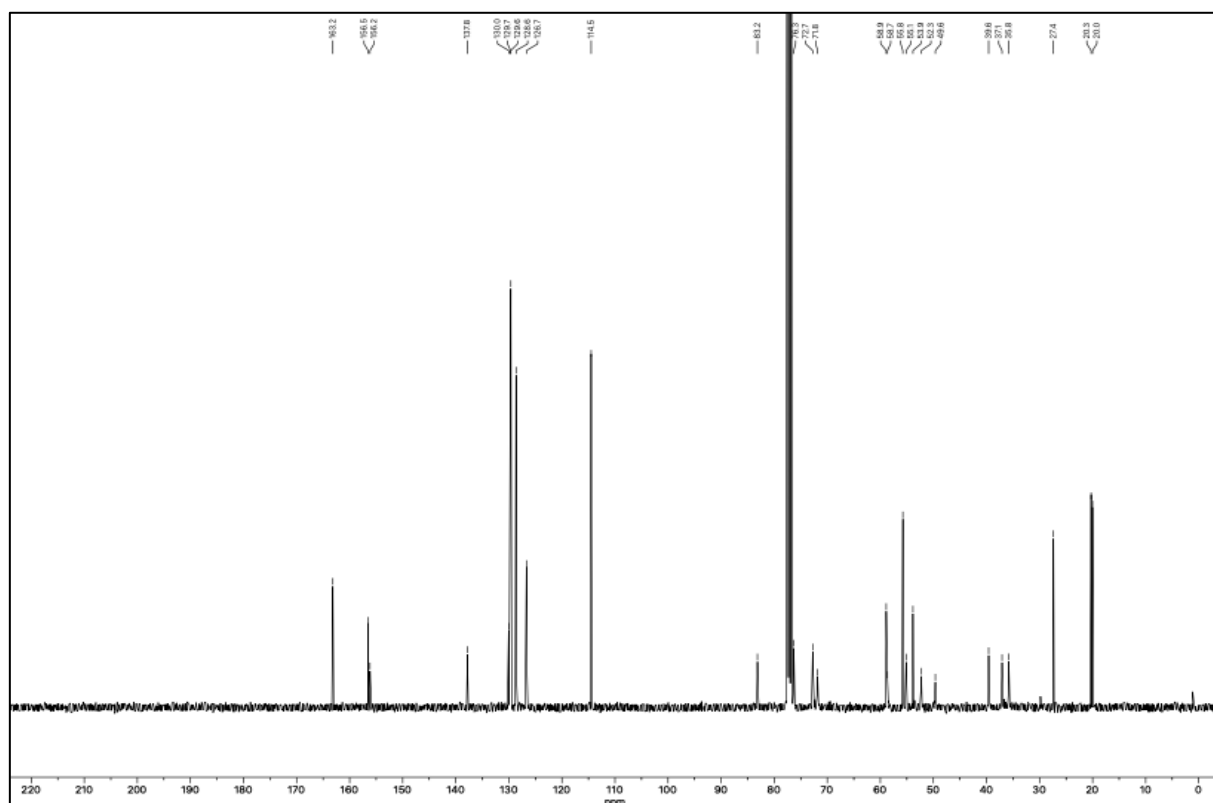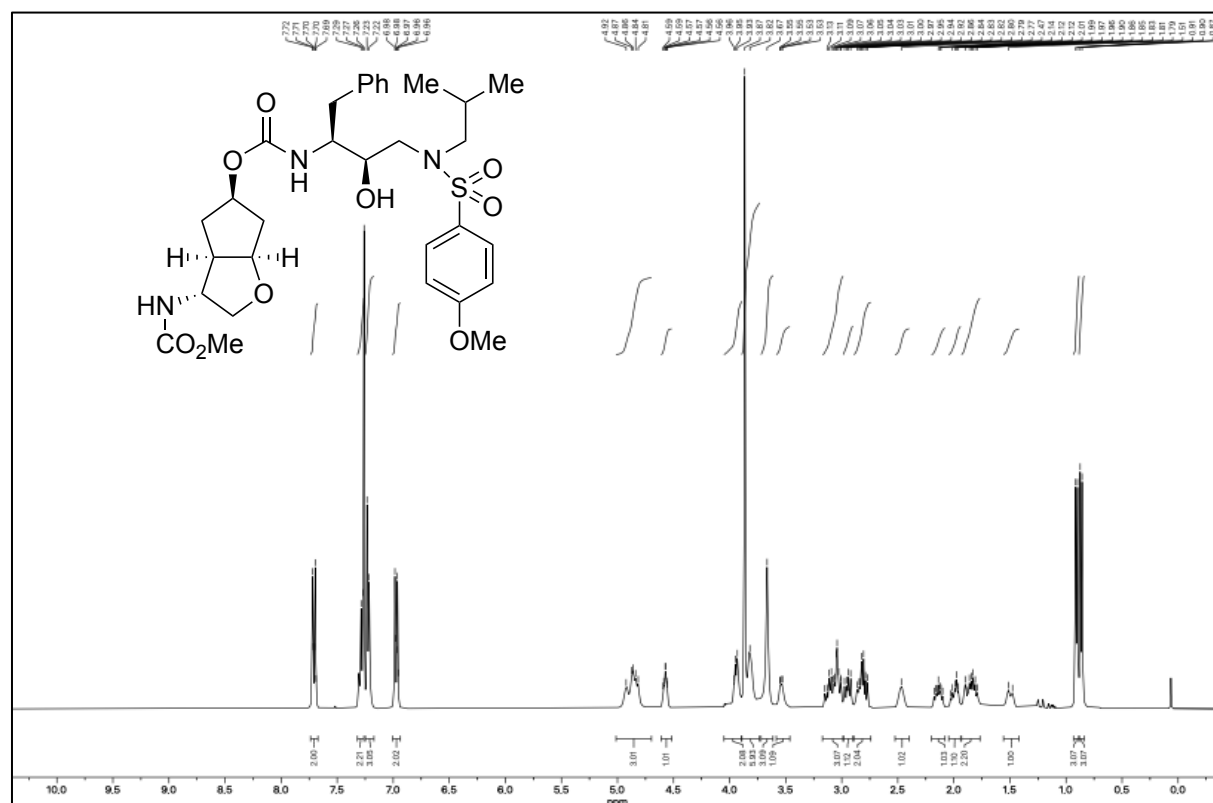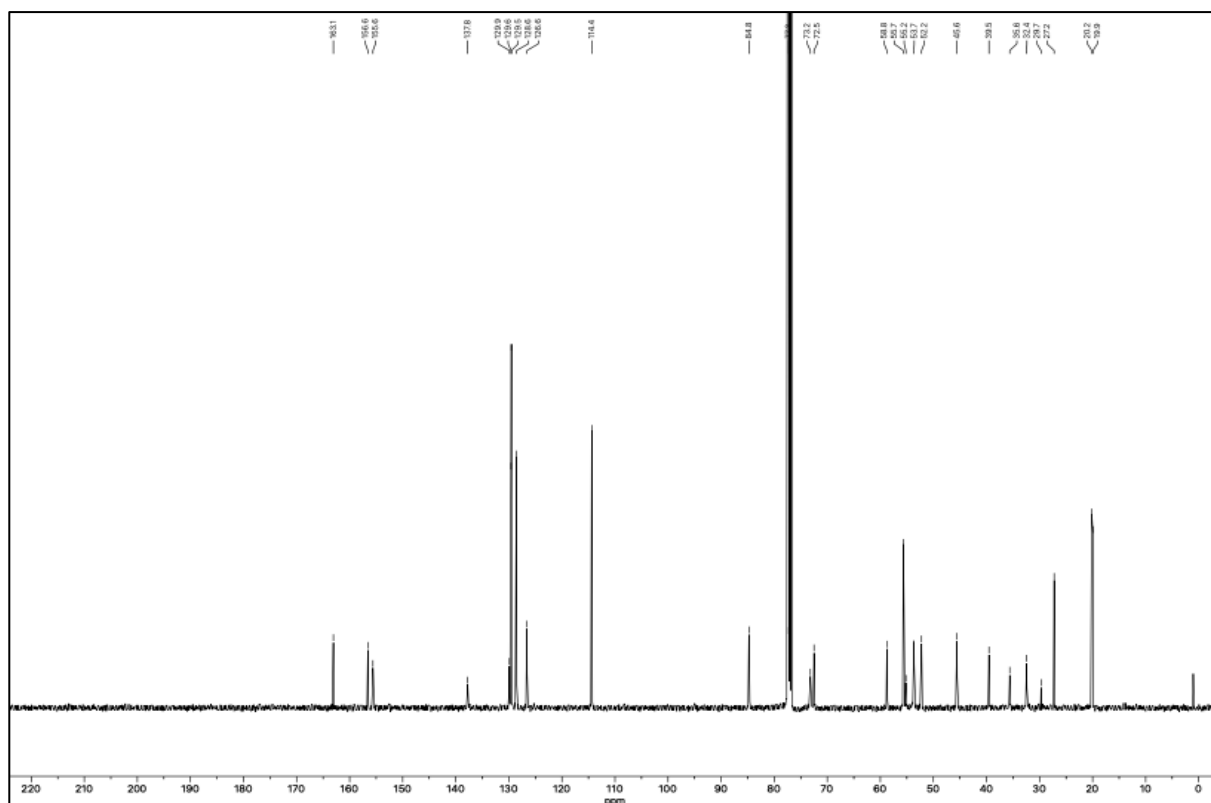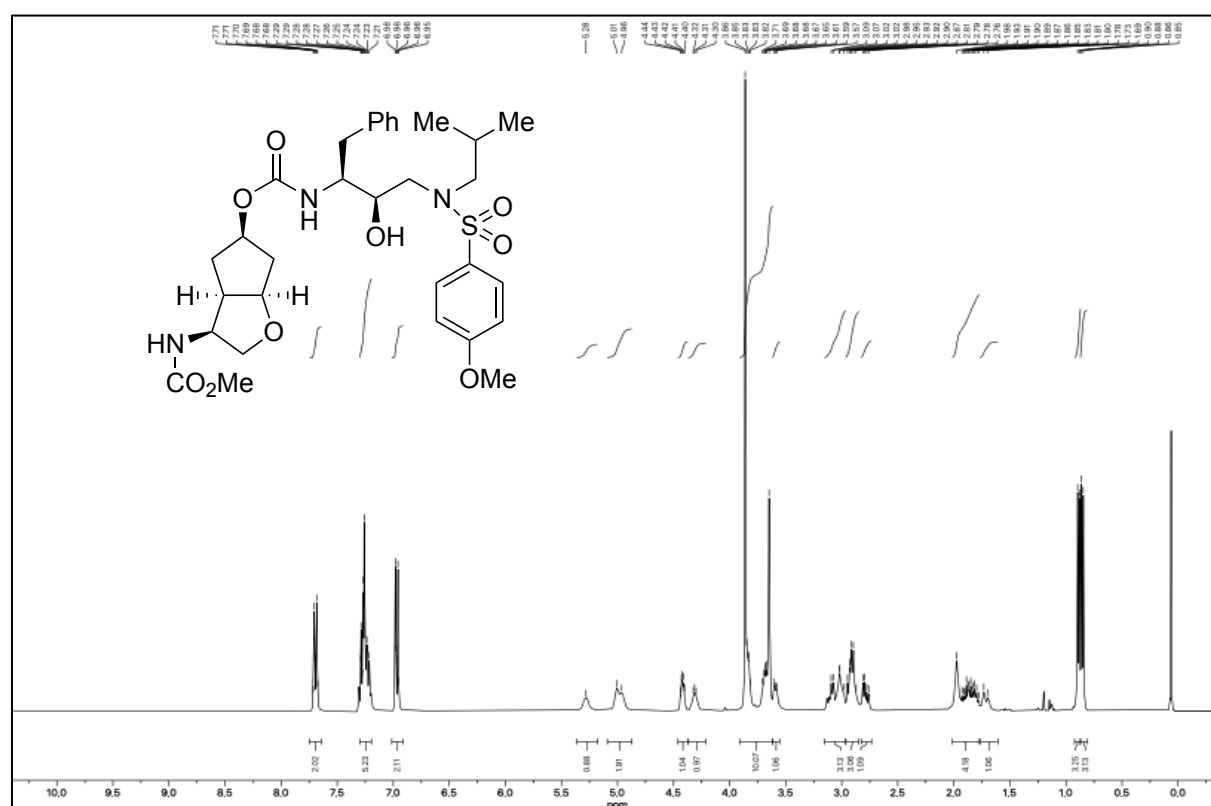
2 Chiral HPLC data

Tert-butyl (4-oxocyclopent-2-en-1-yl) carbonate (118)
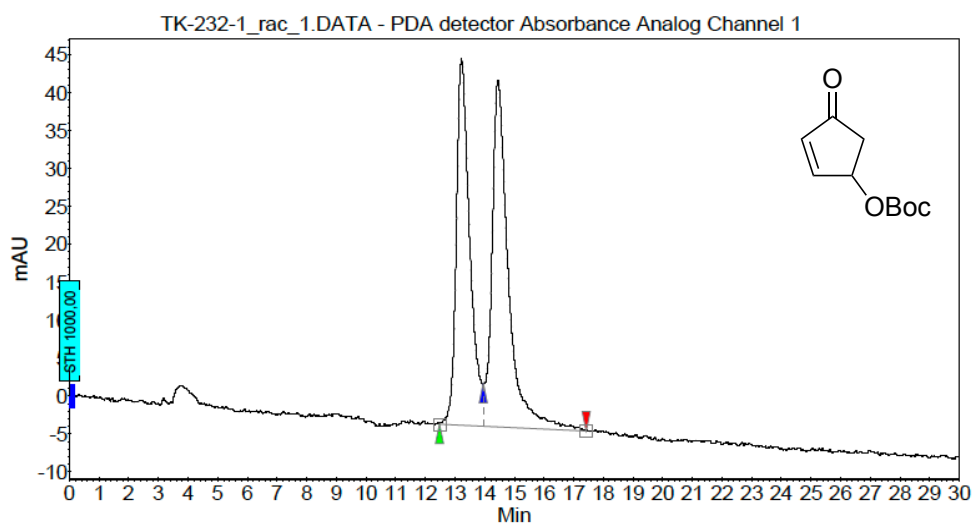
Peak Results :

Index	Name	Time [Min]	Quantity [% Area]	Height [mAU]	Area [mAU.Min]	Area % [%]
1	UNKNOWN	13,22	46,26	48,3	25,3	46,261
2	UNKNOWN	14,45	53,74	45,7	29,4	53,739
Total			100,00	94,0	54,7	100,000

Figure S75. HPLC chromatogram of racemic **118** (OJ-H, *i*-propanol/*n*-heptane = 1/99, flow rate = 1.0 mL/min, I = 215 nm, **racemic sample**).

(S)-Tert-butyl (4-oxocyclopent-2-en-1-yl) carbonate ((*S*)-118)
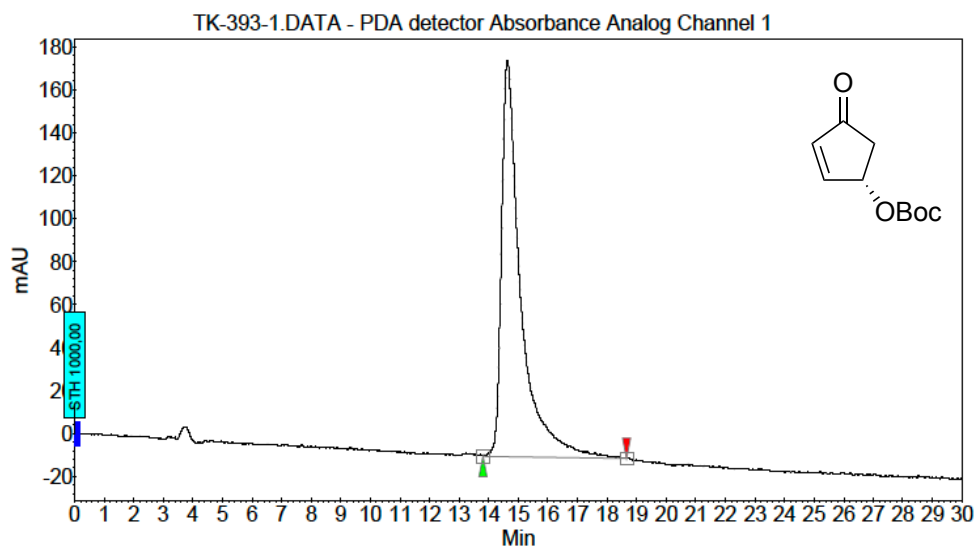
Peak Results :

Index	Name	Time [Min]	Quantity [% Area]	Height [mAU]	Area [mAU.Min]	Area % [%]
1	UNKNOWN	14,63	100,00	184,7	139,1	100,000
Total			100,00	184,7	139,1	100,000

Figure S76. HPLC chromatogram of (*S*)-**118** (OJ-H, *i*-propanol/*n*-heptane = 1/99, flow rate = 1.0 mL/min, I = 215 nm, **>99% ee**).

(R)-Tert-butyl (4-oxocyclopent-2-en-1-yl) carbonate ((*R*)-118)
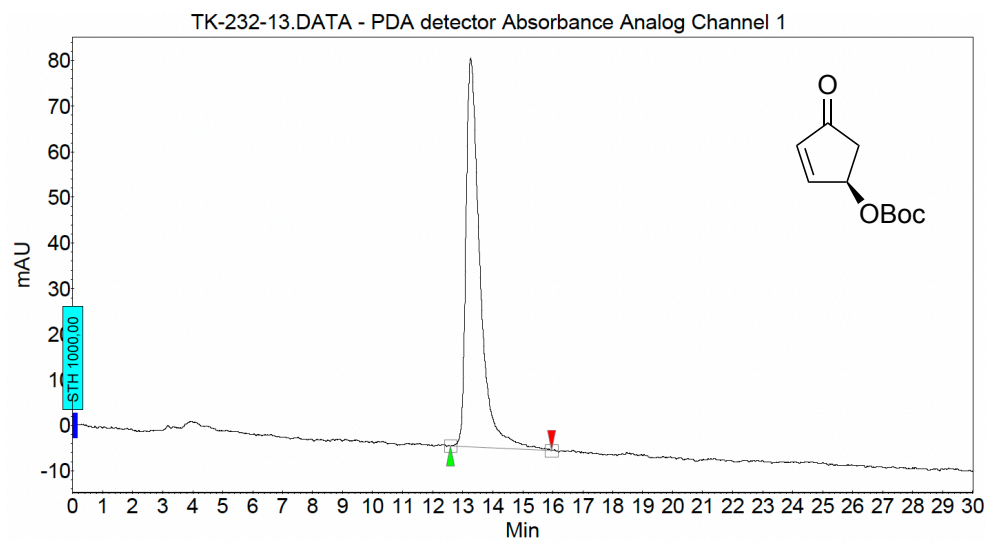
Figure S77. HPLC chromatogram of (*R*)-**118** (OJ-H, *i*-propanol/*n*-heptane = 1/99, flow rate = 1.0 mL/min, I = 215 nm, **>99% *ee***).

4-Benzhydrylcyclopent-2-en-1-one (188)
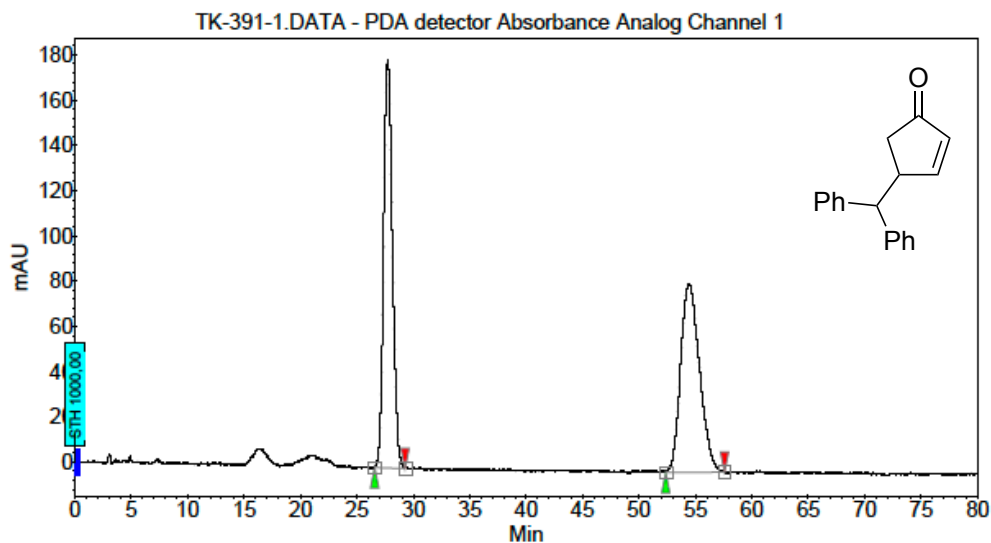
Figure S78. HPLC chromatogram of racemic **188** (Amylose-1, *i*-propanol/*n*-heptane = 20/80, flow rate = 1.0 mL/min, I = 215 nm, **racemic sample**).

(*S*)-4-Benzhydrylcyclopent-2-en-1-one ((*S*)-188)
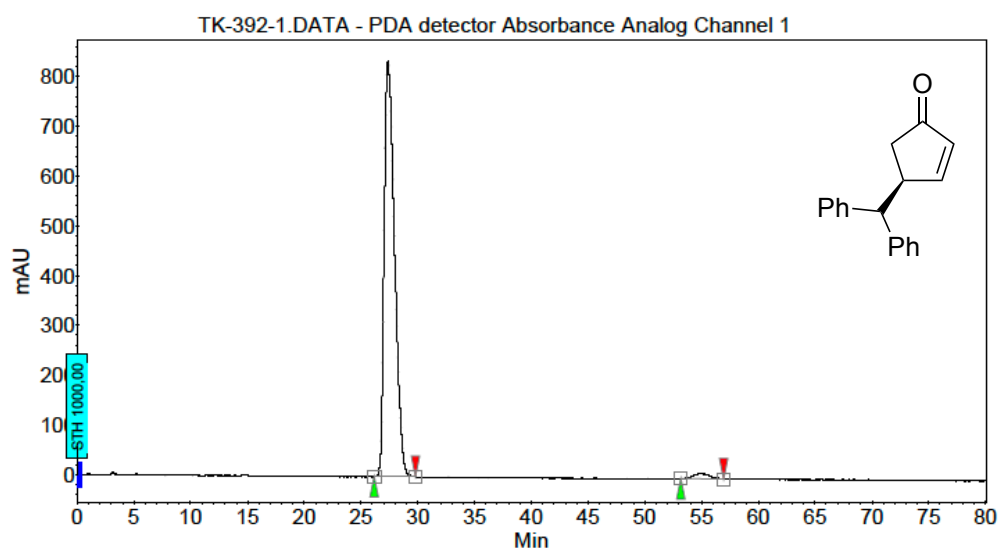
Figure S79. HPLC chromatogram of (*S*)-**188** (Amylose-1, *i*-propanol/*n*-heptane = 20/80, flow rate = 1.0 mL/min, I = 215 nm, **96% *ee***).

(±)-(9*H*-fluoren-9-yl)Methyl ((3*S*,3a*S*,6a*S*)-5-oxohexahydro-2*H*-cyclopenta[*b*]furan-3-yl)carbamate (*exo*-157)
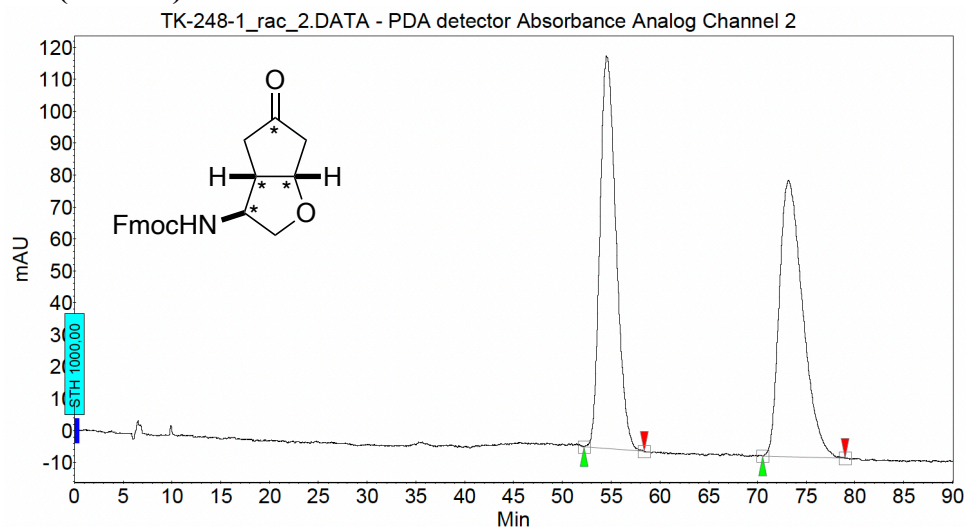
Peak Results :

Index	Name	Time [Min]	Quantity [% Area]	Height [mAU]	Area [mAU.Min]	Area % [%]
1	UNKNOWN	54,54	49,45	123,0	235,9	49,451
2	UNKNOWN	73,18	50,55	86,6	241,1	50,549
Total			100,00	209,6	477,0	100,000

Figure S80. HPLC chromatogram of *exo*-**157** (AS-H, *i*-propanol/*n*-heptane = 20/80, flow rate = 0.5 mL/min, I = 215 nm, **racemic sample**).

(9*H*-fluoren-9-yl)Methyl ((3*S*,3a*S*,6a*S*)-5-oxohexahydro-2*H*-cyclopenta[*b*]furan-3-yl)carbamate ((3*S*)-157)
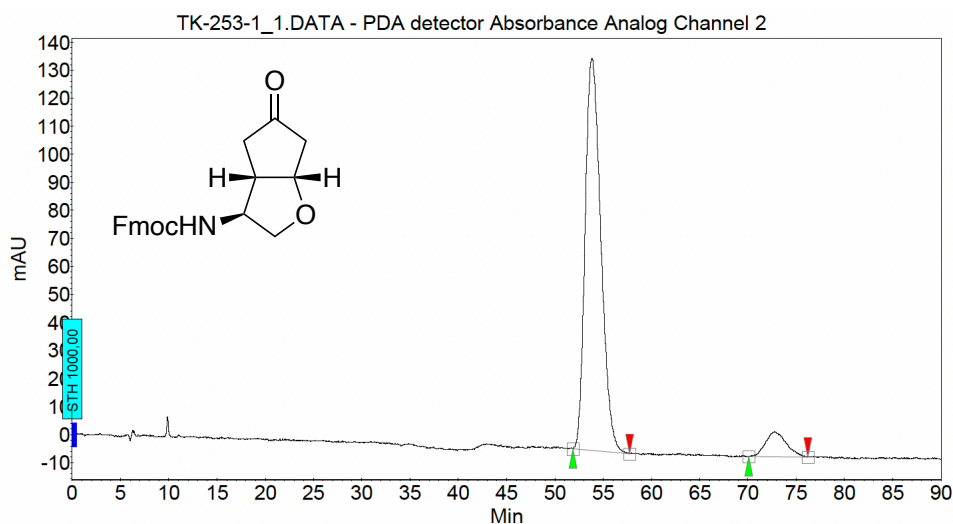
Peak Results :

Index	Name	Time [Min]	Quantity [% Area]	Height [mAU]	Area [mAU.Min]	Area % [%]
1	UNKNOWN	53,84	92,14	140,0	263,6	92,136
2	UNKNOWN	72,76	7,86	9,0	22,5	7,864
Total			100,00	149,0	286,1	100,000

Figure S81. HPLC chromatogram of (3*S*)-**157** (AS-H, *i*-propanol/*n*-heptane = 20/80, flow rate = 0.5 mL/min, I = 254 nm, **84% *ee***).

(±)-Methyl ((3R,3aR,5R,6aR)-5-(((4-nitrophenoxy)carbonyl)oxy)hexahydro-2H-cyclopenta[b]furan-3-yl)carbamate (exo-191)

Peak Results :

Index	Name	Time [Min]	Quantity [% Area]	Height [mAU]	Area [mAU.Min]	Area % [%]
1	UNKNOWN	19,39	49,51	199,2	121,0	49,511
2	UNKNOWN	23,28	50,49	175,9	123,4	50,489
Total			100,00	375,1	244,3	100,000
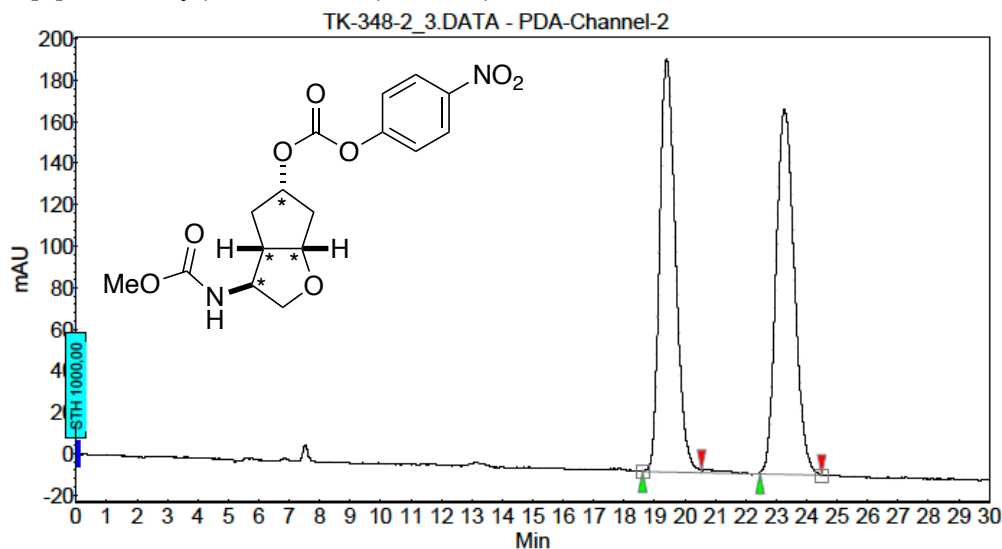
Figure S82. HPLC chromatogram of *exo*-**191** (Cellulose-1, *i*-propanol/*n*-heptane = 40/60, flow rate = 0.5 mL/min, I = 254 nm, **racemic sample**).

Methyl ((3R,3aR,5R,6aR)-5-(((4-nitrophenoxy)carbonyl)oxy)hexahydro-2H-cyclopenta[b]furan-3-yl)carbamate ((3R)-191)

Peak Results :

Index	Name	Time [Min]	Quantity [% Area]	Height [mAU]	Area [mAU.Min]	Area % [%]
1	UNKNOWN	19,36	8,15	28,6	15,2	8,154
2	UNKNOWN	23,05	91,85	234,7	171,1	91,846
Total			100,00	263,3	186,2	100,000
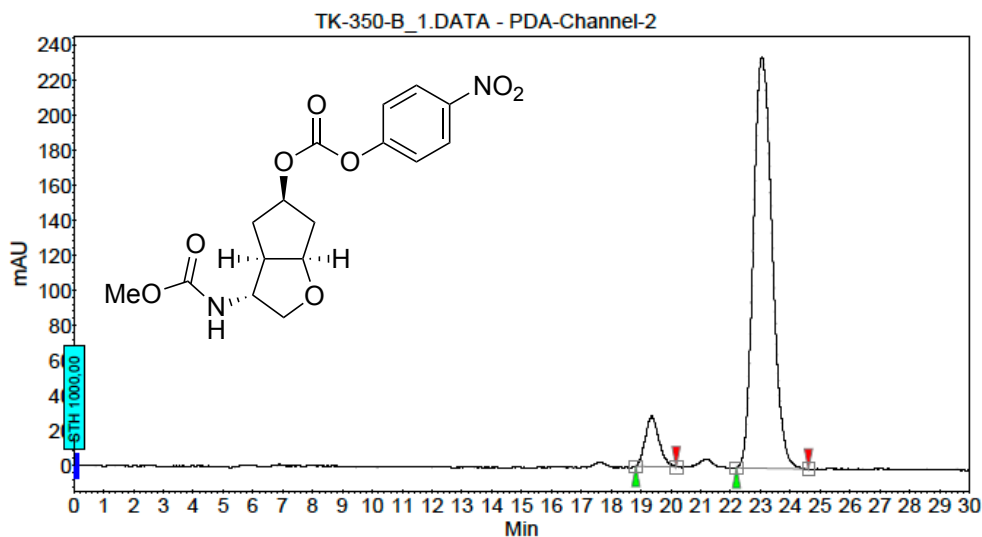
Figure S83. HPLC chromatogram of (3R)-**191** (Cellulose-1, *i*-propanol/*n*-heptane = 40/60, flow rate = 0.5 mL/min, I = 254 nm, **84% *ee***).

(±)-Methyl ((3*S*,3a*R*,5*R*,6a*R*)-5-(((4-nitrophenoxy)carbonyl)oxy)hexahydro-2*H*-cyclopenta[*b*]furan-3-yl)carbamate (*endo*-191)

Peak Results :

Index	Name	Time [Min]	Quantity [% Area]	Height [mAU]	Area [mAU.Min]	Area % [%]
1	UNKNOWN	39,98	50,35	37,7	46,4	50,346
2	UNKNOWN	44,05	49,65	34,4	45,7	49,654
Total			100,00	72,1	92,1	100,000
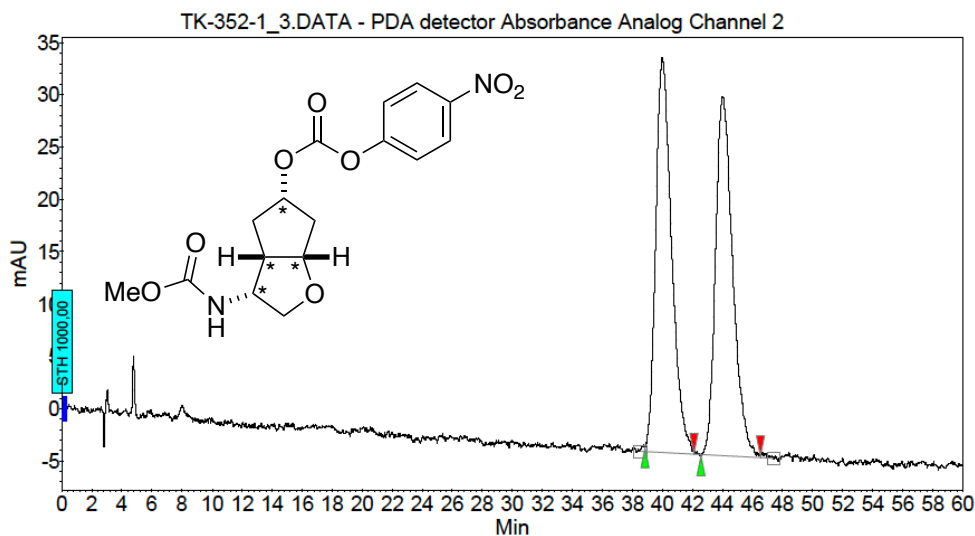
Figure S84. HPLC chromatogram of *endo*-191 (Cellulose-1, *i*-propanol/*n*-heptane = 10/90, flow rate = 1.0 mL/min, I = 254 nm, **racemic sample**).

Methyl ((3*S*,3a*R*,5*R*,6a*R*)-5-(((4-nitrophenoxy)carbonyl)oxy)hexahydro-2*H*-cyclopenta[*b*]furan-3-yl)carbamate ((3*S*)-191)

Peak Results :

Index	Name	Time [Min]	Quantity [% Area]	Height [mAU]	Area [mAU.Min]	Area % [%]
1	UNKNOWN	40,28	4,15	4,9	5,5	4,150
2	UNKNOWN	43,68	95,85	92,4	128,0	95,850
Total			100,00	97,3	133,5	100,000
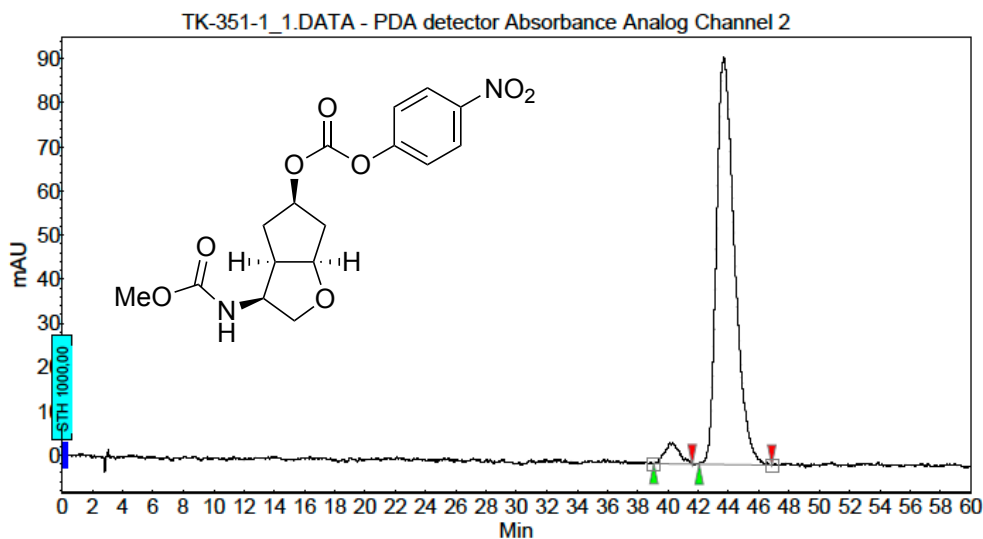
Figure S85. HPLC chromatogram of (3*S*)-191 (Cellulose-1, *i*-propanol/*n*-heptane = 10/90, flow rate = 1.0 mL/min, I = 254 nm, **92% *ee***).

Tert-butyl ((2*S*,3*R*)-3-hydroxy-4-((*N*-isobutyl-4-methoxyphenyl)sulfonamido)-1-phenylbutan-2-yl)carbamate (194)
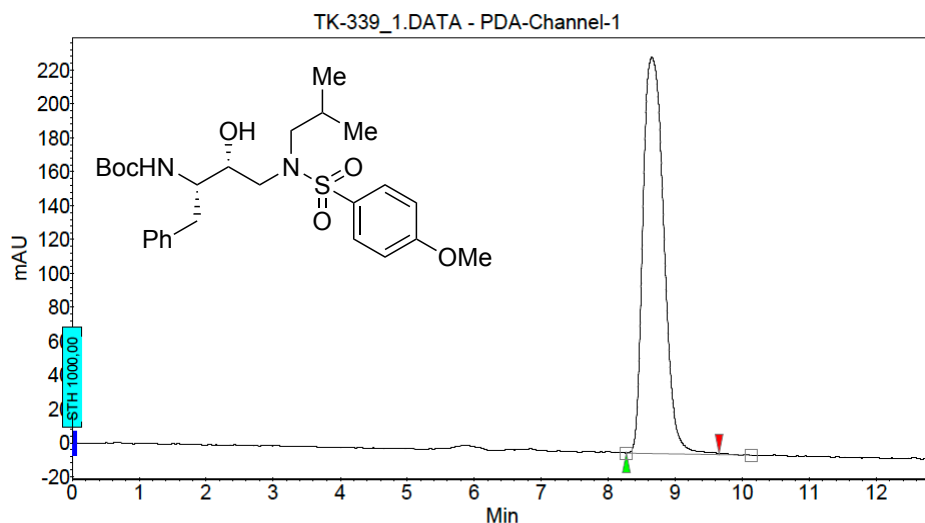
Figure S86. HPLC chromatogram of **194** (Cellulose-1, *i*-propanol/*n*-heptane = 40/60, flow rate = 0.5 mL/min, I = 215 nm, **>99% ee**).

The reference samples for chiral HPLC analysis for inhibitors **125** and **126**, namely (*rac*)-**125** and (*rac*)-**126**, were synthesized by coupling the racemic and diastereopure Cp-THF carbonates *exo*-**191** and *endo*-**191** with enantiopure amine **134** (Scheme S1), which was obtained via a literature procedure[124] starting from a commercially available and optically pure epoxide precursor. The optical purity of **134** is proved by the purity of its protected precursor **194** (see figure S79).
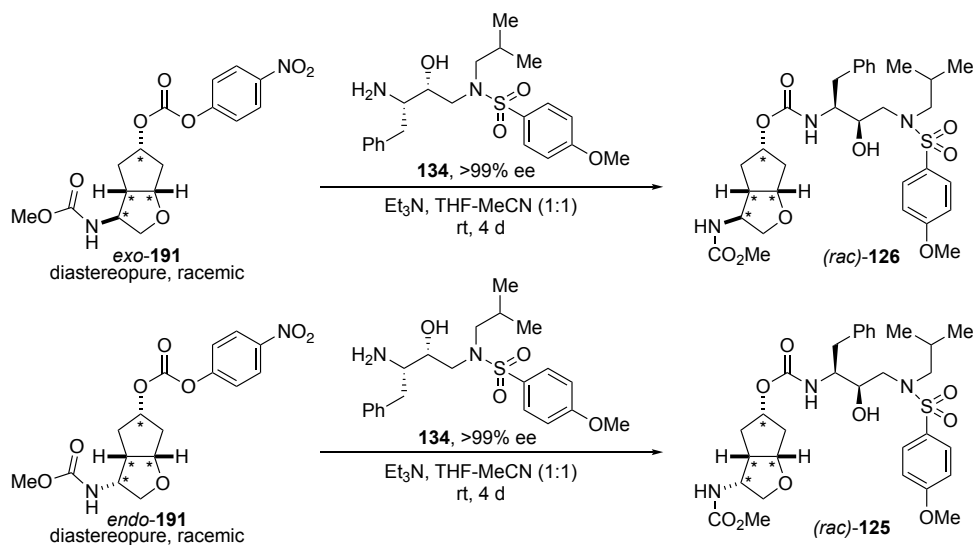
Scheme S1. Synthesis of chiral reference samples (*rac*)-**125** and (*rac*)-**126**.

3-((Methoxycarbonyl)amino)hexahydro-2*H*-cyclopenta[*b*]furan-5-yl ((2*S*,3*R*)-3-hydroxy-4-((*N*-isobutyl-4-methoxyphenyl)sulfonamido)-1-phenylbutan-2-yl)carbamate (*rac*-126)

Peak Results :

Index	Name	Time [Min]	Quantity [% Area]	Height [mAU]	Area [mAU.Min]	Area % [%]
1	UNKNOWN	35,36	49,49	161,7	256,5	49,492
2	UNKNOWN	43,72	50,51	139,9	261,8	50,508
Total			100,00	301,5	518,3	100,000
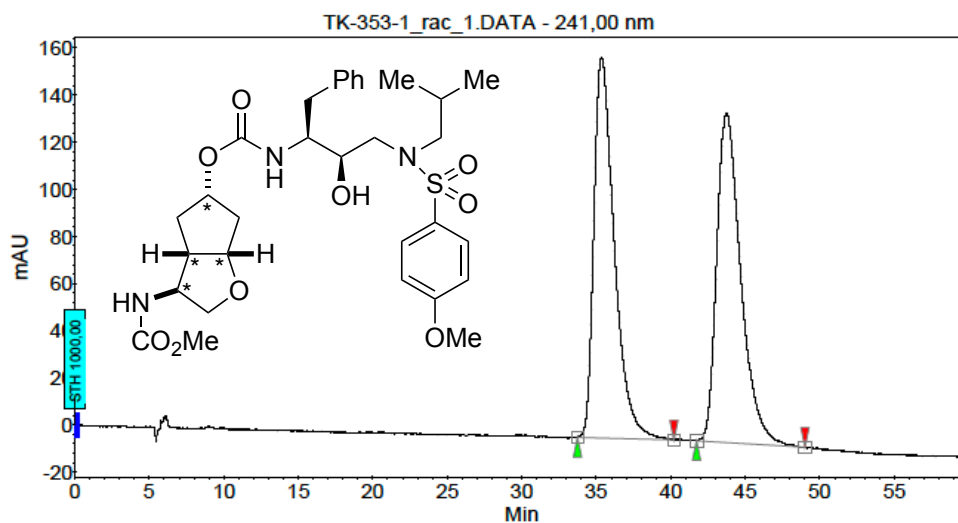
Figure S87. HPLC chromatogram of *rac*-126 (Cellulose-1, *i*-propanol/*n*-heptane = 20/80, flow rate = 0.5 mL/min, I = 254 nm, **racemic Cp-THF moiety** (*exo*)).

(3*R*,3a*R*,5*R*,6a*R*)-3-((Methoxycarbonyl)amino)hexahydro-2*H*-cyclopenta[*b*]furan-5-yl ((2*S*,3*R*)-3-hydroxy-4-((*N*-isobutyl-4-methoxyphenyl)sulfonamido)-1-phenylbutan-2-yl)carbamate (126)

Peak Results :

Index	Name	Time [Min]	Quantity [% Area]	Height [mAU]	Area [mAU.Min]	Area % [%]
1	UNKNOWN	35,78	6,89	34,8	54,4	6,893
2	UNKNOWN	43,37	93,11	392,6	734,3	93,107
Total			100,00	427,4	788,7	100,000
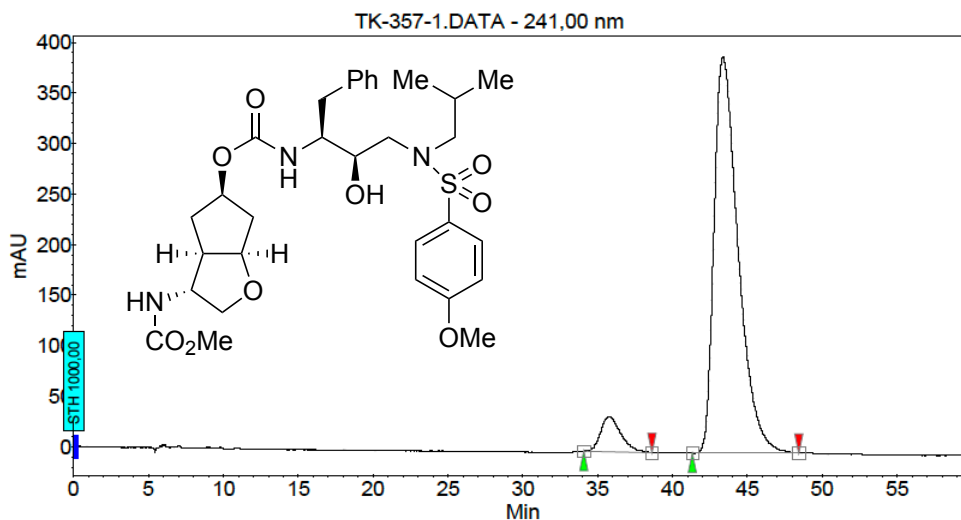
Figure S88. HPLC chromatogram of **126** (Cellulose-1, *i*-propanol/*n*-heptane = 20/80, flow rate = 0.5 mL/min, I = 254 nm, **86% *de***).

3-((Methoxycarbonyl)amino)hexahydro-2*H*-cyclopenta[*b*]furan-5-yl ((2*S*,3*R*)-3-hydroxy-4-((*N*-isobutyl-4-methoxyphenyl)sulfonamido)-1-phenylbutan-2-yl)carbamate (*rac*-125)

Peak Results :

Index	Name	Time [Min]	Quantity [% Area]	Height [mAU]	Area [mAU.Min]	Area % [%]
1	UNKNOWN	12,63	48,97	290,8	160,4	48,967
2	UNKNOWN	18,75	51,03	212,2	167,2	51,033
Total			100,00	503,0	327,6	100,000
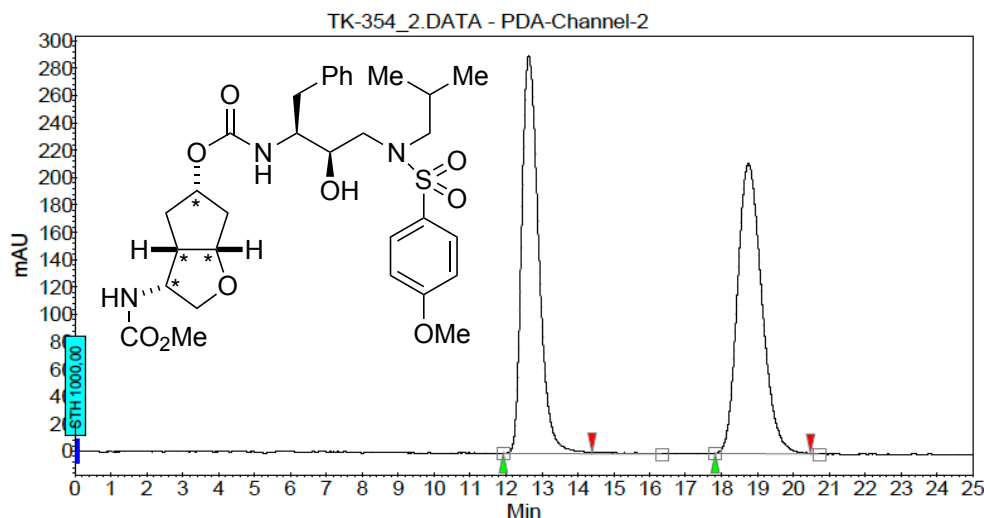
Figure S89. HPLC chromatogram of *rac*-125 (Cellulose-1, *i*-propanol/*n*-heptane = 40/60, flow rate = 0.5 mL/min, I = 254 nm, **racemic Cp-THF moiety** (*endo*)).

(3*S*,3a*R*,5*R*,6a*R*)-3-((Methoxycarbonyl)amino)hexahydro-2*H*-cyclopenta[*b*]furan-5-yl ((2*S*,3*R*)-3-hydroxy-4-((*N*-isobutyl-4-methoxyphenyl)sulfonamido)-1-phenylbutan-2-yl)carbamate (125)

Peak Results :

Index	Name	Time [Min]	Quantity [% Area]	Height [mAU]	Area [mAU.Min]	Area % [%]
1	UNKNOWN	12,78	4,66	19,0	9,9	4,662
2	UNKNOWN	18,63	95,34	250,2	202,8	95,338
Total			100,00	269,2	212,8	100,000
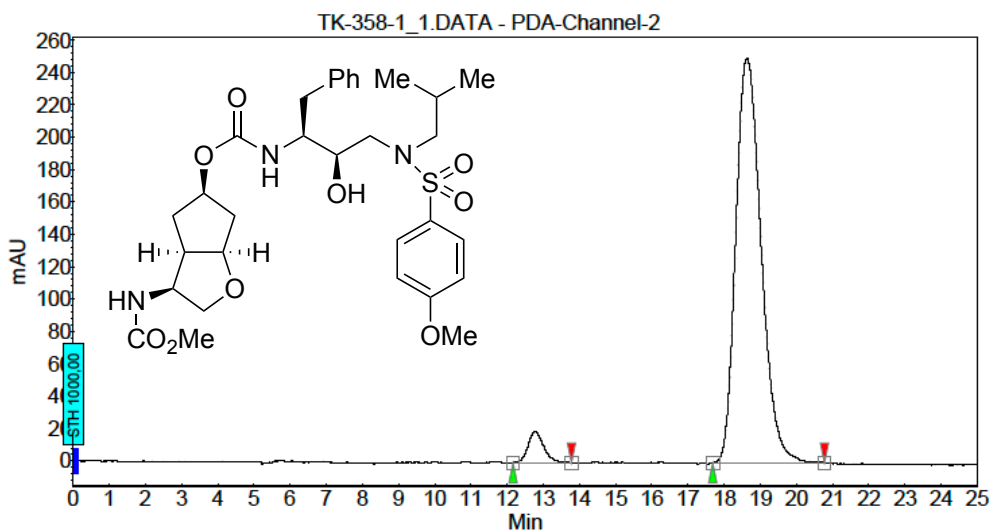
Figure S90. HPLC chromatogram of **125** (Cellulose-1, *i*-propanol/*n*-heptane = 40/60, flow rate = 0.5 mL/min, I = 254 nm, **91% *de***).

160

3   X-ray crystallographic data

(±)-*Tert*-butyl ((3*S*,3a*S*,6a*S*)-5-oxohexahydro-2*H*-cyclopenta[*b*]furan-3-yl)carbamate (*exo*-151)

CCDC: 2085697
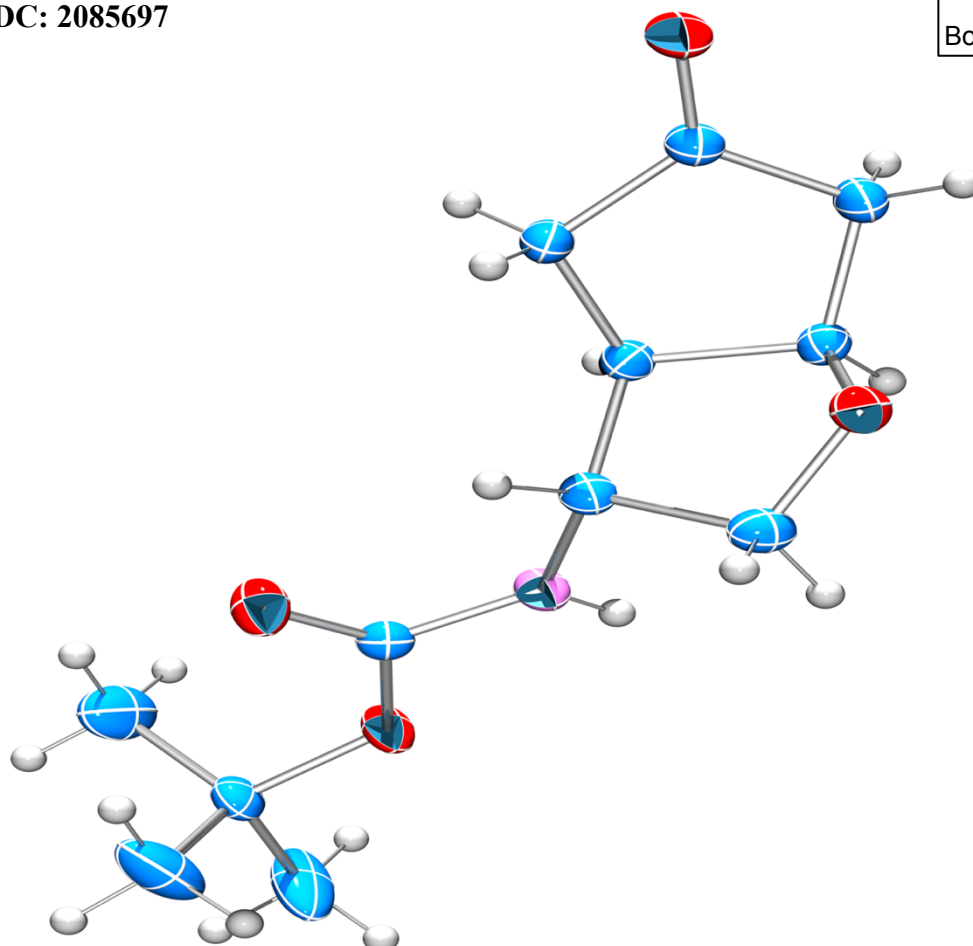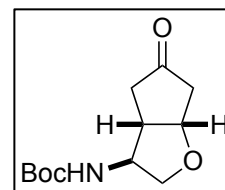
Figure S91. X-Ray crystallographic structure of *exo*-151 (ORTEP view with 50% thermal ellipsoid contour probability, CCDC 2085697).

Method for X-Ray quality crystal growth

Suitable crystals for X-Ray analysis were obtained by slow evaporation of a Et₂O solution containing *exo*-151. The crystals obtained were colourless and prism-shaped.

Table S1. Crystal data and structure refinement for *exo*-**151**.

Formula	$C_{12}H_{19}NO_4$
$D_{calc.}$/ g cm^{-3}	1.290
μ/mm^{-1}	0.798
Formula Weight	241.28
Colour	clear colourless
Shape	prism
Size/mm^3	0.39×0.32×0.32
T/K	122.9(4)
Crystal System	monoclinic
Space Group	$P2_1/n$
a/Å	5.83180(10)
b/Å	28.7066(3)
c/Å	7.42780(10)
α/°	90
β/°	92.2270(10)
γ/°	90
V/Å^3	1242.56(3)
Z	4
Z'	1
Wavelength/Å	1.54184
Radiation type	Cu K$_\alpha$
Θ_{min}/°	3.079
Θ_{max}/°	73.898
Measured Refl.	14114
Independent Refl.	2500
Reflections with I > 2(I)	2452
R_{int}	0.0229
Parameters	157
Restraints	0
Largest Peak	0.483
Deepest Hole	-0.315
GooF	1.071
wR_2 (all data)	0.1114
wR_2	0.1110
R_1 (all data)	0.0445
R_1	0.0440

Table S2: Fractional Atomic Coordinates (×10⁴) and Equivalent Isotropic Displacement Parameters (Å²×10³) for *exo*-**151**. U_{eq} is defined as 1/3 of the trace of the orthogonalised U_{ij}.

Atom	x	y	z	U_{eq}
O2	217.8(16)	4345.2(3)	4022.8(13)	24.3(2)
O4	6641.6(19)	3465.5(4)	8953.7(13)	27.7(3)
O3	3025.4(19)	4597.6(4)	-679.9(13)	29.2(3)
O1	6456.7(18)	3163.8(4)	6112.5(14)	30.1(3)
N1	4575(2)	3827.6(4)	6839.5(15)	22.1(3)
C8	5939(2)	3455.8(5)	7203.8(18)	20.0(3)
C5	3383(2)	3888.8(5)	5102.4(17)	20.6(3)
C3	2166(2)	4650.1(5)	4015.5(17)	20.4(3)
C4	4217(2)	4310.5(5)	4011.2(17)	20.5(3)
C1	3197(2)	4578.4(5)	950.9(18)	22.2(3)
C2	2111(3)	4911.9(5)	2245.3(18)	24.2(3)
C6	809(2)	3994.2(5)	5323.0(19)	25.0(3)
C9	8161(2)	3099.3(5)	9734.2(19)	25.5(3)
C7	4570(3)	4215.7(5)	2004.7(19)	28.0(3)
C10	10462(3)	3121.3(7)	8896(3)	42.9(4)
C12	7095(3)	2620.2(6)	9480(3)	49.5(5)
C11	8348(5)	3232.7(8)	11696(2)	61.1(7)

Table S3: Anisotropic Displacement Parameters (×10⁴) for *exo*-**151**. The anisotropic displacement factor exponent takes the form: $-2\pi^2[h^2a^{*2} \times U_{11} + \ldots + 2hka^* \times b^* \times U_{12}]$

Atom	U_{11}	U_{22}	U_{33}	U_{23}	U_{13}	U_{12}
O2	18.7(5)	30.1(5)	23.9(5)	3.0(4)	-1.9(4)	1.2(4)
O4	37.6(6)	27.3(5)	17.8(5)	-0.1(4)	-4.8(4)	13.6(4)
O3	37.3(6)	33.1(6)	17.0(5)	0.1(4)	-3.1(4)	8.5(4)
O1	35.2(6)	29.6(5)	25.1(5)	-7.3(4)	-5.5(4)	8.6(4)
N1	28.9(6)	21.8(6)	15.3(5)	-1.3(4)	-2.9(4)	4.4(4)
C8	20.3(6)	21.1(6)	18.7(6)	0.9(5)	0.3(5)	-1.8(5)
C5	23.7(6)	22.1(6)	15.7(6)	-1.2(5)	-2.0(5)	1.8(5)
C3	22.0(6)	21.5(6)	17.7(6)	-2.3(5)	1.2(5)	1.8(5)
C4	18.7(6)	24.9(6)	17.8(6)	1.1(5)	-0.5(5)	2.3(5)
C1	24.3(6)	23.9(7)	18.3(6)	0.5(5)	-0.7(5)	2.1(5)
C2	28.8(7)	22.6(7)	21.3(7)	0.3(5)	0.9(5)	6.5(5)
C6	23.5(7)	30.3(7)	21.1(7)	2.6(5)	-0.7(5)	-2.1(5)
C9	28.0(7)	25.6(7)	22.6(7)	4.4(5)	-2.7(5)	9.0(6)
C7	31.4(7)	33.5(8)	19.5(7)	3.3(6)	4.1(6)	14.0(6)
C10	26.3(8)	57.9(11)	44.2(10)	14.1(8)	-2.3(7)	4.5(7)
C12	39.3(10)	35.2(9)	72.9(14)	24.5(9)	-10.0(9)	-3.1(7)
C11	91.0(16)	67.2(14)	23.9(9)	-0.8(8)	-13.3(9)	52.6(13)

Table S4: Bond Lengths in Å for *exo*-**151**.

Atom	Atom	Length/Å
O2	C3	1.4346(16)
O2	C6	1.4285(17)
O4	C8	1.3480(16)
O4	C9	1.4786(16)
O3	C1	1.2129(17)
O1	C8	1.2124(17)
N1	C8	1.3520(17)
N1	C5	1.4524(16)
C5	C4	1.5459(18)
C5	C6	1.5462(19)
C3	C4	1.5432(18)
C3	C2	1.5137(18)
C4	C7	1.5367(18)
C1	C2	1.5129(19)
C1	C7	1.5131(19)
C9	C10	1.503(2)
C9	C12	1.518(2)
C9	C11	1.507(2)

.

Table S5: Bond Angles in ° for *exo*-**151**

Atom	Atom	Atom	Angle/°
C6	O2	C3	105.22(10)
C8	O4	C9	121.23(11)
C8	N1	C5	122.06(11)
O4	C8	N1	109.33(11)
O1	C8	O4	125.78(12)
O1	C8	N1	124.88(12)
N1	C5	C4	114.26(11)
N1	C5	C6	111.27(11)
C4	C5	C6	103.24(10)
O2	C3	C4	103.21(10)
O2	C3	C2	108.43(11)
C2	C3	C4	107.58(11)
C3	C4	C5	103.52(10)
C7	C4	C5	115.25(12)
C7	C4	C3	104.29(10)
O3	C1	C2	125.86(13)
O3	C1	C7	124.70(13)
C2	C1	C7	109.44(11)
C1	C2	C3	104.05(11)
O2	C6	C5	106.03(11)
O4	C9	C10	109.81(12)
O4	C9	C12	111.06(12)
O4	C9	C11	102.61(11)
C10	C9	C12	110.76(15)
C10	C9	C11	110.95(16)
C11	C9	C12	111.38(17)
C1	C7	C4	106.96(11)

Table S6: Hydrogen Fractional Atomic Coordinates ($\times 10^4$) and Equivalent Isotropic Displacement Parameters ($\text{Å}^2 \times 10^3$) for *exo*-**151**. U_{eq} is defined as 1/3 of the trace of the orthogonalised U_{ij}.

Atom	x	y	z	U_{eq}
H1	4408.47	4034.29	7662.19	26
H5	3536.68	3604.51	4386.68	25
H3	2236.95	4859.62	5057.97	24
H4	5590	4450.56	4589.45	25
H2A	547.56	4985.23	1851.67	29
H2B	2985.05	5198.76	2351.56	29
H6A	-105.31	3716.18	5104.67	30
H6B	547.29	4105.51	6530.93	30
H7A	6183.23	4239.21	1745.74	34
H7B	4038.32	3905.31	1683.92	34
H10A	10296.17	3041.22	7642.98	64
H10B	11492.23	2905.66	9495.9	64
H10C	11069.45	3431.14	9013.97	64
H12A	5590.02	2618.91	9958.99	74
H12B	8036.79	2392.59	10101.05	74
H12C	6985.57	2546.23	8219.21	74
H11A	8947.9	3543.24	11809.79	92
H11B	9358.91	3019.86	12331.31	92
H11C	6857.2	3220.13	12198.46	92

***Tert*-butyl (2*R*,5*R*,5a*S*,8a*S*)-7-oxooctahydro-4*H*-2,5-methanocyclopenta[*f*][1,4]oxazepine-4-carboxylate ((5a*S*,8a*S*)-179a)**

CCDC: 2085792
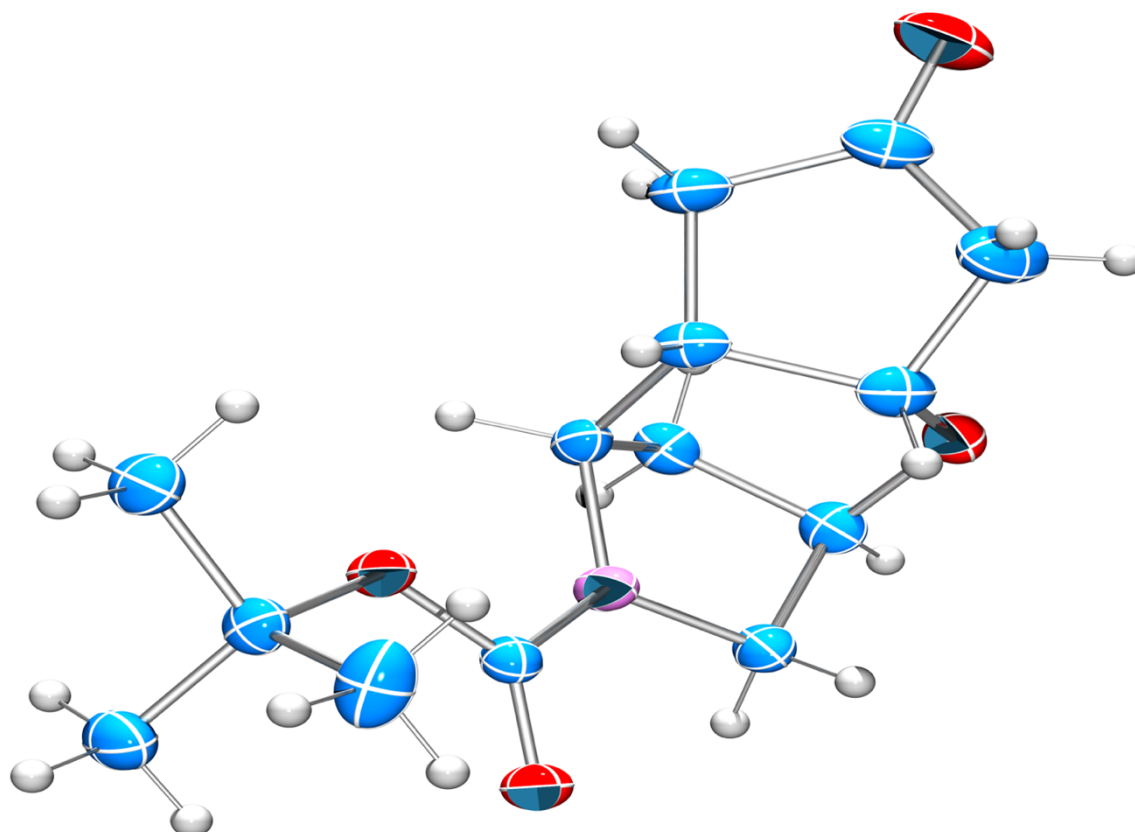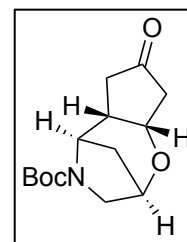
Figure S92. X-Ray crystallographic structure of (5aS,8aS)-**179a** (ORTEP view with 50% thermal ellipsoid contour probability, CCDC: 2085792).

Method for X-Ray quality crystal growth

Suitable crystals for X-Ray analysis were obtained by slow evaporation of a Et$_2$O solution containing a mixture of both diastereomers of **179a**. The crystals obtained were colourless and prism-shaped.

Table S7. Crystal data and structure refinement for (5a*S*,8a*S*)-**179a**.

Formula	$C_{14}H_{21}NO_4$
$D_{calc.}$/ g cm^{-3}	1.271
μ/mm^{-1}	0.553
Formula Weight	267.32
Colour	clear colourless
Shape	prism
Size/mm^3	0.23×0.17×0.10
T/K	123.00(10)
Crystal System	monoclinic
Flack Parameter	0.05(9)
Hooft Parameter	0.06(8)
Space Group	$P2_1$
a/Å	10.8409(3)
b/Å	10.1683(2)
c/Å	13.5231(3)
α/°	90
β/°	110.407(3)
γ/°	90
V/Å^3	1397.14(6)
Z	4
Z'	2
Wavelength/Å	1.39222
Radiation type	Cu K
Θ_{min}/°	3.148
Θ_{max}/°	59.955
Measured Refl's.	8183
Ind't Refl's	4762
Refl's with I > 2(I)	4597
R_{int}	0.0161
Parameters	349
Restraints	1
Largest Peak	0.173
Deepest Hole	-0.163
GooF	1.027
wR_2 (all data)	0.0758
wR_2	0.0748
R_1 (all data)	0.0314
R_1	0.0302

Table S8: Fractional Atomic Coordinates (×10^4) and Equivalent Isotropic Displacement Parameters (Å^2×10^3) for (5aS,8aS)-**179a**. U_{eq} is defined as 1/3 of the trace of the orthogonalised U_{ij}.

Atom	x	y	z	U_{eq}
O2	1192.1(14)	1956.4(13)	8095.7(11)	25.1(3)
O1	-50.9(15)	2173.7(14)	9148.8(11)	27.7(3)
O6	6237.1(14)	4457.6(13)	7941.9(10)	24.8(3)
O3	-313.5(14)	6576.9(15)	7577.1(10)	27.7(3)
O5	4949.6(15)	4605.7(14)	8968.2(11)	29.1(3)
O7	4905.2(14)	9085.4(14)	7871.9(10)	27.1(3)
O8	5130(2)	10134.8(17)	5169.0(12)	43.7(4)
N1	804.5(17)	3935.6(17)	8601.9(13)	24.8(4)
N2	6037.6(17)	6370.0(18)	8651.2(12)	24.7(4)
O4	577.9(19)	7481(2)	5137.2(13)	50.9(5)
C5	588.7(19)	2639(2)	8652.2(14)	21.9(4)
C19	5669.7(19)	5095(2)	8550.1(14)	23.4(4)
C25	4506.7(19)	8105(2)	7056.3(15)	25.5(4)
C20	5497(2)	7313(2)	9214.7(15)	26.3(4)
C16	5935(2)	3067.6(19)	7656.0(16)	25.9(4)
C8	1872(2)	5899(2)	8600.4(15)	26.5(4)
C22	7124(2)	8322(2)	8660.1(15)	26.7(4)
C23	6702(2)	7060(2)	8016.6(15)	23.2(4)
C9	1582(2)	4573(2)	8029.9(15)	23.8(4)
C28	6155(2)	8210(2)	6191.3(15)	28.7(4)
C27	5069(2)	9206(2)	5711.4(15)	30.2(5)
C17	6757(2)	2804(2)	6966.9(16)	29.6(5)
C2	1037(2)	517(2)	7978.3(15)	25.4(4)
C7	512(2)	6209(2)	8628.5(15)	26.3(4)
C11	-546(2)	5547(2)	6806.2(15)	28.4(4)
C24	5682(2)	7355(2)	6926.0(14)	23.1(4)
C26	3902(2)	8853(3)	6022.5(16)	33.5(5)
C6	119(2)	4919(2)	9012.2(15)	25.5(4)
C10	710(2)	4763(2)	6877.5(15)	26.0(4)
C21	5852(2)	8634(2)	8854.0(15)	26.2(4)
C14	1350(2)	5526(2)	6198.2(16)	32.8(5)
C4	1740(2)	224(2)	7208.6(17)	33.7(5)
C1	1745(2)	-142(2)	9029.1(17)	34.9(5)
C13	362(2)	6557(3)	5612.0(15)	34.6(5)
C18	4485(2)	2910(3)	7026(2)	40.3(6)
C15	6409(3)	2217(2)	8636.5(18)	37.9(5)
C12	-936(2)	6240(3)	5743.5(17)	41.9(6)
C3	-405(2)	152(3)	7505(2)	41.9(6)

Table S9: Anisotropic Displacement Parameters (×10⁴) for (5a*S*,8a*S)*-**179a**. The anisotropic displacement factor exponent takes the form: $-2\pi^2[h^2a^{*2} \times U_{11} + ... +2hka^* \times b^* \times U_{12}]$

Atom	U_{11}	U_{22}	U_{33}	U_{23}	U_{13}	U_{12}
O2	34.1(7)	18.2(7)	29.2(7)	-0.3(5)	18.8(6)	0.7(6)
O1	34.4(8)	25.2(8)	29.6(7)	3.2(6)	18.9(6)	1.4(7)
O6	33.7(8)	17.0(7)	28.0(7)	-0.2(5)	16.0(6)	-0.3(6)
O3	31.2(7)	25.9(8)	26.7(7)	3.0(6)	10.8(6)	4.5(7)
O5	35.3(8)	25.3(8)	31.3(7)	-0.8(6)	17.3(6)	-4.1(7)
O7	33.1(8)	23.2(7)	24.0(7)	-1.8(6)	8.5(6)	5.3(6)
O8	63.8(11)	32.4(9)	33.0(8)	9.0(7)	14.6(8)	1.5(9)
N1	33.6(9)	19.9(9)	26.9(8)	0.3(7)	18.0(7)	2.4(7)
N2	32.3(9)	20.2(8)	26.1(8)	0.9(7)	15.8(7)	-0.2(8)
O4	60.2(12)	50.9(12)	41.3(9)	19.9(9)	17.5(9)	-2.3(10)
C5	24.3(9)	22.5(10)	18.8(8)	0.5(7)	7.3(7)	1.6(8)
C19	26.4(9)	22.3(10)	22.2(8)	0.8(7)	9.2(8)	0.4(8)
C25	23.2(9)	28.6(11)	23.6(9)	-3.8(8)	7.1(7)	-1.4(9)
C20	32.2(10)	25.3(11)	23.0(9)	-2.4(8)	11.8(8)	-1.7(9)
C16	32.5(11)	16.5(10)	29.5(10)	-2.6(8)	11.7(8)	-1.0(9)
C8	29.4(11)	22.8(10)	25.1(9)	-1.3(8)	6.7(8)	-2.5(9)
C22	26.9(10)	24.7(10)	24.4(9)	1.8(8)	3.9(8)	-3.9(9)
C23	25.1(9)	19.6(10)	27.7(9)	2.7(8)	12.9(8)	-0.5(8)
C9	26.2(9)	20.2(10)	29.3(10)	1.6(8)	15.0(8)	0.9(8)
C28	33.3(11)	30.5(11)	24.6(9)	3.4(9)	13.0(8)	-1.2(10)
C27	41.0(12)	26.9(11)	18.9(9)	-3.5(8)	5.6(8)	-0.5(10)
C17	33.7(11)	25.8(11)	30.5(10)	-2.2(8)	12.8(9)	2.8(9)
C2	29.2(10)	18.5(10)	29.4(9)	-2.9(8)	11.5(8)	-0.1(9)
C7	34.0(11)	21.7(10)	23.6(9)	-5.1(8)	10.3(8)	0.4(9)
C11	26.0(10)	34.8(12)	23.6(9)	-0.8(9)	7.4(8)	-6.8(9)
C24	28.5(10)	19.2(10)	23.7(9)	-2.0(8)	11.9(8)	-1.6(8)
C26	30.2(11)	42.1(14)	24.3(10)	-0.1(9)	4.6(8)	6.1(10)
C6	32.5(10)	24.6(11)	22.3(9)	-0.7(8)	13.1(8)	5.1(9)
C10	35.0(11)	22.0(10)	25.0(9)	-4.6(8)	15.6(8)	-6.7(9)
C21	33.6(11)	21.7(11)	21.1(9)	-4.6(7)	6.9(8)	-2.4(9)
C14	38.8(12)	35.5(12)	30.5(10)	1.8(9)	20.5(9)	-3.7(10)
C4	44.6(13)	28.0(12)	32.6(10)	-3.0(9)	18.8(10)	5.9(10)
C1	46.3(13)	25.3(12)	37.3(11)	3.8(9)	19.9(10)	5.8(10)
C13	43.2(12)	39.9(13)	19.6(9)	0.8(9)	9.5(9)	-6.3(11)
C18	33.8(12)	40.5(14)	47.4(13)	-17.1(11)	15.2(10)	-5.8(11)
C15	54.9(15)	24.2(12)	41.3(12)	7.6(10)	25.3(11)	4.3(11)
C12	35.0(12)	61.3(17)	25.0(10)	6.8(11)	4.9(9)	-3.8(12)
C3	30.7(11)	32.6(13)	58.9(15)	-15.6(11)	11.2(11)	-2.9(10)

Table S10: Bond Lengths in Å for (5a*S*,8a*S*)-**179a**.

Atom	Atom	Length/Å
O2	C5	1.349(2)
O2	C2	1.475(2)
O1	C5	1.216(2)
O6	C19	1.352(2)
O6	C16	1.472(2)
O3	C7	1.440(2)
O3	C11	1.437(3)
O5	C19	1.218(2)
O7	C25	1.437(2)
O7	C21	1.442(2)
O8	C27	1.212(3)
N1	C5	1.345(3)
N1	C9	1.477(2)
N1	C6	1.466(3)
N2	C19	1.350(3)
N2	C20	1.468(3)
N2	C23	1.476(2)
O4	C13	1.207(3)
C25	C24	1.546(3)
C25	C26	1.524(3)
C20	C21	1.523(3)
C16	C17	1.520(3)
C16	C18	1.513(3)
C16	C15	1.515(3)
C8	C9	1.531(3)
C8	C7	1.521(3)
C22	C23	1.528(3)
C22	C21	1.524(3)
C23	C24	1.533(3)
C9	C10	1.527(3)
C28	C27	1.516(3)
C28	C24	1.537(3)
C27	C26	1.509(3)
C2	C4	1.519(3)
C2	C1	1.515(3)
C2	C3	1.514(3)
C7	C6	1.525(3)
C11	C10	1.552(3)
C11	C12	1.522(3)
C10	C14	1.541(3)
C14	C13	1.511(3)
C13	C12	1.513(3)

Table S11: Bond Angles in ° for (5a*S*,8a*S*)-**179a.**

Atom	Atom	Atom	Angle/°
C5	O2	C2	120.74(15)
C19	O6	C16	120.90(15)
C11	O3	C7	114.75(15)
C25	O7	C21	114.39(15)
C5	N1	C9	126.68(16)
C5	N1	C6	121.98(17)
C6	N1	C9	110.86(16)
C19	N2	C20	121.53(16)
C19	N2	C23	125.78(16)
C20	N2	C23	110.81(16)
O1	C5	O2	126.06(19)
O1	C5	N1	123.49(18)
N1	C5	O2	110.45(16)
O5	C19	O6	126.02(19)
O5	C19	N2	124.03(18)
N2	C19	O6	109.94(16)
O7	C25	C24	112.98(16)
O7	C25	C26	106.01(18)
C26	C25	C24	104.43(16)
N2	C20	C21	102.62(15)
O6	C16	C17	101.90(16)
O6	C16	C18	109.97(17)
O6	C16	C15	110.00(16)
C18	C16	C17	110.63(17)
C18	C16	C15	113.64(19)
C15	C16	C17	110.08(18)
C7	C8	C9	99.49(16)
C21	C22	C23	99.41(16)
N2	C23	C22	100.25(15)
N2	C23	C24	108.51(16)
C22	C23	C24	110.84(16)
N1	C9	C8	100.19(15)
N1	C9	C10	109.08(16)
C10	C9	C8	110.38(16)
C27	C28	C24	105.68(17)
O8	C27	C28	125.6(2)
O8	C27	C26	125.6(2)
C26	C27	C28	108.84(18)
O2	C2	C4	101.70(16)
O2	C2	C1	109.64(16)
O2	C2	C3	110.52(18)
C1	C2	C4	110.15(18)
C3	C2	C4	110.70(18)
C3	C2	C1	113.49(19)
O3	C7	C8	107.65(16)
O3	C7	C6	114.07(17)
C8	C7	C6	102.58(17)
O3	C11	C10	113.64(16)
O3	C11	C12	105.56(19)
C12	C11	C10	104.18(17)
C23	C24	C25	109.49(15)
C23	C24	C28	116.17(17)
C28	C24	C25	105.59(17)
C27	C26	C25	103.90(17)
N1	C6	C7	102.68(15)
C9	C10	C11	110.23(15)
C9	C10	C14	115.16(17)

Atom	Atom	Atom	Angle/°
C14	C10	C11	105.79(17)
O7	C21	C20	113.42(17)
O7	C21	C22	107.72(15)
C20	C21	C22	102.50(17)
C13	C14	C10	106.11(18)
O4	C13	C14	125.8(2)
O4	C13	C12	126.1(2)
C14	C13	C12	108.03(19)
C13	C12	C11	104.27(18)

Table S12: Torsion Angles in ° for (5a*S*,8a*S*)-**179a**.

Atom	Atom	Atom	Atom	Angle/°
O3	C7	C6	N1	85.90(19)
O3	C11	C10	C9	38.1(2)
O3	C11	C10	C14	-87.0(2)
O3	C11	C12	C13	85.6(2)
O7	C25	C24	C23	40.9(2)
O7	C25	C24	C28	-84.82(19)
O7	C25	C26	C27	85.43(19)
O8	C27	C26	C25	-153.7(2)
N1	C9	C10	C11	55.4(2)
N1	C9	C10	C14	174.97(17)
N2	C20	C21	O7	85.39(19)
N2	C20	C21	C22	-30.44(18)
N2	C23	C24	C25	53.9(2)
N2	C23	C24	C28	173.37(17)
O4	C13	C12	C11	-149.8(2)
C5	O2	C2	C4	173.80(16)
C5	O2	C2	C1	-69.6(2)
C5	O2	C2	C3	56.2(2)
C5	N1	C9	C8	-159.89(19)
C5	N1	C9	C10	84.2(2)
C5	N1	C6	C7	-171.48(18)
C19	O6	C16	C17	178.74(16)
C19	O6	C16	C18	61.4(2)
C19	O6	C16	C15	-64.5(2)
C19	N2	C20	C21	-163.90(18)
C19	N2	C23	C22	-167.59(18)
C19	N2	C23	C24	76.2(2)
C25	O7	C21	C20	-46.8(2)
C25	O7	C21	C22	65.9(2)
C20	N2	C19	O6	175.90(15)
C20	N2	C19	O5	-5.3(3)
C20	N2	C23	C22	27.90(19)
C20	N2	C23	C24	-88.31(19)
C16	O6	C19	O5	4.8(3)
C16	O6	C19	N2	-176.39(16)
C8	C9	C10	C11	-53.8(2)
C8	C9	C10	C14	65.8(2)
C8	C7	C6	N1	-30.20(18)
C22	C23	C24	C25	-55.2(2)

Atom	Atom	Atom	Atom	Angle/°
C22	C23	C24	C28	64.2(2)
C23	N2	C19	O6	12.9(3)
C23	N2	C19	O5	-168.25(18)
C23	N2	C20	C21	1.4(2)
C23	C22	C21	O7	-72.50(18)
C23	C22	C21	C20	47.39(17)
C9	N1	C5	O2	0.1(3)
C9	N1	C5	O1	179.13(18)
C9	N1	C6	C7	1.1(2)
C9	C8	C7	O3	-73.51(18)
C9	C8	C7	C6	47.13(17)
C9	C10	C14	C13	-131.71(19)
C28	C27	C26	C25	26.2(2)
C27	C28	C24	C25	-13.9(2)
C27	C28	C24	C23	-135.40(18)
C2	O2	C5	O1	4.6(3)
C2	O2	C5	N1	-176.39(17)
C7	O3	C11	C10	-44.6(2)
C7	O3	C11	C12	-158.16(17)
C7	C8	C9	N1	-45.05(18)
C7	C8	C9	C10	69.85(18)
C11	O3	C7	C8	64.7(2)
C11	O3	C7	C6	-48.4(2)
C11	C10	C14	C13	-9.7(2)
C24	C25	C26	C27	-34.1(2)
C24	C28	C27	O8	172.3(2)
C24	C28	C27	C26	-7.6(2)
C26	C25	C24	C23	155.68(17)
C26	C25	C24	C28	29.9(2)
C6	N1	C5	O2	171.44(16)
C6	N1	C5	O1	-9.5(3)
C6	N1	C9	C8	27.9(2)
C6	N1	C9	C10	-87.96(19)
C10	C11	C12	C13	-34.4(2)
C10	C14	C13	O4	167.1(2)
C10	C14	C13	C12	-11.8(2)
C21	O7	C25	C24	-47.8(2)
C21	O7	C25	C26	-161.54(16)
C21	C22	C23	N2	-45.17(17)
C21	C22	C23	C24	69.29(18)
C14	C13	C12	C11	29.1(3)
C12	C11	C10	C9	152.44(18)
C12	C11	C10	C14	27.3(2)

Table S13: Hydrogen Fractional Atomic Coordinates (×10^4) and Equivalent Isotropic Displacement Parameters (Å^2×10^3) for (5a*S*,8a*S*)-**179a**. U_{eq} is defined as 1/3 of the trace of the orthogonalised U_{ij}.

Atom	x	y	z	U_{eq}
H25	3869.74	7493.99	7170.09	31
H20A	5902	7209.6	9972.78	32
H20B	4551.42	7214.7	9014.82	32
H8A	2522.75	5819.41	9303.81	32
H8B	2159.28	6550.66	8203.71	32
H22A	7851.55	8170.5	9313.89	32
H22B	7357.34	9009.9	8260.42	32
H23	7455.37	6563.45	7971.04	28
H9	2387.35	4083.87	8101.14	29
H28A	6972.78	8650.01	6586.17	34
H28B	6295.14	7676.67	5645.26	34
H17A	6526.77	3424.55	6396.24	44
H17B	6589.11	1927.85	6687.8	44
H17C	7673.52	2893.6	7381.71	44
H7	557.89	6921.6	9128.44	32
H11	-1247.21	4956.72	6836.3	34
H24	5359.03	6518.39	6570.39	28
H26A	3285.57	8303.6	5490.36	40
H26B	3449.37	9636.29	6123	40
H6A	411.38	4890.21	9776.36	31
H6B	-826.65	4790.42	8726.3	31
H10	443.34	3894.98	6559.27	31
H21	6000.77	9299.93	9407.09	31
H14A	2162.89	5937.28	6640.68	39
H14B	1544.94	4939.87	5705.97	39
H4A	1356.52	737.55	6580.29	50
H4B	1653.72	-694.04	7031.17	50
H4C	2655.72	442.33	7528.04	50
H1A	2660.84	89.48	9267.83	52
H1B	1655.27	-1078.7	8947.84	52
H1C	1367.7	146.35	9537.29	52
H18A	3985.52	3029.96	7482.53	60
H18B	4326.52	2045.41	6723.34	60
H18C	4222.87	3555.4	6473.71	60
H15A	7323.65	2390.74	9014.78	57
H15B	6297.34	1306.58	8436.84	57
H15C	5907.7	2414.35	9079.16	57
H12A	-1466.56	5669.53	5181.05	50
H12B	-1427.71	7036.55	5744.57	50
H3A	-837.9	370.04	7993.57	63
H3B	-485.21	-774.52	7362.1	63
H3C	-805.6	630.39	6860.25	63

***Tert*-butyl ((3*R*,3a*R*,5*R*,6a*R*)-5-hydroxyhexahydro-2*H*-cyclopenta-[*b*]furan-3-yl)carbamate ((3*R*)-189)**

CCDC: 2085696
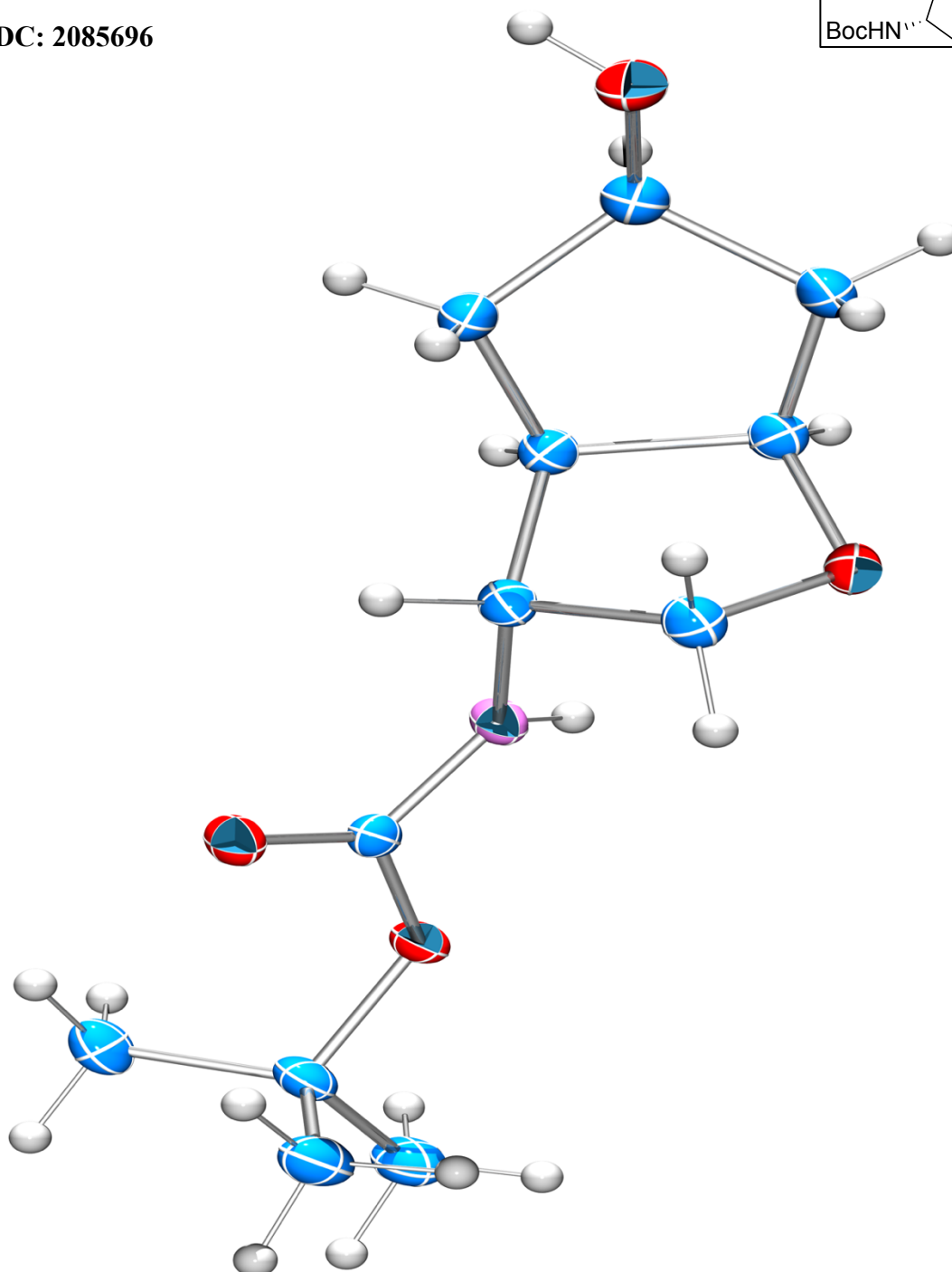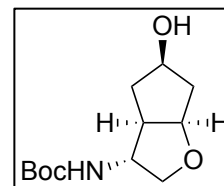
Figure S93. X-Ray crystallographic structure of (3*R*)-**189** (ORTEP view with 50% thermal ellipsoid contour probability, CCDC: 2085696).

Method for X-Ray quality crystal growth

Suitable crystals for X-Ray analysis were obtained by slow evaporation of a EtOAc solution containing (*3R*)-**10**. The crystals obtained were colourless and prism-shaped.

Table S14. Crystal data and structure refinement for (3*R*)-**189**.

Formula	$C_{12}H_{21}NO_4$
$D_{calc.}$/ g cm^{-3}	1.245
μ/mm^{-1}	0.765
Formula Weight	243.30
Colour	clear colourless
Shape	prism
Size/mm^3	0.12×0.07×0.06
T/K	100.00(10)
Crystal System	monoclinic
Flack Parameter	-0.07(7)
Hooft Parameter	-0.11(5)
Space Group	$P2_1$
a/Å	9.65750(10)
b/Å	5.88650(10)
c/Å	11.55820(10)
α/°	90
β/°	99.0470(10)
γ/°	90
V/Å^3	648.896(14)
Z	2
Z'	1
Wavelength/Å	1.54184
Radiation type	Cu K$_\alpha$
Θ_{min}/°	3.873
Θ_{max}/°	73.071
Measured Refl's.	28032
Indep't Refl's	2521
Refl's I≥2 σ(I)	2422
R_{int}	0.0415
Parameters	158
Restraints	1
Largest Peak	0.275
Deepest Hole	-0.278
GooF	1.053
wR_2 (all data)	0.0714
wR_2	0.0706
R_1 (all data)	0.0284
R_1	0.0272

Table S15: Fractional Atomic Coordinates (×10⁴) and Equivalent Isotropic Displacement Parameters (Å²×10³) for (3*R*)-**189**. U_{eq} is defined as 1/3 of the trace of the orthogonalised U_{ij}.

Atom	x	y	z	U_{eq}
O2	8764.1(13)	5381(2)	7928.2(10)	21.3(3)
O1	7055.0(12)	8077(2)	7739.3(10)	19.9(3)
O3	5526.3(12)	2780(2)	4628.2(10)	21.3(3)
O4	8556.2(14)	-666(3)	2454.1(13)	33.3(4)
N1	7280.0(15)	5905(3)	6209.4(12)	18.9(3)
C5	7780.4(17)	6365(3)	7344.6(14)	16.7(3)
C6	7688.1(17)	3804(3)	5684.5(15)	18.6(4)
C8	6340.1(18)	3379(3)	3727.0(15)	20.9(4)
C2	7412.9(19)	8828(3)	8977.7(14)	21.7(4)
C7	7818.1(17)	4074(3)	4381.1(14)	20.1(4)
C3	8872(2)	9844(3)	9194.2(16)	25.1(4)
C12	6512.7(18)	2060(3)	5617.1(15)	21.6(4)
C4	7231(2)	6872(3)	9802.0(16)	27.0(4)
C11	8837.3(18)	2348(4)	3967.3(17)	25.9(4)
C10	8094.9(19)	1502(4)	2778.6(17)	27.4(4)
C1	6320(2)	10658(4)	9055.6(17)	29.9(4)
C9	6568.3(19)	1340(4)	2950.9(16)	28.1(4)

Table S16: Anisotropic Displacement Parameters (×10⁴) for (3*R*)-**189**. The anisotropic displacement factor exponent takes the form: $-2\pi^2[h^2a^{*2} \times U_{11}+ ... +2hka^* \times b^* \times U_{12}]$

Atom	U_{11}	U_{22}	U_{33}	U_{23}	U_{13}	U_{12}
O2	19.6(6)	24.1(7)	18.7(6)	0.0(5)	-1.5(5)	3.9(5)
O1	20.2(6)	23.3(6)	15.5(5)	-4.3(5)	0.3(5)	3.4(5)
O3	16.0(6)	26.9(7)	20.6(6)	-0.1(5)	1.4(5)	-2.0(5)
O4	22.5(7)	40.4(9)	37.8(8)	-19.8(7)	7.5(6)	-2.2(6)
N1	18.0(7)	19.7(7)	17.7(7)	-1.7(6)	-1.1(5)	3.7(6)
C5	15.5(8)	17.8(8)	17.0(7)	-0.5(7)	3.3(6)	-2.8(7)
C6	17.6(8)	18.0(8)	19.5(8)	-2.2(7)	0.8(6)	2.0(7)
C8	18.6(8)	25.9(10)	17.9(8)	0.0(7)	1.9(7)	1.1(7)
C2	25.1(9)	23.9(9)	15.0(8)	-5.1(7)	-0.1(7)	-0.3(7)
C7	18.6(8)	21.5(9)	20.3(8)	-2.9(7)	3.8(7)	-1.3(7)
C3	27.6(10)	22.1(9)	23.6(9)	-1.6(7)	-1.6(8)	-3.7(7)
C12	22.1(9)	21.7(9)	20.2(8)	0.6(7)	1.5(7)	-1.4(7)
C4	32.3(10)	28.9(10)	20.1(9)	-2.9(8)	5.3(7)	-7.2(8)
C11	16.6(8)	34.0(11)	27.3(9)	-10.5(8)	3.9(7)	-1.3(8)
C10	22.8(9)	33.9(11)	25.7(9)	-7.6(8)	4.4(7)	-1.2(8)
C1	31.5(10)	33.1(11)	24.6(9)	-9.3(8)	3.1(8)	5.8(9)
C9	20.2(9)	39.0(11)	23.8(9)	-11.3(8)	-1.0(7)	0.1(9)

Table S17: Bond Lengths in Å for (3*R*)-**189**.

Atom	Atom	Length/Å
O2	C5	1.221(2)
O1	C5	1.347(2)
O1	C2	1.4859(19)
O3	C8	1.444(2)
O3	C12	1.432(2)
O4	C10	1.422(2)
N1	C5	1.353(2)
N1	C6	1.458(2)
C6	C7	1.540(2)
C6	C12	1.523(2)
C8	C7	1.561(2)
C8	C9	1.535(3)
C2	C3	1.515(3)
C2	C4	1.522(3)
C2	C1	1.521(3)
C7	C11	1.542(2)
C11	C10	1.530(2)
C10	C9	1.521(3)

Table S18: Bond Angles in ° for (3*R*)-**189**.

Atom	Atom	Atom	Angle/°
C5	O1	C2	119.61(13)
C12	O3	C8	106.19(12)
C5	N1	C6	119.66(14)
O2	C5	O1	124.65(15)
O2	C5	N1	124.67(16)
O1	C5	N1	110.68(14)
N1	C6	C7	112.87(14)
N1	C6	C12	110.16(14)
C12	C6	C7	101.20(13)
O3	C8	C7	105.94(13)
O3	C8	C9	112.04(15)
C9	C8	C7	106.47(14)
O1	C2	C3	110.24(14)
O1	C2	C4	110.23(14)
O1	C2	C1	102.08(14)
C3	C2	C4	113.03(15)
C3	C2	C1	110.30(16)
C1	C2	C4	110.41(15)
C6	C7	C8	103.76(13)
C6	C7	C11	112.95(15)
C11	C7	C8	104.88(14)
O3	C12	C6	103.78(14)
C10	C11	C7	105.14(14)
O4	C10	C11	114.03(17)
O4	C10	C9	109.19(16)
C9	C10	C11	103.29(14)
C10	C9	C8	104.99(15)

Table S19: Torsion Angles in ° for (3*R*)-**189**.

Atom	Atom	Atom	Atom	Angle/°
O3	C8	C7	C6	-0.53(18)
O3	C8	C7	C11	118.18(15)
O3	C8	C9	C10	-137.61(16)
O4	C10	C9	C8	158.88(15)
N1	C6	C7	C8	-92.87(16)
N1	C6	C7	C11	154.13(15)
N1	C6	C12	O3	77.95(16)
C5	O1	C2	C3	65.39(19)
C5	O1	C2	C4	-60.08(19)
C5	O1	C2	C1	-177.41(15)
C5	N1	C6	C7	-146.11(15)
C5	N1	C6	C12	101.59(18)
C6	N1	C5	O2	14.6(3)
C6	N1	C5	O1	-166.08(14)
C6	C7	C11	C10	136.49(16)
C8	O3	C12	C6	43.21(16)
C8	C7	C11	C10	24.18(19)
C2	O1	C5	O2	-2.0(2)
C2	O1	C5	N1	178.69(14)

Atom	Atom	Atom	Atom	Angle/°
C7	C6	C12	O3	-41.70(16)
C7	C8	C9	C10	-22.23(19)
C7	C11	C10	O4	-156.56(15)
C7	C11	C10	C9	-38.2(2)
C12	O3	C8	C7	-26.23(17)
C12	O3	C8	C9	89.47(16)
C12	C6	C7	C8	24.83(17)
C12	C6	C7	C11	-88.17(17)
C11	C10	C9	C8	37.2(2)
C9	C8	C7	C6	-119.97(15)
C9	C8	C7	C11	-1.25(19)

Table S20: Hydrogen Fractional Atomic Coordinates (×10^4) and Equivalent Isotropic Displacement Parameters (Å^2×10^3) for (3R)-**189**. U_{eq} is defined as 1/3 of the trace of the orthogonalised U_{ij}.

Atom	x	y	z	U_{eq}
H4	9373.58	-558	2296.44	50
H1	6711.08	6866.97	5789.6	23
H6	8576.68	3190.21	6137.58	22
H8	5893.19	4667	3241.61	25
H7	8060.64	5668.71	4192.38	24
H3A	9559.9	8675.45	9077.55	38
H3B	9074.02	10414.51	9999.55	38
H3C	8926.13	11097.81	8645.55	38
H12A	6863.8	512.19	5495.15	26
H12B	6084.47	2073.29	6341.07	26
H4A	6297.53	6202.5	9581.14	41
H4B	7329.83	7440.41	10607.85	41
H4C	7947.2	5715.21	9747.92	41
H11A	9738.74	3085.15	3887.32	31
H11B	9022.53	1073.99	4529.48	31
H10	8196.09	2642.37	2156.11	33
H1A	6423.67	11872.04	8495.71	45
H1B	6451	11283.95	9850.92	45
H1C	5379.71	9995.83	8870.36	45
H9A	6390.78	-104.54	3341.12	34
H9B	5937.09	1426.79	2189.46	34

G References

[1] J.-P. Lange, *Biofuels Bioprod. Bioref.* **2007**, *1*, 39–48.

[2] Statistisches Bundesamt (2021, 06. December). *Energieverbrauch in der Industrie 2020 um 1.9% gegenüber dem Vorjahr gesunken.*
https://www.destatis.de/DE/Presse/Pressemitteilungen/2021/12/PD21_551_435.html
(accessed: 23.06.2022).

[3] Verband der Chemischen Industrie e.V. (2022, 25. May). *Energiestatistik – Daten und Fakten.*
https://www.vci.de/ergaenzende-downloads/energiestatistik-2022.pdf
(accessed: 23.06.2022).

[4] E. S. Beach, Z. Cui, P. T. Anastas, *Energy Environ. Sci.* **2009**, *2*, 1038–1049.

[5] P. T. Anastas, J. C. Warner, *Green Chemistry: Theory and Practice*, Oxford University Press, Oxford, **1998**.

[6] P. T. Anastas and N. Eghbali, *Chem. Soc. Rev.* **2010**, *39*, 301–312.

[7] P. Gallezot, *Chem. Soc. Rev.* **2012**, *41*, 1538–1558.

[8] J. Schwarz, B. König, *Green Chem.* **2016**, *18*, 4743–4749.

[9] E. Scott, F. Peter, J. Sanders, *Appl. Microbiol. Biotechnol.* **2007**, *75*, 751–762.

[10] L. J. Gooßen, N. Rodriguez, K. Gooßen, *Angew. Chem. Int. Ed.* **2008**, *47*, 3100–3120.

[11] D. M. Kitcatt, S. Nicolle, A.-L. Lee, *Chem. Soc. Rev.* **2022**, *51*, 1415–1453.

[12] J. Xuan, Z.-G. Zhang, W.-J. Xiao, *Angew. Chem. Int. Ed.* **2015**, *54*, 15632–15641.

[13] J. Schwarz, B. König, *Green Chem.* **2018**, *20*, 323–361.

[14] H. Kolbe, *Liebigs Ann. Chem.* **1848**, *64*, 339–341.

[15] H. Hunsdiecker, C. Hunsdiecker, *Chem. Ber.* **1942**, *75*, 291–297.

[16] D. H. R. Barton, E. P. Serebryakov, *Proc. Chem. Soc.* **1962**, 309.

[17] H. Huang, K. Jia, Y. Chen, *ACS Catal.* **2016**, *6*, 4983–4988.

[18] C. K. Prier, D. A. Rankic, D. W. C. MacMillan, *Chem. Rev.* **2013**, *113*, 5322–5363.

[19] L. Marzo, S. K. Pagire, O. Reiser, B. König, *Angew. Chem. Int. Ed.* **2018**, *57*, 10034–10072.

[20] A. Hossain, A. Bhattacharyya, O. Reiser, *Science* **2019**, *364*, eaav9713.

[21] A. L. Gant Kanegusuku, J. L. Roizen, *Angew. Chem. Int. Ed.* **2021**, *60*, 21116–21149.

[22] L. McMurray, T. M. McGuire, R. L. Howells, *Synthesis* **2020**, *52*, 1719–1737.

[23] B. Giese, *Angew. Chem. Int. Ed. Engl.* **1983**, *22*, 753–764.

[24] (a) K. U. Ingold, J. K. Kochi, *Free Radicals, Vol. 1*, Wiley, New York, **1973**;
(b) H. Knoll, *Z. Chem.* **1982**, *22*, 245–252.

25 F. De Vleeschouwer, V. Van Speybroeck, M. Waroquier, P. Geerlings, F. De Proft, *Org. Lett.* **2007**, *9*, 2721–2724.

26 F. Parsaee, M. C. Senarathna, P. B. Kannangara, S. N. Alexander, P. D. E. Arche, E. R. Wein, *Nat. Rev. Chem, 2021, 5*, 486–499.

27 L. Chu, C. Ohta, Z. Zuo, D. W. C. MacMillan, *J. Am. Chem. Soc*. **2014**, *136*, 10886–10889.

28 C. A. Martinez, S. Hu, Y. Dumond, J. Tao, P. Kelleher, L. Tully, *Org. Process Res. Dev.* **2008**, *12*, 392–398.

29 S. J. McCarver, J. X. Qiao, J. Carpenter, R. M. Borzilleri, M. A. Poss, M. D. Eastgate, M. M. Miller, D. W. C. Macmillan, *Angew. Chem. Int. Ed*. **2017**, *56*, 728–732.

30 A. Piserchio, G. D. Salinas, T. Li, J. Marshall, M. R. Spaller, D. F. Mierke, *Chem. Biol*. **2004**, *11*, 469–473.

31 P. Fernandez-Rodriguez, F. Legros, T. Maier, A. Weber, M. Mendez, V. Derdau, G. Hessler, M. Kurz, A. Villar-Garea, S. Ruf, *Eur. J. Org. Chem*. **2021**, 782–787.

32 A. Noble, D. W. C. MacMillan, *J. Am. Chem. Soc*. **2014**, *136*, 11602–11605.

33 Y. Duan, M. Zhang, R. Ruzi, Z. Wu, C. Zhu, *Org. Chem. Front.* **2017**,*4*, 525–528.

34 L. M. Kammer, B. Lipp, T. Opatz*, J. Org. Chem.* **2019**, *84*, 2379–2392.

35 (a) J. T. Palmer, D. Rasnick, J. L. Klaus, D. J. Bromme, *Med. Chem.* **1995**, *38*, 3193–3196. (b) J. C. Engel, P. S. Doyle, I. Hseih, J. H. McKerrow, *J. Exp. Med*. **1998**, *188*, 725–734.

36 C. Shu, R. S. Mega, B. J. Andreassen, A. Noble, V. K. Aggarwal, *Angew. Chem. Int. Ed*. **2018**, *57*, 15430–15434.

37 G. Ernouf, E. Chirkin, L. Rhyman, P. Ramasami, J.-C. Cintrat, *Angew. Chem. Int. Ed*. **2020**, *59*, 2618–2622.

38 K. B. Wiberg, G. M. Lampman, R. P. Ciula, D. S. Connor, P. Schertler, J. Lavanish, *Tetrahedron* **1965**, *21*, 2749–2769.

39 C. Chatgilialoglu, D. Crich, M. Komatsu, I. Ryu*, Chem. Rev.* **1999**, *99*, 1991–2070.

40 G.-Z. Wang, R. Shang, W.-M. Cheng, Y. Fu, *Org. Lett*. **2015**, *17*, 4830–4833.

41 Z. Chen, F. Lu, F. Yuan, J. Sun, L. Du, Z. Li, M. Gao, R. Shi, A. Lei, *Sci. China Chem.* **2019**, *62*, 1497–1500.

42 M. Zhang, J. Xi, R. Ruzi, N. Li, Z. Wu, W. Li, C. Zhu, *J. Org. Chem*. **2017**, *82*, 9305–9311.

43 T. Xiao, L. Li, L. Zhou, *J. Org. Chem.* **2016**, *81*, 7908–7916.

44 Q.-F. Bai, C. Jin, J.-Y. He, G. Feng, *Org. Lett*. **2018**, *20*, 2172–2175.

45 J.-Q. Chen, R. Chang, Y.-L. Wei, J.-N. Mo, Z.-Y. Wang, P.-F. Xu, *J. Org. Chem*. **2018**, *83*, 253–259.

[46] A. Noble, R. S. Mega, D. Pflästerer, E. L. Myers, V. K. Aggarwal, *Angew. Chem., Int. Ed.* **2018**, *57*, 2155–2159.

[47] V. R. Yatham, P. Bellotti, B. König, *Chem. Commun.* **2019**, *55*, 3489–3492.

[48] A. Hu, J.-J. Guo, H. Pan, Z. Zuo, *Science* **2018**, *361*, 668–672.

[49] R. A. Sheldon, J. K. Kochi, *J. Am. Chem. Soc.* **1968**, *90*, 6688–6698.

[50] O. Zhang, J. W. Schubert, *J. Org. Chem.* **2020**, *85*, 6225–6232.

[51] M. Erak, K. Bellmann-Sickert, S. Els-Heindl, A. G. Beck-Sickinger, *Bioorg. Med. Chem.* **2018**, *26*, 2759−2765.

[52] P. Chandu, D. Das, K. G. Ghosh, D. Sureshkumar, *Adv. Synth. Catal.* **2022**, *364*, 1–7.

[53] D. J. Van Hoomissen, S. Vyas, *J. Org. Chem.* **2017**, *82*, 5731–5742.

[54] Y. Miyake, K. Nakajima, Y. Nishibayashi, *Chem. Commun.* **2013**, *49*, 7854–7856.

[55] L. Capaldo, L. Buzzetti, D. Merli, M. Fagnoni, D. Ravelli, *J. Org. Chem.* **2016**, *81*, 7102–7109.

[56] J. Guo, Q.-L.Wu, Y. Xie, J. Weng, G. Lu, *J. Org. Chem.* **2018**, *83*, 12559–12567.

[57] S. Zhang, Z. M. Tan, H. N. Zhang, J. L. Liu, W. T. Xu, K. Xu, *Chem. Commun.* **2017**, *53*, 11642–11645.

[58] H. Huang, C. Yu, Y. Zhang, Y. Zhang, P. S. Mariano, W. Wang, *J. Am. Chem. Soc.* **2017**, *139*, 9799–9802.

[59] T. Guo, L. Zhang, Y. Fang, X. Jin, Y. Li, R. Li, X. Li, W. Cen, X. Liu, Z. Tian, *Adv. Synth. Catal.* **2018**, *360*, 1352–1357.

[60] T. Krolo, *Photochemical derivatization of 4-hydroxy-2-cyclopentenone and derivatives*. Masterthesis, University of Regensburg, Regensburg, **2018**.

[61] F. W. Lichtenthaler, *Carbohydr. Res.* **1998**, *313*, 69–89.

[62] K. Ulbrich, P. Kreitmeier, O. Reiser, *Synlett* **2010**, *13*, 2037–2040.

[63] F. Rodrigues, R. Guirardello, *Chem. Eng. Technol.* **2008**, *31*, 883–892.

[64] B. C. Saha, *J. Ind. Microbiol. Biotechnol.* **2003**, *30*, 279–291.

[65] A. Corma, S. Iborra, A. Velty, *Chem. Rev.* **2007**, *107*, 2411–2502.

[66] G. Piancatelli, A. Scettri, S. Barbadoro, *Tetrahedron Lett.* **1976**, *17*, 3555–3558.

[67] S. P. Roche, D. J. Aitken, *Eur. J. Org. Chem.* **2010**, 5339–5358.

[68] D. Dobler, *Conversion of 4-hydroxy-2-cyclopentenone derivatives into valuable fine chemicals*. Dissertation, University of Regensburg, Regensburg, **2017**.

[69] T. Krolo, A. Bhattacharyya, O. Reiser, *Org. Lett.* **2021**, *23*, 6283-6287.

[70] B.-B. Gu, W. Wu, F.-R. Jiao, W.-H. Jiao, L. Li, F. Sun, S.-P. Wang, F. Yang, H.-W. Lin, *J. Org. Chem.* **2019**, *84*, 300–306.

References

[71] K.-I. Nihei, F. J. Hanke, Y. Asaka, T. Matsumoto, I. Kubo, *J. Agric. Food Chem.* **2002,** *50*, 5048–5052.

[72] (a) A. K. Ghosh, K. Xi, *Org. Lett.* **2007,** *9*, 4013–4016. (b) A. K. Ghosh, K. Xi, *J. Org. Chem.* **2009,** *74*, 1163–1170.

[73] (a) K. Murai, S.-I. Katoh, D. Urabe, M. Inoue, *Chem. Sci.* **2013,** *4*, 2364–2368. (b) S. Hashimoto, S.-I. Katoh, T. Kato, D. Urabe, M. Inoue, *J. Am. Chem. Soc.* **2017,** *139*, 16420–16429.

[74] (a) S. Hirose, Y. O. Kamatari, E. Yanase, *Tetrahedron Lett.* **2020,** *61*, 151601. (b) S. Hirose, K. Tomatsu, E. Yanase, *Tetrahedron Lett.* **2013,** *54*, 7040–7043.

[75] C. Jing, S. Mallah, E. Kriemen, S. H. Bennett, V. Fasano, A. J. J. Lennox, I. Hers, V. K. Aggarwal, *ACS Central Science* **2020,** *6*, 995–1000.

[76] H. Wakita, H. Yoshiwara, H. Nishiyama, H. Nagase, *Heterocycles* **2000,** *53*, 1085–1110.

[77] Y. Koh, H. Nakata, K. Maeda, H. Ogata, G. Bilcer, T. Devasamudram, J. F. Kincaid, P. Boross, Y.-F. Wang, Y. Tie, P. Volarath, L. Gaddis, R. W. Harrison, I. T. Weber, A. K. Ghosh, H. Mitsuya, *Antimicrob. Agents Chemother.* **2003**, *47*, 3123–3129.

[78] A. K. Ghosh, B. D. Chapsal, M. Steffey, J. Agniswamy, Y.-F. Wang, M. Amano, I. T. Weber, H. Mitsuya, *Bioorg. Med. Chem. Lett.* **2012,** *22*, 2308–2311.

[79] A. K. Ghosh, B. D. Chapsal, G. L. Parham, M. Steffey, J. Agniswamy, Y.-F. Wang, M. Amano, I. T. Weber, H. Mitsuya, *J. Med. Chem.* **2011,** *54*, 5890–5901.

[80] F. Cottiglia, L. Casu, M. Leonti, P. Caboni, C. Floris, B. Busonera, P. Farci, A. Ouhtit, G. Sanna, *J. Nat. Prod.* **2012,** *75*, 225–229.

[81] M. Miyano, C. R. Dorn, *J. Org. Chem.* **1972,** *37*, 1818–1823.

[82] J.-R. Weng, M.-I. Chung, M.-H. Yen, C.-N. Lin, R.-R. Wu, *Helvetica Chimica Acta* **2001,** *84*, 1976–1979.

[83] G. Coulthard, W. Erb, V. K. Aggarwal, *Nature* **2012,** *489*, 278–281.

[84] Z. Lv, B. Chen, C. Zhang, G. Liang, *Chem. Eur. J.* **2018,** *24*, 9773–9777.

[85] (a) L. A. Paquette, Z. Zhao, F. Gallou, J. Liu, *J. Am. Chem. Soc.* **2000,** *122*, 1540–1541. (b) G. Mehta, A. Srikrishna, A. V. Reddy, M. S. Nair, *Tetrahedron* **1981,** *37*, 4543–59.

[86] A. V. Baranovsky, D. A. Bolibrukh, J. R. Bull, *Eur. J. Org. Chem.* **2007**, 445–454.

[87] M. Inoue, S. Yamashita; Y. Ishihara, M. Hirama, *Org. Lett.* **2006,** *8*, 5805–5808.

[88] J. Montgomery, M. V. Chevliakov, H. L. Brielmann, *Tetrahedron* **1997,** *53*, 16449–16462.

[89] (a) J. Yan, J. W. Herndon, *J. Org. Chem.* **1998,** *63*, 2325–2331. (b) F. P. Marmsater, J. A. Vanecko, F. G. West, *Tetrahedron* **2002,** *58*, 2027–2040.

References

[90] E. Fanales-Belasio, M. Raimondo, B. Suligoi, S. Butto, *Ann Ist Super Sanita*. **2010**, *46*, 5–14.

[91] UNAIDS. *Global HIV & AIDS statistics – Fact sheet*. https://www.unaids.org/en/resources/fact-sheet (accessed: 06.06.2022).

[92] V. Le Douce, A. Janossy, H. Hallay, S. Ali, R. Riclet, O. Rohr, C. Schwartz , *J Antimicrob Chemother*. **2012**, *67*, 1063–74.

[93] N. Squillace, G. Bozzi, E. Colella, A. Gori, A. Bandera, *Drug Des Devel Ther*. **2018**, *12*, 3635–3643.

[94] E. D. Deeks, *Drugs* **2018**, *78*, 1013–1024.

[95] A. K. Ghosh, J. Takayama, *Tetrahedron Lett*. **2008,** *49*, 3409–3412.

[96] M. G. Atta, S. De Seigneux, G. M. Lucas, *Clin J Am Soc Nephrol*. **2019**, 14, 435–444.

[97] A. K. Ghosh, P. R. Sridhar, N. Kumaragurubaran, Y. Koh, I. T. Weber, H. Mitsuya, *ChemMedChem*. **2006**, *1*, 939–950.

[98] M. Kožíšek, M. Lepšík, K. Grantz Šašková. J. Brynda, J. Konvalinka, P. Řezáčová, *FEBS J*. **2014**, *281*, 1834–1847.

[99] A. K. Ghosh, S. B. Markad, W. L. Robinson, *J. Org. Chem.* **2021**, *86*, 1216–1222.

[100] A. K. Ghosh, P. R. Sridhar, S. Leshchenko, A. K. Hussain, J. Li, A. Y. Kovalevsky, D. E. Walters, J. E. Wedekind, V. Grum-Tokars, D. Das, Y. Koh, K. Maeda, H. Gatanaga, I. T. Weber, H. Mitsuya, *J. Med. Chem.* **2006**, *49*, 5252–5261.

[101] A. K. Ghosh, S. Leshchenko, M. Noetzel, *J. Org. Chem*. **2004**, *69*, 7822–7829.

[102] H. Mihara, Y. Sohtome, S. Matsunaga, M. Shibasaki, *Chemistry - An Asian Journal* **2008,** *3*, 359–366.

[103] M. S. Lowry, J. I. Goldsmith, J. D. Slinker, R. Rohl, R. A. Pascal, G. G. Malliaras, S. Bernhard, *Chem. Mater*. **2005**, *17*, 5712–5719.

[104] J. D. Slinker, A. A. Gorodetsky, M. S. Lowry, J. Wang, S. Parker, R. Rohl, S. Bernhard, G. G. Malliaras, *J. Am. Chem. Soc*. **2004**, *126*, 2763–2767.

[105] L. Flamigni, A. Barbieri, C. Sabatini, B. Ventura, F. Barigelletti, *Top. Curr. Chem*. **2007**, *281*, 143–203.

[106] A. Juris, V. Balzani, P. Belser, A. von Zelewsky, *Helv. Chim. Acta* **1981**, *64*, 2175–2182.

[107] J. M. Kern, J.-P. Sauvage, *J. Chem. Soc., Chem. Commun*. **1987**, 546–548.

[108] P. Wuts, T. Greene, *Greene's Protective Groups in Organic Synthesis*, 4th edition, John Wiley & Sons, Hoboken, New Jersey, **2006**.

[109] J. L. Bilke, P. O'Brien, J. Org. Chem. **2008**, *73*, 6452–6454.

[110] A. Moussa, P. Meffre, J. Martinez, V. Rolland, *Amino Acids* **2012**, *42***,** 1339–1348.

[111] F. Ishikawa, T.Tsumuraya, I. Fujii, *J. Am. Chem. Soc.* **2009**, *131*, 456–457.

[112] N. A. Romero, D. A. Nicewicz, *Chem. Rev.* **2016,** *116*, 10075–10166.

[113] A. C. Benniston, A. Harriman, P. Li, J. P. Rostron, H. J. van Ramesdonk, M. M. Groeneveld, H. Zhang, J. W. Verhoeven, *J. Am. Chem. Soc*. **2005**, *127*, 16054−16064.

[114] Y. Wang, O. Haze, J. P. Dinnocenzo, S. Farid, R. S. Farid, I. R. Gould, *J. Org. Chem*. **2007**, *72*, 6970−6981.

[115] T. Shen, Z.-G. Zhao, Q. Yu, H.-J. Xu, *J. Photochem. Photobiol*., A **1989**, *47*, 203−212.

[116] S. Yasui, M. Tsujimoto, K. Itoh, A. Ohno, *J. Org. Chem*. **2000**, *65*, 4715−4720.

[117] T.-Y. Shang, L.-H. Lu, Z. Cao, Y. Liu, W.-M. He, B. Yu, *Chem. Commun*. **2019**, *55*, 5408–5419.

[118] H. Kilic, S. Bayindir, E. Erdogan, N. Saracoglu, *Tetrahedron* **2012,** *68*, 5619–5630.

[119] R. K. Boeckman, D. O. Tusch, K. F. Biegasiewicz, *Org. Synth*. **2015**, *92*, 320–327.

[120] Y. Itou, K. Ishida, H. J. Shin, M. Murakami, *Tetrahedron* **1999**, *55*, 6871–6882.

[121] N. Arisetti, O. Reiser, *Org. Lett.* **2015**, *17*, 94–97.

[122] B. M. Trost, D. L. Van Vranken, C. Bingel, *J. Am. Chem. Soc.* **1992**, *114*, 9327–9343.

[123] A. K. Ghosh, B. D. Chapsal, A. Baldridge, K. Ide, Y. Koh, H. Mitsuya, *Org. Lett.* **2008,** *10*, 5135–5138.

[124] A. K. Ghosh, S. Fidanze, *J. Org. Chem.* **1998,** *63*, 61466152.

[125] G. L. Bundy, J. M. Baldwin, *Tetrahedron Lett. 1978*, *16*, 1371–1374.

[126] K. C. Nicolaou, W. E. Barnette, G. P. Gasic, R. L. Magolda, *J. Am. Chem. Soc.* **1977**, *99*, 7736–7738.

[127] D. R. Nicponski, J. M. Marchi, *Synthesis* **2014**, *46*, 1725–1730.

[128] K. Donabauer, M. Maity, A. L. Berger, G. S. Huff, S. Crespi, B. König, *Chem. Sci.* **2019**, *10*, 5162–5166.

[129] W. L. F. Armarego, *Purification of laboratory chemicals,* 8. edition, Butterworth-Heinemann, **2017**, pp. 4–52.

[130] O. V. Dolomanov, L. J. Bourhis, R. J. Gildea, J. A. K. Howard, H. Puschmann, *J. Appl. Cryst.* **2009**, *42*, 339–341.

[131] G.M. Sheldrick, *Acta Cryst.* **2015**, *A71*, 3–8.

[132] G.M. Sheldrick, *Acta Cryst.* **2015**, *C71*, 3–8.

[133] S. Lenz, P. Horx, A. Geyer, *J. Pept. Sci.* **2018**, *24*, e3075.

H Curriculum Vitae

Name	Tomislav Krolo
Date / place of birth	07.10.1994 in Regensburg
Citizenship	German, Croatian
Marital status	Unmarried
E-Mail	tomislav.krolo@gmx.net

Education ——————————————————————

10/2018 – 07/2022 PhD (Dr. rer. nat.), Organic Chemistry
University of Regensburg

Dissertation: Photoredox-Catalyzed Decarboxylative Radical
Conjugate Addition-Elimination-Oxa-Michael Reaction:
A ustainable approach towards potent HIV-1 Protease Inhibitors

04/2019 – 07/2022 Bachelor of Science (B. Sc.), Business Chemistry
University of Regensburg

Bachelor thesis: Totalsynthese von 6-alkylsubstituierten
2-Pyronderivaten ausgehend von erneuerbaren Rohstoffen und
deren Bewertung hinsichtlich kostenwirtschaftlicher Effizienz

10/2016 – 09/2018 Master of Science (M. Sc.), Chemistry
University of Regensburg

Master thesis: Photochemical derivatization of 4-hydroxy-2-
cyclopentenone and derivatives

10/2013 – 09/2016 Bachelor of Science (B. Sc.), Chemistry
University of Regensburg

Bachelor thesis: Totalsynthese von 6-Propyl-2*H*-pyran-2-on,
6-Pentyl-2*H*-pyran-2-on und 6-Heptyl-2*H*-pyran-2-on ausgehend
von erneuerbaren Ressourcen

09/2005 – 06/2013   General Qualification for the University Entrance
Donau-Gymnasium Kelheim

Degree: Allgemeine Hochschulreife

Professional References

Prof. Dr. Oliver Reiser   Institut für Organische Chemie
Universität Regensburg, Universitätsstr. 31
93053 Regensburg, Germany
Phone: +49 941 9434631
E-mail: oliver.reiser@chemie.uni-regensburg.de

List of Publications

"Accessing HIV-1 Protease Inhibitors through Visible-Light-Mediated Sequential Photocatalytic Decarboxylative Radical Conjugate Addition-Elimination–Oxa-Michael Reactions" (*2021*)

T. Krolo, A. Bhattacharyya, O. Reiser, *Org. Lett.* **2021**, *23*, 6283–6287.

I   Acknowledgement

Zunächst möchte ich mich ganz herzlich bei meinem Doktorvater Prof. Dr. Oliver Reiser für die Aufnahme in seinen Arbeitskreis, die interessante Themenstellung, die anregenden Diskussionen chemischer als auch nicht chemischer Art und seine stete Unterstützung während der Durchführung dieser Arbeit bedanken. Vielen Dank dafür, dass du mir diese Möglichkeit gegeben hast, Oliver!

An dieser Stelle möchte ich mich auch besonders bei Herrn Prof. Dr. Alexander Breder für die Übernahme des Amtes des 2. Gutachters, bei Herrn Prof. Dr. Frank-Michael Matysik für die Übernahme des Amtes des 3. Prüfers sowie bei Herrn Prof. Dr. Alkwin Slenczka für die Übernahme des Prüfungsvorsitzes bedanken, vielen Dank für Ihre Zeit!

Großen Dank auch an Dr. Peter Kreitmeier für die zahlreichen chemischen Hilfestellungen und seine praktische Hilfe jeglicher Art. Für die technische Unterstützung bedanke ich mich bei Johannes Floss, Brigitte Eichenseher, Roxane Harteis, Klaus Döring und Helena Konkel. Herzlich bedanken möchte ich mich auch bei unseren Sekretärinnen Anja Titze, Michaela Schüle und Antje Weigert für ihre herzliche Art und ihre umfangreiche Unterstützung bei organisatorischen Problemen.

Bei allen Mitarbeitern der zentralen Analytik möchte ich mich bedanken. Besonders bedanke ich mich dabei bei den Mitarbeitern der NMR Abteilung Dr. Ilya Shenderovich und Fritz Kastner sowie bei den Mitarbeitern der X-Ray Abteilung Sabine Stempfhuber, Birgit Hischa und Dr. Michael Bodensteiner. Darüber hinaus bedanke ich mich bei Josef Kiermaier und Wolfgang Söllner für die Messung der Massenspektren.

Bei allen aktuellen und ehemaligen Mitarbeitern des Arbeitskreises möchte ich mich für die gute Atmosphäre und die vielen schönen Stunden bedanken. Besonders bedanken möchte ich mich dabei bei meinen Freunden, aktuellen und ehemaligen Kollegen Roxane Harteis, Dr. Thomas Weinbender, Dr. Robert Eckl, Dr. Natalija Moor, Anurag Chincole und Marco Henriquez. Ganz besonderer Dank geht hierbei an die drei Kindsköpfe aus Labor 33.1.20, die auf die Namen Sebastian Fischer, Andreas Ratzenböck und Viktor Klöpfer hören. Danke für die vielen lustigen Momente, für das stets gute Arbeitsklima und die richtige Portion Pledzin. Herzlicher Dank gilt auch meiner zukünftigen Kollegin Carina Sonnleitner, die mir vor allem in den letzten Wochen mit Rat und Tat zur Seite stand.

J Declaration

Herewith I declare that this present thesis is a presentation of my original work prepared single-handed. Wherever contributions from others are involved, all of them are marked clearly, with reference to the literature, license, and acknowledgement of collaborative research.

Regensburg, 27.07.2022

_____

Tomislav Krolo